DOCTORAL THESIS

Presented to the Department of Pharmacy
Graduate School of Pharmaceutical Science, XXXIII Cycle

University of Naples Federico II

"Design of Small Molecules with Antitumor Activity through Computational Methodologies"

Ph.D. Thesis
Pasquale Russomanno

Approved by
Ph.D. Supervisor: Prof. Luciana Marinelli
Ph.D. Program Coordinator: Prof. Maria Valeria D'Auria

Abstract

Today, there are multiple targeted therapies against cancer. The most relevant ones are those aimed at the stop of cancer cells from growing, or at the halting of signals that stimulate blood vessels, or at helping the immune system destroy cancer cells, and many others. The last one, has achieved impressive results to date. Indeed, the immuno-oncology field is entering a new, exciting phase having the potential to change the current cancer treatment either as a standalone therapy or in combination. Recently, many innovative strategies exist to overcome tumor-induced immunosuppression. Currently the main ones are checkpoint blockade inhibitors, adoptive T cell transfers, and vaccination strategies. To date, the immuno-oncology therapeutics on the market are mostly biologic products (e.g. monoclonal antibodies (mAbs), proteins, engineered cells, and oncolytic viruses). However, for example, antibodies have specific drawbacks: high production costs, lack of oral bioavailability, poor tumor penetrating capacity, Fc-related toxicities, and immunogenic properties. In this perspective, small molecules could potentially overcome many of these issues and be complementary to, and potentially synergistic with, biologic therapeutics too.

In this context, my PhD work was focused on discovery of small molecules targeting three different proteins: MDM2 (Mouse Double Minute 2) the PD-1/PD-L1 axis (Programmed cell Death protein-1/ Programmed Death-ligand 1), and STING protein (STimulator of INterferon Genes). For all targets, a tandem approach of computational studies/NMR spectroscopy was applied.

Abbreviations

Abs	Antibodies
ABZI	2-[(1-ethyl-3-methyl-1H-pyrazole-5-carbonyl)amino]-1-[(2R)-2-hydroxy-2 phenylethyl]-1H-benzimidazole-5-carboxamide
ADU-S100	2'3'-c-di-AM(PS)2 (Rp,Rp
a-MG	alpha-Mangostin
APCs	antigen-presenting cells
BMS	Bristol-Myers-Squibb
BNBC	6-bromo-N-(Naphtalen-1-yl)-benzo[d][1,3]dioxole-5carboxamide
cAIMP	Cyclic adenine monophosphate-inosine monophosphate
CD	circular dichroism
CDNs	cyclic dinucleotides
c-di-AMP	Cyclic diadenyl acid
c-di-GMP	Cyclic diguanyl acid
cGAMP	Cyclic guanosine monophosphate–adenosine monophosphate
cGAS	cyclic GMP-AMP synthase
CMA	carboxymethiyl-9-acridanone
DAMPs	danger-associated molecular patterns
DCs	dendritic cells
di-ABZI	1,1'-(Butane-1,4-diyl)bis(2-(1-ethyl-3-methyl-1H-pyrazole-5-carboxamido)-1H-benzo[d]imidazole-5-carboxamide)
DMXAA	5,6-dimethylxanthenone-4-acetic acid
DMSO	dimethyl sulphoxide
DSC	Differential scanning calorimetry
EC_{50}	Half maximal effective concentration
E.coli	Escherichia Coli
ER	endoplasmic reticulum
FAA	flavone acetic acid
FRET	fluorescence resonance energy transfer
GF	gel-filtration
HNSCC	head and neck squamous cell carcinoma
HSQC	Heteronuclear Single-Quantum Correlation

HTRF	homogeneous time-resolved fluorescence
HTS	High-throughput screening
IC_{50}	half maximal inhibitory concentration
ICRs	Immune Checkpoint Receptors
IFN-I	type I interferons
IFN-α	interferon alpha
IFN-β	interferon beta
IFNs	interferons
IgV	immunoglobulin-variable
IKK	IkB kinase
IL-2	interleukin-2
IPTG	isopropyl β-D-1-thiogalactopyranoside
IRF3	Interferon Regulatory Factor 3
ISG	IFN-stimulated genes
LB	lysogeny broth
mAbs	monoclonal antibodies
MES	2-(N-morpholino)ethanesulfonic acid
MHCI	major histocompatibility complex class I
MSA-2	benzothiophene oxobutanoic acid
MW	molecular weight
NF-κB	Nuclear factor-kappaB
NMR	nuclear magnetic resonance
NOE	nuclear Overhauser effect
NSCLC	non-small cell lung cancer
OD	optical density
PAMPs	pathogen-associated molecular patterns
PBMCs	peripheral blood mononuclear cell
PDB	protein data bank
PD-1	Programmed cell Death protein-1
PD-L1	Programmed cell Death-Ligand 1
PPI	protein-protein interaction
SBVS	structure-based virtual screening
SR-717	2-(6-(1H-Imidazol-1-yl)pyridazine-3-carboxamido)-4,5-difluorobenzoic

SDS-PAGE	sodium dodecyl sulfate polyacrylamide gel electrophoresis
STD	Saturation Transfer Difference
STING	STimulator of INterferon Genes
T-eff	effector T
Tm	melting temperature
TME	tumor microenvironment
TBK1	TANK-binding kinase 1
VS	Virtual Screening
WL	WaterLOGSY (Water-Ligand Observed by Gradient SpectroscopY).
XAA-5Me	2-(5-methyl-9-oxoxanthen-4-yl)acetic acid
XAA-8Me	2-(8-methyl-9-oxoxanthen-4-yl)acetic acid
XRD	X-ray diffraction

Index

Chapter 1
INTRODUCTION

1.1. Cancer

National cancer institute defines cancer as *"disease in which some of the body's cells grow uncontrollably and spread to other parts of the body."*

This disease is caused by changes to genes that control all cellular processes, particularly cell growth and cell division. [1,2] These genetic changes that induce cancer are caused by several reasons, such as errors during cell division, DNA damage caused by environmental factors, or more simply genetic factors. Three main genes are involved in cancer: Proto-oncogenes, tumor suppressor genes, and DNA repair genes. These are called "drivers" of cancer.

Proto-oncogenes are genes involved in cell growth and division. When these genes mutate or are more active than normal, they become oncogenes (carcinogenic genes) and cause the growth and survival of cancer cells. Tumor suppressor genes, also called antioncogenes, such as proto-oncogenes are implicated in cell growth and division. When these genes are altered, cancer cells are divided in an uncontrolled manner. In the end, the DNA repair genes are involved in fixing damaged DNA[2–6]

The body normally eliminates cells with damaged DNA before they become cancerous, but this ability of the organism often fails. Cancer can be described as a multistep process characterized by abnormal and uncontrolled proliferation of cells, growth suppressors evasion, immortal replication, angiogenesis induction, spread in surrounding tissue and formation of metastases in distant organs through the blood or lymphatic system[1,7,8]

This multistep process called tumorigenesis involves two phases: Tumor Initiation and Tumor Promotion.

During the first phase (Tumor initiation) genetic mutations occur in pro-oncogenes such as RAS and MYC or in tumor suppressor genes such as BRCA1, BRCA2 and P53. Once mutated, cancer cells may remain in a dormant state or proliferate. The second phase (Tumor Promotion) consists of several phases: hyperplasia (increase in the number of cells), dysplasia (phenotypic changes in cells), carcinoma in situ (early-stage cancer) and finally invasive carcinoma (cancer spread on surrounding tissues)[8–13]

Most of cancer treatments that exist today affect the gene mutations listed above. These "targeted therapies" target proteins that control how cancer cells grow, divide, and spread. Today there are various targeted therapies that treat cancer in many ways such as helping the immune system destroy cancer cells, stopping cancer cells from growing, stopping

signals that help form blood vessels, delivering cell-killing substances to cancer cells and many other.[14–17]

1.2. P53 and MDM2 in Cancer

Tumor suppressor p53 protects organisms from DNA damage and cancer. It is one of defenses against kind of damage such as abnormal and uncontrolled proliferation of cells and growth suppressors evasion and is one of the most studied regulators of cell when the integrity of the genome is damaged. p53 tumor suppressor is normally present in minimal amounts, but when DNA damage is detected, its levels increase, and defense mechanisms begin. [18,19] The p53 binds to regulatory sites in genome and starts the production of proteins that stop cell division until the damage is repaired. On the other hand, if the damage is too serious, p53 begins the process of programmed cell death, or apoptosis. The p53 action must be carefully controlled. [5,6,20,21]

This is the task of MDM2 (mouse double minute 2, an oncoprotein discovered the first time in the mouse) that supervises the p53 so that it comes into action only when it is absolutely necessary. Normally MDM2 remains attached to p53 and performs several sequential actions first in the nucleus and then in the cytoplasm. In the nucleus, a MDM2 domain binds to the p53 transactivation domain, blocking its DNA transcription activation action. Then, another MDM2 domain binds an export signal from the nucleus, which is used to drag the p53 out of the nucleus.[21–24]

Finally, in the cytoplasm MDM2 bind ubiquitin and add it to the p53 marking for destruction in proteasomes. Normally the cell synthesizes enough MDM2 to control the p53. However, when there is damage or infection, MDM2 is deactivated to allow p53 to activate. Most cancer cells have developed methods to overcome this process. In some cases, the p53 is altered and so the cell no longer has tools to protect itself. In other cases, cancer cells synthesize more MDM2. This high amount of MDM2 blocks p53 thus stopping the induced apoptosis.[15,23,25–29] Thus, the finding of MDM2 inhibitors represented so far a valuable strategies to overcome such mechanism.

1.3. Immune System and Cancer: Axis PD-1/PD-L1 and STING Protein

The immune system protects us against disease due to "non-self" substances and from all kinds of invasions strangers. In addition it is involved in the prevention, development and defense of cancer, because cancer cells, recognized as non-self, differ from normal cells in biological behavior, antigenic structure and biochemical composition.[30]

An intimate relationship between cancer and immune function was firstly proposed more than a century ago by Rudolf Virchow, who observed the prevalence of leukocytes in tumours.[31] Also in 1890, William Cooley observed that some cancer patients, after contracting an acute infection, had spontaneous remission of the tumor. This observation led him to develop a primordial immunotherapy treatment by injecting directly into the tumor site a bacterial concentrate of killed colonies of Streptococcus pyogenes and Serratia marcescens (Cooley's toxin)[32,33]

Since then and for at least the following 100 years, there were limited advancements in the comprehension of the biological pathways activated upon interaction between cancer cells and immune system.

We must wait until 1980 to have new discoveries. In fact, in those years Lewis Thomas and Mcfarlane Burnet proposed the theory of "immune surveillance of cancer" which suggested that lymphocytes identified and eliminated all mutated cells and therefore differed from "normal" cells. This theory stated that the immune system was capable of destroying cancer.[30,32,34–36]

The true development of immunotherapy occurs between the end of 1900 and the beginning of 2000 with the discovery of the gene coding an antigen by T lymphocytes[37] and with the approval of interferon-alpha (IFN- α) and interleukin-2 (IL-2) as a treatment against melanoma. [32]

In addition, studies by in 2001 and Koebel in 2007 demonstrated the immunosurveillance theory (integrated in the immunoediting theory)[38] and the equilibrium phase of cancer theory[39] respectively. These theories were used by Galon et al. and Wang et al. to explain how the infiltration of adaptive system cells[40] and an active-tumor microenvironment

conducive to immune recognition[41] were important for the survival of cancer patients. [32,36]

Today, it is known that the immune system recognizes cancer cells due to their biochemical differences with self-cells. There is an initial dynamic period, called immunoediting, in which immune cells destroy cancer cells, but at a later stage cancer cells manage to evade the immune system through various mechanisms. Immunoediting is the most correct term to use compared to immunosurveillance, because it includes all stages of cancer and all stages of interaction with the immune system and so the immunosurveillance is only a part of the process. [30,36,42]

Immunoediting (Figure 1) is divided into three steps: elimination, equilibrium and escape. [30,36,42,43]

- The first step is the elimination. During this step, the immunosurveillance is active and both the innate and adaptive immune systems cooperate to eradicate the tumor. The damaged cells and therefore malignant or potentially malignant cells are initially identified through the release of so called "danger signals" and then killed. The destruction of cancer cells occurs first thanks to innate immunity, then thanks to development of tumor antigens, dendritic cells and specific cancer cells CD4+ and CD8+ T. At this stage (undetectable and early stage of tumor development) cancer cells are destroyed before they become clinically relevant, although they are not always completely eliminated. [30,36,42,43]

- The second step is the equilibrium. During this step, the not destroyed cancer cells coexist with the immune system. They are unable to progress and are kept in a state of dormancy. This phase is the longest of the three. Theoretically it could last for years since the cancer cells are kept under control. Unfortunately, the lack of control of these cells by the immune system, allow them to escape. [30,36,42,43]

- The third step is the escape. During this step, the immune system lack of the control and growth of cancer cells. Through multiple mechanisms, cancer cells elude elimination by the immune system, sometimes even suppressing it, thus succeeding in advancing and forming metastases. [30,36,42,43]
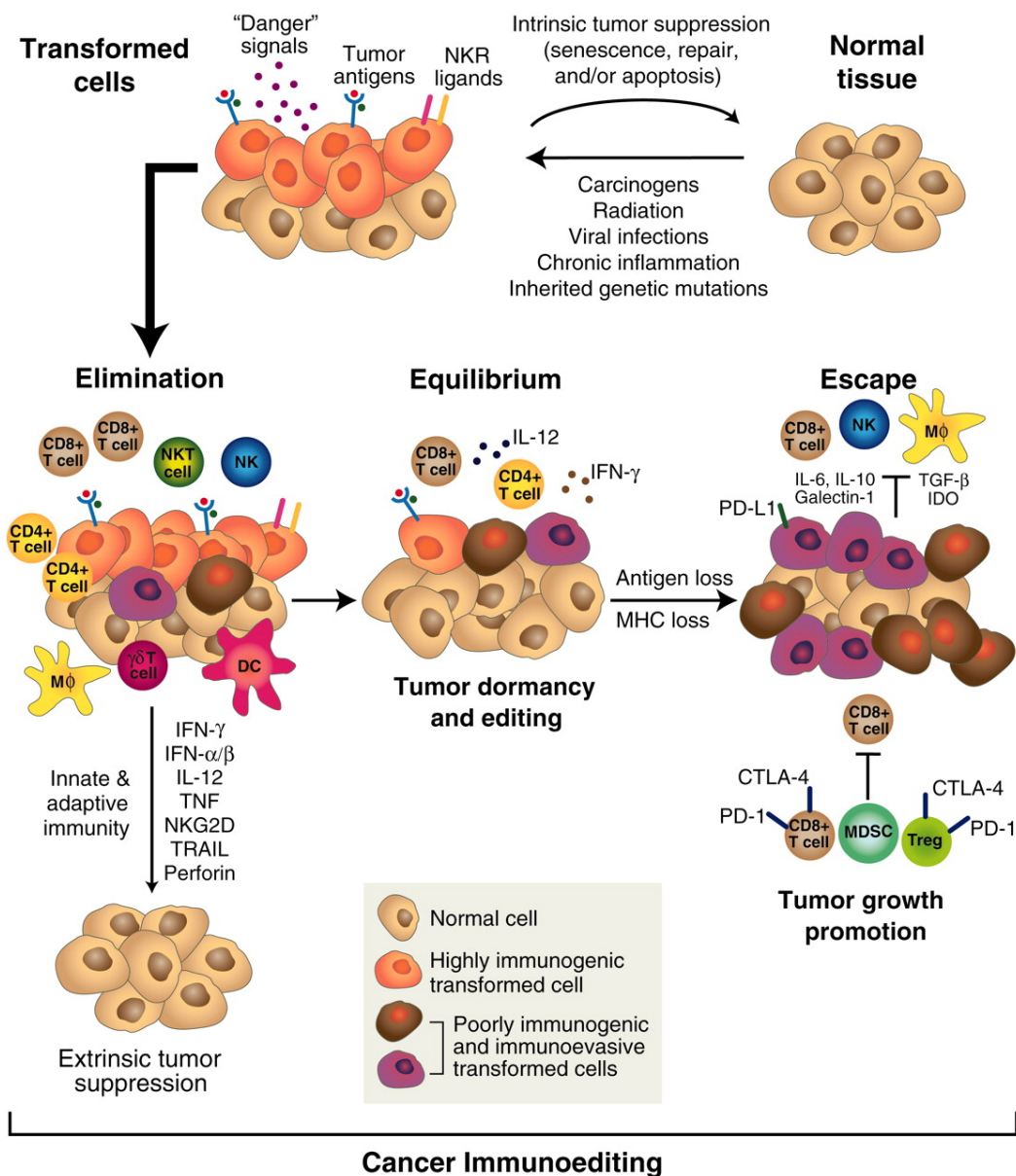
Figure 1. The cancer immunoediting (adopted from Robert D. Schreibe et al. [42])

Although much remains to be understood, it is now clear that many immunorelated factors play an important role in cancer. In fact, cancer cells manipulate the immune system not to attack the malignant cells, and that this "tolerance" is obtained by multiple mechanisms such as, for example, chemokines, immunosuppressive cytokines or the so-called Immune Checkpoint Receptors (ICRs). All the previous mentioned molecular mechanisms contribute to the local remodeling of the tumor microenvironment (TME) and in secondary organs predispose "premetastatic niches", where a fertile soil for immune escape and cancer growth is guaranteed.[31,44]

Very interesting and increasingly studied is the mechanism of ICRs. With this mechanism cancer cells are able to express the molecules of the immune checkpoint on their cell surface, such as those found on normal cells, and therefore are able to suppress T cells and avoid attack by the immune system.[30,45,46]

This is just one of many mechanisms used by cancer cells. Often more mechanisms are activated simultaneously. The ability to evade the immune attack is considered one of the distinctive signs of tumor genesis. For this reason, therapeutic intervention, which increases the ability of the immune system to attack the tumor and to circumvent immunosuppressive mediators, can be of importance in the treatment of cancer.[30,45,46]

For cancer immunotherapy to be successful, a number of steps must occur successfully, as recently described by Chen et Al in Oncology Meets Immunology: The Cancer-Immunity Cycle.[45]

Figure 2 shows the various steps of this cycle and what are the different factors influencing an anticancer response.
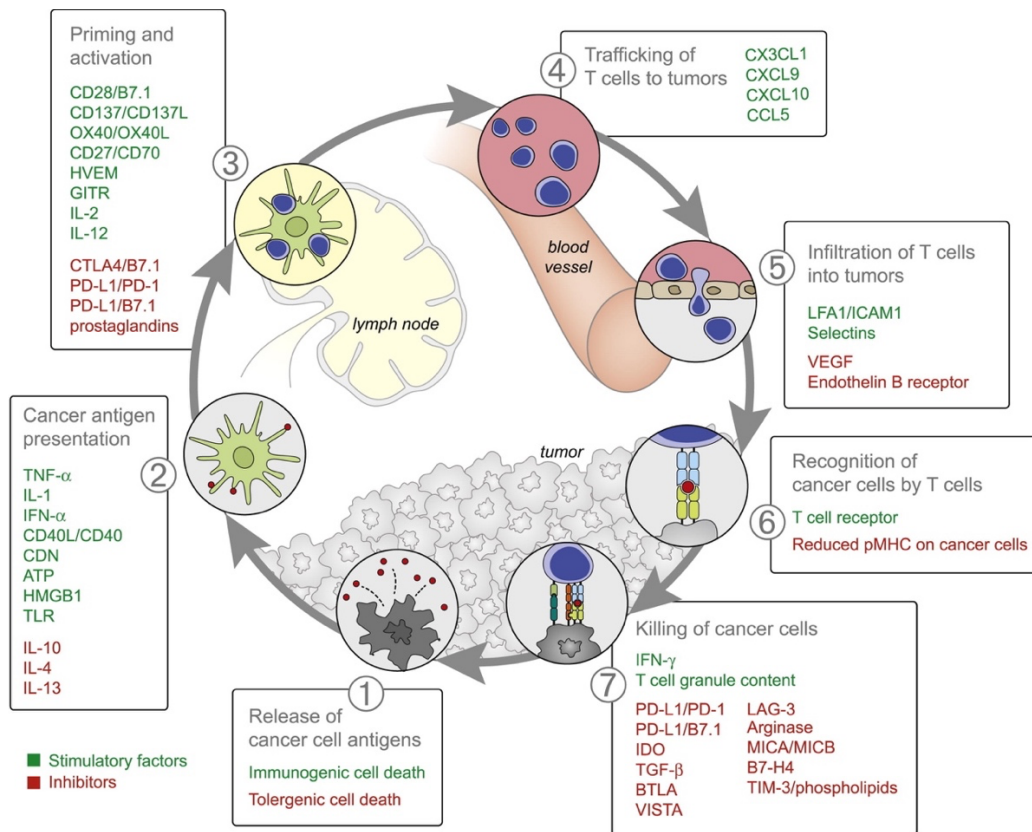

Figure 2. The Cancer-Immunity Cycle and Stimulatory and Inhibitory Factors (adopted from Daniel S. Chen et al. [45])

In the first step, tumor antigens created during oncogenesis are released and captured by dendritic cells (DCs). Subsequently, dendritic cells process the tumor antigen and present it on their surface. At this point the lymphocytes are activated and move towards the tumor bed and infiltrate. Finally, T cells are able to recognize cancer cells, thanks to the interaction between their antigens and those of cancer cells, leading to their death.

Various methods of immunotherapy have been developed from this knowledge. Indeed, National cancer institute defines immunotherapy as "A type of therapy that uses substances to stimulate or suppress the immune system to help the body fight cancer, infection, and other diseases. Some types of immunotherapies only target certain cells of the immune system. Others affect the immune system in a general way. Types of immunotherapies include cytokines, vaccines, bacillus Calmette-Guerin (BCG), and some monoclonal antibodies."

The goal of immunotherapy is to exploit the immune system to eliminate cancer cells by avoiding uncontrolled inflammatory autoimmune responses. [30]

Anticancer immunotherapy is generally divided into two different family: active and passive immunotherapy. [32,46,47]

- Active immunotherapy stimulates the immune response of patients and includes DNA vaccines, Peptide vaccines, Immunostimulatory cytokines, Oncolytic viruses and Dendritic cell-based vaccines. [32,46,47]

- Passive immunotherapy, on the other hand, involves the administration of active immune components for direct anticancer effects and includes Immunization using antibodies, adoptive transfer of in vitro activated cells, e.g. T cells or NK cells, Inhibition of immunosuppression and (low-dose) chemotherapy . [32,46,47]

The research efforts, undertaken until now to reawaken the immune system against tumors, brought to the market several immuno-oncology therapeutics.

Currently the main ones are the following four:

- immune stimulation eg. Stimulation of STING Protein [32,46–48]
- adoptive T cell transfers [32,46,47,49]
- vaccination strategies such as Sipuleucel-T or gp100 vaccine in combination with IL-2 [32,46,47,50]
- checkpoint blockade inhibitors such as Ipilimumab (anti-CTLA4 monoclonal antibody) and the PD-1/PD-1 inhibitors [32,46,47,51]

1.4. Checkpoint Blockade Inhibitors Against Cancer

Today, we can assert that the field of anti-cancer immune therapy has joined surgery, radiation, and chemotherapy, as the fourth pillar of cancer therapy because recently, many innovative strategies to overcome tumor-induced immunosuppression have been emerged. However, the immuno-oncology therapeutics on the market are mostly biologic products (e.g. monoclonal antibodies (mAbs), proteins, engineered cells, and oncolytic viruses). Antibodies (Abs) as immune checkpoint agents have emerged and are on the market for the treatment of melanoma, lung cancer, kidney cancer, and many other tumor types. The ipilimumab (Ab against CTLA-4) was approved in 2011, while the two Ab against PD-1 (pembrolizumab and nivolumab) were approved in 2014. Surely, these drugs represent a radical and disruptive change in cancer therapy as they do not target the tumor cell, but the soldiers of the immune system (T cells), removing their inhibitory brakes. However, these breakthrough medicines are all monoclonal antibodies that have well-known drawbacks as therapeutics: high production costs, lack of oral bioavailability, poor tumor penetrating capacity, Fc-related toxicities, and immunogenic properties. In this perspective, small molecules could potentially overcome many of these issues, can offer several unique advantages and are complementary to, and potentially synergistic with, biologic therapeutics too. [30,32,45–47,52,53]

1.5. The STING Receptor

The STING protein plays an important role in the innate immune pathway because is essential for controlling the transcription of numerous host defense genes type I interferons (IFNs-I) and pro-inflammatory cytokines, and also for the recognition of cyclic dinucleotides (CDNs) or mutant DNA species in the cytosol of the cell, so as to be identified as a potent target of anticancer therapies.[54–58] Within this system STING is a key sensor and the one of the most important mediators of the signaling triggered by cytosolic nucleic acid derived from DNA pathogens (viruses and bacteria) or self-DNA in the cytosol. [54,58] These cytosolic nucleic acids are powerful PAMPs (pathogen-associated molecular patterns)/ DAMPs (danger-associated molecular patterns) for which host organism possesses like STING a sensors and downstream adaptors to induce innate immune responses.[54,57,59]

STING, unlike other nucleic acid sensors, does not directly bind DNA and instead recognizes cyclic dinucleotides (CDNs) of either exogenous (e.g., bacterial) or endogenous origin. [60] It is a central player in the innate immune response to nucleic acids,[61] particularly CDNs, because stimulates the transcription of numerous innate immune genes in response to various invading DNA pathogens or transfected DNA, indeed STING promotes immunity to DNA viruses and retro-viruses, suppresses replication of RNA viruses and activation of innate immune genes to prevent dangerous bacterial infection.[55] The CDNs bind STING in its C-terminal domain and activate it; furthermore, the presence of the cytosolic exogenous DNA and also endogenous damaged DNA in cytoplasm of mammalian cells is a danger signal that generates the production of second messenger cGAMP by the DNA sensor protein cyclic GMP-AMP synthase (cGAS) and induce a STING-dependent type I IFN response.[62–66]

STING activation induces its dimerization and translocation from ER to the Golgi by mechanism similar to autophagy, and then initiates the downstream TBK1-IRF3 cascade to induce type I interferons. [65–70] Within this system at first the association between STING-TBK1 leads to autophosphorylation of TBK1, its activation, and then STING phosphorylation by TBK1. [65,66,69–71]

STING phosphorylation is important for the recruitment of IRF3 in proximity to TBK1, and then to phosphorylate and activate IRF3. Activated IRF3 translocated into the nucleus and promotes expression of type I interferons. [65,66,69,72]

STING have also been shown to activate NF-κB pathway through phosphorylation of TKB1 and then its interaction and phosphorylation of IKK (IkB kinase). STING-TBK1-IKK axis, regulates the activation loop of IKKα/β releasing p65 to form active dimers with p50. Then the NF-kB complex translocated into the nucleus and promotes expression of type I interferons like the STING-TBK1-IRF3 axis. [65,66,69,70,73]

STING activation induces type I IFN (IFN-I) production and increased expression of IFN-stimulated genes (ISG). [74] The two major IFN-I, are IFN-α and β, are important for protecting the cell against for viral and bacterial infections and many tumor, indeed STING agonists have been used against the development of cancer by promoting antitumor immune responses.[55] Particularly the major STING antitumor effects depend by production of IFN-b production by antigen-presenting cells (APCs) that promotes CD8$^+$ T cell priming against tumor-associated antigens. [66] Specifically, dendritic cells (DCs) absorb dying cancer cells and the tumor DNA activates STING pathway to induce the expression of interferons. Interferons stimulate the maturation of DCs and facilitates presentation of tumor associated antigens on MHCI. Finally, DCs migrates to lymph nodes and activates CD8+ T cells, which seek and attack tumors in target tissues. [70] Based on these finding and cancer control via host immune cell activation, the antitumor therapy is based on activation of the STING pathway. Indeed, the latter strategy surely represent a new, and stimulating frontier of research in the anticancer field. Moreover, recent studies have demonstrated that combination of STING agonists with PD-1/PD-L1 antibodies or inhibitors further boost antitumor immunity and to enforce control of tumor growth. [55,75]

1.6. References

(1)   Bray, F.; Ferlay, J.; Soerjomataram, I.; Siegel, R. L.; Torre, L. A.; Jemal, A. Global Cancer Statistics 2018: GLOBOCAN Estimates of Incidence and Mortality Worldwide for 36 Cancers in 185 Countries. *CA. Cancer J. Clin.* **2018**, *68* (6), 394–424.

(2)   Haberkorn, U. What Is Cancer? *Adv. Nucl. Oncol.* **2007**, *62* (4), 1–16.

(3)   Hussain, S. P.; Harris, C. C. Molecular Epidemiology of Human Cancer: Contribution of Mutation Spectra Studies of Tumor Suppressor Genes. *Cancer Res.* **1998**, *58* (18), 4023–4037.

(4)   Hanahan, D.; Weinberg, R. A. Hallmarks of Cancer: The next Generation. *Cell* **2011**, *144* (5), 646–674.

(5)   Blagih, J.; Buck, M. D.; Vousden, K. H. P53, Cancer and the Immune Response. *J. Cell Sci.* **2020**, *133* (5), 1–13.

(6)   Ozaki, T.; Nakagawara, A. Role of P53 in Cell Death and Human Cancers. *Cancers (Basel).* **2011**, *3* (1), 994–1013.

(7)   Bertucci, F.; Finetti, P.; Birnbaum, D. Basal Breast Cancer: A Complex and Deadly Molecular Subtype. *Curr. Mol. Med.* **2011**, *12* (1), 96–110.

(8)   Nelson, D. A.; Tan, T. T.; Rabson, A. B.; Anderson, D.; Degenhardt, K.; White, E. Hypoxia and Defective Apoptosis Drive Genomic Instability and Tumorigenesis. *Genes Dev.* **2004**, *18* (17), 2095–2107.

(9)   Downward, J. Targeting RAS Signalling Pathways in Cancer Therapy. *Nat. Rev. Cancer* **2003**, *3* (1), 11–22.

(10)   Friedenson, B. The BRCA1/2 Pathway Prevents Hematologic Cancers in Addition to Breast and Ovarian Cancers. *BMC Cancer* **2007**, *7*, 1–11.

(11)   Baker, S. J.; Markowitz, S.; Fearon, E. R.; Willson, J. K. V; Baker, S. J.; Markowitz, S.; Fearon, E. R.; Willson, J. K. V; Vogelstein, B. Suppression of Human Colorectal Carcinoma Cell Growth by Wild-Type P53 Bert Vogelstein Published by : American Association for the Advancement of Science Stable URL : Http://Www.Jstor.Org/Stable/2877961 Digitize , Preserve and Extend Access to Science Sup. *Science (80-.).* **2018**, *249* (4971), 912–915.

(12)   Devilee, P.; Cornelisse, C. J. Somatic Genetic Change in Human Breast Cancer. *Biochim. Biophys. Acta* **1994**, *1198*, 113–130.

(13)   Van De Vijver, M. J. Genetic Alterations in Breast Cancer. *Curr. Diagnostic Pathol.* **2000**, *6* (4), 271–281.

(14)   Gotwals, P.; Cameron, S.; Cipolletta, D.; Cremasco, V.; Crystal, A.; Hewes, B.; Mueller, B.; Quaratino, S.; Sabatos-Peyton, C.; Petruzzelli, L.; Engelman, J. A.; Dranoff, G. Prospects for Combining Targeted and Conventional Cancer Therapy with Immunotherapy. *Nat. Rev. Cancer* **2017**, *17* (5), 286–301.

(15)   Wang, W.; Qin, J. J.; Rajaei, M.; Li, X.; Yu, X.; Hunt, C.; Zhang, R. Targeting MDM2 for Novel Molecular Therapy: Beyond Oncology. *Med. Res. Rev.* **2020**, *40* (3), 856–880.

(16)   Wang, J. J.; Lei, K. F.; Han, F. Tumor Microenvironment: Recent Advances in Various Cancer Treatments. *Eur. Rev. Med. Pharmacol. Sci.* **2018**, *22* (12), 3855–3864.

(17)   Lheureux, S.; Denoyelle, C.; Ohashi, P. S.; De Bono, J. S.; Mottaghy, F. M. Molecularly Targeted Therapies in Cancer: A Guide for the Nuclear Medicine Physician. *Eur. J. Nucl. Med. Mol. Imaging* **2017**, *44*, 41–54.

(18)   Lai, Z.; Auger, K. R.; Manubay, C. M.; Copeland, R. A. Thermodynamics of P53 Binding to Hdm2(1-126): Effects of Phosphorylation and P53 Peptide Length. *Arch. Biochem. Biophys.* **2000**, *381* (2), 278–284.

(19)   Chen, L.; Yin, H.; Farooqi, B.; Sebti, S.; Hamilton, A. D.; Chen, J. Interaction and Activate P53. *Interactions* **2005**, *4* (June), 1019–1025.

(20)   Vassilev, L. T. P53 Activation by Small Molecules: Application in Oncology. *J. Med. Chem.* **2005**, *48* (14), 4491–4499.

(21)   Chen, L.; Yin, H.; Farooqi, B.; Sebti, S.; Hamilton, A. D.; Chen, J. P53 A-Helix Mimetics Antagonize P53/MDM2 Interaction and Activate P53. *Interactions* **2005**, *4* (June), 1019–1025.

(22)   Wang, S.; Zhao, Y.; Aguilar, A.; Bernard, D.; Yang, C. Y. Targeting the MDM2-P53 Protein-Protein Interaction for New Cancer Therapy: Progress and Challenges. *Cold Spring Harb. Perspect. Med.* **2017**, *7* (5), 1–10.

(23)   Vassilev, L. T.; Vu, B. T.; Graves, B.; Carvajal, D.; Filipovic, Z.; Kong, N.; Kammlott, U.; Lukacs, C.; Fotouhi, N.; Liu, E. A. In Vivo Activation of the P53 Pathway by Small-Molecule Antagonists of MDM2. *Science (80-.).* **1881**, *os-2* (57), 341–342.

(24)   Hou, H.; Sun, D.; Zhang, X. The Role of MDM2 Amplification and Overexpression in Therapeutic Resistance of Malignant Tumors. *Cancer Cell Int.* **2019**, *19* (1), 1–8.

(25)   Giustiniano, M.; Daniele, S.; Pelliccia, S.; La Pietra, V.; Pietrobono, D.; Brancaccio, D.; Cosconati, S.; Messere, A.; Giuntini, S.; Cerofolini, L.; Fragai, M.; Luchinat, C.; Taliani, S.; La Regina, G.; Da Settimo, F.; Silvestri, R.; Martini, C.;

Novellino, E.; Marinelli, L. Computer-Aided Identification and Lead Optimization of Dual Murine Double Minute 2 and 4 Binders: Structure-Activity Relationship Studies and Pharmacological Activity. *J. Med. Chem.* **2017**, *60* (19), 8115–8130.

(26)   Brancaccio, D.; Di Maro, S.; Cerofolini, L.; Giuntini, S.; Fragai, M.; Luchinat, C.; Tomassi, S.; Limatola, A.; Russomanno, P.; Merlino, F.; Novellino, E.; Carotenuto, A. HOPPI-NMR: Hot-Peptide-Based Creening Assay for Inhibitors of Protein-Protein Interactions by NMR. *ACS Med. Chem. Lett.* **2020**, *11* (5), 1047–1053.

(27)   Schon, O.; Friedler, A.; Bycroft, M.; Freund, S. M. V.; Fersht, A. R. Molecular Mechanism of the Interaction between MDM2 and P53. *J. Mol. Biol.* **2002**, *323* (3), 491–501.

(28)   Hou, H.; Sun, D.; Zhang, X. The Role of MDM2 Amplification and Overexpression in Therapeutic Resistance of Malignant Tumors. *Cancer Cell Int.* **2019**, *19* (1), 1–16.

(29)   Wienken, M.; Moll, U. M.; Dobbelstein, M. Mdm2 as a Chromatin Modifier. *J. Mol. Cell Biol.* **2017**, *9* (1), 74–80.

(30)   Abbott, M.; Ustoyev, Y. Cancer and the Immune System: The History and Background of Immunotherapy. *Semin. Oncol. Nurs.* **2019**, *35* (5), 150923.

(31)   Balkwill, F.; Mantovani, A. Inflammation and Cancer: Back to Virchow? *Lancet* **2001**, *357* (9255), 539–545.

(32)   Galon, J.; Angell, H. K.; Bedognetti, D.; Marincola, F. M. The Continuum of Cancer Immunosurveillance: Prognostic, Predictive, and Mechanistic Signatures. *Immunity* **2013**, *39* (1), 11–26.

(33)   Cooley, W. B. The Treatment of Malignant Tumors by Inoculations of Erysipelas. *J. Am. Med. Assoc.* **1893**, *105* (22), 487–511.

(34)   Burnet, F. M. The Concept of Immunological Surveillance. *Prog. Exp. Tumor Res* **1970**, *13*, 1–27.

(35)   Thomas, L. On Immunosurveillance in Human Cancer. *Yale J. Biol. Med.* **1982**, *55* (3–4), 329–333.

(36)   Muenst, S.; Läubli, H.; Soysal, S. D.; Zippelius, A.; Tzankov, A.; Hoeller, S. The Immune System and Cancer Evasion Strategies: Therapeutic Concepts. *J. Intern. Med.* **2016**, *279* (6), 541–562.

(37)   Van Der Bruggen, P.; Traversari, C.; Chomez, P.; Lurquin, C.; De Plaen, E.; Van Den Eynde, B.; Knuth, A.; Boon, T. A Gene Encoding an Antigen Recognized by Cytolytic T Lymphocytes on a Human Melanoma. *Science (80-.).* **1991**, *254* (5038),

1643–1647.

(38)   Shankaran, V.; Ikeda, H.; Bruce, A. T.; White, J. M.; Swanson, P. E.; Old, L. J.; Shreiber, R. D. IFNgamma and Lympohcytes Prevent Primary Tomour Development and Shape Tomour Immunogenicity. *Nature* **2001**, *410* (6832), 1107–1111.

(39)   Koebel, C. M.; Vermi, W.; Swann, J. B.; Zerafa, N.; Rodig, S. J.; Old, L. J.; Smyth, M. J.; Schreiber, R. D. Adaptive Immunity Maintains Occult Cancer in an Equilibrium State. *Nature* **2007**, *450* (7171), 903–907.

(40)   Galon, J.; Fridman, W. H.; Pages, F. The Adaptive Immunologic Microenvironment in Colorectal Cancer: A Novel Perspective. *Cancer Res.* **2007**, *67* (5), 1883–1886.

(41)   Wang, E.; Miller, L. D.; Ohnmacht, G. A.; Mocellin, S.; Perez-Diez, A.; Petersen, D.; Zhao, Y.; Simon, R.; Powell, J. I.; Asaki, E.; Alexander, H. R.; Duray, P. H.; Herlyn, M.; Restifo, N. P.; Liu, E. T.; Rosenberg, S. A.; Marincola, F. M. Prospective Molecular Profiling of Melanoma Metastases Suggests Classifiers of Immune Responsiveness. *Cancer Res.* **2002**, *62* (13), 3581–3586.

(42)   Schreiber, R. D.; Old, L. J.; Smyth, M. J. Cancer Immunoediting: Integrating Immunity's Roles in Cancer Suppression and Promotion. *Science (80-.).* **2011**, *331* (6024), 1565–1570.

(43)   Drew Pardoll. Cancer and the Immune System: Basic Concepts and Targets for Intervention Drew. *Semin Oncol.* **2015**, *42* (4), 523–538.

(44)   Qin, S.; Xu, L.; Yi, M.; Yu, S.; Wu, K.; Luo, S. Novel Immune Checkpoint Targets: Moving beyond PD-1 and CTLA-4. *Mol. Cancer* **2019**, *18* (1), 1–14.

(45)   Chen, D. S.; Mellman, I. Oncology Meets Immunology: The Cancer-Immunity Cycle. *Immunity* **2013**, *39* (1), 1–10.

(46)   Oiseth, S. J.; Aziz, M. S. Cancer Immunotherapy: A Brief Review of the History, Possibilities, and Challenges Ahead. *J. Cancer Metastasis Treat.* **2017**, *3* (10), 250.

(47)   Li, B.; Chan, H. L.; Chen, P. Immune Checkpoint Inhibitors: Basics and Challenges. *Curr. Med. Chem.* **2019**, *26* (17), 3009–3025.

(48)   Hollinshead, A. C.; Stewart, T. H. M. Specific and Nonspecific Immunotherapy as an Adjunct to Curative Surgery for Cancer of the Lung. *Yale J. Biol. Med.* **1981**, *54* (5), 367–379.

(49)   Rosenberg, S. A.; Restifo, N. P. Adoptive Cell Transfer as Personalized Immunotherapy for Human Cancer. *Science (80-.).* **2015**, *348* (6230), 62–68.

(50)   Guo, C.; Manjili, M. H.; Subjeck, J. R.; Sarkar, D.; Fisher, P. B.; Wang, X. Y.

Therapeutic Cancer Vaccines. Past, Present, and Future. *Adv. Cancer Res.* **2013**, *119* (804), 421–475.

(51)   Haanen, J. B. A. G.; Robert, C. Immune Checkpoint Inhibitors. *Prog. tumor Res.* **2015**, *42*, 55–66.

(52)   Scott McComb, Aude Thiriot, Bassel Akache, Lakshmi Krishnan, and F. S. Chapter 1. Introduction to the Immune Response. *Immunoproteomics Methods Protoc. Methods Mol. Biol.* **2014**, *2024*, 1–24.

(53)   Candeias, S. M.; Gaipl, U. S. The Immune System in Cancer Prevention, Development and Therapy. *Anticancer. Agents Med. Chem.* **2016**, *16* (1), 101–107.

(54)   Sokolowska, O.; Nowis, D. STING Signaling in Cancer Cells: Important or Not? *Arch. Immunol. Ther. Exp. (Warsz).* **2018**, *66* (2), 125–132.

(55)   Barber, G. N. STING: Infection, Inflammation and Cancer. *Nat. Rev. Immunol.* **2015**, *15* (12), 760–770.

(56)   Qi, L.; Kash, J. C.; Dugan, V. G.; Jagger, B. W.; Lau, Y.; Crouch, E. C.; Hartshorn, K. L.; Taubenberger, J. K. STING Ligand C-Di-GMP Improves Cancer Vaccination against Metastatic Breast Cancer. *Cancer Immunol Res* **2012**, *412* (2), 426–434.

(57)   Deng, L.; Liang, H.; Xu, M.; Yang, X.; Burnette, B.; Arina, A.; Li, X. D.; Mauceri, H.; Beckett, M.; Darga, T.; Huang, X.; Gajewski, T. F.; Chen, Z. J.; Fu, Y. X.; Weichselbaum, R. R. STING-Dependent Cytosolic DNA Sensing Promotes Radiation-Induced Type I Interferon-Dependent Antitumor Immunity in Immunogenic Tumors. *Immunity* **2014**, *41* (5), 843–852.

(58)   Weinmann, H. Cancer Immunotherapy: Selected Targets and Small-Molecule Modulators. *ChemMedChem* **2016**, *11* (5), 450–466.

(59)   Liu, X.; Wang, C. The Emerging Roles of the STING Adaptor Protein in Immunity and Diseases. *Immunology* **2016**, *147* (3), 285–291.

(60)   Paludan, S. R.; Bowie, A. G. Immune Sensing of DNA. *Immunity* **2013**, *38* (5), 870–880.

(61)   Burdette, D. L.; Vance, R. E. STING and the Innate Immune Response to Nucleic Acids in the Cytosol. *Nat. Immunol.* **2013**, *14* (1), 19–26.

(62)   Hopfner, K. P.; Hornung, V. Molecular Mechanisms and Cellular Functions of CGAS–STING Signalling. *Nat. Rev. Mol. Cell Biol.* **2020**, *21* (9), 501–521.

(63)   Yu, L.; Liu, P. Cytosolic DNA Sensing by CGAS : Regulation , Function , and Human Diseases. *Signal Transduct. Target. Ther.* **2021**, *6* (170), 1–15.

(64)   Cai, X.; Chiu, Y. H.; Chen, Z. J. The CGAS-CGAMP-STING Pathway of Cytosolic DNA Sensing and Signaling. *Mol. Cell* **2014**, *54* (2), 289–296.

(65)   Balka, K. R.; De Nardo, D. Molecular and Spatial Mechanisms Governing STING Signalling. *FEBS J.* **2020**.

(66)   Zhu, Y.; An, X.; Zhang, X.; Qiao, Y.; Zheng, T.; Li, X. STING: A Master Regulator in the Cancer-Immunity Cycle. *Mol. Cancer* **2019**, *18* (1), 1–15.

(67)   Decout, A.; Katz, J. D.; Venkatraman, S.; Ablasser, A. The CGAS–STING Pathway as a Therapeutic Target in Inflammatory Diseases. *Nat. Rev. Immunol.* **2021**.

(68)   Nicole Dobbs, Nikolay Burnaevskiy, Didi Chen, Vijaya K Gonugunta, N. M. A. and N. Y. STING Activation by Translocation from the ER Is Associated with Infection and Autoinflammatory Disease. *Cell Host Microbe* **2015**, *18* (2), 157–168.

(69)   Yum, S.; Li, M.; Fang, Y.; Chen, Z. J. TBK1 Recruitment to STING Activates Both IRF3 and NF-KB That Mediate Immune Defense against Tumors and Viral Infections. *PNAS* **2021**, *118* (14), 1–9.

(70)   Chen, Q.; Sun, L.; Chen, Z. J. Regulation and Function of the CGAS-STING Pathway of Cytosolic DNA Sensing. *Nat. Immunol.* **2016**, *17* (10), 1142–1149.

(71)   Conggang Zhang, Guijun Shang, Xiang Gui, Xuewu Zhang, Xiao-chen Bai, Z. J. C. Structural Basis of STING Binding with and Phosphorylation by TBK1. *Nature* **2019**, *567* (7748), 394–398.

(72)   Tanaka, Y.; Chen, Z. J. STING Specifies IRF3 Phosphorylation by TBK1 in the Cytosolic DNA Signaling Pathway. *Sci. Signal.* **2012**, *5* (214), 1–12.

(73)   Abe, T.; Barber, G. N. Cytosolic-DNA-Mediated, STING-Dependent Proinflammatory Gene Induction Necessitates Canonical NF- B Activation through TBK1. *J. Virol.* **2014**, *88* (10), 5328–5341.

(74)   Bridget Larkin, Vladimir Ilyukha, Maxim Sorokin, Anton Buzdin, Edouard Vannier, and A. P. Activation of STING in T Cells Induces Type I IFN Responses and Cell Death Bridget. *J Immunol.* **2017**, *199* (2), 397–402.

(75)   Khoo, L. T.; Chen, L. Role of the CGAS–STING Pathway in Cancer Development and Oncotherapeutic Approaches. *EMBO Rep.* **2018**, *19* (12).

Chapter 2
Aims of the Work

This PhD thesis was focused on discover and development of small molecules targeting the 3 receptors as already described in the Introduction: hMDM2 protein (Mouse Double Minute 2), PD-1/PDL-1 axis (Programmed cell Death protein-1/ Programmed Death-ligand 1), and on STING protein (STimulator of INterferon Genes).

Specifically, as regards the targeting of hMDM2, the main aim was to discover and develop novel selective and potent inhibitors. In a previous work done by the research group in which I work, a Virtual Screening was carried out on the crystal structures of MDM2 (PDB 3LBL) by using our in-house database, and a 2-phenylindole molecule (RS3760) was found to be capable of disrupting the MDM2/p53 interaction with an IC50 of 270 nM. I use this compound as a precious starting point for a ligand-based lead optimization. My aim was also to study the interaction with the protein and its exact binding mode. To do so, a combined approach of modeling/NMR was used.

As regards the PD-1/PDL-1 axis, I was involved in a project having as aim the switching from monoclonal antibody (mAbs) to small molecule able to disrupt the interaction among the two above-mentioned proteins. In our program of ligands finding, design and NMR study of a series of compounds were accomplished. The ultimate aim was the design of a second round of lead optimization guided by docking results.

At the end, I dealt with STING receptor, for which an extensive computational work was performed starting from the available X-ray hSTING co-crystal structures with its physiological agonist. Computational methods such as receptor-based VS, Core Hopping and De Novo design were applied go generate/finding structurally new ligands. All the found molecules were assayed through an NMR-based screening protocol.

For all three proteins, I've been focused also on expression, purification, biochemical and structural characterization. The proteins were recombinantly expressed in *E.coli*, purified and preliminary characterized through NMR, UV-vis spectroscopy and size exclusion chromatography.

Chapter 3
Targeting MDM2 through a combined approach of Modeling/NMR

3.1. Brief Introduction

Tumor suppressor p53 protects organisms from DNA damage and cancer. It is one of defenses against kind of damage such as abnormal and uncontrolled proliferation of cells and growth suppressors evasion and is one of the most studied regulators of cell when the integrity of the genome is damaged.

p53 tumor suppressor is normally present in minimal amounts, but when DNA damage is detected, its levels increase, and defense mechanisms begin. [1,2]

The p53 binds to regulatory sites in genome and starts the production of proteins that stop cell division until the damage is repaired. On the other hand, if the damage is too serious, p53 begins the process of programmed cell death, or apoptosis. The p53 action must be carefully controlled. [3–6]

This is the task of MDM2 (mouse double minute 2, an oncoprotein discovered the first time in the mouse) that supervises the p53 so that it comes into action only when it is absolutely necessary. Normally MDM2 remains attached to p53 and performs several sequential actions first in the nucleus and then in the cytoplasm. In the nucleus, a MDM2 domain binds to the p53 transactivation domain, blocking its DNA transcription activation action. Then, another MDM2 domain binds an export signal from the nucleus, which is used to drag the p53 out of the nucleus.[5,7–9]

Finally, in the cytoplasm MDM2 bind ubiquitin and add it to the p53 marking for destruction in proteasomes. Normally the cell synthesizes enough MDM2 to control the p53. However, when there is damage or infection, MDM2 is deactivated to allow p53 to activate. Most cancer cells have developed methods to overcome this process. In some cases, the p53 is altered and so the cell no longer has tools to protect itself. In other cases, cancer cells synthesize more MDM2. This high amount of MDM2 blocks p53 and allows cancer cells to grow without control.[8,10–15]

In this scenario are possible three different anticancer therapies:

1. targeting of mutated p53 that restore p53 wt function
2. gene therapy
3. inhibition of MDM2

During the three years of my PhD course, I focused on discover and development of small molecules targeting to inhibition of MDM2.

MDM2 is a protein of 491 amino acids composed of several connected domains, each with a specific function.

N-terminal of MDM2 is the domain that specifically binds p53 transactivation domain, blocking its action. At the center there is a domain of MDM2 that contains a finger of zinc and bind the ribosomal protein L11. The C-terminal end of MDM2 is the domain called ring, which contains two zinc fingers. Together with MDMX bind ubiquitin and its carrier Ubch5b and then transfer the ubiquitin to p53.[16]

```
000    MCNTNMSVPTDGAVTTSQIPASEQETLVRPKPLLLKLLKSVGAQKDTYTM
050    KEVLFYLGQYIMTKRLYDEKQQHIVYCSNDLLGDLFGVPSFSVKEHRKIY
100    TMIYRNLVVVNQQESSDSGTSVSENRCHLEGGSDQKDLVQELQEEKPSSS
150    HLVSRPSTSSRRRAISETEENSDELSGERQRKRHKSDSISLSFDESLALC
200    VIREICCERSSSSESTGTPSNPDLDAGVSEHSGDWLDQDSVSDQFSVEFE
250    VESLDSEDYSLSEEGQELSDEDDEVYQVTVYQAGESDTDSFEEDPEISLA
300    DYWKCTSCNEMNPPLPSHCNRCWALRENWLPEDKGKDKGEISEKAKLENS
350    TQAEEGFDVPDCKKTIVNDSRESCVEENDDKITQASQSQESEDYSQPSTS
400    SSIIYSSQEDVKEFEREETQDKEESVESSLPLNAIEPCVICQGRPKNGCI
491    VHGKTGHLMACFTCAKKLKKRNKPCPVCRQPIQMIVLTYFP
```

Figure 1. Amino acid sequence of hMDM2

More MDM2 X-ray crystallographic structural complexes linked to p53, p53-mimicking peptide or non-peptide molecules are available. Crystallographic studies demonstrated that N-terminal region of p53 protein interacts with MDM2, forming an amphipathic α-helix, with the binding key residues L54, L57, I61, M62, Y67, Q72, V75, F86, F91, V93, H96, I99, Y100, and I103 of MDM2. [16] [10,11,17]
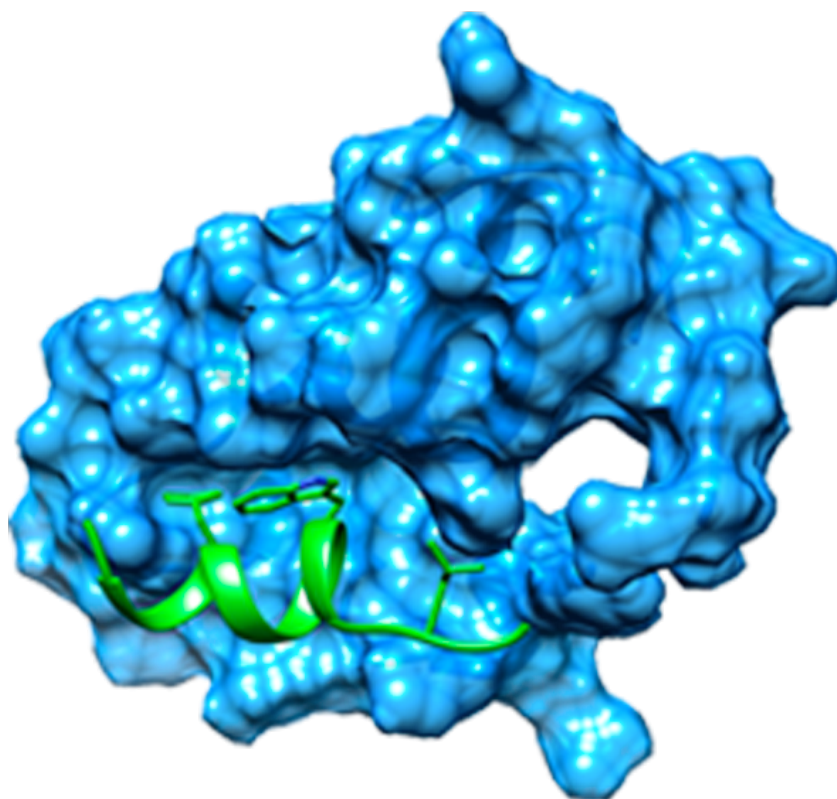
Figure 2. Crystal structure of hMDM2 N-term and p53-mimicking peptide

A lot of MDM2 antagonists have been described in patent and scientific literature and they are divided in three classes of small molecule inhibitors. These compounds are able to disrupt MDM2-p53 binding with high (nM) affinity and specificity.

The first and best-documented compound is Nutlin-3 discovered during a HTS. The second class of potent and selective inhibitors are spiro-oxindoles derivates. The compound MI-219 and MI-63 of this class, bind MDM2 better than the p53 wt peptide. The third group of MDM2-p53 inhibitors present a benzodiazepine dione core. [16]
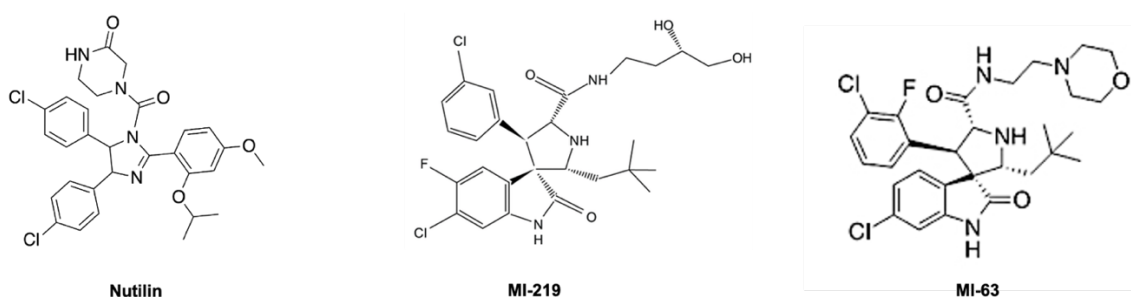
Figure 3. MDM2 inhibitor compounds

3.2. Results and Discussion

The first part of my PhD project was aimed to discover and develop new inhibitors for MDM2/p53 interaction through computational methods. In particular, I was involved in of sMDM2 inhibitors ligand-based lead optimization, starting from literature studies.

In a previous work [10] done by the research group in which I work, a Virtual Screening was carried out on the crystal structures of MDM2 (PDB 3LBL)[16,18] by using our in-house database. One of the molecules selected, a 2-phenylindole molecule (RS3760), was found to be capable of disrupting the MDM2/p53 interaction with an IC50 of 270 nM.

In this scenario, the discovery of RS3760 has represented a precious starting point for ligand-based optimization. In collaboration with the research groups of Simona Daniele of University of Pisa and Romano Silvestri of University of Roma, we select a number of compounds derivates of RS3760 (compound 4-9 in figure. 4) and also, longer molecules endowed with a sulfonyl-phenyl branch (compound 10-13 in figure. 4). These compounds are displayed in the Figure 4 below.
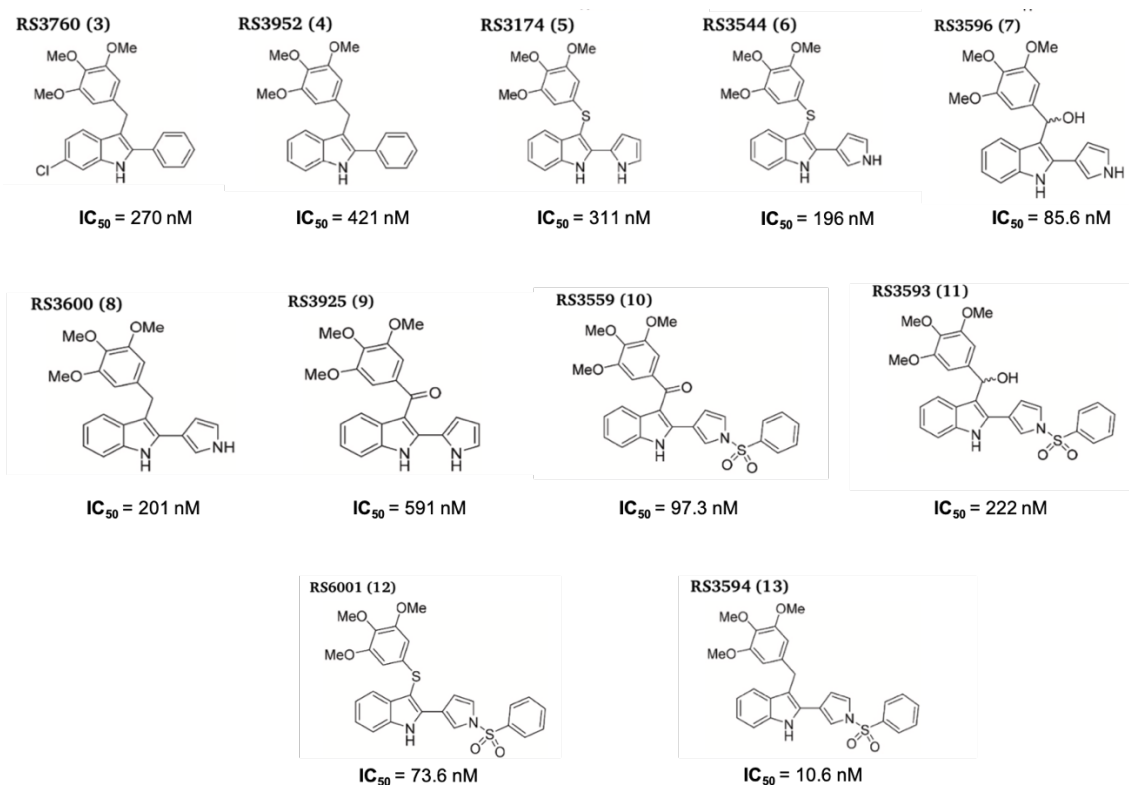

Figure 4 Compounds derivates of RS3760

In order to elucidate at an atomistic level, the binding mode of our compounds at MDM2 receptor, molecular docking studies were performed. As shown in figure 5 the MDMs binding subpockets are depicted as blue (Phe19), red (Trp23), yellow (Leu26), and green (N-terminus) dots, in accordance with the p53 interacting side chains. All compounds (4-13) occupy the MDM2 subpockets. In addiction an extensive occupancy of the binding site, including the Leu26 subpocket and/or the N-terminus region, is important to reach a high affinity toward the MDM2 protein.[19]
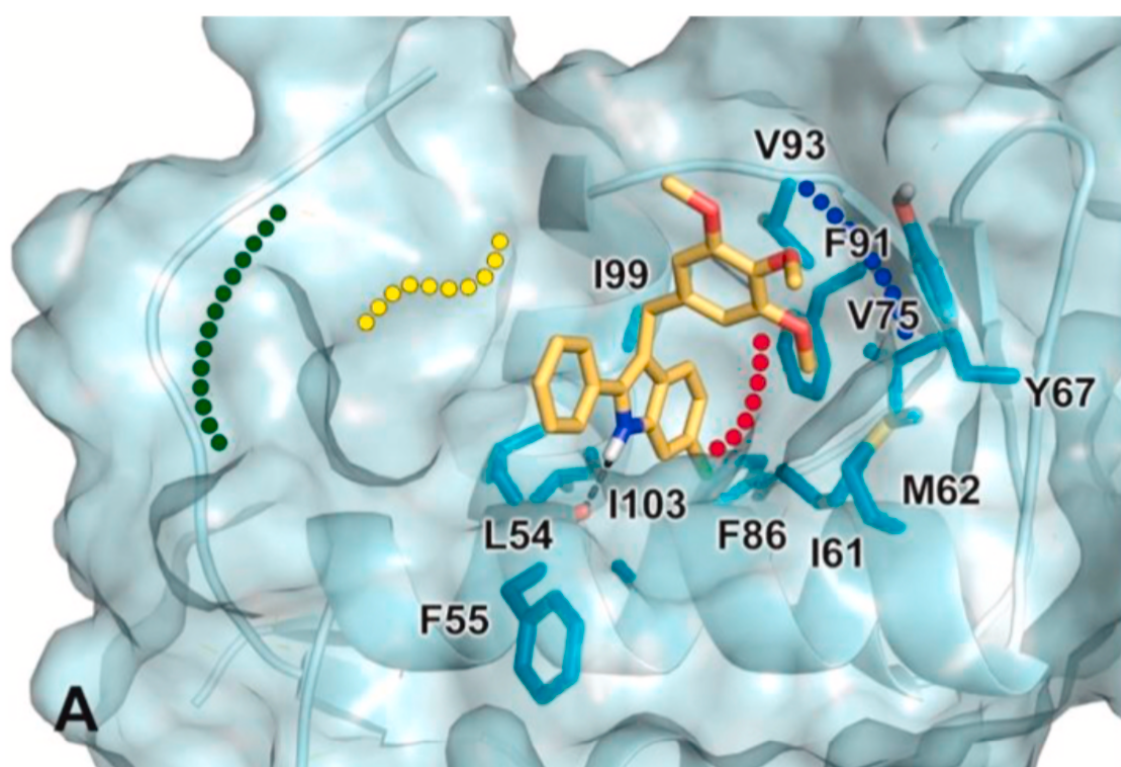
Figure 5. Docking poses of compound 3 (RS3760) in MDM2 (A) binding cavity (adopted from Simona Daniele et al. [17])

These compounds were synthesized, qualitatively tested by 1D 1H-NMR, and then quantitatively selected for binding assays. One of them, RS3594 molecules endowed with a sulfonyl-phenyl branch, was identified as the most potent compound.

The ability of compounds 3–13 to inhibit interaction between p53 from MDM2 was analysed with an immunoenzymatic assay. One of them, RS3594 compound, was identified as the most potent early lead and through NMR was shown to specifically bind MDM2.

In order to elucidate at an atomistic level, the binding mode of 13 (RS3594) at the MDM2 receptor, molecular docking studies were performed. As for the protein tridimensional structure selection, the X-ray complex of MDM2 (PDB code: 3LBL)[16] was chosen. Docking of RS3594 predicted that the indole scaffold plunges into the Trp23 pockets (interacting residues in MDM2: L54, F86, F91, I99, I103) H-bonding the L54 and the M50 backbone respectively, while the trimethoxy-phenyl ring occupies the Phe19 sites (interacting residues in MDM2: I61, M62, Y67, V75, V93). the pyrrole ring in position 2 is oriented toward the Phe55 residue, and the sulfonyl-phenyl moiety stretches along the α2 helix and, thanks to the considerable bending, almost reaches the internal cavity of the N-terminus region where hydrophobic contacts are established with the Q24 side chain and the K41 carbon atoms. Also, a slight movement of the flexible K41 side chain could allow the formation of a cation-pi interaction. This theoretical binding mode is in accordance with the NMR data shown later on and justify the low nanomolar IC_{50}.
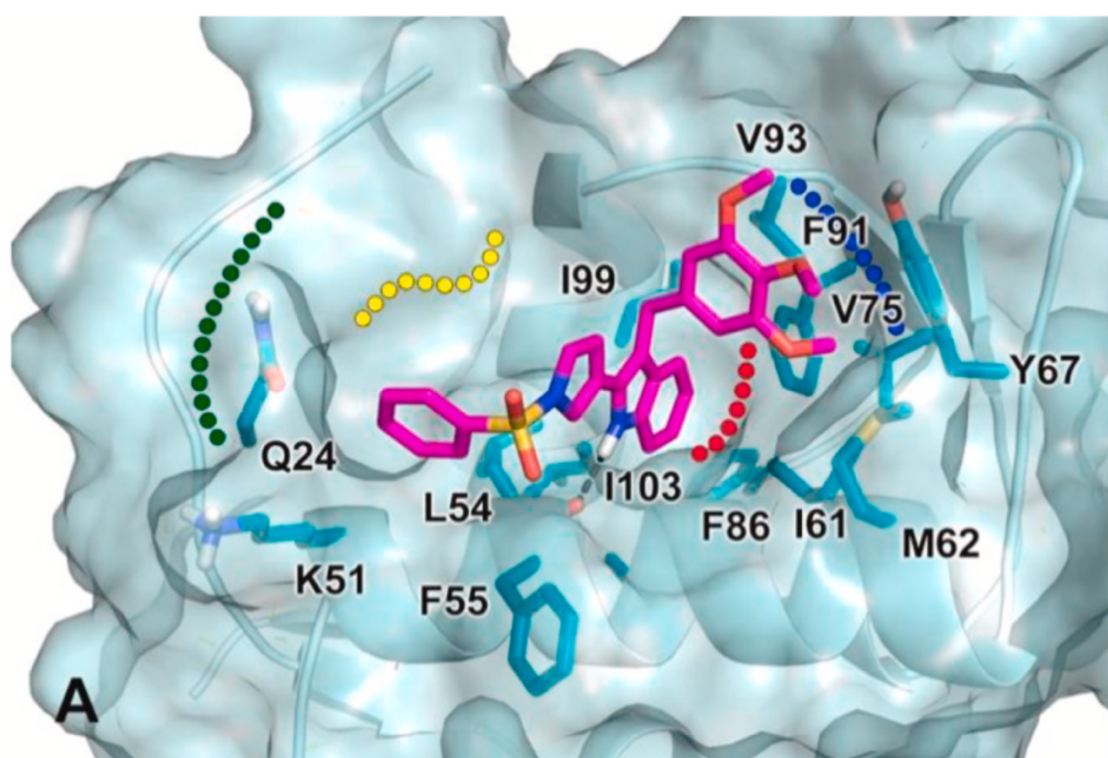

Figure 6. Docking poses of RS3594 in MDM2 (A) binding cavity (Adopted from Simona Daniele et al. [17])

In addiction the docking poses prediction of compounds 4-12 are in line with the experimental IC50s listed in figure 4. In fact, looking at the activity of compounds 10, 12, and RS3594, as predicted, it is evident that a broader aromatic moiety allows a better occupancy of the binding clefts in MDM2 and confers lower IC_{50} values with respect to

their smaller precursors 5, 6, 8 and 9. Moreover, it appears that the flexibility of the linker connecting the indole scaffold with the trimethoxy-phenyl moiety also affects the binding affinities. In fact, compound 9, endowed with a rigid carbonyl linker, showed remarkably reduced activity with respect to its more conformationally free analogues 5, 6, 7, and 8. This different ability in ligand accommodation is also observed when the sulfonyl-phenyl branch is introduced. In fact, the derivatives 10, 12 and 13 (RS3594) possess decreasing IC_{50} values 97nM, 73nM, 10nM on MDM2, respectively. Only, compound 11 deviates from this trend. Docking pose prediction of this compound show that the steric hindrance of the linker hydroxyl group hampers the proper accommodation of the trimethoxy-phenyl group into the Phe19 subpocket, which is consistent with its high IC50 value.

As mentioned above, the compounds were qualitatively tested by 1D ^{1}H-NMR and 2D ^{1}H–^{15}N HSQC, in fact in second part of my PhD project I've been working on expression, extraction and purification samples of hMDM2, as described in methods section (6.2.1.), in order to analyze the protein obtained in their free state and then evaluate the interaction with the designed ligands, through NMR experiments.

The binding mode of RS3594 on MDM2 protein has been investigated by monitoring the changes in cross-peak intensity ratio (I/I_0) occurring in the 2D ^{1}H–^{15}N HSQC spectrum of the uniformly ^{15}N-labeled protein upon the addition of increasing amounts (to reach concentrations of 100, 200, 400, and 800 µM) of RS3594 (solubilized in DMSO-d6), versus the free protein in solution (I_0). The concentration of the protein used for the NMR titrations was 50 µM in 50 mM KH2PO4, 50 mM Na2HPO4, 150 mM NaCl, at pH 7.5 The residues T10, Y56, L57, G58, Q59, I61, M62, D68, V75, Y76, V93, H96, Y100 displayed the highest intensity decreases, while I19, D46, F55, G58, Q59, M62, H73, C77, D84, F91, S92, H96 exhibited the highest chemical shift perturbations. Mapping the residues of MDM2 protein, it is clear that RS3594 binds the protein's canonical site. In fact, all these residues are located on the α2 helix, L2 and L5 loops, and β1 and β2 strands, which are all segments lining the p53-binding cavity.
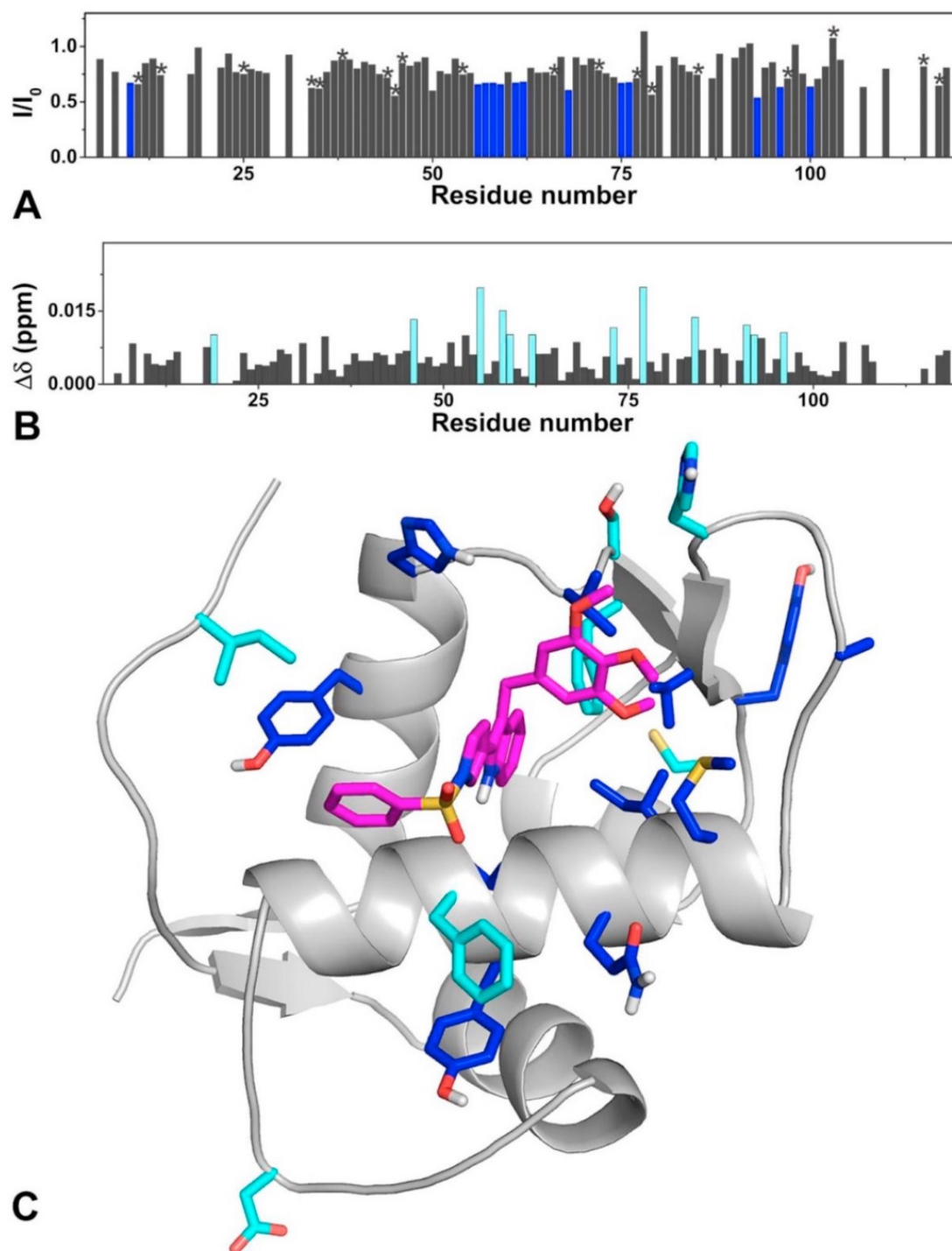
Figure 7 Intensity decreases of NMR signals and the chemical shift perturbations. (A) Residues exhibiting the highest intensity decreases are highlighted in blue. The overlapping signals have been marked with a star and not considered in the selection. (B) Residues exhibiting the highest chemical shift perturbations are highlighted in cyan, residues with the highest intensity decreases are in blue. (Adopted from Simona Daniele et al. [17])

Immunoenzymatic assay was used to evaluate the ability of all compounds and RS3594 to dissociate p53 from MDM2. For this experiment was used cell lysates obtained from U87MG expressing high levels of the p53-MDM2 and Nutlin-1 was used as a control. All the tested compounds were able to bind MDM2 in the nanomolar range. Compounds 3–6, 8, 9 and 11 showed moderate affinity in the medium-high nanomolar range. Instead compounds 7, 10, and 12 showed IC_{50} values below 100 nM and displayed a good ability to bind MDM2. In conclusion, the most potent inhibitor compound is RS3594 with an IC_{50} value of 10 nM

To verify that the most active compound RS3594 could restore the p53-MDM2 axis, p53 protein accumulation was demonstrated with GBM cell treatment. For this purpose, the IV grade-astrocytoma cell line, U87MG, was chosen as an appropriate cellular model expressing a wild-type p53 and CXCR4 [20,21] RS3594 was tested at concentrations corresponding to about 100- or 1000-fold of its IC50, consistent with the activity of these nuclear-target compounds in cells. The choice of AMD3100 (CXCR4 Antagonist) was based on literature data.

As shown in Figure 8 treatment with AMD3100 or RS3594 ligands induced a significant accumulation of p53. Interestingly, AMD3100 also accumulated p53 protein (Figure 8A and B), suggesting that a CXCR4 antagonism can trans reactivate the p53 pathway. CXCR4 activation has repeatedly proven to reduce neuronal p53 content[22]. The combined ligands treatment demonstrated an improved p53 protein accumulation compared to cells treated with either AMD3100 or RS3594 alone (Figure 8A and B). Then, Real-Time PCR analysis was conducted to assess the transcriptional activity of p53. Treating cells with RS3594 or AMD3100 caused significant induction of the p53-target gene, MDM2 (Figure 8C). Moreover, RS3594 induced a significant improvement in PUMA and p21 mRNA expression compared to control cells (Figure 4D). The p53-upregulated modulator of apoptosis (PUMA) is a promoter of apoptosis induced in response to ER stress and directly attaches to the Bcl-2 and antagonizes this antiapoptotic mediator[23]. These findings prove that RS3594 and AMD3100 were able to reactivate p53. Then, to investigate a link between the p53/MDMs axis and CXCR4 in GBM, the assay was carried out in the presence of the CXCR4 antagonist AMD3100. When combined, the two compounds showed a significantly greater upregulation of MDM2 mRNA (Figure 8C) with respect to the single-treated cells. It can be concluded that the CXCR4 receptor

antagonism synergizes in reactivating the p53 pathway when combined with a disruptor of the MDMs-p53 complex.
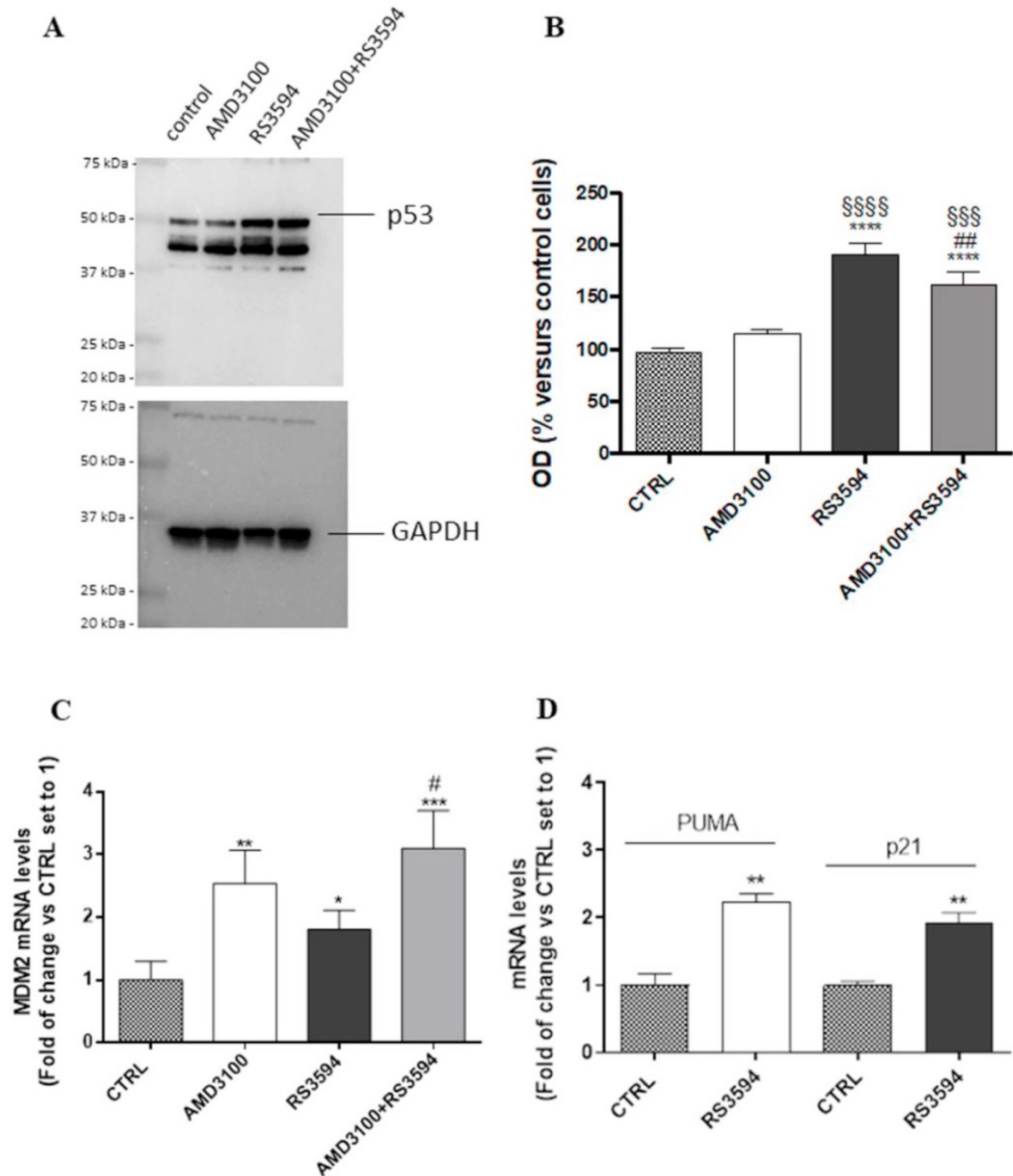

Figure 8. Effects of RS3594 and AMD3100 on the p53 pathway's reactivation. (A, B) U87MG cells were treated with RS3594 (1 μM) and AMD3100 (10 μM), alone or in combination, for 24 h. Cell lysates were subjected to Western blot analysis using a specific antibody for p53. GAPDH was used as the loading control. A representative image is shown in panel A. (B) Densitometric analysis was performed using ImageJ

software. The data are shown as optical density (OD) versus control cells. (C, D) U87MG cells were treated with RS3594 (1 μM) and AMD3100 (10 μM), alone or in combination, for 8 h. Following treatments, total RNA was extracted, and the expression levels of MDM2, p21, and PUMA were evaluated by quantitative Real-Time RT-PCR, as reported in the experimental section. The data are expressed as the fold change versus control level (mean values ± S.D. of three different experiments performed in duplicate). $*P < 0.05$, $**P < 0.01$ and $***P < 0.001$ versus the control. $\#P < 0.05$ and $\#\#\#P < 0.001$ versus cells treated with RS3594. $\$\$\$P < 0.001$ versus the cells treated with AMD3100. (Adopted from Simona Daniele et al. [17])

Subsequently the demonstration of the p53 reactivation, the cell viability was evaluated upon GBM cell treatment with RS3594 in the absence and presence of AMD3100. In particular, the compounds were tested in order to assed their antiproliferative effects in the GBM cell lines (U87MG and U343MG cells) expressing a wild type p53. Moreover, considering the demonstrated efficacy of CXCR4 blockers in breast cancer, the breast cancer cells (MCF-7) were used as a comparison in selected experiments. Both cell lines have been demonstrated to express MDM2[24] and CXCR4 receptors [25]

After 72 h of incubation compound RS3594 induced a significant inhibition of U87MG cell proliferation with an IC50 of 1.37 μM (Figure 9A). Similar effects were obtained in MCF-7 cells (IC_{50} 1.9 μM, Figure 9B). Moreover, RS3594 induced an important inhibition of U343MG cell proliferation following 72 h of incubation, with a maximum effect comparable to that obtained in U87MG cells (Figure 9C). Contrarily, the antiproliferative effects were lower in p53-mutated cells (e.g T98G cells, Figure 9C) with respect to p53-wild type GBM cells. These data demonstrate that RS3594 acts through p53-dependent mechanisms, at least in the tested GBM cells.

In contrast, compound AMD3100 did not significantly affect cellular proliferation at 10 μM neither in U87MG (Figure 9D) nor MCF-7 cells. However, the addiction of RS3594 (10 μM) to AMD3100-treated cells induced a significant reduction of proliferative cells (Figure 5D). The observed effects were significantly higher when compared to single compound treated cells (Figure 9C). These results demonstrate that AMD3100 sensitized glioma cells to the antiproliferative action of RS3594.

To test the compounds' putative toxicity on non-cancer cells, the microglia C20 cell line was employed for viability assays. As shown in Figure 9 (panel E), the highest concentrations of AMD3100 and RS3594 appreciably decreased the proliferation rate of

microglia cells. The percentage of cell proliferation was higher in microglia C20 cell line than U87MG after treatment with RS3594 alone (74% vs 46%, P = 0,0092, respectively) and in combination with AMD3100 (88% vs 39%, P = 0,0026, respectively).

Furthermore, we investigated if the antiproliferative effects of the compounds could be associated with apoptosis. The number of living, early, and late apoptosis cells were analyzed by Annexin assay. After treatment, RS3594 and the co-treatment were able to significantly enhance the percentage of cells in the early apoptosis, suggesting an apoptosis activation.
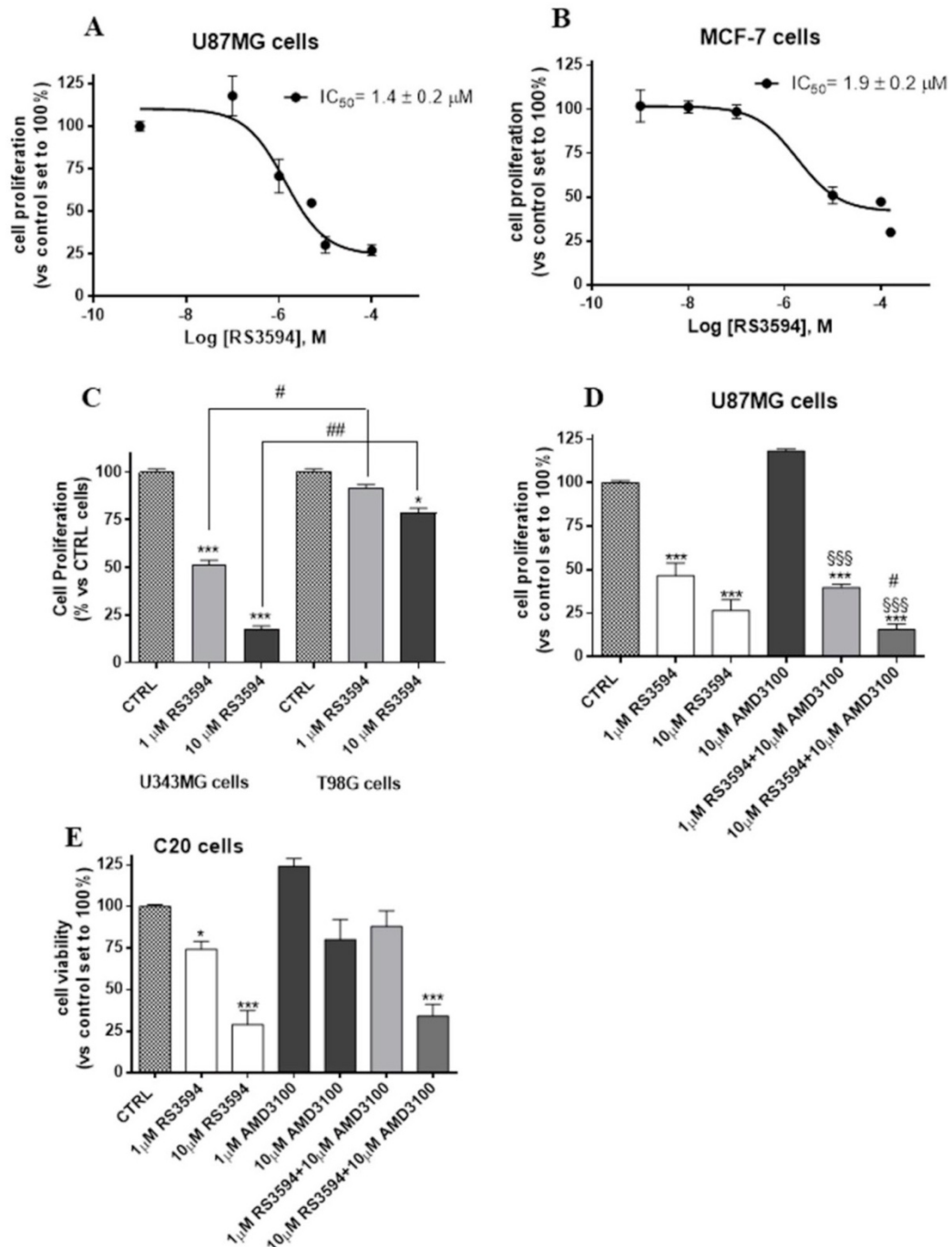
Figure 9. Effect of RS3594 and AMD3100 on cell proliferation. U87MG (A) and MCF-7 (B) were treated with increasing concentrations (1 nM-100 μM) of RS3594. (C) U343MG and T98G were treated with RS3594 (1 μM and 10 μM). U87MG (D) and C20 cells (E) were treated with RS3594 (1 μM and 10 μM) and AMD3100 (1 μM and 10 μM), alone or in combination. Following 72 h, cell viability was evaluated by MTS assay as described in the experimental section. Data are reported as a percentage with respect to control, set to 100% (mean ± S.D. of three different experiments conducted in triplicate). $*P < 0.05$, $***P < 0.001$ vs the control. $\#P < 0.05$ versus cells treated with RS3594. $\$\$\$P < 0.001$ versus the cells treated with AMD3100. (Adopted from Simona Daniele et al. [17])

Given the crucial role of CXCR4 in controlling cell migration and invasiveness[26], and the interplay registered in breast cancer between MDM2 and CXCR4, additional experiments were conducted to investigate the effects of AMD3100 alone or in combination with the MDM2 inhibitor RS3594 in GBM (U87MG cells). Matrigel assay was performed on control and treated cells by counting invading cells on the lower surface of the transwell membrane after fixing with p-formaldehyde and staining with crystal violet [27]. The results showed that the AMD3100 reduced the percentages of invading cells compared to untreated samples (Figure 10A and B). A significant reduction of U87MG cellular invasiveness was also evident in samples treated with RS3594 (Figure 10A and B), tested at 1 μM and 10 μM, in a concentration-dependent manner. When cells were incubated in combination of AMD3100 and RS3594, additive/synergic effects were observed (Figure 10A and B). Because the reduction in cell viability at 24 h, particularly for AMD3100, was not significant following 24 h of incubation, these results may be ascribed to an invasion phenomenon rather than a decrease in cell number.

To confirm these data, a wound-healing assay was performed. In particular, cells were scratched and then treated with RS3594, alone or in combination with AMD3100, for 24 h. As showed in Figure 11, AMD3100 significantly reduced the migration distance of U87MG cells with respect to control cells. Quantitative analysis of the gap area proved that RS3594 (1 μM) decreased glioma migration (Figure 11A and B). When GBM cells were challenged with AMD3100 and RS3594 simultaneously, the gap area increased (Figure 11A and B) with respect to untreated and single-treated cells, thus reducing the glioma migration.
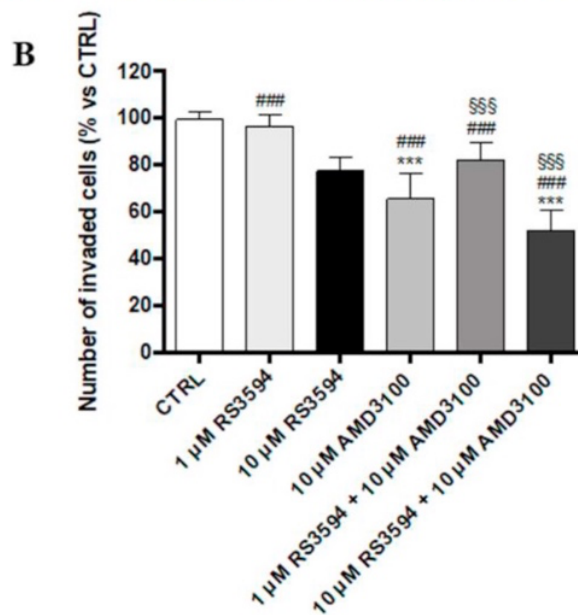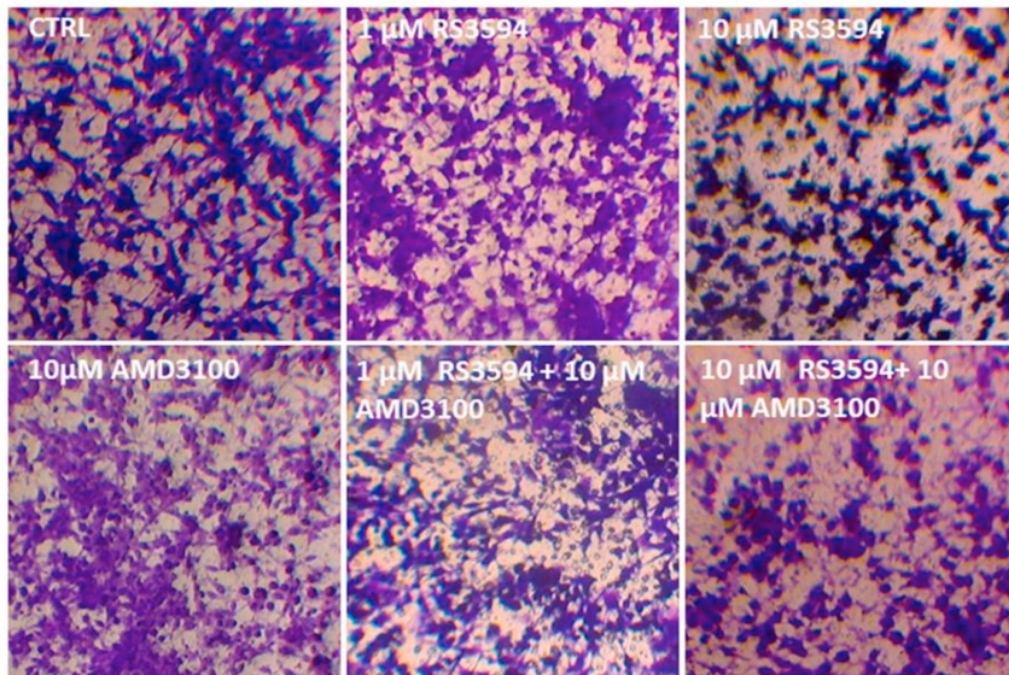
Figure 10. Effect of RS3594 and AMD3100 on U87MG cell invasiveness. Cell invasion was analysed through the Matrigel basement membrane transwell system, as described in the experimental section. (A) Representative images of U87MG incubated with RS3594 (10 μM and 1 μM) and AMD3100 (10 μM) alone or in combination for 24 h. (B) Cell invasiveness was measured by counting the number of cells that migrated into the lower face of the transwell mem- brane. ***P < 0.001 versus control. ###P < 0.001, ##P < 0.01 versus cells treated with RS3594 (10 μM). §§§P < 0.001 versus cells treated with AMD3100 (10 μM). (Adopted from Simona Daniele et al. [17])
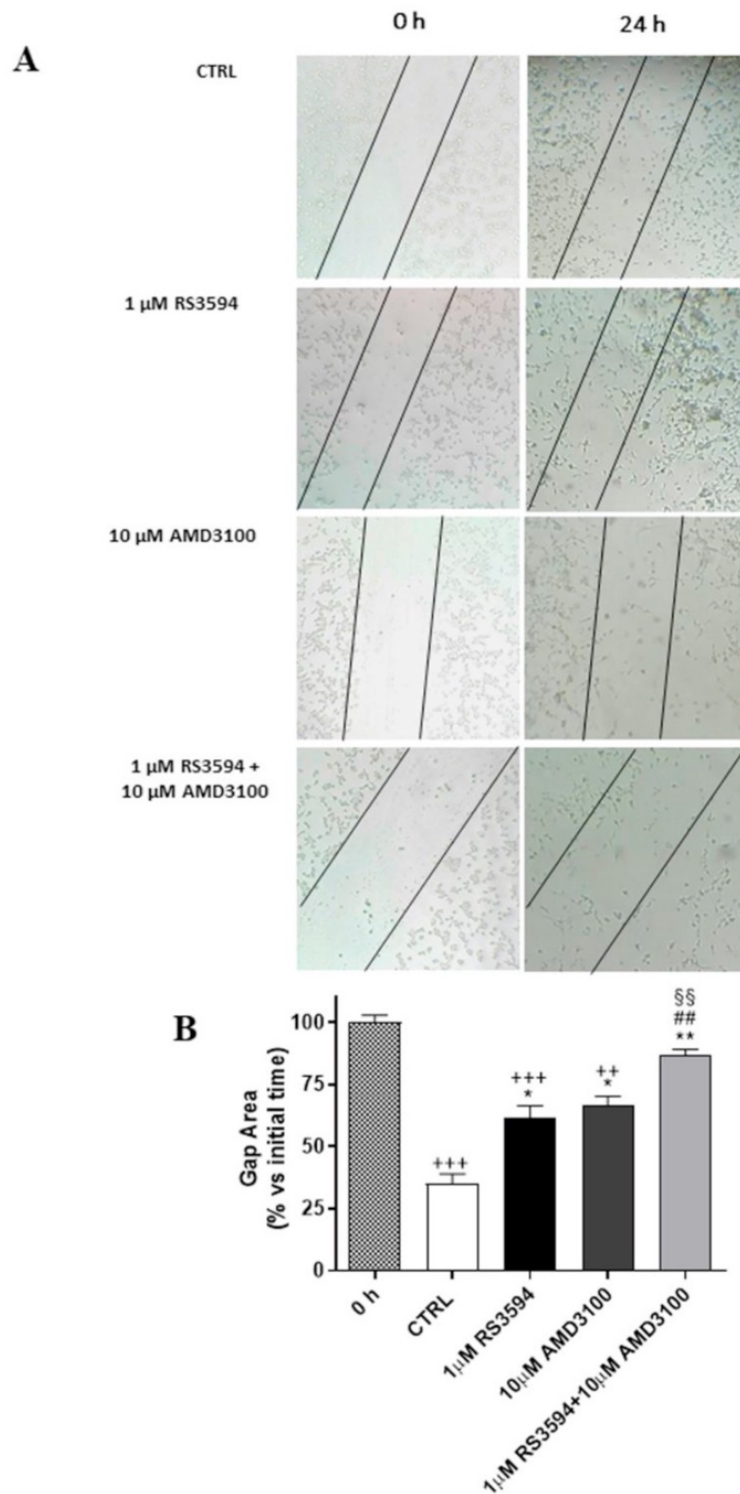
Figure 11. Effect of RS3594 and AMD3100 on U87MG cell migration. The cells were treated with RS3594 (1 μM) and AMD3100 (10 μM), alone or in combi- nation, and the healing of the scratch wounds were evaluated. A) Representa- tive pictures of the scratch wounds at 0 h and 24 h. Dashed lines were shown in the images. B) The percentage of gap closure compared to the respective gap at t0. The data are presented as the means ± S.D. of at least two different ex- periments performed in triplicate. ++P < 0.01 and +++P < 0.001 versus 0 h *P < 0.05 and **P < 0.01 versus the control. ##P < 0.01 versus the
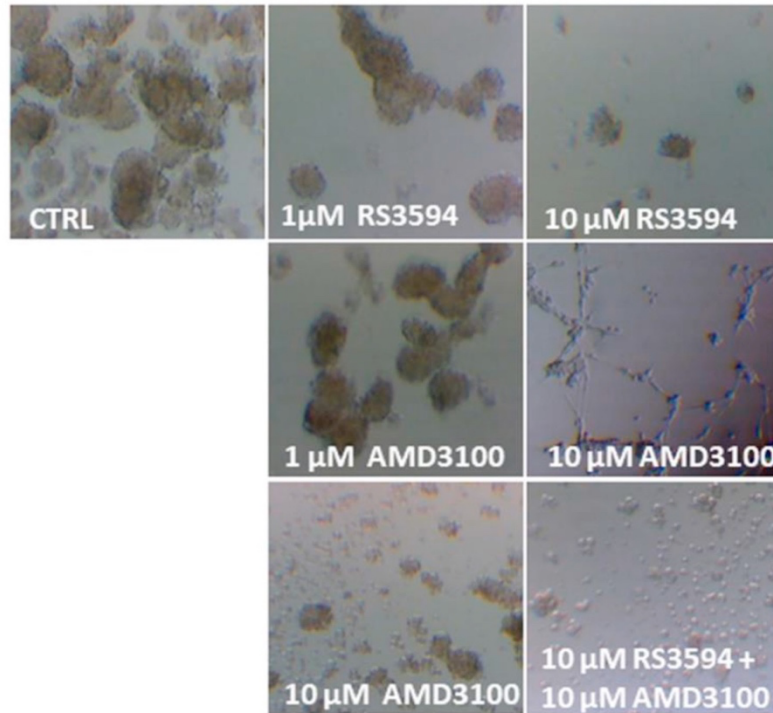
cells treated with RS3594 (1 μM). §§P < 0.01 versus the cells treated with AMD3100 (10 μM). (Adopted from Simona Daniele et al. [17])

GBM stem-like cells (GSCs) have been proven to possess a high tumorigenic capacity and a significant radio- and chemoresistance, highlighting the need for a "stem cell-oriented therapy" to reduce tumor recurrence and improve GBM prognosis[28,29]. In this sense, both CXCR4 and p53/MDMs axis[28] have been demonstrated to affect the proliferation of neurospheres

Further experiments were achieved to assess the effects of RS3594 on neurospheres. Especially, studies were carried out on the stem cell component of U87MG cells by culturing the cells in a defined serum-free medium that allows isolating cancer stem cells as "neurospheres".[28,30–32] These cells were demonstrated to present an enhancement in the mRNA expression of the stem cell marker (CD133) and a decrease of the glial marker GFAP (glial fibrillary acidic protein), confirming the validity of this established protocol.[28,30–32] The use of these spheroids as a GSC model presents limitations but can be a starting point to test the efficacy of new compounds in a cell subpopulation that is richer in cancer stem cells.

Figure below (Figure 12A) shows representative images of neurospheres treated for seven days with RS3594, alone or in combination with AMD3100. RS3594 reduced the number and the area (Figure 12A and B and C) of neurospheres in culture significantly. Of note, the first effect occurred in a concentration-dependent manner. In contrast, AMD3100 did not affect their area (Figure 12A and C), but it slightly reduced their number when used at 10 μM (Figure 12A and B). The area of neurospheres (Figure 12A and C) was significantly decreased when AMD3100 was combined with RS3594, although with a percentage of reduction comparable to those observed with RS3594 alone. Interestingly, AMD3100 was proven to induce cellular sprouting of cultured neurospheres (Figure 12A and D), suggesting that blocking CXCR4 can induce differentiation.
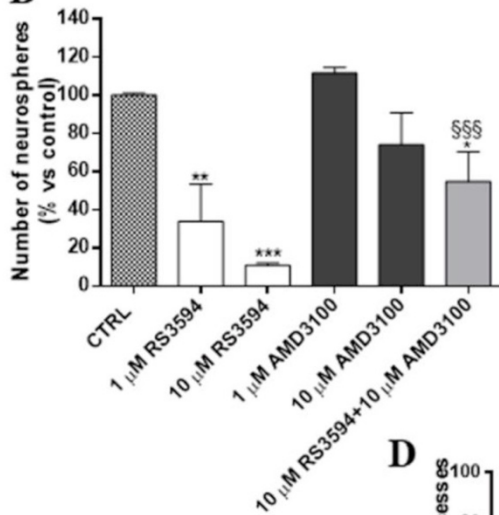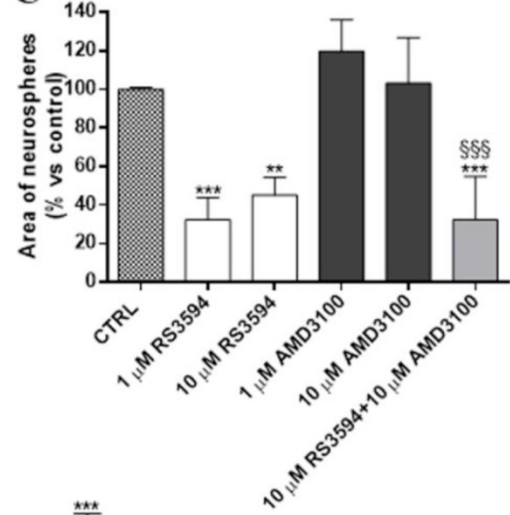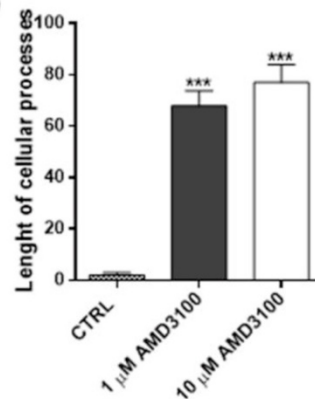
Figure 12. Effects of RS3594 and AMD3100 on sphere-derived cell morphology. Neurospheres were treated for 7 days with RS3594 (1 μM and 100 μM) and AMD3100 (1 μM and 10 μM) in complete NSC medium. (A) Representative pictures of the neurospheres after 7 days of incubation were shown. The number (B), area (C), and length of cellular processes (D) of the newly formed spheres were scored after 7 days of

treatments. The data represent the mean ± S.D. of three pictures from two different experiments. *P < 0.05, **P < 0.01, ***P < 0.001 versus the control. §§§P < 0.001 versus the cells treated with AMD3100 (10 μM). (Adopted from Simona Daniele et al. [17])

Clonogenic assay was used to verify the ability of RS3594 on the formation of neurospheres and so they were dissected. This test was performed after 7 days of treatment with subtoxic concentrations of AMD3100 or RS3594 (Figure 13A and B). In particular, it was crucial to use non- toxic concentrations of the compounds in this assay. Otherwise, the reduction in the clonogenic potential could be ascribed to a toxic effect rather than an inhibition of the cell clonogenic ability.

In conclusion RS3594 significantly reduced the total sphere number (Figure 13A and B) in a concentration-dependent manner. Similar results were obtained with AMD3100 (Figure 13A and B). When the lowest concentration of RS3594 was combined with the lowest concentration of AMD3100, the anti-clonogenic effect was enhanced compared to single-treated cells (Figure 13A and B).
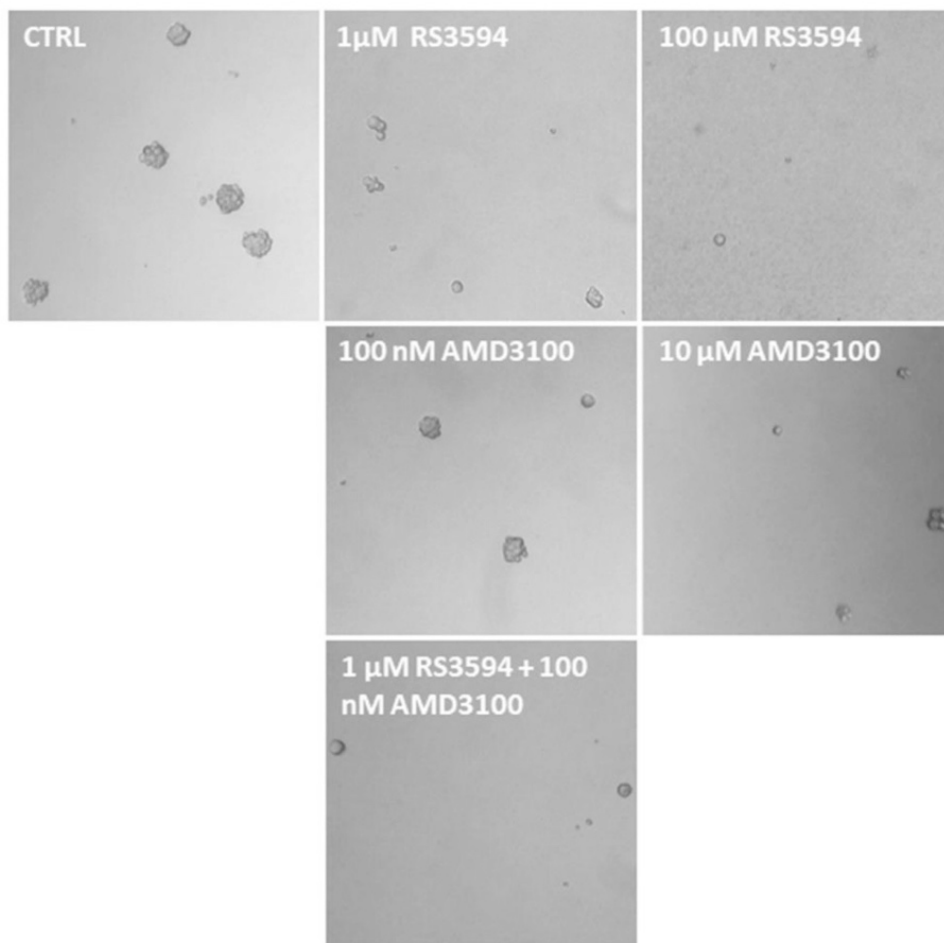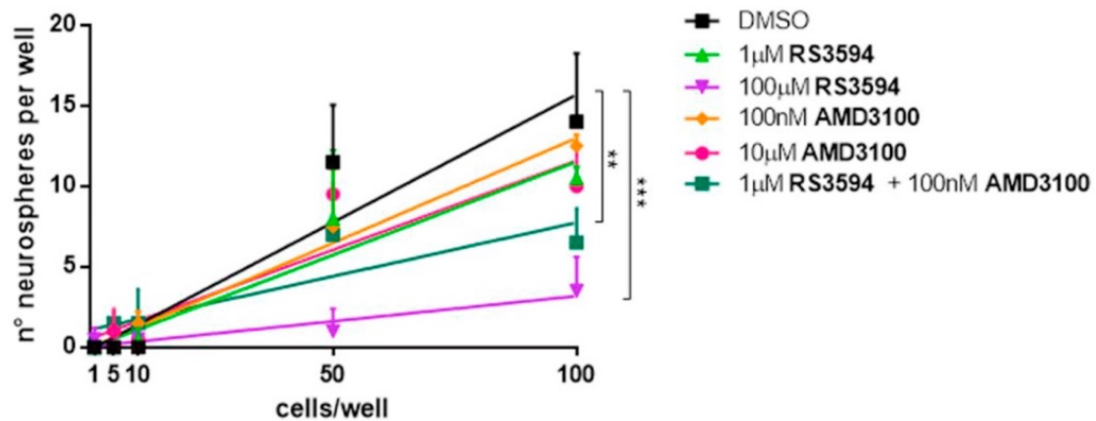
Figure 13. Effects of RS3594 and AMD3100 on the clonogenic potential of GBM cells. (A) Representative microscopic images of neurospheres (100 cells/well) after 7 days of treatment with RS3594 (1 μM and 100 μM) and AMD3100 (100 nM and 10 μM), alone or in combination. (B) Quantitative results of the clonogenic assay. Data are presented as the mean ± S.D. of two different experiments. **P < 0.01, ***P < 0.001 versus the control, as indicated in panel B. (Adopted from Simona Daniele et al. [17])

In a second work MDM2/p53 complex was chosen as a case study in order to evaluate the possibility for screening applications by protein- and ligand- based NMR. MDM2/p53 complex was selected because this PPI (Protein−protein interactions) is one of the most studied for its implications in several cancer types. Development of inhibitors to disrupt this interaction has been the object of intensive pharmaceutical efforts for anti-cancer therapies. As shown also in the previous work, a short segment of the N-terminal region of the p53 interacts with MDM2, forming an amphipathic α-helix, with Phe19, Trp23, and Leu26 being crucial interacting residues. Three peptides, having different K_D's for MDM2: p53[16-27] (K_D = 0.060 μM), 20 p53[19-26] (K_D = 0.80 μM) and p53[19-25] (K_D = 150 μM) were selected as potential hot-peptides in our study.

At first, in collaboration with research group of Prof. Fragai of CERM, University of Firenze, we validated that the selected peptides interacted with MDM2 by acquiring the 2D ^{1}H−^{15}N HSQC spectrum of the ^{15}N-MDM2 N- terminal domain (residues 1−112) alone and after the addition of three peptides.

As expected, residues that are mainly affected by all peptides are within the known binding site of MDM2 for p53 interaction, indicating that the binding is specific even for the weak ligand p53[19-25]. As expected, residues influenced by interaction with all three peptides are within the known MDM2 binding site for p53 interaction and also in accordance with the K_d we can see that the three complexes have different exchange regimes. In addition to evaluate the possibility for screening applications by protein-based NMR, nutlin-3a (inhibitor of the MDM2/p53 complex) was added to complex and the HSQC spectra were reacquired. Moreover, was acquired the HSQC spectrum of the complex MDM2/nutlin-3a without peptides (Figure14 and 15).

All HSQC spectra in the presence of nutlin-3a are identical, this shows that MDM2/peptide interactions have been inhibited and the effective application of the protein-based NMR procedure as a screening test.

Figure 14. (a−c) Full spectra of 2D $^1H-^{15}N$ HSQC of the MDM2 N-terminal domain alone (blue spectra), after the addition of peptides (green spectra) p53[19-26] (a), p53[19-25] (b), p53[16-27] (c), and nutlin-3a to the complexes (red spectra). (d) Selected regions of 2D $^1H-^{15}N$ HSQC spectra of the MDM2 N-terminal domain alone (blue spectra) and after addition of nutlin-3a (red spectra).

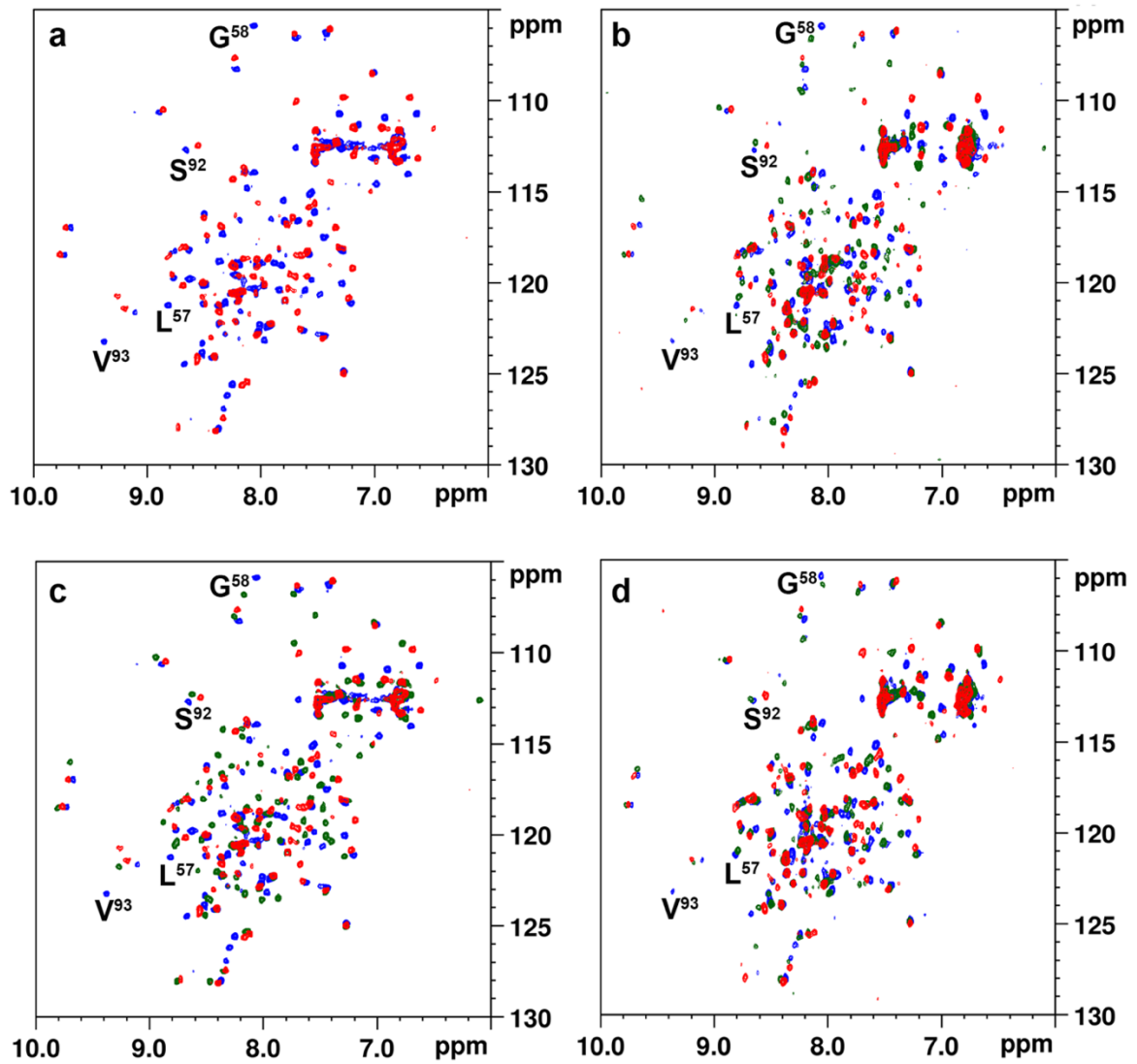(Adopted from Diego Brancaccio et al.[11])

Figure 15. (a−c) Selected regions of 2D $^1H-^{15}N$ HSQC spectra of the MDM2 N-terminal domain alone (blue spectra), after the addition of peptides (green spectra) p53[19-26] (a), p53[19-25] (b), p53[16-27] (c), and nutlin-3a to the complexes (red spectra). (d) Selected regions of 2D $^1H-^{15}N$ HSQC spectra of the MDM2 N-terminal domain alone (blue spectra) and after addition of nutlin-3a (red spectra). (Adopted from Diego Brancaccio et al.[11])
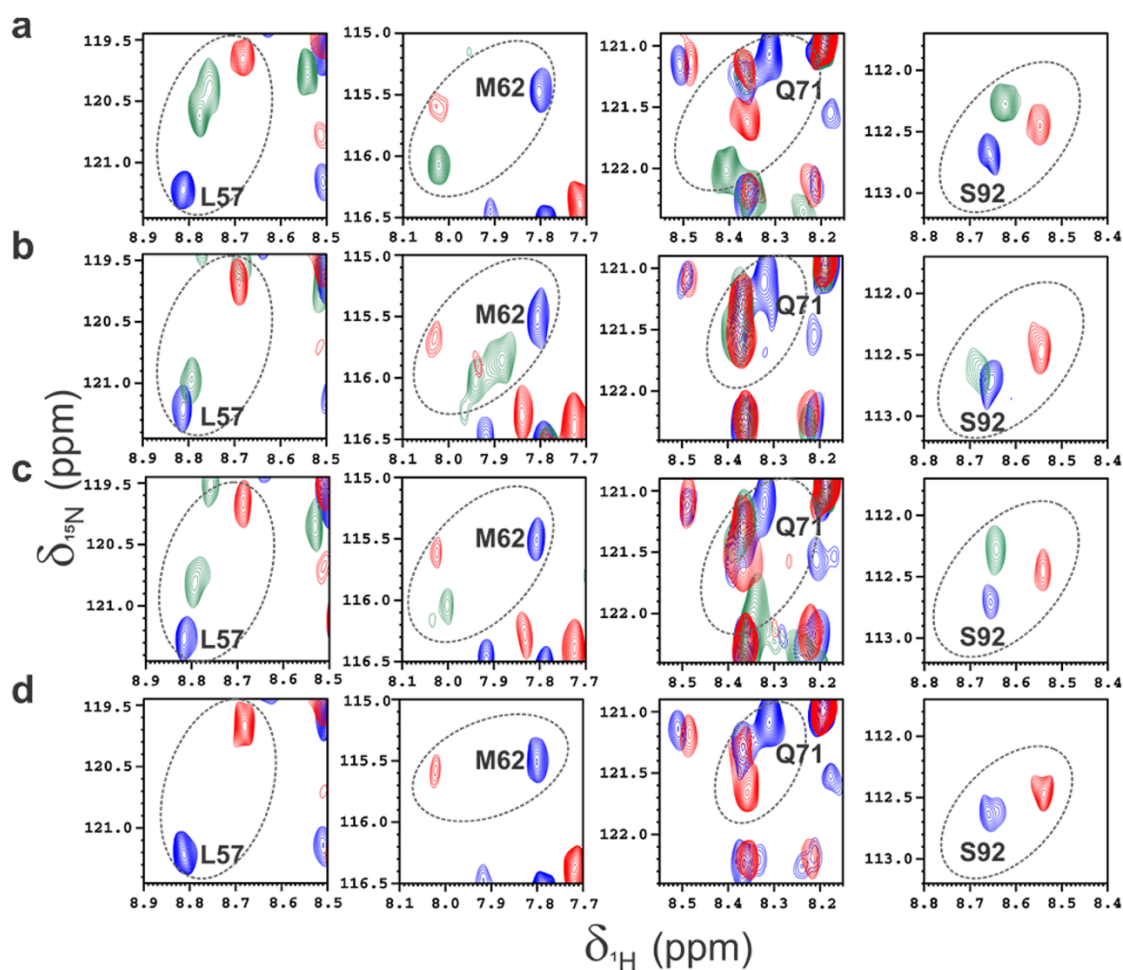
1D ^1H Ligand-based NMR experiments were used to detect the interaction between the hMDM2 protein not labelled, expressed and purified as previously described and the three peptides.

In the present NMR assay, we have acquired the 1D ^1H STD an WL NMR spectra of investigated peptides (1.0 mM) in the presence and absence of hMDM2 (0.020 mM), the potential use of this techniques for inhibitor screening was then assessed by adding nutlin-3a as positive control.

The figure 16 show positive signals observed in the STD-NMR spectra of the p53[19-26] peptides mixed with MDM2. After the addition of nutlin-3a for the competition

experiments, aromatic and methyl signal STD intensities of peptides p53[19-26] were significantly reduced. The same behavior we get with the other two peptides.

Figure 16. 1H NMR (a) and STD spectra of 1.0 mM p53[19-26] alone (b), in the presence of 0.020 mM MDM2 solution (c), and after the addition of 0.100 mM nutlin-3a (d). Buffer impurity is marked with a hash symbol. (Adopted from Diego Brancaccio et al.)

Figure 17 show the WL spectra of p53[19-26]. In this spectrum, signal intensities of aromatic and methyl protons significantly change from peptide alone to the spectrum of the complex with MDM2. After the addition of nutlin-3a, the same signals reduced their

intensities coming back to the free state situation. The same behavior we get with the other two peptides.
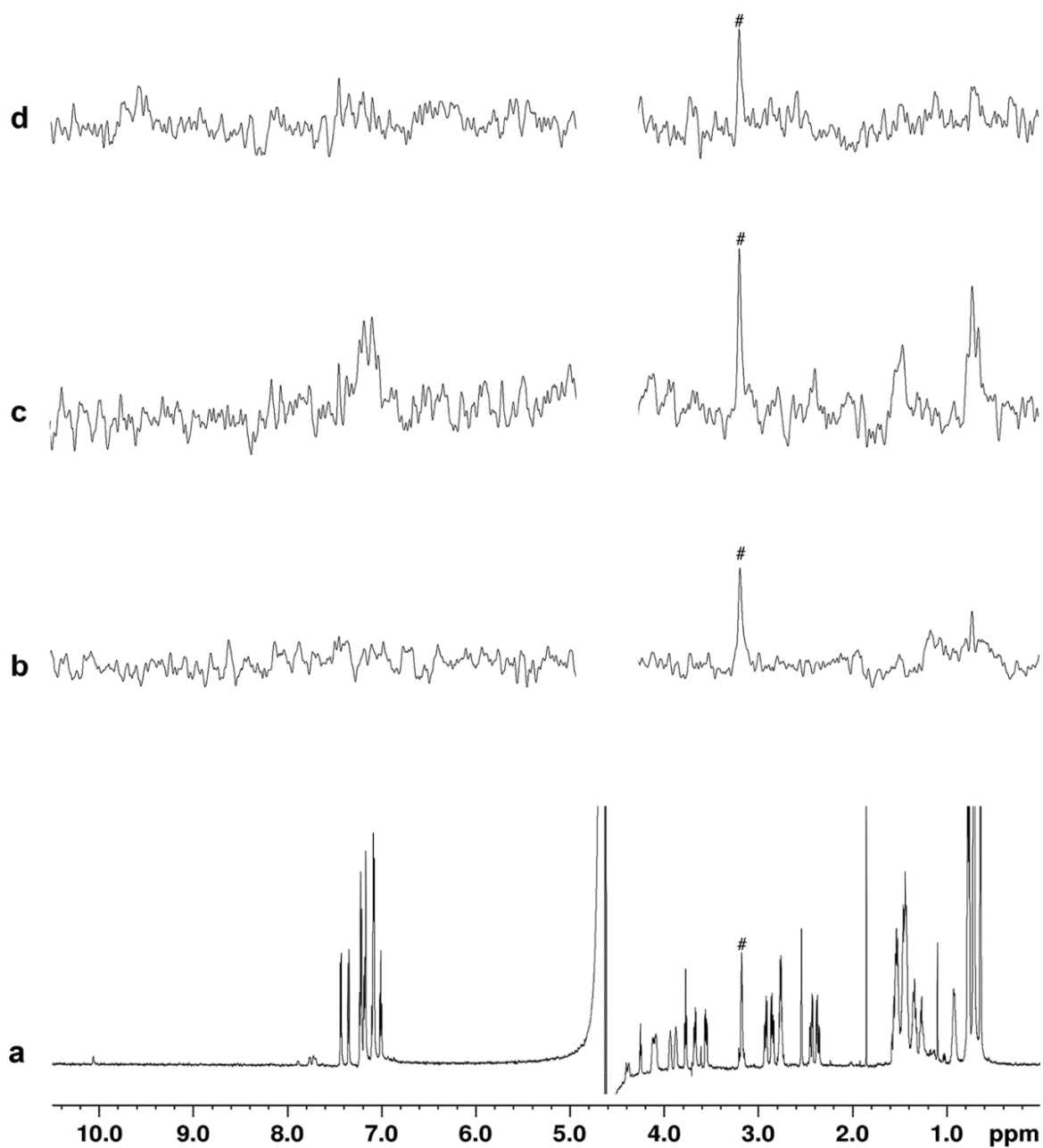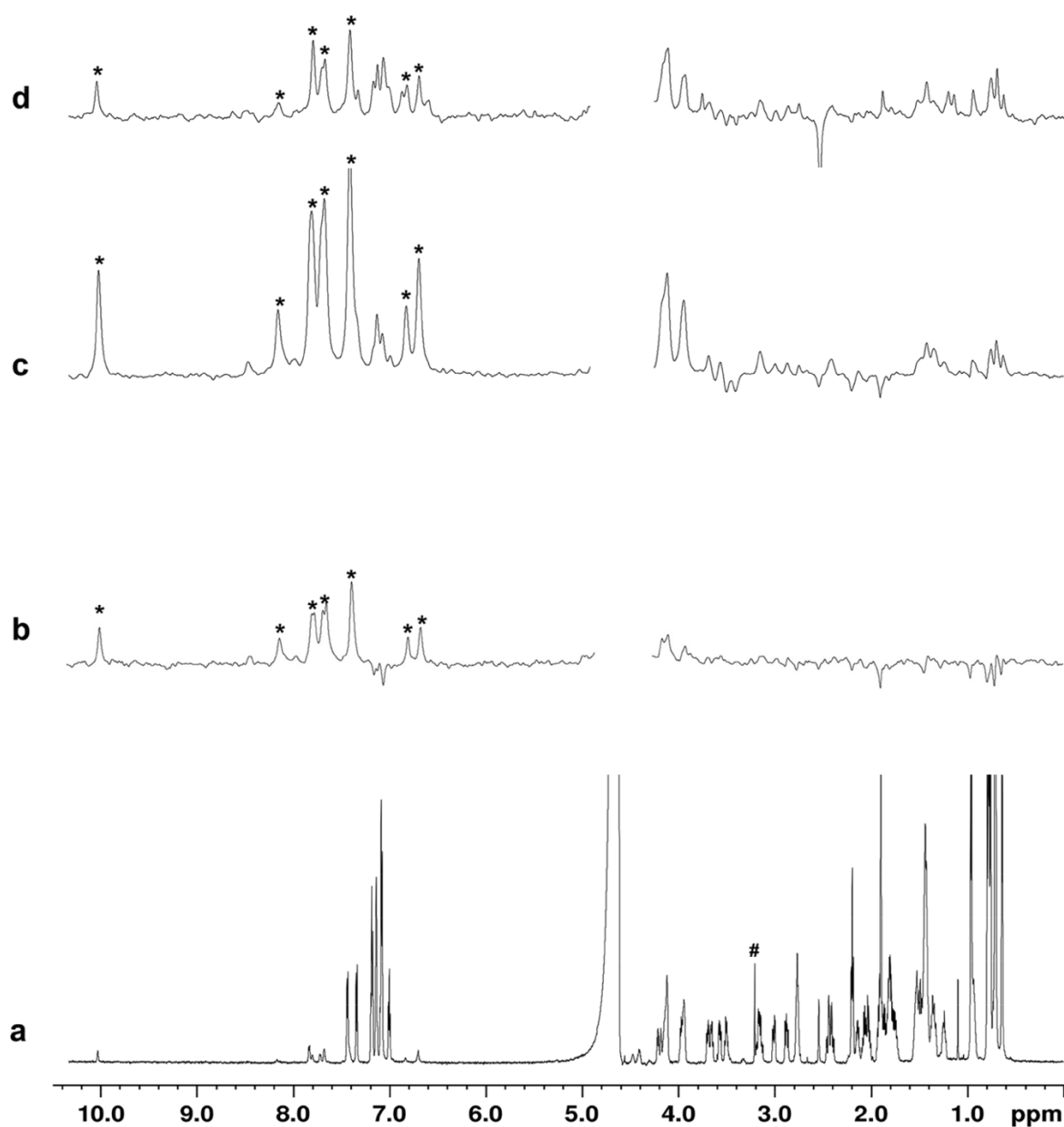

Figure 17. 1H NMR (a) and WL spectra of 1.0 mM p53[16-27] alone (b), in the presence of 0.020 mM MDM2 solution (c), and after the addition of 0.100 mM of nutlin-3a (d). Stars indicate the position of exchangeable proton signals. Buffer impurity is marked with a hash symbol.

Noteworthy, after analysis of 2D ^{1}H–^{15}N HSQC and 1D ^{1}H STD an WL NMR spectra, it is clear how this screening method was effective in the identification of new of MDM2 inhibitor binder. In this work, we described an efficient and simple method for the screening of PPI inhibitors (HOPPI-NMR) in which one of the two interacting proteins

is replaced by a short peptide (hot-peptide). This method may be used in the future not only for similar system (protein−protein interaction), but also with ligand-protein interaction in order to identify new small molecules inhibitors.

Finally, one last work on MDM2/p53 complex is still ongoing. In this scenario, given the results of the two previous works, in collaboration with Professor Mai of the University of Rome, the same method of VS of the first work was applied to a virtual database of molecules of his research group. About one hundred of them showed the same binding mode of the molecules described in the first work of this chapter.

Our screening method, developed and published in the article HOPPI-NMR: Hot-Peptide-Based Screening Assay for Inhibitors of Protein−Protein Interactions by NMR, was then used to detect the interaction between the hMDM2 protein, expressed and purified as described in methods section (6.2.1), and these compounds. Experiments performed so far indicate that three of these (Figure 18) showed interacting with the protein MDM2, but analyses are still ongoing.
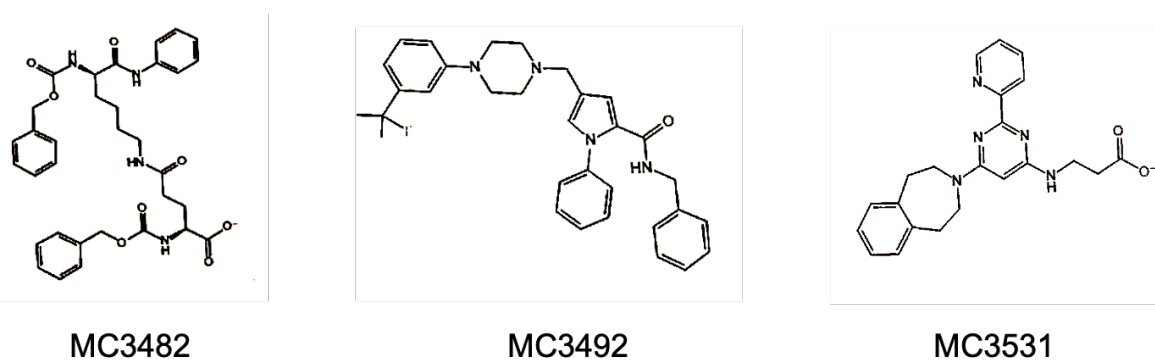

MC3482   MC3492   MC3531

Figure 18. MDM2 Binder of University of Roma Database

3.3. Conclusion

MDM2/p53 protein complex is one of the most widely studied complexes for its implications in several cancer types. Development of inhibitors to disrupt this interaction has been the object of intensive pharmaceutical efforts for anticancer therapies. In fact, a number of MDM2 inhibitors have been described in patent and scientific literature. However, in a previous work, through a virtual screening performed on MDM2 the lead compound RS3760 was identified. It was found to be capable of disrupting the MDM2/p53 interaction with an IC_{50} of 270 nM. Herein a ligand-based lead optimization was carried out and a series of RS3760 derivates was synthetized and assayed for their ability to dissociate p53 from MDM2. One our compound (RS3594) showed a highest affinity, with an IC_{50} value of 10 nM. The binding mode of RS3594 to MDM2 protein was evaluated by 2D ^1H–^{15}N HSQC NMR and molecular docking. After this combined approach of Modeling/NMR, MDM2 inhibitor, RS3594, was combined with the CXCR4 antagonist, AMD3100, in human GBM cells and tested in GBM stem-like cells (neurospheres), which are crucial for tumor recurrence and chemotherapy resistance. RS3594 and AMD3100 reduced GBM cell invasiveness and migration in single-agent treatment and mainly in combination. These two compounds present synergic effects on cancer stem component: RS3594 efficiently blocks the growth of neurospheres and inhibits their formation. At the same time, AMD3100 induces the differentiation of neurospheres and acts synergistically with RS3594 in blocking their proliferation and clonogenic ability. Globally, our data showed that the inhibition of the two pathways synergistically reduces the invasiveness and the migration of GBM cells and that the CXCR4 antagonist AMD3100 is able to sensitize GBM cells to the antiproliferative activity of the dual MDMs inhibitor RS3594. Of most importance, the experiments herein reported demonstrated that similar to what happens in breast cancer, the two pathways greatly affect the stem cell component of the GBM. These results confirm that the CXCR4/MDM2 block can represent a valuable strategy to reduce GBM proliferation and invasiveness, acting, most importantly, on the stem cell component. Of note, the efficacy of the proposed therapeutic strategy is limited to GBM tumors expressing wild-type p53. Specific compounds are needed in the case of a mutated p53 since conventional reactivators would not be effective.

As mentioned above MDM2/p53 complex is one of the most studied PPI (Protein−protein interactions) for its implications in several cancer types and so in a second work MDM2/p53 complex was chosen as a case study in order to evaluate the possibility for screening applications by protein- and ligand- based NMR. In this work, we described an efficient and simple method for the screening of PPI inhibitors (HOPPI-NMR), in which one of the two interacting proteins is replaced by a short peptide (hot-peptide). The replacement, among other benefits, allows the application of fast, low-consuming, ligand-based NMR techniques for the investigation of unlabeled samples. In addition, the HOPPI method can, in principle, be used in combination with any other screening technique (SPR, fluorescence spectroscopy, etc.). The combination of HOPPI-NMR and fragment-based drug discovery (FBDD) methods would be a straightforward way to boost the discovery of PPI inhibitors, allowing researchers to detect also small fragments tested in FBDD which often display weak binding; hence, HOPPI-NMR emerges as a suitable tool to reliably and efficiently detect such weak binding. We envisage that the appropriate choice of hot-peptides will enable the discovery of hit compounds with weak binding affinity, potentially useful in FBDD investigations, providing new opportunities for the highly expanding field of medicinal chemistry devoted to the identification of effective PPI Inhibitors.

Finally, this method may be used in the future not only for similar system (protein−protein interaction), but also with ligand-protein interaction in order to identify new small molecules inhibitors. In fact, in collaboration with Professor Mai of the University of Rome, this method was used to detect the interaction between the hMDM2 protein, and 3 new compounds presents on his virtual database, after a previous VS computational method. The analyses of this compounds are still ongoing.

3.4. References

(1)   Lai, Z.; Auger, K. R.; Manubay, C. M.; Copeland, R. A. Thermodynamics of P53 Binding to Hdm2(1-126): Effects of Phosphorylation and P53 Peptide Length. *Arch. Biochem. Biophys.* **2000**, *381* (2), 278–284.

(2)   Chen, L.; Yin, H.; Farooqi, B.; Sebti, S.; Hamilton, A. D.; Chen, J. Interaction and Activate P53. *Interactions* **2005**, *4* (June), 1019–1025.

(3)   Vassilev, L. T. P53 Activation by Small Molecules: Application in Oncology. *J. Med. Chem.* **2005**, *48* (14), 4491–4499.

(4)   Ozaki, T.; Nakagawara, A. Role of P53 in Cell Death and Human Cancers. *Cancers (Basel).* **2011**, *3* (1), 994–1013.

(5)   Chen, L.; Yin, H.; Farooqi, B.; Sebti, S.; Hamilton, A. D.; Chen, J. P53 A-Helix Mimetics Antagonize P53/MDM2 Interaction and Activate P53. *Interactions* **2005**, *4* (June), 1019–1025.

(6)   Blagih, J.; Buck, M. D.; Vousden, K. H. P53, Cancer and the Immune Response. *J. Cell Sci.* **2020**, *133* (5), 1–13.

(7)   Wang, S.; Zhao, Y.; Aguilar, A.; Bernard, D.; Yang, C. Y. Targeting the MDM2-P53 Protein-Protein Interaction for New Cancer Therapy: Progress and Challenges. *Cold Spring Harb. Perspect. Med.* **2017**, *7* (5), 1–10.

(8)   Vassilev, L. T.; Vu, B. T.; Graves, B.; Carvajal, D.; Filipovic, Z.; Kong, N.; Kammlott, U.; Lukacs, C.; Fotouhi, N.; Liu, E. A. In Vivo Activation of the P53 Pathway by Small-Molecule Antagonists of MDM2. *Science (80-.).* **1881**, *os-2* (57), 341–342.

(9)   Hou, H.; Sun, D.; Zhang, X. The Role of MDM2 Amplification and Overexpression in Therapeutic Resistance of Malignant Tumors. *Cancer Cell Int.* **2019**, *19* (1), 1–8.

(10)   Giustiniano, M.; Daniele, S.; Pelliccia, S.; La Pietra, V.; Pietrobono, D.; Brancaccio, D.; Cosconati, S.; Messere, A.; Giuntini, S.; Cerofolini, L.; Fragai, M.; Luchinat, C.; Taliani, S.; La Regina, G.; Da Settimo, F.; Silvestri, R.; Martini, C.; Novellino, E.; Marinelli, L. Computer-Aided Identification and Lead Optimization of Dual Murine Double Minute 2 and 4 Binders: Structure-Activity Relationship Studies and Pharmacological Activity. *J. Med. Chem.* **2017**, *60* (19), 8115–8130.

(11)   Brancaccio, D.; Di Maro, S.; Cerofolini, L.; Giuntini, S.; Fragai, M.; Luchinat, C.; Tomassi, S.; Limatola, A.; Russomanno, P.; Merlino, F.; Novellino, E.; Carotenuto, A. HOPPI-NMR: Hot-Peptide-Based Creening Assay for Inhibitors of Protein-Protein

Interactions by NMR. *ACS Med. Chem. Lett.* **2020**, *11* (5), 1047–1053.

(12)   Schon, O.; Friedler, A.; Bycroft, M.; Freund, S. M. V.; Fersht, A. R. Molecular Mechanism of the Interaction between MDM2 and P53. *J. Mol. Biol.* **2002**, *323* (3), 491–501.

(13)   Hou, H.; Sun, D.; Zhang, X. The Role of MDM2 Amplification and Overexpression in Therapeutic Resistance of Malignant Tumors. *Cancer Cell Int.* **2019**, *19* (1), 1–16.

(14)   Wienken, M.; Moll, U. M.; Dobbelstein, M. Mdm2 as a Chromatin Modifier. *J. Mol. Cell Biol.* **2017**, *9* (1), 74–80.

(15)   Wang, W.; Qin, J. J.; Rajaei, M.; Li, X.; Yu, X.; Hunt, C.; Zhang, R. Targeting MDM2 for Novel Molecular Therapy: Beyond Oncology. *Med. Res. Rev.* **2020**, *40* (3), 856–880.

(16)   Popowicz, G. M.; Czarna, A.; Wolf, S.; Wang, K.; Wang, W.; Dömling, A.; Holak, T. A. Structures of Low Molecular Weight Inhibitors Bound to MDMX and MDM2 Reveal New Approaches for P53-MDMX/MDM2 Antagonist Drug Discovery. *Cell Cycle* **2010**, *9* (6), 1104–1111.

(17)   Daniele, S.; La Pietra, V.; Piccarducci, R.; Pietrobono, D.; Cavallini, C.; D'Amore, V. M.; Cerofolini, L.; Giuntini, S.; Russomanno, P.; Puxeddu, M.; Nalli, M.; Pedrini, M.; Fragai, M.; Luchinat, C.; Novellino, E.; Taliani, S.; La Regina, G.; Silvestri, R.; Martini, C.; Marinelli, L. CXCR4 Antagonism Sensitizes Cancer Cells to Novel Indole-Based MDM2/4 Inhibitors in Glioblastoma Multiforme. *Eur. J. Pharmacol.* **2021**, *897* (January), 173936.

(18)   Chang, Y. S.; Graves, B.; Guerlavais, V.; Tovar, C.; Packman, K.; To, K. H.; Olson, K. A.; Kesavan, K.; Gangurde, P.; Mukherjee, A.; Baker, T.; Darlak, K.; Elkin, C.; Filipovic, Z.; Qureshi, F. Z.; Cai, H.; Berry, P.; Feyfant, E.; Shi, X. E.; Horstick, J.; Annis, D. A.; Manning, A. M.; Fotouhi, N.; Nash, H.; Vassilev, L. T.; Sawyer, T. K. Stapled α-Helical Peptide Drug Development: A Potent Dual Inhibitor of MDM2 and MDMX for P53-Dependent Cancer Therapy. *Proc. Natl. Acad. Sci. U. S. A.* **2013**, *110* (36), 3445–3454.

(19)   Merlino, F.; Daniele, S.; La Pietra, V.; Di Maro, S.; Di Leva, F. S.; Brancaccio, D.; Tomassi, S.; Giuntini, S.; Cerofolini, L.; Fragai, M.; Luchinat, C.; Reichart, F.; Cavallini, C.; Costa, B.; Piccarducci, R.; Taliani, S.; Da Settimo, F.; Martini, C.; Kessler, H.; Novellino, E.; Marinelli, L. Simultaneous Targeting of RGD-Integrins and Dual Murine Double Minute Proteins in Glioblastoma Multiforme. *J. Med. Chem.* **2018**, *61*

(11), 4791–4809.

(20)   Hira, V. V. V.; Verbovšek, U.; Breznik, B.; Srdič, M.; Novinec, M.; Kakar, H.; Wormer, J.; der Swaan, B. Van; Lenarčič, B.; Juliano, L.; Mehta, S.; Van Noorden, C. J. F.; Lah, T. T. Cathepsin K Cleavage of SDF-1α Inhibits Its Chemotactic Activity towards Glioblastoma Stem-like Cells. *Biochim. Biophys. Acta - Mol. Cell Res.* **2017**, *1864* (3), 594–603.

(21)   Nimmagadda, S.; Pullambhatla, M.; Pomper, M. G. Immunoimaging of CXCR4 Expression in Brain Tumor Xenografts Using SPECT/CT. *J. Nucl. Med.* **2009**, *50* (7), 1124–1130.

(22)   Khan, M. Z.; Shimizu, S.; Patel, J. P.; Nelson, A.; Le, M. T.; Mullen-Przeworski, A.; Brandimarti, R.; Fatatis, A.; Meucci, O. Regulation of Neuronal P53 Activity by CXCR4. *Mol. Cell. Neurosci.* **2005**, *30* (1), 58–66.

(23)   Najafi, M.; Salehi, E.; Farhood, B.; Nashtaei, M. S.; Hashemi Goradel, N.; Khanlarkhani, N.; Namjoo, Z.; Mortezaee, K. Adjuvant Chemotherapy with Melatonin for Targeting Human Cancers: A Review. *J. Cell. Physiol.* **2019**, *234* (3), 2356–2372.

(24)   Wang, C. L.; Wang, J. Y.; Liu, Z. Y.; Ma, X. M.; Wang, X. W.; Jin, H.; Zhang, X. P.; Fu, D.; Hou, L. J.; Lu, Y. C. Ubiquitin-Specific Protease 2a Stabilizes MDM4 and Facilitates the P53-Mediated Intrinsic Apoptotic Pathway in Glioblastoma. *Carcinogenesis* **2014**, *35* (7), 1500–1509.

(25)   Mercurio, L.; Ajmone-Cat, M. A.; Cecchetti, S.; Ricci, A.; Bozzuto, G.; Molinari, A.; Manni, I.; Pollo, B.; Scala, S.; Carpinelli, G.; Minghetti, L. Targeting CXCR4 by a Selective Peptide Antagonist Modulates Tumor Microenvironment and Microglia Reactivity in a Human Glioblastoma Model. *J. Exp. Clin. Cancer Res.* **2016**, *35* (1), 1–15.

(26)   Guo, S.; Xiao, D.; Liu, H.; Zheng, X.; Liu, L.; Liu, S. Interfering with CXCR4 Expression Inhibits Proliferation, Adhesion and Migration of Breast Cancer MDA-MB-231 Cells. *Oncol. Lett.* **2014**, *8* (4), 1557–1562.

(27)   Nuti, E.; Casalini, F.; Santamaria, S.; Gabelloni, P.; Bendinelli, S.; Da Pozzo, E.; Costa, B.; Marinelli, L.; La Pietra, V.; Novellino, E.; Margarida Bernardo, M.; Fridman, R.; Da Settimo, F.; Martini, C.; Rossello, A. Synthesis and Biological Evaluation in U87MG Glioma Cells of (Ethynylthiophene)Sulfonamido-Based Hydroxamates as Matrix Metalloproteinase Inhibitors. *Eur. J. Med. Chem.* **2011**, *46* (7), 2617–2629.

(28)   Daniele, S.; Costa, B.; Zappelli, E.; Da Pozzo, E.; Sestito, S.; Nesi, G.; Campiglia, P.; Marinelli, L.; Novellino, E.; Rapposelli, S.; Martini, C. Combined Inhibition of

AKT/MTOR and MDM2 Enhances Glioblastoma Multiforme Cell Apoptosis and Differentiation of Cancer Stem Cells. *Sci. Rep.* **2015**, *5* (9956), 1–14.

(29)   Liu, G.; Yuan, X.; Zeng, Z.; Tunici, P.; Ng, H.; Abdulkadir, I. R.; Lu, L.; Irvin, D.; Black, K. L.; Yu, J. S. Analysis of Gene Expression and Chemoresistance of CD133+ Cancer Stem Cells in Glioblastoma. *Mol. Cancer* **2006**, *5* (67), 1–12.

(30)   Daniele, S.; Giacomelli, C.; Zappelli, E.; Granchi, C.; Trincavelli, M. L.; Minutolo, F.; Martini, C. Lactate Dehydrogenase-A Inhibition Induces Human Glioblastoma Multiforme Stem Cell Differentiation and Death. *Sci. Rep.* **2015**, *5* (September), 1–17.

(31)   Daniele, S.; Sestito, S.; Pietrobono, D.; Giacomelli, C.; Chiellini, G.; Di Maio, D.; Marinelli, L.; Novellino, E.; Martini, C.; Rapposelli, S. Dual Inhibition of PDK1 and Aurora Kinase A: An Effective Strategy to Induce Differentiation and Apoptosis of Human Glioblastoma Multiforme Stem Cells. *ACS Chem. Neurosci.* **2017**, *8* (1), 100–114.

(32)   Daniele, S.; Pietrobono, D.; Costa, B.; Giustiniano, M.; La Pietra, V.; Giacomelli, C.; La Regina, G.; Silvestri, R.; Taliani, S.; Trincavelli, M. L.; Da Settimo, F.; Novellino, E.; Martini, C.; Marinelli, L. Bax Activation Blocks Self-Renewal and Induces Apoptosis of Human Glioblastoma Stem Cells. *ACS Chem. Neurosci.* **2018**, *9* (1), 85–99.

Chapter 4
Targeting PD-1/PD-L1 axis

4.1. Brief Introduction

PD-1 is a cell-surface receptor expressed by CD8^{+} T cells on activation, during priming or expansion. It is now known that TME can prompt overexpression of the PD-1 receptor on infiltrated T cells, while its physiological ligand PD-L1 is overexpressed on tumor cell membranes. [1,2]

PD-1 is a type I transmembrane receptor of 288 amino acids (about 31,6 kDa) composed by 3 domains: extracellular, transmembrane and Cytoplasmatic (Figure 1A). The extracellular domain (red in Figure 1A) assumes a b-sandwich immunoglobulin-variable (IgV)-type topology conformation through a disulfide bridge between Cys54 and Cys123. [10]

Similarly to PD-1, PD-L1 is composed by 290 amino acids (about 33,3 kDa) divided in extracellular, transmembrane and cytoplasmatic domain (Figure 2A). Its extracellular domain (red in Figure 2A) is characterized by the Ig V-type topology, as in PD-1. [10]

```
A   000   MQIPQAPWPVVWAVLQLGWRPGWFLDSPDRPWNPPTFSPALLVVTEGDNA
    050   TFTCSFSNTSESFVLNWYRMSPSNQTDKLAAFPEDRSQPGQDCRFRVTQL
    100   PNGRDFHMSVVRARRNDSGTYLCGAISLAPKAQIKESLRAELRVTERRAE
    150   VPTAHPSPSPRPAGQFQTLVVGVVGGLLGSLVLLVWVLAVICSRAARGTI
    200   GARRTGQPLKEDPSAVPVFSVDYGELDFQWREKTPEPPVPCVPEQTEYAT
    288   IVFPSGMGTSSPARRGSADGPRSAQPLRPEDGHCSWPL

B   000   MRIFAVFIFMTYWHLLNAFTVTVPKDLYVVEYGSNMTIECKFPVEKQLDL
    050   AALIVYWEMEDKNIIQFVHGEEDLKVQHSSYRQRARLLKDQLSLGNAALQ
    100   ITDVKLQDAGVYRCMISYGGADYKRITVKVNAPYNKINQRILVVDPVTSE
    150   HELTCQAEGYPKAEVIWTSSDHQVLSGKTTTTTNSKREEKLFNVTSTLRIN
    200   TTTNEIFYCTFRRLDPEENHTAELVIPELPLAHPPNERTHLVILGAILLC
    290   LGVALTFIFRLRKGRMMDVKKCGIQDTNSKKQSDTHLEET
```

Figure 1. Amino acid sequence of PD-1 (A) and PD-L1 (B). The signal peptide is reported in black, the extracellular domain in red, the transmembrane domain in yellow and the cytosolic domain in green.

In according to crystal structure (figure 2, PDB:4ZQK) interaction between PD-1 and PD-L1 occurs through the two extracellular domains and resembles that one between the Ig V domains of antibodies and T-cell receptors. This contact involves hydrophobic and

polar interactions around a central hydrophobic core of both extracellular domains, in particular involving non-polar residues of PD1 Val64, Ile126, Leu128, Ala132, Ile134 and those of PD-L1 Ile54, Tyr56, Met115, Ala121, Tyr123. [10]
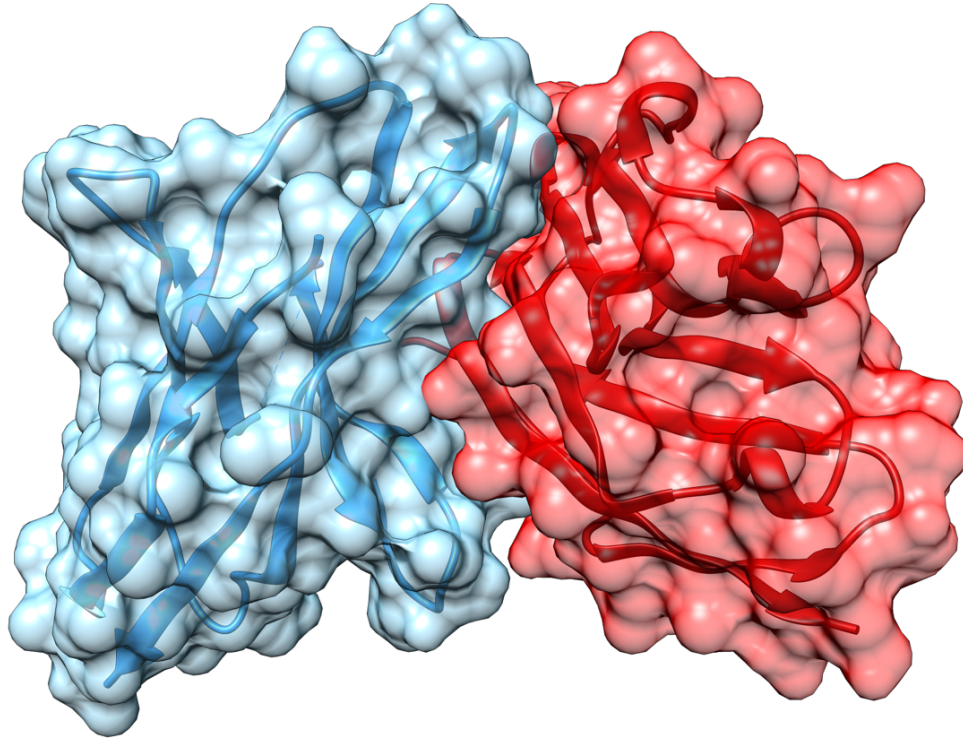

Figure 2. Crystal structure (PDB:4ZQK) of PD-1(light blu)/PD-L1 (red) complex.

PD-1/PD-L1 recognition and binding generate an inhibitory signal that attenuates the activity of T cells in cancer patients, thus inhibiting the antitumor immunity and causing T-cell exhaustion. The 'exhaustion' of effector T (T-eff) cells was found to be an important negative feedback loop that ensures immune homeostasis against cancer. In this perspective, the PD-1/PD-L1 axis can be impaired by targeting either PD-1 or PD-L1 with antibodies. In fact, two PD-1 specific mAbs, Pembrolizumab (Keytruda by Merck)[3] and Nivolumab (Opdivo by Bristol-Myers Squibb)[4], were among the first clinical proofs that cancer can be treated through the modulation of the immune response.[5] Following this success, PD-L1 specific antibodies (atezolizumab, durvalumab, atezolizumab, avelumab) entered the marked too.[6,7] At present, anti-PD-1/anti-PD-L1 antibodies have been tested in more than 1000 clinical trials and approved for several cancers including melanoma, renal cell carcinoma, Hodgkin's lymphoma, bladder cancer, head and neck squamous cell carcinoma (HNSCC), and more recently non-small cell lung cancer (NSCLC).[8,9] However, despite their remarkable success in patients bearing a particular

type of tumor, antibodies have specific well known drawbacks as therapeutics, including but not limited to high production costs, lack of oral bioavailability, long circulating half-life, poor tissue and tumor penetrating capacity,[10] and immune-related adverse events.[11] In the attempt to overcome some of these problems, a number of small molecules, such as macrocyclic peptides, and organic compounds targeting PD-L1 have been reported, primarily in patent applications.[12-33] Bristol-Myers Squibb (BMS) was the first company to patent a series of dibenzyl ether-based compounds (BMS-202, see Figure 3), able to disrupt the PD-1/PD-L1 complex with an IC_{50} ranging from 1 to 300 nM.[12,13] Only in 2015, the structural basis for the human PD-1/PD-L1 protein-protein interaction (PPI) was unraveled by X-ray crystallography[2]. Later on, structures of PD-L1 in complex with antibodies, peptide macrocycles and small organic compounds (eg. BMS202) have been released too,[14–16] revealing that ligands can recognize partially overlapping regions on the PD-L1 surface.[15,17–20] However, the flat and hydrophobic binding surface of PD-L1 made immediately clear that the rational design of small inhibitors would have been all but easy. In this scenario, the discovery of BMS202 has represented a precious starting point for ligand-based design or "me too" strategies that led to the discovery of compounds 1-5 (Figure3).[25,-27,29,31]

BMS202
$IC_{50} = 18$ nM

1
$IC_{50} = 92.3$ nM

2
$IC_{50} = 132$ nM

3
$IC_{50} = 15$ nM

4
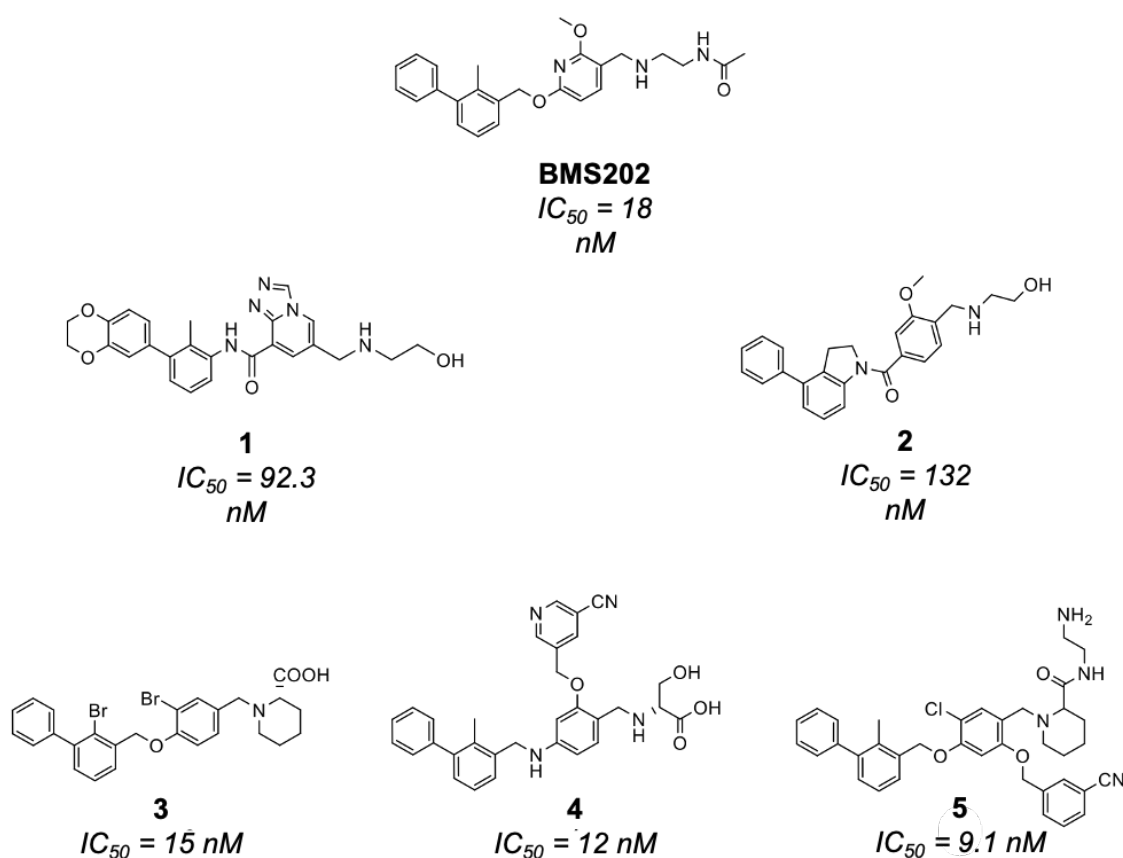$IC_{50} = 12$ nM

5
$IC_{50} = 9.1$ nM

Figure 3. Chemical structures of representative small molecules as direct inhibitors of PD-L1/PD-1 binding

Thus, a number of studies aiming at the evaluation of the *in vivo* anti-cancer properties of the biphenyl-based compounds are quickly arising. Although some studies are of doubtful value with respect to PD-L1-dependent effects in mice, as 1 has been used in animal models expressing mouse PD1/PD-L1[25] and evidence exist that BMS202 does not bind mouse PD-L1,[26] thus some off-target should be responsible of the anticancer results, other studies seem more meaningful and promising in this respect. For example, 4 and 5 was challenged in an immune checkpoint humanized mouse model demonstrating to be highly effective in suppressing tumor growth, [22,23] thus prompting further development of biphenyl-based compounds. In fact, development of structurally new PD-L1 small ligands would be of the outmost importance for a complete understanding of the full potentialities of small molecule PD-L1/PD-1 inhibitors.

4.2. Results and Discussion

This paragraph describes all studies and all results obtained during my three years of PhD regarding PD-1/PD-L1 project. The first paragraph concerns the computational studies applied on hPD-1/hPD-L1 axis to due to discover and develop new inhibitors, the successive analysis and experiments achieved by NMR ad integrated methodologies. The last section of this paragraph describes further tests carried out, in collaboration with other research groups, to quantify and characterize the interaction between the hPD-L1 and our compounds, quantitatively tests such as HTFR, DSC and in vitro tests.

I was involved in of hPD-L1 inhibitors design, starting from literature studies. Few macrocyclic peptides and organic molecules developed by Bristol-Myers Squibb (BMS) have been recently well characterized in their exact mechanism of action. [15,27] BMS was the first company to patent a series of dibenzyl ether-based compounds (eg. BMS-202, see Figure 3 and 4), able to disrupt the PD-1/PD-L1 complex with an IC50 ranging from 1 to 300 nM. Indeed, a macrocyclic compound has been crystallized in complex with PDL-1[2], as well as an organic molecule (BMS-202).[14]

The BMS-202/PD-L1 X-ray complex together with some biochemical data revealed that upon binding BMS-202 induces the dimerization of PD-L1, so that the latter protein can't interact with its receptor PD-1. [14] This X-ray complex (PDB code 5J89) show that the polar arm in BMS-202 (see Figure 3 and 4) is a key element for binding.
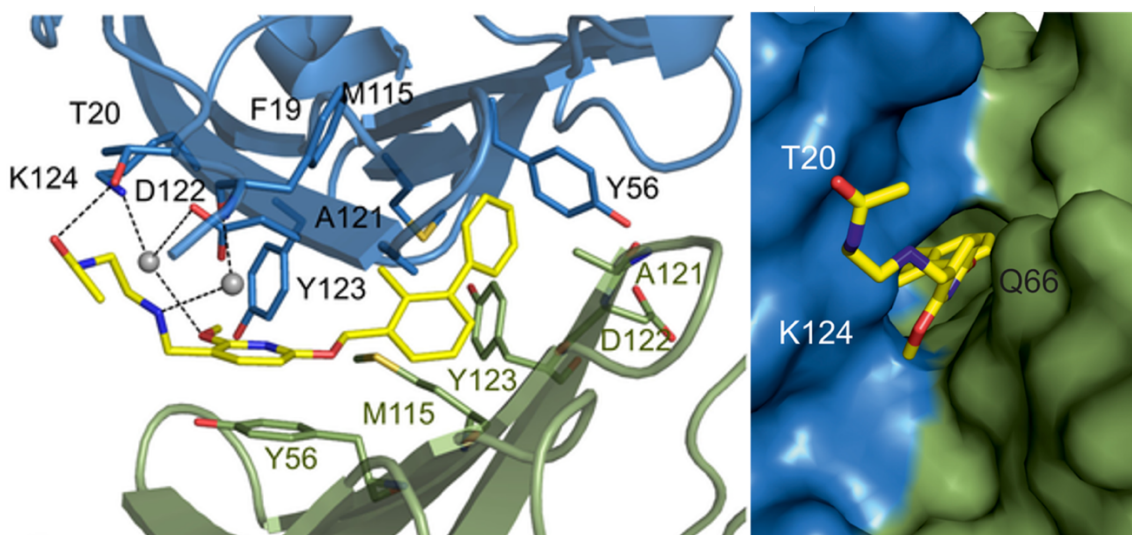

Figure 4 Detailed interactions of BMS-202 at the binding cleft of PD-L1 dimer (adopted from Krzysztof M. Zak, Tad A Holak et al. [3])

In this scenario, the discovery of BMS202 has represented a precious starting point for ligand-based design or "me too" strategies that led to the discovery of compounds 1-5 (Figure 3). [21–23,28–31] Thus, a number of studies aiming at the evaluation of the in vivo anti-cancer properties of the biphenyl-based compounds are quickly arising.[22,23,25,26] Aware that the biphenyl ether moiety in BMS202 and in compounds 1-5 is the driving group for PD-L1 surface binding [21] and that a central aromatic core is necessary to oppositely orient the two main PD-L1 interacting chains, in collaboration of research group of Prof. Seneci of University of Milano, we looked for an accessible and synthetically flexible ring replacement.

We selected one new core, conscious that its electrostatic properties are substantially diverse with respect to the pyridine ring (core of BMS202) and benzene (core of 1-5), and we selected two different substitutions on this central core despite the relative orientation of substituents are similar but not fully superimposable (para-orientation in the most active compounds, meta-orientation in our molecules).

Unfortunately, now I can't show the structures of these compounds because they are in the process of publication and patent.

The two compounds' series were synthesized, qualitatively tested by 1D ^{1}H-NMR, and then quantitatively tested through a homogeneous time-resolved fluorescence (HTRF) binding assay, that furnished an IC_{50} for each binder found through NMR.

One of them, a disubstituted compound, was identified as the most potent early lead and through NMR was shown to specifically bind PD-L1 and not to PD-1. Moreover, two biotinylated, either trisubstituted or disubstituted derivatives were synthetized and used in immunofluorescent double-staining experiments on four different cell lines expressing diverse levels of PD-L1, to demonstrate the capability of our compounds to bind PD-L1 cell membranes, besides the isolated protein.

In order to elucidate at an atomistic level, the binding mode of our most potent compound at the PD-L1 receptor, molecular docking studies were performed. As for the protein tridimensional structure selection, the X-ray complex of homodimeric PD-L1 (monomers A and B) with the known inhibitor BMS202 (PDB code: 5J89) [14] was chosen, based on the structural similarity between this compound and our binder. Docking of our binder predicted that this molecule can be hosted, similarly to BMS202, in the so-called cylindrical hydrophobic pocket defined at the interface between the two PD-L1 monomers. [16] In detail, the 2-methylbiaryl moiety deepens in the bottom part of the binding site, engaging a T-shaped stacking interaction with the phenol moiety of $_A$Y56 as well as multiple lipophilic contacts with the sidechains of $_A$M115, $_B$M115 and $_B$A121 analogously to what found for BMS202. Besides, while new core establishes a π-stacking with the $_B$Y56 side chain, the hydrophilic alkylamino chain interacts through water-bridge with the side chains of $_A$K124 and $_A$D122, and H-bonds with the cationic head of $_A$K124. Although, the predicted binding mode of our compound is mostly superimposable with the crystallographic pose of BMS202, important differences arise in the positioning of the central cores and in the interaction between the polar side chains and the receptor amino acids. The above-mentioned diversities are mostly due to the fact that our new core, differently from the pyridine, does support the *meta-* and not the *para*-substitution, thus it spatially rearranges itself toward the Y123 to properly orient the biphenyl moiety and the polar side chain along with the cylinder-shaped pocket. Moreover, the polar chain

of our compound lacks a methylene unit connecting the hydrophilic alkylamino chain group, with respect to BMS202. This variation could probably be responsible for the different binding affinity of the two compounds. In fact, looking at the predicted binding pose, the aminoethyl group of our compound seems not optimized to H-bond the $_AD22$ side chain as for BMS202, due the reduced basicity and altered spatial arrangement of the same group. This provides useful information about the ideal chemical requirements of the ligand polar chain, which will be exploited in a next lead optimization cycle.

As mentioned above, the two compounds' series were qualitatively tested by 1D ^{1}H-NMR, in fact in second part of my PhD project I've been working on expression, extraction and purification samples of hPD-L1 and hPD-1 in order to analyze the two proteins obtained in their free state and then evaluate their interaction with the designed ligands, through NMR experiments.

I started working on expression, extraction and purification samples of hPD-L1 and hPD-1 not labeled and ^{15}N-labeled, as described by Holak et al. [14,15] implementing the extraction method through multiple cycles of sonication and buffers, as widely described in method chapter (6.2.2)

It is well known that the dimeric state of hPD-L1 is obtained only in the presence of a binder, while in solution it is monomeric. Therefore, it was essential to assess that the recombinant protein expressed was indeed monomer. Size exclusion chromatography and SDS-PSAGE were carried out (Figure 5) on nl-hPD-L1, ^{15}N-hPD-L1, nl-hPD-1 and ^{15}N-hPD-1 samples. These techniques proved that the proteins were in monomeric state.
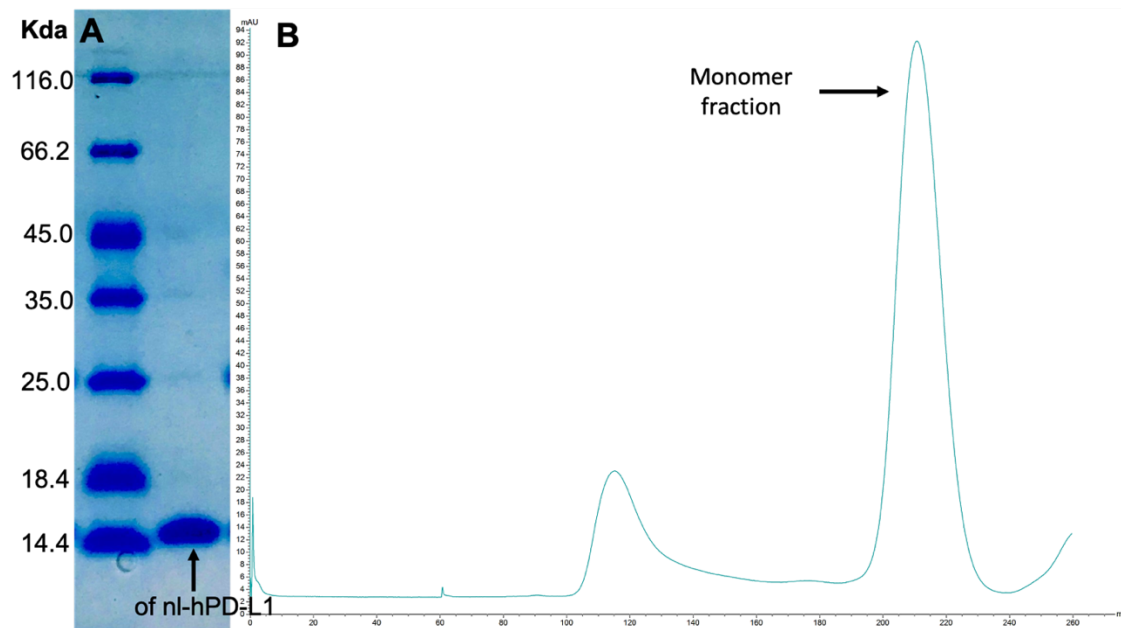
Figure 5 SDS-PAGE gel (A) and gel-filtration chromatogram (B) of nl-hPD-L1

Assessed the monomeric structures of the h-PD-1 and h-PD-L1, not labelled and labelled samples were used to analyze the proteins folding. In collaboration with research group of Prof. Fragai of CERM, University of Firenze, we used the nuclear magnetic resonance spectroscopy for this purpose.

Therefore, 1D-^{1}H NMR and HSQC spectra were acquired on free hPD-1 and hPD-L1 protein
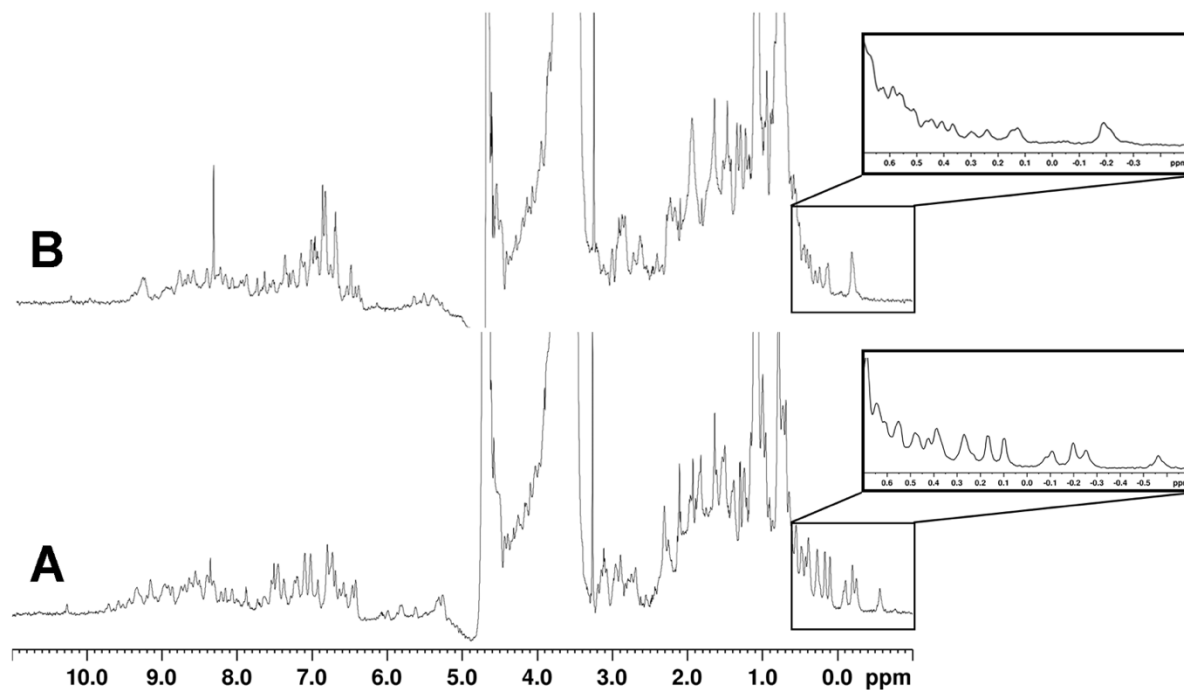
Figure 6 1D-^{1}H NMR spectra of 10 μM hPD-L1 (B) and hPD-1 (A) in 10 mM Tris-HCl, pH 8.0, 20 mM NaCl buffer and 10% D$_2$O,

As shown in Figure 6, in 1D-^{1}H NMR spectra of 10 μM hPD-L1 (B) and hPD-1 (A) in 10 mM Tris-HCl, pH 8.0, 20 mM NaCl buffer and 10% D$_2$O, the methyl signals under 0 ppm and the NH signals at 9-10 ppm indicate that protein is folded in the proper way. The methyl signal under 0 ppm indicates the presence of a hydrophobic region like a binding pocket and the good dispersion of NH signals at 9-10 ppm indicates the presence of tertiary and secondary structures of proteins.

With these preliminary results in hand, we acquired 2D ^{1}H–^{15}N HSQC spectra of the free state uniformly ^{15}N-labeled proteins.

The hPD-1 2D ^{1}H–^{15}N HSQC spectrum was compared with that deposited on the BMRB website (code: 18908). The two HSQC spectra are similar. This confirms unequivocally the proper folding of hPD-1 obtained with the expression and purification procedure previously shown.

As regard PD-L1 unfortunately there is no reference HSQC spectrum, as for PD-1. Analysis of the HSCQ spectrum, together with the 1D-^{1}H spectrum, however, indicates that the hPD-L1 protein obtained with the expression and purification procedure previously shown is folded in the proper way.
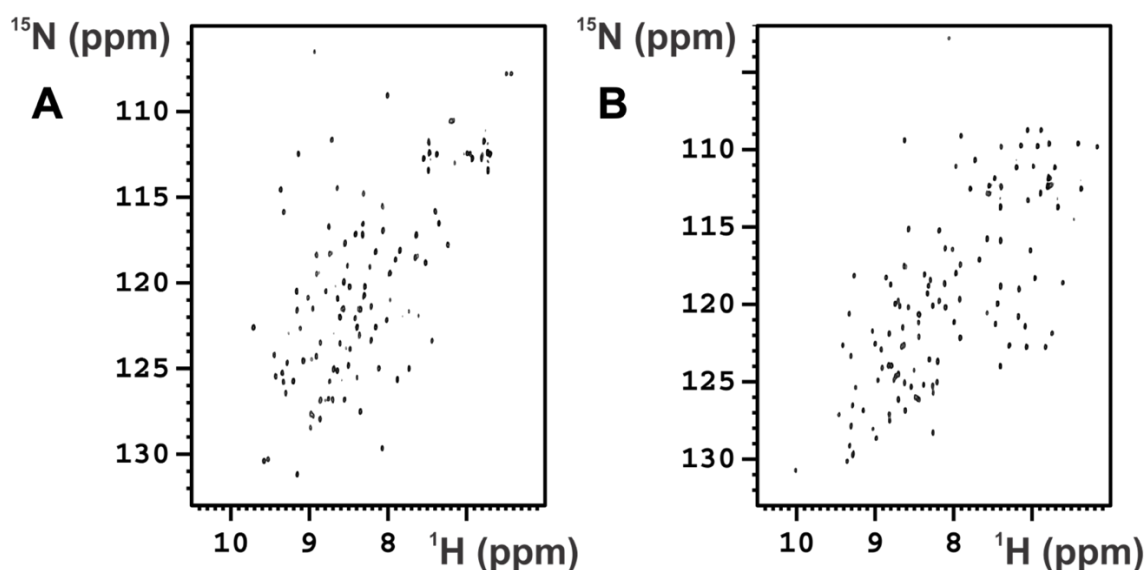
Figure 7 2D ^{1}H–^{15}N HSQC spectra of 50 μM ^{15}N-hPD-1 (A) and ^{15}N-hPD-L1 (B) in 10 mM Tris-HCl, pH 8.0, 20 mM NaCl buffer and 10% D$_2$O,

Assessed the monomeric structure and the correct folding of the proteins, 1D ^{1}H Macromolecule-based NMR experiments were used to detect the interaction between the hPD-L1 protein not labelled, expressed and purified as described in methods chapter (6.2.2) [14,15], and the our small library of synthesized compounds. 1D ^{1}H NMR spectra of 10 μM PD-L1 nl were acquired in the presence of different ligands (protein:ligand ratio equal to 1:1 and 1:10), and the NMR proton line width of the protein signals were analyzed to discover a new binding ligand. Particularly, in such experiments, the chemical shift as well as the decreases of the resonance signals intensities of PD-L1 were monitored to follow the formation of the ligand-protein complex (Figure 8).

In the present NMR assay, we have compared the 1D ^{1}H NMR spectra of PD-L1 in the presence of the new investigated ligands with those of free PD-L1 and PD-L1 in the presence of the well-known binder BMS-202, which has been exploited as reference control.

As an example, Figure 8 shows the comparison among the 1D ^{1}H NMR spectra of the free protein (Figure 8 c), the protein in presence of BMS-202 (Figure 8 b), and the protein in presence of the newly identified binder (Figure 8 a). When BMS202 is added to hPDL-1, also at stoichiometric ratio, a decrease in the intensity of the signals of the free protein, as well as the appearance of new signals, is observed (Figure 8 b). Comparable results were obtained with our compound (Figure 8 a). In fact, the 1D ^{1}H-NMR spectrum of PD-L1 in the presence of this compound is similar to that of PD-L1 induced by the presence of BMS202. The line broadening of the signals of the two protein-ligand complexes is similar and much larger than that of the free protein (Figure 8 c). This confirms unequivocally the formation of our compound-PD-L1 complex, presumably very similar to that of the BMS202-PD-L1 complex since the spectra of the two complexes are comparable. The formation of the complex between PD-L1 and the above-mentioned ligands is better highlighted in the comparison of the aliphatic regions of the spectra of the free protein (Figure 8 c) and in presence of BMS-202 (Figure 8 b) and our compound (Figure 8 a).

Noteworthy, comparing the NMR spectra (Figure 8), it is clear how 1D ^{1}H Macromolecule-based NMR experiment was effective in the identification of new of PD-

L1 binders, even if a quantitative evaluation of the binding potency is not feasible with this methodology.
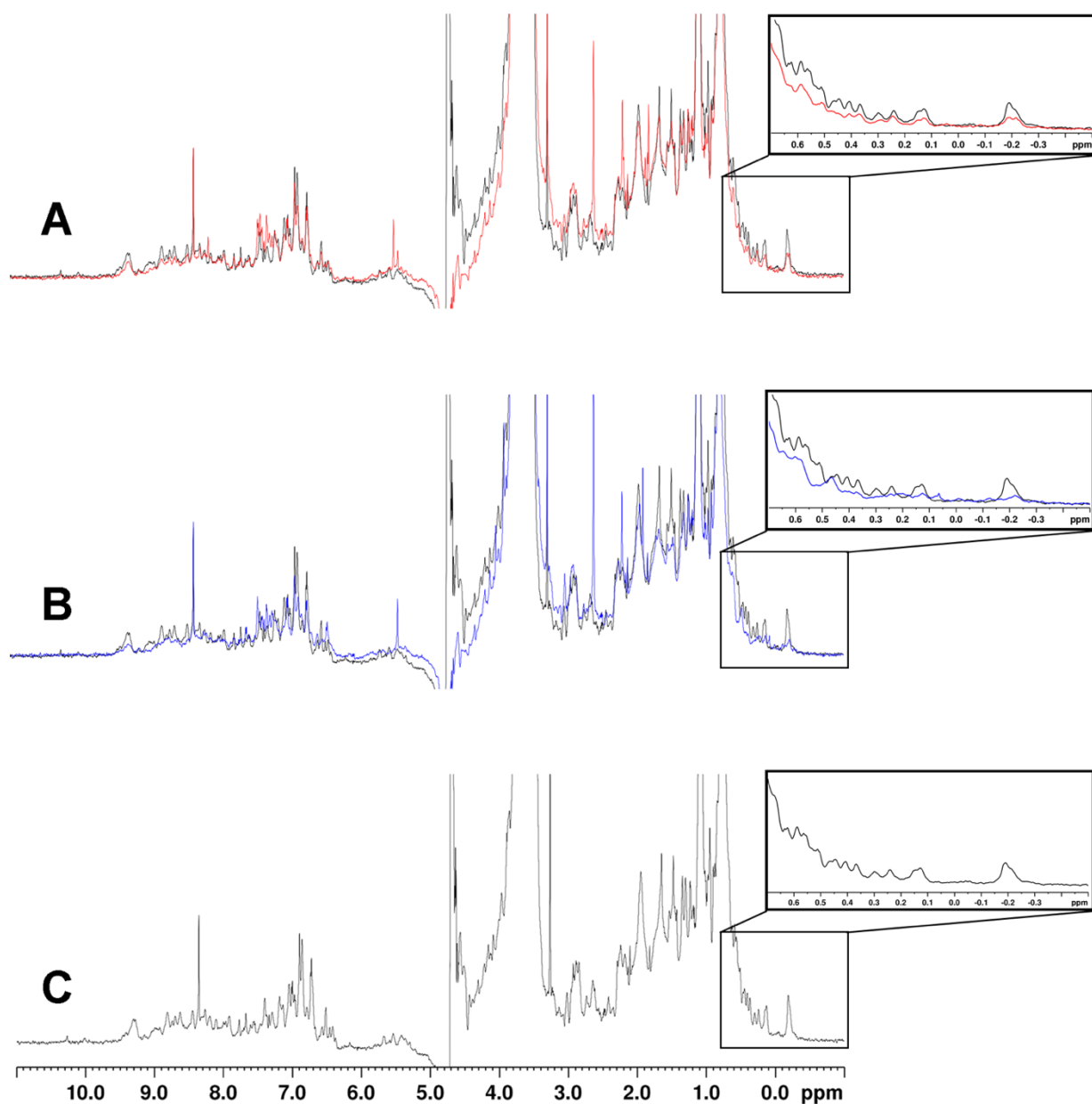

Figure 8. 1D-1H NMR spectra of PDL1 (10 mM) in absence (C, black), and in presence of BMS-202 (B, blue) and our binder (A, red)

Further 1D 1H experiments based on NMR macromolecule were carried out to detect the non-interaction between the protein hPD-1 not labelled, expressed and purified as previously described in the methods chapter (6.3.5) [14,15] and our most potent binder

In this NMR experiment, we have compared the 1D ^{1}H NMR spectra of hPD-1 in absence (Figure 9 B) and in presence of our compound (Figure 9A). As shown in figure 9A, the two spectra are perfectly identical. This confirms unequivocally the non-interaction between hPD-1 and our compound.
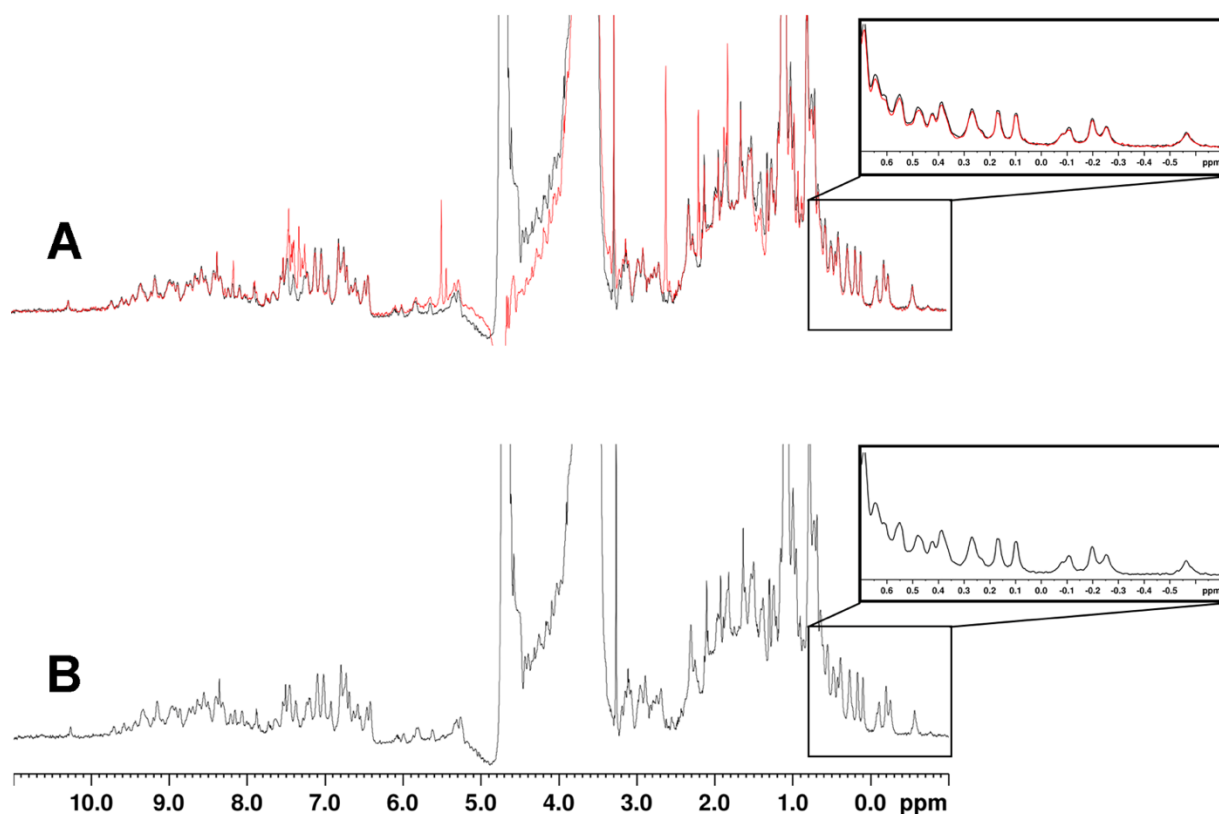

Figure 9. 1D-1H NMR spectra of PD-1 (10 mM) in absence (B, black), and in presence of our binder (A, red)

In the end, using HSQC NMR experiment, we have been investigated the binding mode of BMS-202 and our most potent binder on PD-L1 protein; and the effect of BMS-202 and our binder on the dissociation of PD-1/PD-L1 complex.

The binding mode of BMS-202 on PD-L1 protein has been investigated by monitoring the changes in cross-peak intensity ratio (I/I_0) occurring in the 2D ^{1}H–^{15}N HSQC spectrum of the uniformly ^{15}N-labeled protein upon the addition of increasing amounts (to reach concentrations of 6.25, 12.5, 18.75, 25, 50 μM) of BMS-202 (solubilized in DMSO-d6), versus the free protein in solution (I_0). The concentration of the protein used

for the NMR titrations was 50 μM in 10 mM Tris buffer at pH 8 with 20 mM NaCl (with proteases inhibitors and 0.1% NaN_3 to preserve the protein stability).

During the NMR titration the cross-peaks of the free protein decrease in intensity upon the addition of increasing concentrations of the ligand, while new cross-peaks, corresponding to the protein in complex with the ligand, appear and increase in intensity. This indicates that the ligand is in slow exchange regime on the NMR timescale and confirm its expected high affinity towards the protein (IC_{50} 18 nM).[14]

In the presence of BMS-202 at the concentration of 12.5 μM (protein:ligand ratio equal to 1:0.25) the cross-peaks corresponding to the free protein and to the protein bound to the ligand have similar intensities (Figure 10). This is in agreement with the binding mode observed in crystal structure of the PDL1/BMS-202 complex[14], where one molecule of ligand binds 2 protein molecules, by inducing protein dimerization.
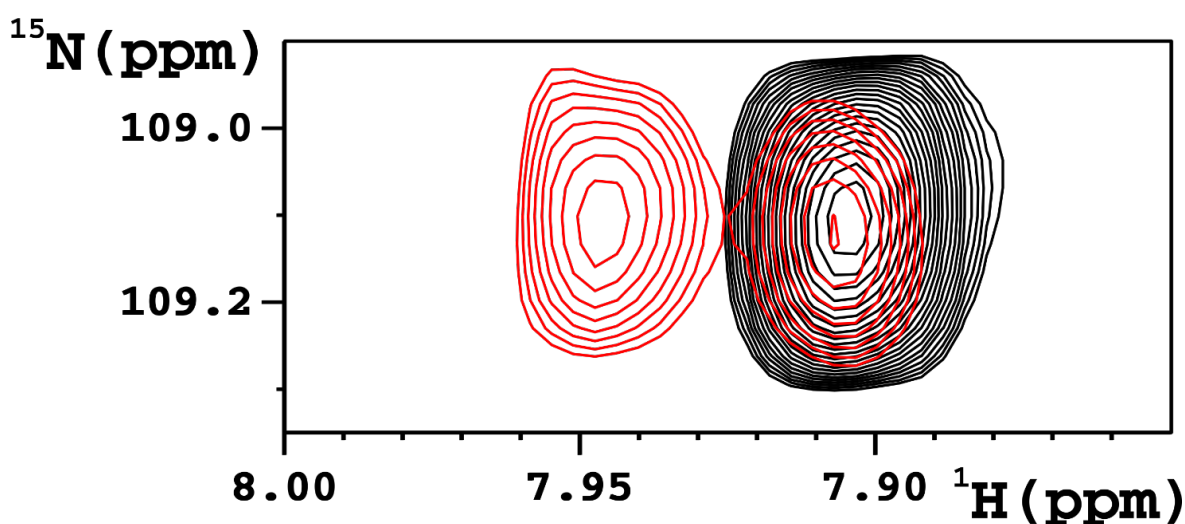

Figure 10. Enlargement of 2D ^1H-^{15}N HSQC spectra of 50 μM free PDL1 (black) and PDL1 in the presence of 12.5 μM BMS-202 (red). The cross-peak displayed is assigned to residue Gly-79.

The residues with the highest decreases in signal intensity at the BMS-202 concentration of 12.5 μM are highlighted in Figure 11.
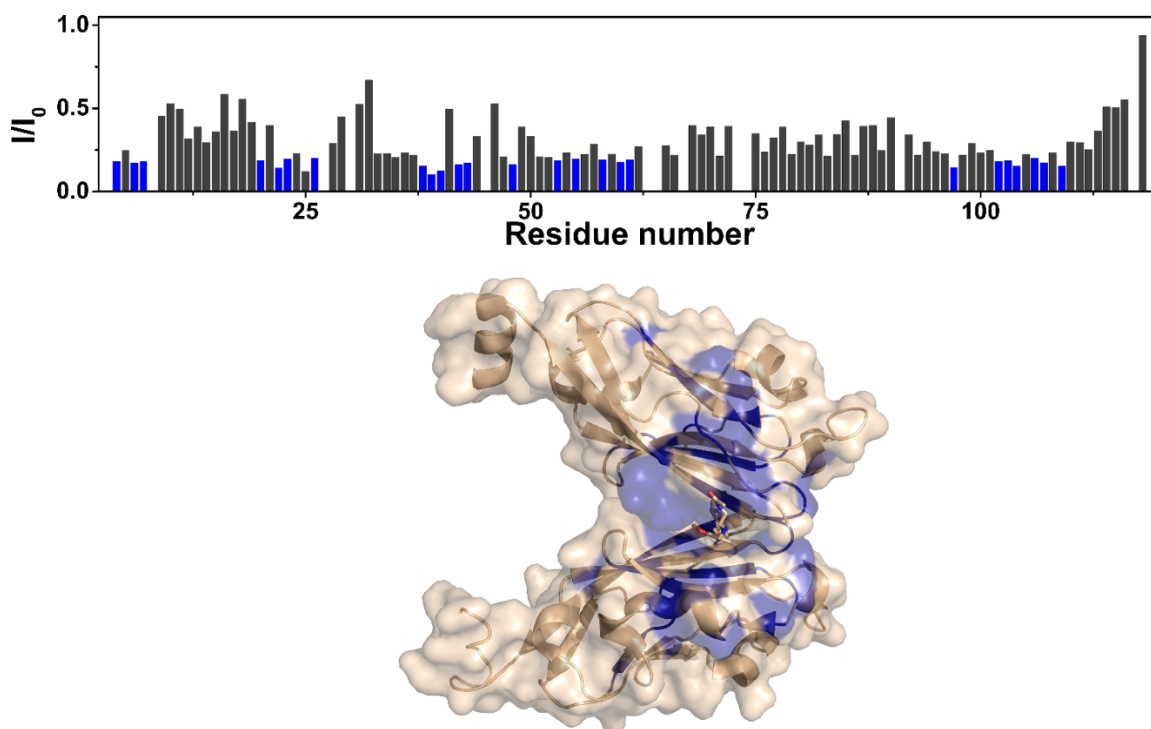
Figure 11. Graphical representation of the intensity changes of PDL1 per residues in the presence of 12.5 µM BMS-202. The residues exhibiting the highest decreases in signal intensities (T4, T6, V7, M20, I22; E23, K25, I38, V39, Y40, E42, M43, I48, H53, E55, L58, V60, Q61, R97, Y102, G103, G104, D106, Y107, R109) have been colored in blue in the plot (A) and on the X-ray structure of the protein in complex with BMS-202 (B) (PDB code: 5J89).

To investigate the binding mode of our binder, a titration in the same conditions used for BMS-202 has been performed. Increasing amounts (to reach concentrations of 6.25, 12.5, 18.75, 25, 50 and 100 µM) of our compound, solubilized in DMSO-d6, were added to the solution of the free protein (at the concentration of 50 µM).

During the NMR titration the cross-peaks of the free protein decrease in intensity upon the addition of increasing concentrations of the ligand, while new cross-peaks, corresponding to the protein in complex with the ligand, appear and increase in intensity. This indicates that the ligand is a in slow exchange regime on the NMR timescale and present a high affinity towards the protein.

In the presence of our binder at the concentration of 12.5 µM (protein:ligand ratio equal to 1:0.25) the signals corresponding to the free protein and to the protein bound to the

ligand display different relative intensities (Figure 12). In particular, the intensity of the signal of the free protein is about the 75% of the total intensity, while the intensity of the signal of the protein bound to ligand is the 25% (Figure 12). This suggests a different high affinity towards the protein respect to the ligand BMS-202.
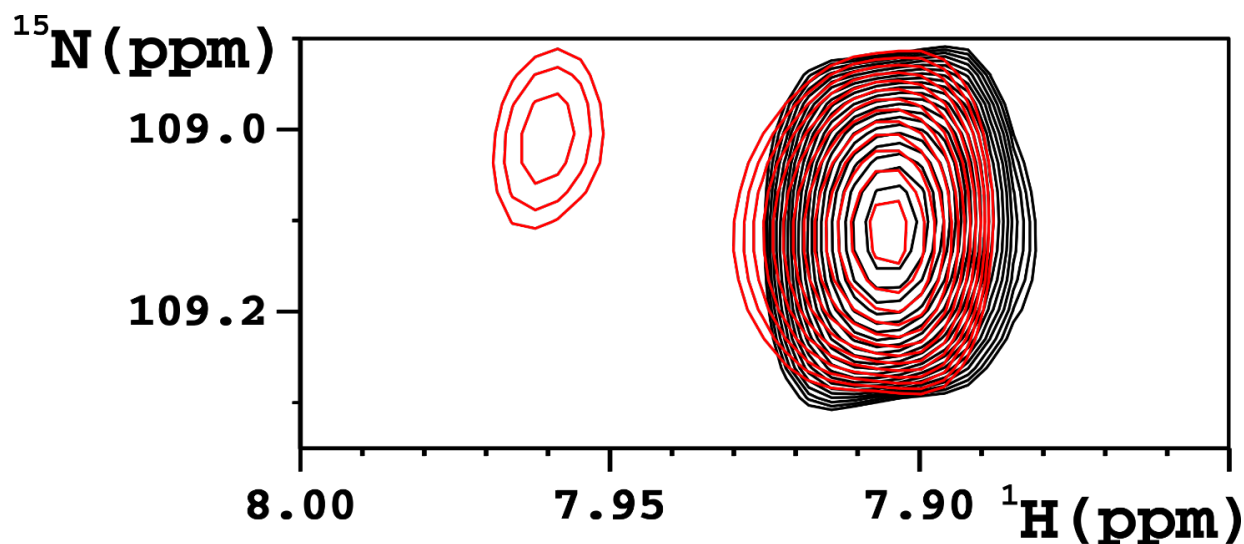

Figure 12. Enlargement of 2D ^{1}H-^{15}N HSQC spectra of 50 μM free PDL1 (black) and PDL1 in the presence of 12.5 μM our bidner (red). The cross-peak displayed is assigned to residue Gly-79.

The residues with the highest decreases in signal intensity at our compound concentration of 12.5 μM are highlighted in Figure 13
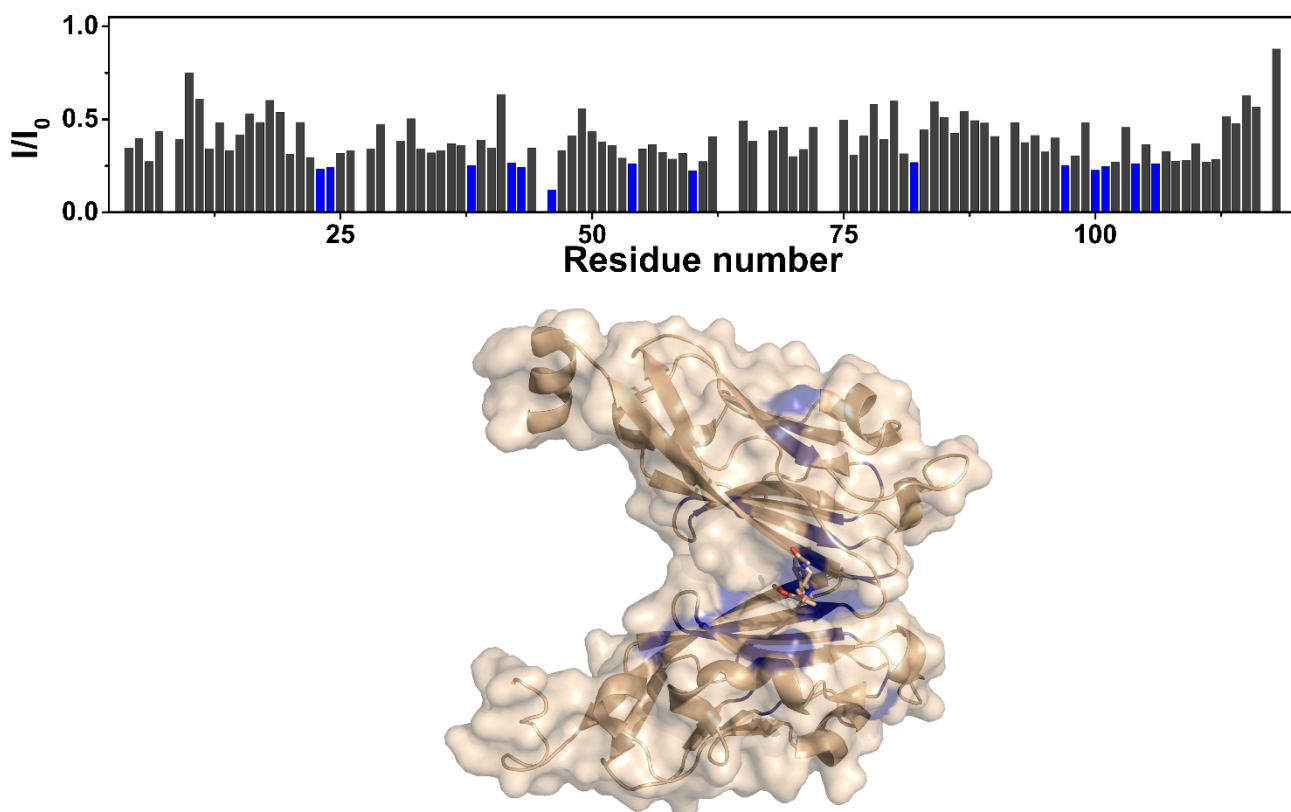
Figure 13. Graphical representation of the intensity changes of PDL1 per residues in the presence of 12.5 μM RS39. The residues exhibiting the highest decreases in signal intensities (E23, C24, I38, E42, M43, K46, G54, V60, A82, R97, I100, S101, G104, D106) have been colored in blue in the plot (A) and on the X-ray structure of the protein in complex with the BMS-202 (B) (PDB code: 5J89).

However, the line broadening of the signals of the two protein-ligand complexes, observed at the end of the titration, is similar and much larger than that of the free protein (Figure 14). The investigation of the mechanism of binding of our compound on hPD-L1 deserve, therefore, further analysis by complementary studies.

Figure 14. Methyl region of 1D ^{1}H spectra of the free protein (red) of the protein in complex with BMS-202 (black, 1:1 ratio) and of the protein in complex with our binder (blue, 1:1 ratio).

The effect of BMS-202 and our binder on the dissociation of PD-1/PD-L1 complex has been evaluated through competition experiments.

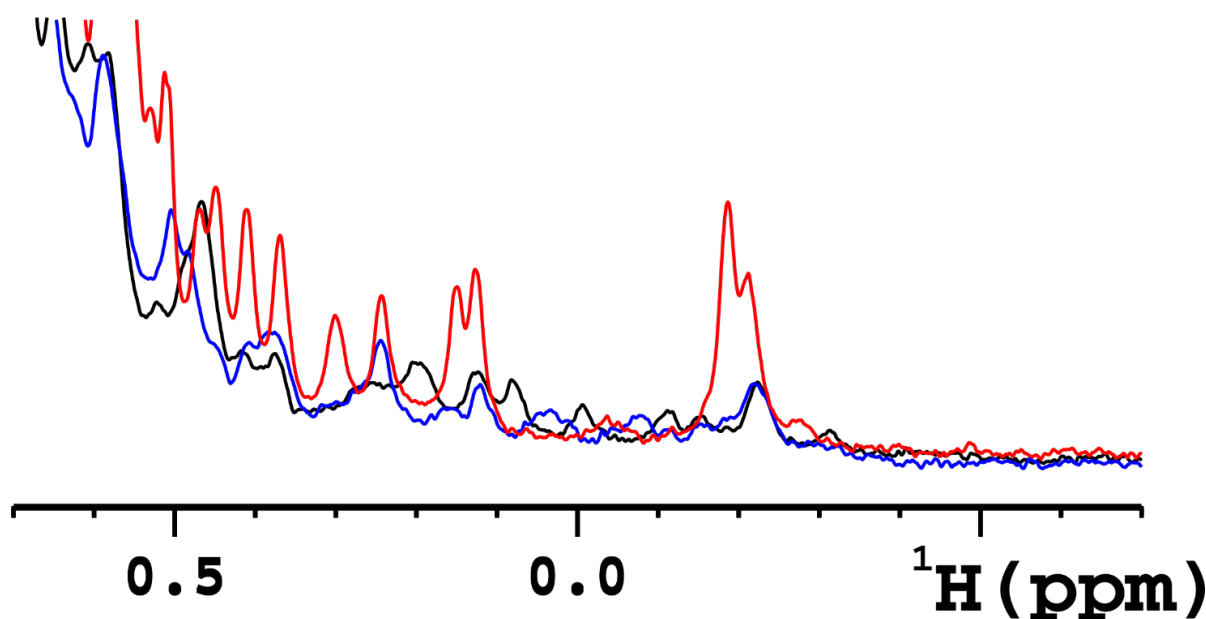First, ^{15}N PD-L1 protein has been titrated with PD-1 protein and the effects monitored through 2D ^{1}H-^{15}N HSQC spectra. Increasing aliquots of PD1 (to reach concentrations of 12.5, 25, 50 37.5, 50, 55 μM) have been added to the solution (1.2 mL) of 50 μM PD-L1 (in 10 mM Tris buffer at pH 8 with 20 mM NaCl, proteases inhibitors and 0.1% NaN$_3$ to preserve the protein stability). During the addition of PD-1 the signals of the free PD-L1 protein decrease in intensity, while simultaneously new cross-peaks, corresponding to the protein-protein complex, appear in the spectra, and increase in intensity with increasing PD-1 concentration. This indicates that the free and bound protein states are in a slow exchange regime on the NMR timescale, as occurs in case of high affinity interactions. Therefore, in our experimental conditions the affinity between the two proteins seems larger (Kd in the nM range) than what has been reported (Kd ~ 8 μM)[14] in other experimental conditions.

The obtained PD-L1/PD-1 complex has been split in two portions, that were titrated with the two different ligands.

The effect of increasing aliquots of BMS-202 (to reach concentrations of 4, 8, 12, 16, 32, 64 μM) on PD-L1/PD-1 complex (32 μM) has been investigated by NMR performing 2D ^{1}H-^{15}N HSQC spectra after each addition of the ligand. During the addition of BMS-202 the cross-peaks corresponding to the PD-L1/PD-1 complex decrease in intensity while new cross-peaks corresponding to the PD-L1/BMS-202 complex appear (Figure 15).

Figure 15. Enlargement of 2D ^{1}H-^{15}N HSQC spectra of PD-L1/PD-1 complex (black), PD-L1/BMS-202 complex (blue) and PD-L1/PD-1 complex (32 μM) in the presence of 16 μM BMS-202 (complex: BMS-202 in 1:0.5 ratio, red).

In the presence of PD-1, the same effects of BMS-202 on PD-L1 protein are visible for higher concentrations of the ligand since different equilibria are present in solution.

At the ligand concentration of 50 μM, however, the PD-1/PD-L1 complex was almost completely dissociated and the complex between PD-L1 and BMS-202 formed. Complete disappearance of the signals of PD-1/PD-L1 complex is observed in the presence of 2 equivalents of the ligand with respect to PD-L1/PD-1 complex.

The effect of increasing aliquots of our binder (to reach concentrations of 4, 8, 12, 16, 32, 64, 160 μM) on PD-L1/PD-1 complex (32 μM) has been investigated by NMR performing 2D ^{1}H-^{15}N HSQC spectra after each addition of the ligand. During the first additions of this compound, few effects are visible and only at high ligand concentrations the cross-peaks corresponding to the PD-L1/PD-1 complex start decreasing in intensity, and new peaks, with low intensity, corresponding to the PD-L1/binder complex appear (Figure 16).
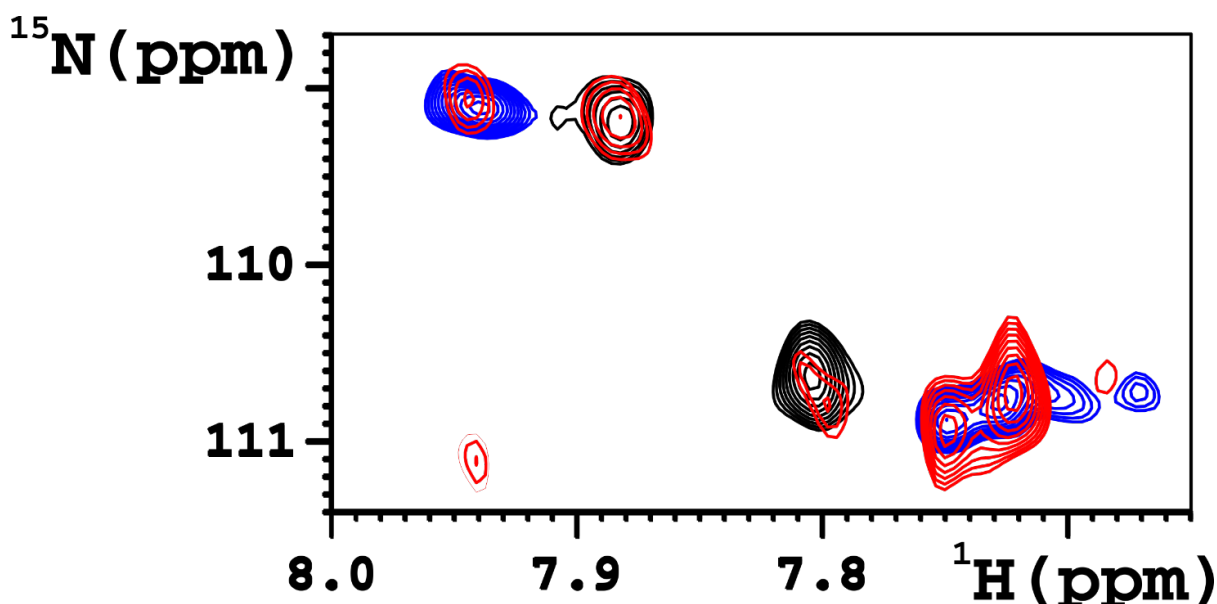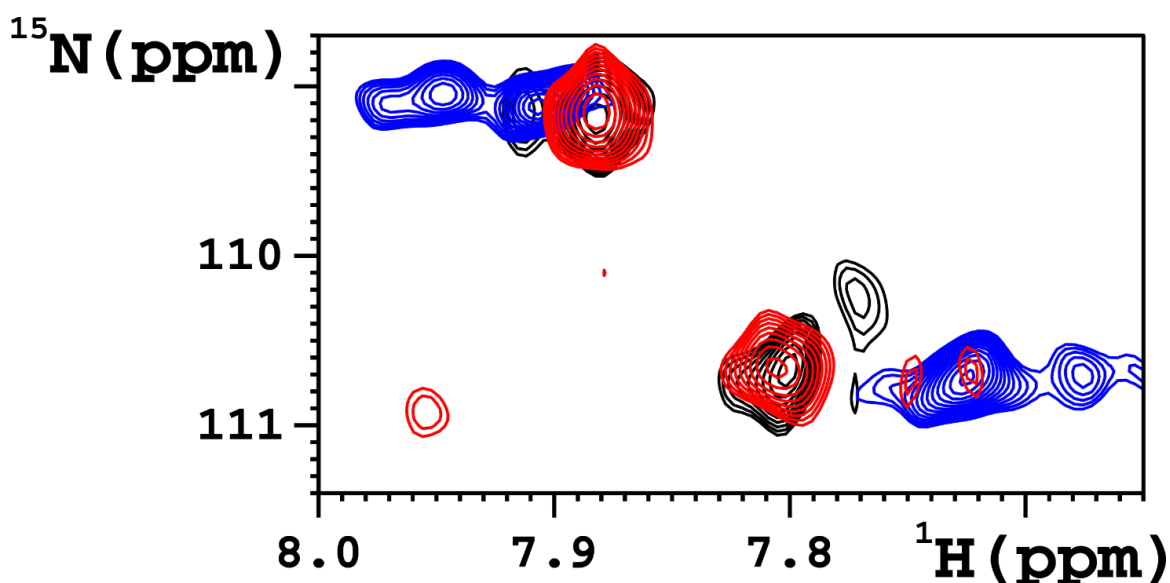
Figure 16. Enlargement of 2D ^{1}H-^{15}N HSQC spectra of PD-L1/PD-1 complex (black), PDL1/binder complex (blue) and PD-L1/PD-1 complex (32 μM) in the presence of 16 μM binder (complex: bidenr in 1:0.5 ratio, red).

At the end of the titration, in the presence of 160μMour compound in solution, the complex among the two proteins was still present in a 1:1 ratio with the complex between the ligand and PD-L1.

As mentioned above, this last section of this paragraph describes further tests carried out, in collaboration with other research groups, to quantify and characterize the interaction between the hPD-L1 and our compounds.

As a further confirm of the NMR assay results and to rank the novel ligands based on their *in vitro* ability to inhibit PD-1/PD-L1 interaction, a homogeneous time-resolved fluorescence (HTRF) binding assay was used. This assay enables a simple and rapid characterization of inhibitors in a high-throughput format. Basically, it uses tagged human recombinant immune checkpoint partners (hPD1 and hPD-L1) and labelled anti-tag reagents for HTRF detection. More in detail, the interaction between hPD-L1 (Tag 1) and hPD1 (Tag2) is detected by using anti-Tag1 labeled with Europium (HTRF donor) and anti-Tag2 labeled with XL665 (HTRF acceptor). Upon hPD-L1 to hPD1 binding, the donor and acceptor antibodies are in close proximity, thus excitation of the donor antibody triggers fluorescence resonance energy transfer (FRET) towards the acceptor antibody, which in turn emits specifically at 665 nm. This signal is directly proportional

to the extent of hPD1/hPD-L1 interaction. Thus, compounds able to inhibit PD1/PD-L1 interaction induce a reduction in HTRF signal.

As shown in NMR experiment, among the newly synthesized compounds, one compound displayed a highest inhibitory potency with a IC_{50} value of 115 ($\pm$ 24) nM. Therefore, this compound was selected for subsequent biophysical and biological evaluations.

Differential scanning calorimetry (DSC) experiments were carried out to compare the behavior of our most potent compound with that of BMS202 in binding and stabilizing the PD-L1 protein. If a compound binds preferentially to a folded protein, the melting temperature (Tm) of the latter will generally increase, and the tighter it binds, the more the Tm increases. [45] Therefore, we performed DSC experiments in which the PD-L1 protein (32 μM) was heated in the absence and presence of both ligands (32 μM), to determine Tm variations. When no ligand was present, we observed a Tm value, corresponding to the maximum of the respective thermogram peak, of 46.5 ($\pm$0.5) °C. In the presence of either compounds we observed Tm values of 49.0 ($\pm$0.5) °C and 53.0 ($\pm$0.5) °C, respectively. Hence, DSC analysis showed that both compounds significantly shifted melting peak of PD-L1, indicating for both a direct binding with a change in the Tm of the protein (ΔTm) of 2.5 and 6.5 °C for our compound and BMS202, respectively
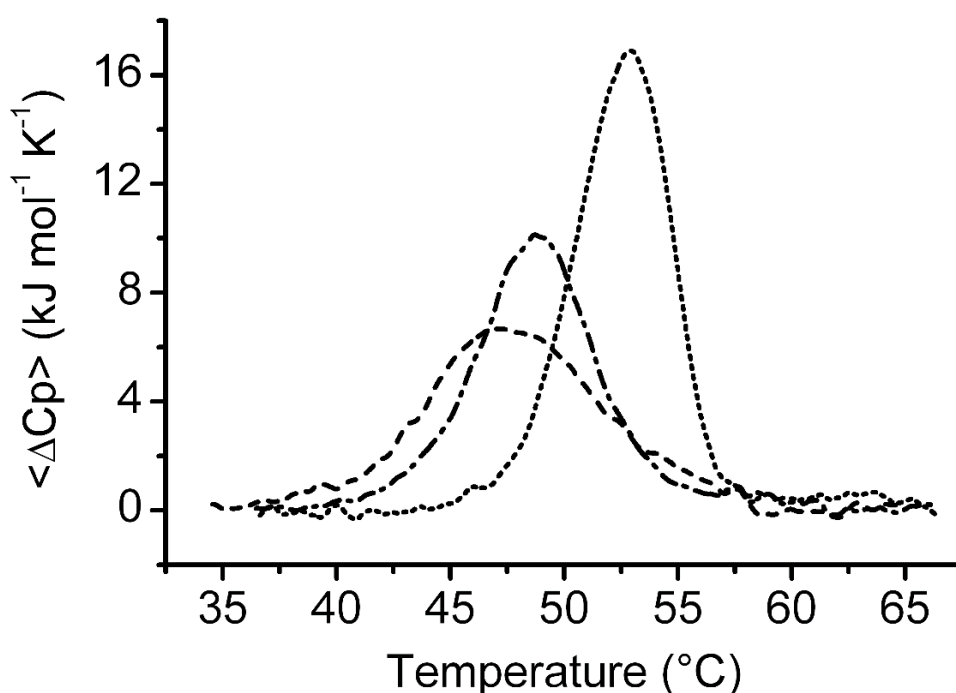
Figure 17. Differential scanning calorimetry (DSC) profiles for PD-L1 in the absence (dashed line) and presence of 1 molar equivalent of our compound (dash-dotted line) or BMS-202 (dotted line), recorded at 0.5 °C/min heating rate.

In order to test the cytotoxicity of our compound, we first determined the expression levels of PD-L1 in both cancer and non-cancer cells. As shown in Figure 18, human Peripheral Blood Mononuclear Cells (PBMCs) did not express PD-L1, while immortalized human keratinocytes (HaCaT) and pulmonary adenocarcinoma cells (PC9) showed a weak expression. Conversely, a high level of PD-L1 expression was detected in lung adenocarcinoma cells (HCC827). Noteworthy, treatment with IFNγ significantly ($P< 0.001$) up-regulated the expression of PD-L1 in both PC9 and HCC827 cells, with a higher ($P<0.05$) expression in HCC827 cells. We next investigated the growth inhibitory effects of our binder in both normal and cancer cells expressing different levels of PD-L1 (Figure 18). PBMCs, HaCaT, PC9 and HCC827 cells were treated with a range of concentrations (0.1, 1, 10 or 100 µM) of standard BMS-202 as a known, positive control, and our binder. Following 24 and 48 h incubation times, no significant cytotoxicity was reported for both compounds at 10 µM. A cytotoxic effect for both compounds was detected both in normal and cancer cells when applied at 100 µM, regardless of PD-L1 expression levels. However, compound BMS-202 ($P<0.05$) inhibited cell growth in general, and in PBMCs in particular, significantly more than our most potent binder (Figure 19). Moreover, it did not affect PBMC proliferation following 24h incubation.
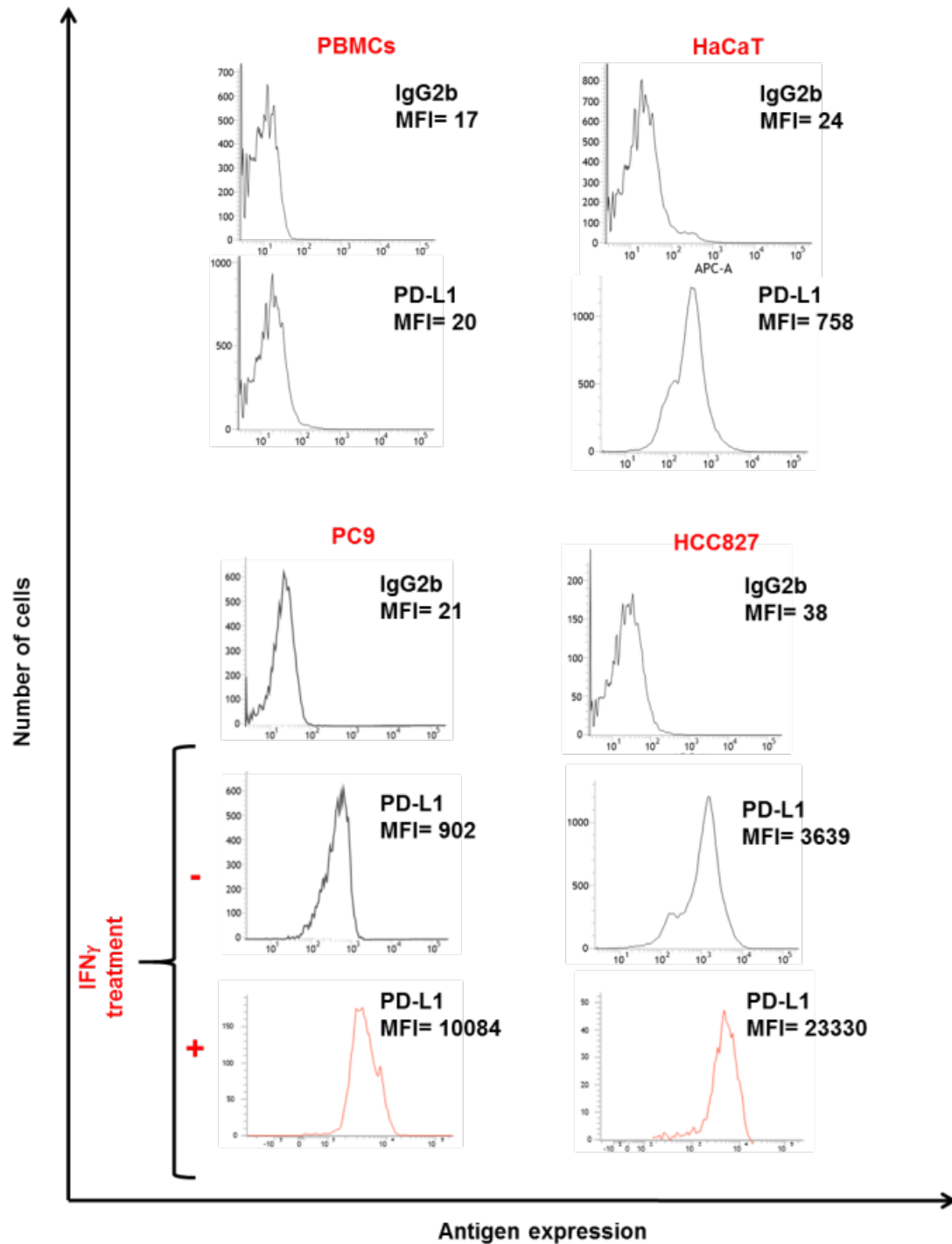
Figure 18. PD-L1 expression levels in normal and cancer cells. PBMCs, HaCaT, PC9 and HCC827 cells were seeded at density of 2×10^5 per well in 6-well plates and incubated with IFNγ (100 IU/mL). Untreated cells were used as a control. Following 24 h incubation at 37 °C in a 5% CO_2 atmosphere, cells were harvested, and the cell surface was stained with an APC-conjugated PD-L1-specific mouse monoclonal antibody (clone 29E.2A3). APC-conjugated mouse IgG2b was used as a specificity control. Representative results are shown.
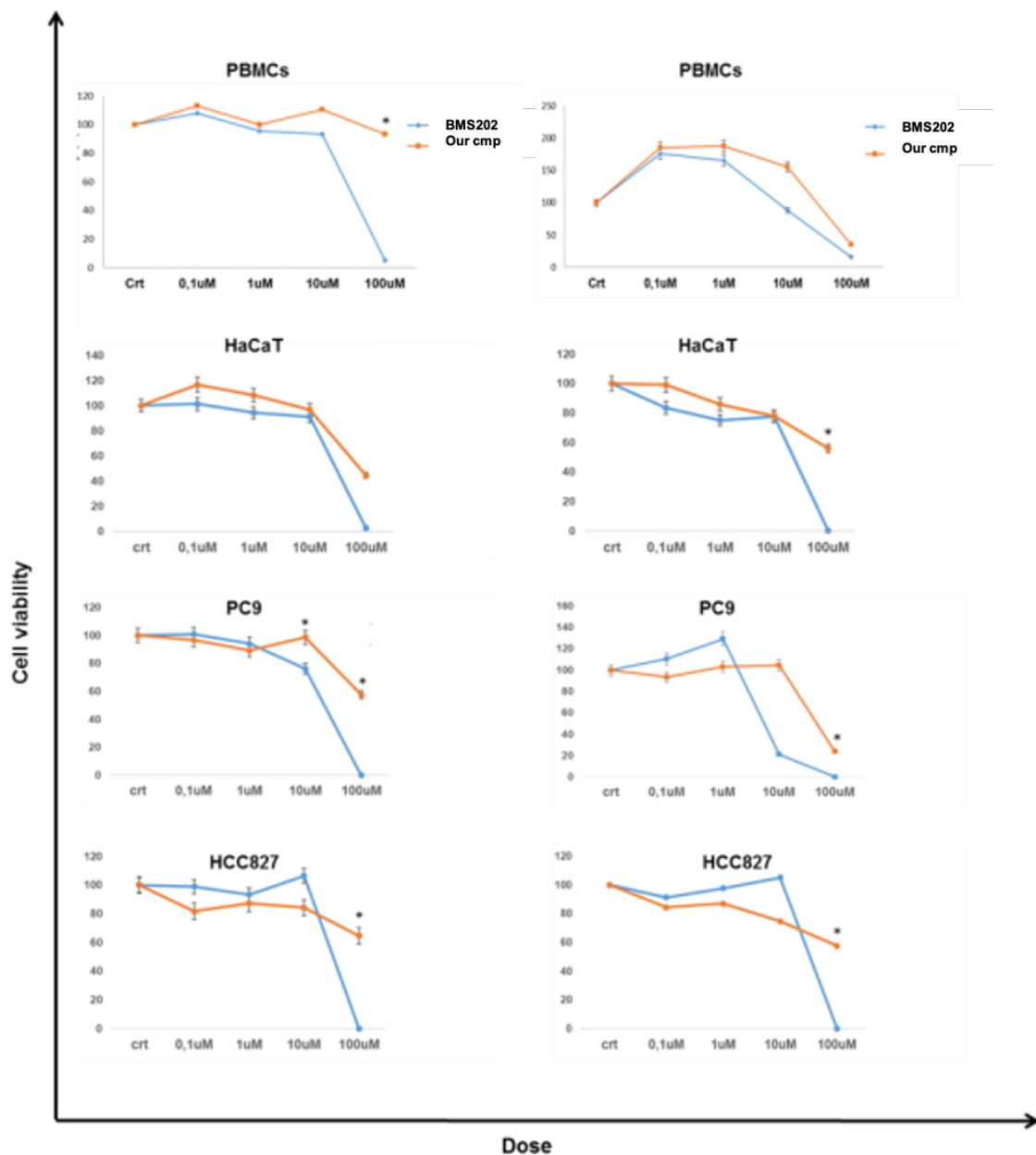
Figure 19. Effects of our compound (orange) on cell viability of normal and cancer cells expressing different levels of PD-L1. PBMCs, HaCaT, PC9 and HCC827 cells were seeded in triplicate in 96-well microtiter plates at the density of 1×10^4 per well and incubated with the indicated doses of our most potent compound or BMS202, the latter used as a control for PD-L1 inhibition. Untreated cells were used as a control. DMSO concentration was maintained at 0.02% in all wells. Following 24 and 48 h incubation at 37 °C in a 5% CO_2 atmosphere, cell viability was determined by a Cell Counting Kit-8 (CCK-8) assay. Data are expressed as mean percent of survival rate ± SD of treated cells as compared to untreated cells. Mean percent of survival rate and SD were calculated from three independent experiments performed in triplicate. The difference between

cytotoxic doses of our binder and bms202 was calculated using unpaired t-test. * indicates P < 0.001

Co-localization of PD-L1 with our biotinylated derivatives

In order to confirm on cell binding of our compounds to PD-L1, we performed an immunofluorescent double-staining to study the possible interaction between cell surface PD-L1 and biotinylated derivatives of our most potent binder on PBMCs, PC9 and HCC827 cells. As shown in Figure 20, PD-L1 expression co-localizes with both two our biotinylated derivatives in PC9 and HCC827 cells, which expressed different levels of PD-L1. In contrast, as expected, these two biotinylated compounds were not detected in PBMCs which do not express PD-L1.
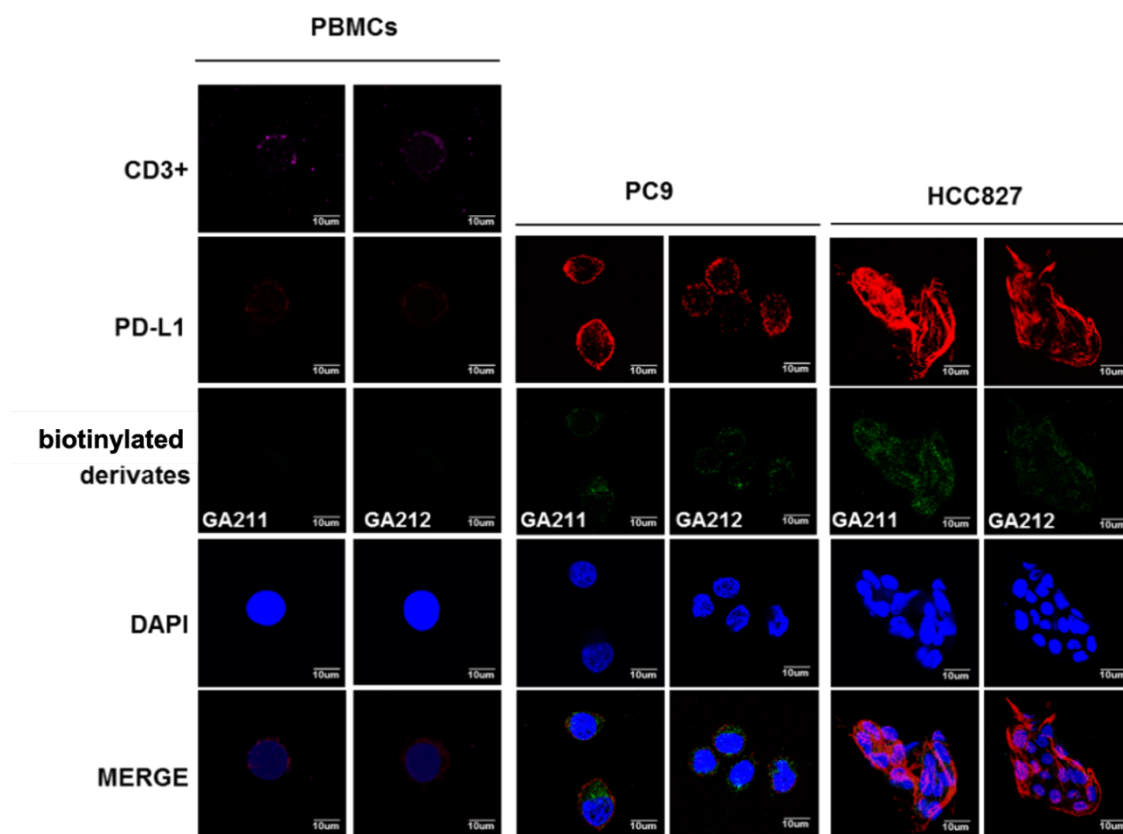
Figure 20. Co-localization of biotinylated compounds and PD-L1 in normal and cancer cells expressing different levels of PD-L1. PBMCs, PC9 and HCC827 cells were incubated with biotinylated derivatives at 1 µM. Following 8 h incubation cells were stained with a PD-L1-specific (Ab 205921) and a CD3-specific monoclonal antibody (Ab17143). Biotinylated compounds were detected utilizing a streptavidin-FITC conjugated antibody (*green*). PD-L1 and CD3 expression were detected utilizing Alexa Fluor-555- (*red*) and Alexa Fluor-649- (*violet*) conjugated anti-rabbit IgG and anti-mouse

IgG1. Nuclei were stained by DAPI (*blue*). Representative immunofluorescent staining is shown. Scale bars are indicated.

To assess the immunomodulatory activity and the putative functional significance of PD-L1 inhibition by our compound, the effect of stimulated PBMCs on recognition of cancer cells following treatment with our binder and positive control BMS202 was investigated. Stimulated PBMCs recognized both PC9 and HCC827 cells, since co-culturing of stimulated PBMCs and cancer cells significantly induced morphological changes of both PC9 and HCC827 cells and increased IFN-γ release ($P < 0.001$) as compared to non-stimulated PBMCs. Specifically, typical signs of cellular damage, including pleomorphism, rupture of the nuclear or plasma membrane, nuclear fragmentation, a shrunken cytosol and disruption of the intercellular junctional complexes were observed. Noteworthy, these morphological changes were significantly increased when PC9 and HCC827 cells were previously incubated either with our most potent binder or BMS202 (1 mM). Conversely, no changes on cancer cells were detected by either non-stimulated co-cultured PBMCs, or by treatment with our most potent binder or BMS202 a single agent or in combination in absence of PBMCs. Moreover, treatment with both our most potent binder or BMS202 significantly ($P < 0.01$) increased IFN-γ release by co-cultured activated PBMCs as compared with untreated cells (figure 21). Lastly, treatment with our most potent binder or BMS202 significantly ($P<0.01$) inhibited survival (figure 22) and increased apoptotic induction (figure 23) for both PC9 and HCC827 cells by co-cultured activated PBMCs as compared to untreated cells. Interestingly, our compound inhibited survival and increased apoptotic induction in PC9 and HCC827 cells in a significantly ($P<0.05$) greater extent when compared to BMS-202
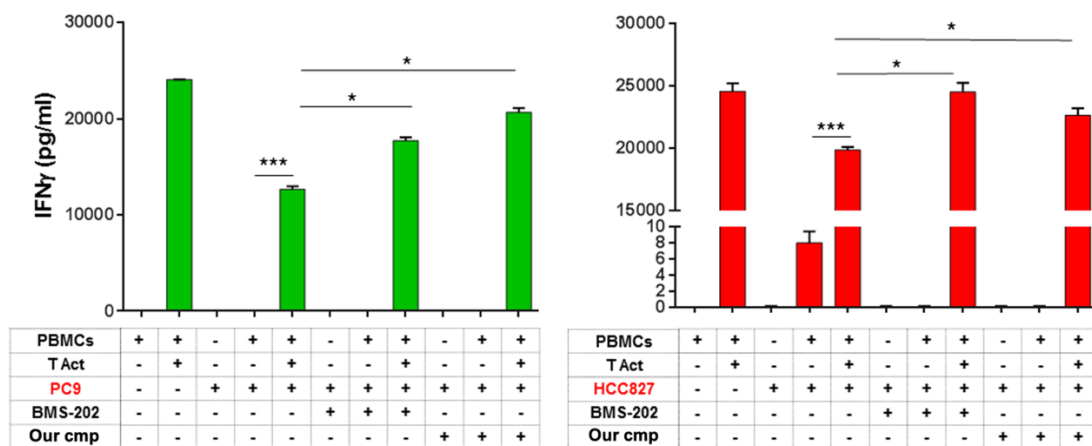
Figure 21. Enhancement of IFNγ release by stimulated PBMCs co-cultured with cancer cells expressing PD-L1 in presence of our most potent binder. PC9 (green) and HCC827 cells (left) were co-cultured with stimulated PBMCs and treated with both compounds (1 µM). PBMCs were stimulated utilizing an anti-CD3 (1 µg/mL) and an anti-CD28 (1 µg/mL) T Cell TransAct™ (T Act). Non-stimulated PBMCs and untreated cancer cells were used as controls. Following 48 h incubation, IFNγ levels in the medium harvested from cultures of PBMCs with cancer cells were measured by ELISA Max Deluxe Set Human IFNγ kit. Data are expressed as IFNγ levels ± SD of the results obtained in three independent experiments; each of them performed in triplicate. *Indicates $P < 0.01$. *** Indicates $P < 0.001$. All P values were calculated using the two-sided Student's t test.

Figure 22. Reduction of cell viability of cancer cells expressing PD-L1 co-cultured with stimulated PBMCs in presence of our most potent binder. PC9 (green) and HCC827 cells (red) were co-cultured with stimulated PBMCs and treated with both compounds (1 µM). PBMCs were stimulated utilizing an anti-CD3 (1 µg/mL) and an anti-CD28 (1 µg/mL) T Cell TransAct™ (T Act). Non-stimulated PBMCs and untreated cancer cells were used as controls. Following 48 h incubation, cell viability was determined by Cell Counting Kit-8 (CCK-8) assay. Cancer cells from cultures of PBMCs were isolated by removing PBMCs with PBS washing. Data are expressed as mean percent of survival rate ± SD of treated cells as compared to untreated cells. Mean percent of survival rate and SD were calculated from three independent experiments performed in triplicate. *Indicates $P < 0.05$. *** Indicates $P < 0.001$. All P values were calculated using the two-sided Student's t test.

PC9

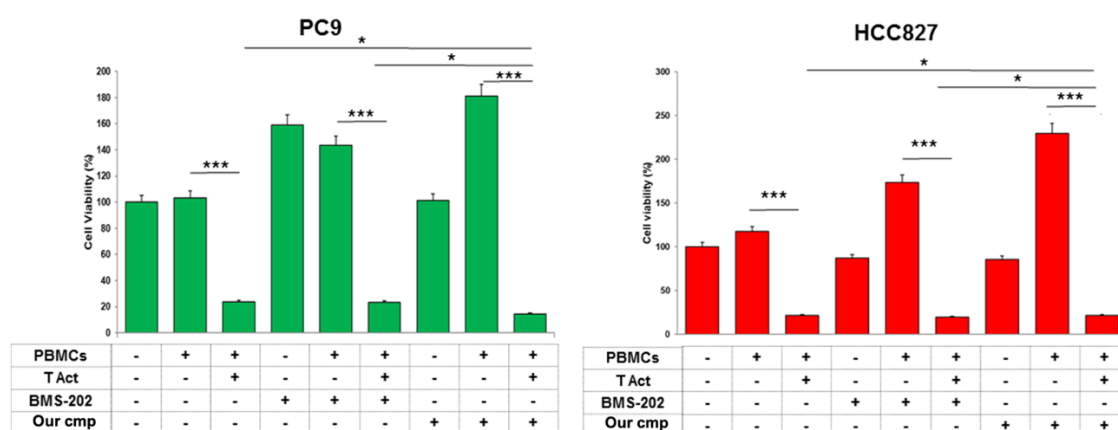| PBMCs	-	+	+	-	+	+	-	+	+
T Act	-	-	+	-	-	+	-	-	+
BMS-202	-	-	-	+	+	+	-	-	-
Our cmp	-	-	-	-	-	-	+	+	+

HCC827

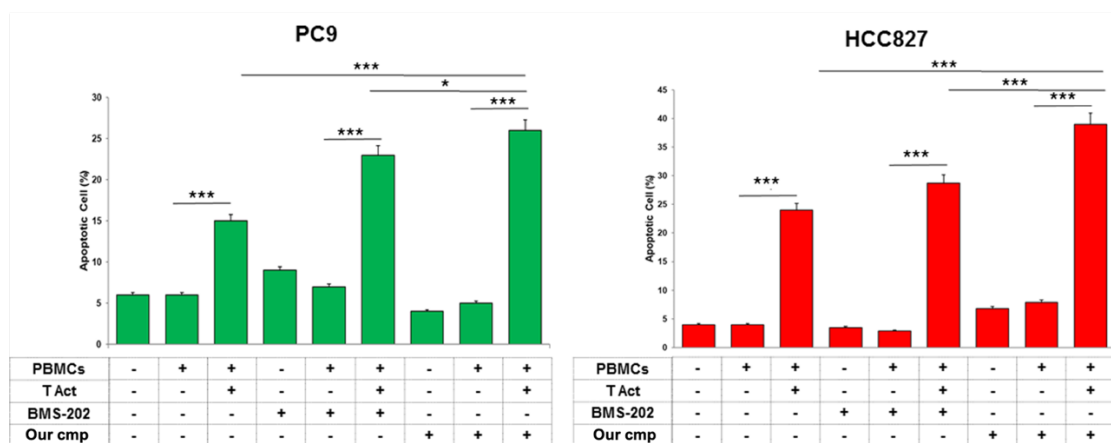| PBMCs	-	+	+	-	+	+	-	+	+
T Act	-	-	+	-	-	+	-	-	+
BMS-202	-	-	-	+	+	+	-	-	-
Our cmp	-	-	-	-	-	-	+	+	+

Figure 23. Enhancement of apoptosis induction of cancer cells expressing PD-L1 co-cultured with stimulated PBMCs in presence of our most potent binder. PC9 (green) and HCC827 cells (red) were co-cultured with stimulated PBMCs and treated with both compunds (1 µM). PBMCs were stimulated utilizing an anti-CD3 (1 µg/mL) and an anti-CD28 (1 µg/mL) T Cell TransAct™ (T Act). Non-stimulated PBMCs and untreated cancer cells were used as controls. Following 48 h incubation, apoptosis induction was determined by flow cytometry analysis of annexin V and PI staining. The levels of apoptosis are plotted and expressed as mean fraction of annexin V^+ cells ± SD of the results obtained in three independent experiments. *Indicates $P < 0.05$. *** Indicates $P < 0.001$. All P values were calculated using the two-sided Student's t test.

4.3. Conclusion

Inhibition of the PD-1/PD-L1 axis by monoclonal antibodies has achieved a remarkable success in treating a growing number of cancers. However, the recent discovery of BMS-202 has fueled efforts directed to a novel class of small molecules as direct and potent PD-L1 inhibitors, although a deeper comprehension of their theragnostic potential is still missing. In this respect, development of structurally new PD-L1 small ligands would be of the outmost importance for a complete understanding of the full potentialities of small molecule PD-L1/PD-1 inhibitors. Herein, a series of compounds was synthetized and assayed for their PD-L1 binding firstly by NMR, and then through HTRF assays. One our compound endowed with a nanomolar IC_{50}, was also subjected to DSC experiments to compare its behavior with positive standard BMS202 in binding and stabilizing the PD-

L1 protein. Furthermore, through NMR, our most potent compound was shown to specifically bounds to PD-L1 and not to PD-1. Then, to demonstrate this compound binds PD-L1 not only on isolated protein, but even on cell membranes, we used two its biotinylated derivatives in an immunofluorescent double-staining assay on PBMCs, PC9 and HCC827 cells. Our most potent compound demonstrated to bind PD-L1 on cell membranes, thus restoring the function of PBMCs co-cultured with lung adenocarcinoma PC9 and HCC827 cells. Indeed, an increased IFN-γ secretion and an augmented apoptotic induction on PC9 and HCC827 cancer cells was clearly visible upon treatment with our compound or with BMS202. Interestingly, even if in HTRF and in DSC assays positive standard BMS202 showed a stronger PD-L1 binding with respect to our compound (IC_{50} 22 nM *vs* 115 nM), in cell assays it was slightly (PC9 cells) or more (HCC827) active than BMS202 in inducing apoptosis after reactivation of PBMCs. Moreover, our most potent binder demonstrated a lower cytotoxicity in healthy cells (lower off-target effect) and a higher induction of IFN-γ in treated cancer cells than BMS202. Today, in a fast-growing field, the identification and characterization of structurally new, direct PD-L1 binders is of outmost importance to fully unravel the full potential of this brand-new class of small molecule immunomodulatory leads. With this in mind, and on the basis of the herein presented encouraging data, a further development for triazine-containing inhibitors is expected. Finally, the structural insight into the binding mode of our most potent ligand on the PD-L1 surface, together with a comparison with the binding mode for BMS202 surely furnish another piece to the precious puzzle of PD-L1/small molecules interactions.

4.4. References

(1)   Qin, S.; Xu, L.; Yi, M.; Yu, S.; Wu, K.; Luo, S. Novel Immune Checkpoint Targets: Moving beyond PD-1 and CTLA-4. *Mol. Cancer* **2019**, *18* (1), 1–14.

(2)   Zak, K. M.; Kitel, R.; Przetocka, S.; Golik, P.; Guzik, K.; Musielak, B.; Dömling, A.; Dubin, G.; Holak, T. A. Structure of the Complex of Human Programmed Death 1, PD-1, and Its Ligand PD-L1. *Structure* **2015**, *23* (12), 2341–2348.

(3)   Poole, R. M. Pembrolizumab: First Global Approval. *Drugs* **2014**, *74* (16), 1973–1981.

(4)   Wang, C.; Thudium, K. B.; Han, M.; Wang, X. T.; Huang, H.; Feingersh, D.; Garcia, C.; Wu, Y.; Kuhne, M.; Srinivasan, M.; Singh, S.; Wong, S.; Garner, N.; Leblanc, H.; Bunch, R. T.; Blanset, D.; Selby, M. J.; Korman, A. J. In Vitro Characterization of the Anti-PD-1 Antibody Nivolumab, BMS-936558, and in Vivo Toxicology in Non-Human Primates. *Cancer Immunol. Res.* **2014**, *2* (9), 846–856.

(5)   Ribas, A.; Wolchok, J. D. Cancer Immunotherapy Using Checkpoint Blockade. *Science (80-.).* **2018**, *359* (6382), 1350–1355.

(6)   Antonia, S. J.; Villegas, A.; Daniel, D.; Vicente, D.; Murakami, S.; Hui, R.; Yokoi, T.; Chiappori, A.; Lee, K. H.; de Wit, M.; Cho, B. C.; Bourhaba, M.; Quantin, X.; Tokito, T.; Mekhail, T.; Planchard, D.; Kim, Y.-C.; Karapetis, C. S.; Hiret, S.; Ostoros, G.; Kubota, K.; Gray, J. E.; Paz-Ares, L.; de Castro Carpeño, J.; Wadsworth, C.; Melillo, G.; Jiang, H.; Huang, Y.; Dennis, P. A.; Özgüroğlu, M. Durvalumab after Chemoradiotherapy in Stage III Non–Small-Cell Lung Cancer. *N. Engl. J. Med.* **2017**, *377* (20), 1919–1929.

(7)   Joseph, J.; Zobniw, C.; Davis, J.; Anderson, J.; Trinh, V. A. Avelumab: A Review of Its Application in Metastatic Merkel Cell Carcinoma. *Ann. Pharmacother.* **2018**, *52* (9), 928–935.

(8)   Sullivan, R. J.; Flaherty, K. T. Immunotherapy: Anti-PD-1 Therapies-a New First-Line Option in Advanced Melanoma. *Nat. Rev. Clin. Oncol.* **2015**, *12* (11), 625–626.

(9)   Khanna, P.; Blais, N.; Gaudreau, P. O.; Corrales-Rodriguez, L. Immunotherapy Comes of Age in Lung Cancer. *Clin. Lung Cancer* **2017**, *18* (1), 13–22.

(10)   Lee, C. M.; Tannock, I. F. The Distribution of the Therapeutic Monoclonal Antibodies Cetuximab and Trastuzumab within Solid Tumors. *BMC Cancer* **2010**, *10* (255).

(11)   Wargo, J. A.; Reuben, A.; Cooper, Z. A.; Oh, K. S.; Sullivan, R. J. Immune Effects

of Chemorapy, Radiation, and Targeted Rapy and Opportunities for Combination with Immunorapy. *Semin. Oncol.* **2015**, *42* (4), 601–616.

(12)   Chupak, L.; Zheng, X. Compounds Useful as Immunomodulators. *Bristol-Myers Squibb* **2015**, No. 12, WO 2015/160641 A1.

(13)   Chupak LS, Ding M, Martin SW, Zheng X, Hewawasam P, Connoly TP, Xu N, Yeung KS, Zhu J, Langley DR, Tenney DJ, S. P. Compounds Useful as Immunomodulators. *Bristol-Myers Squibb Co.* **2015**, *12* (WO 2015/160641 A2), WO 2015/160641 A2.

(14)   Zak, K. M.; Grudnik, P.; Guzik, K.; Zieba, B. J.; Musielak, B.; Dömling, A.; Dubin, G.; Holak, T. A. Structural Basis for Small Molecule Targeting of the Programmed Death Ligand 1 (PD-L1). *Oncotarget* **2016**, *7* (21), 30323–30335.

(15)   Guzik, K.; Zak, K. M.; Grudnik, P.; Magiera, K.; Musielak, B.; Törner, R.; Skalniak, L.; Dömling, A.; Dubin, G.; Holak, T. A. Small-Molecule Inhibitors of the Programmed Cell Death-1/Programmed Death-Ligand 1 (PD-1/PD-L1) Interaction via Transiently Induced Protein States and Dimerization of PD-L1. *J. Med. Chem.* **2017**, *60* (13), 5857–5867.

(16)   Skalniak, L.; Zak, K. M.; Guzik, K.; Magiera, K.; Musielak, B.; Pachota, M.; Szelazek, B.; Kocik, J.; Grudnik, P.; Tomala, M.; Krzanik, S.; Pyrc, K.; Dömling, A.; Dubin, G.; Holak, T. A. Small-Molecule Inhibitors of PD-1/PD-L1 Immune Checkpoint Alleviate the PD-L1-Induced Exhaustion of T-Cells. *Oncotarget* **2017**, *8* (42), 72167–72181.

(17)   Amaral, M.; Kokh, D. B.; Bomke, J.; Wegener, A.; Buchstaller, H. P.; Eggenweiler, H. M.; Matias, P.; Sirrenberg, C.; Wade, R. C.; Frech, M. Protein Conformational Flexibility Modulates Kinetics and Thermodynamics of Drug Binding. *Nat. Commun.* **2017**, *8* (1), 2276.

(18)   Perry, E.; Mills, J. J.; Zhao, B.; Wang, F.; Sun, Q.; Christov, P. P.; Tarr, J. C.; Rietz, T. A.; Olejniczak, E. T.; Lee, T.; Fesik, S. Fragment-Based Screening of Programmed Death Ligand 1 (PD-L1). *Bioorganic Med. Chem. Lett.* **2019**, *29* (6), 786–790.

(19)   Basu, S.; Yang, J.; Xu, B.; Magiera-Mularz, K.; Skalniak, L.; Musielak, B.; Kholodovych, V.; Holak, T. A.; Hu, L. Design, Synthesis, Evaluation, and Structural Studies of C2-Symmetric Small Molecule Inhibitors of Programmed Cell Death-1/Programmed Death-Ligand 1 Protein-Protein Interaction. *J. Med. Chem.* **2019**, *62* (15), 7250–7263.

(20)   Cheng, B.; Yuan, W. E.; Su, J.; Liu, Y.; Chen, J. Recent Advances in Small Molecule Based Cancer Immunotherapy. *Eur. J. Med. Chem.* **2018**, *157*, 582–598.

(21)   Konieczny, M.; Musielak, B.; Kocik, J.; Skalniak, L.; Sala, D.; Czub, M.; Magiera-Mularz, K.; Rodriguez, I.; Myrcha, M.; Stec, M.; Siedlar, M.; Holak, T. A.; Plewka, J. Di-Bromo-Based Small-Molecule Inhibitors of the PD-1/PD-L1 Immune Checkpoint. *J. Med. Chem.* **2020**, *63* (19), 11271–11285.

(22)   Guo, J.; Luo, L.; Wang, Z.; Hu, N.; Wang, W.; Xie, F.; Liang, E.; Yan, X.; Xiao, J.; Li, S. Design, Synthesis, and Biological Evaluation of Linear Aliphatic Amine-Linked Triaryl Derivatives as Potent Small-Molecule Inhibitors of the Programmed Cell Death-1/Programmed Cell Death-Ligand 1 Interaction with Promising Antitumor Effects in Vivo. *J. Med. Chem.* **2020**, *63* (22), 13825–13850.

(23)   Cheng, B.; Wang, W.; Niu, X.; Ren, Y.; Liu, T.; Cao, H.; Wang, S.; Tu, Y.; Chen, J.; Liu, S.; Yang, X.; Chen, J. Discovery of Novel and Highly Potent Resorcinol Dibenzyl Ether-Based PD-1/PD-L1 Inhibitors with Improved Drug-like and Pharmacokinetic Properties for Cancer Treatment. *J. Med. Chem.* **2020**, *63* (24), 15946–15959.

(24)   Qin, M.; Cao, Q.; Wu, X.; Liu, C.; Zheng, S.; Xie, H.; Tian, Y.; Xie, J.; Zhao, Y.; Hou, Y.; Zhang, X.; Xu, B.; Zhang, H.; Wang, X. Discovery of the Programmed Cell Death-1/Programmed Cell Death-Ligand 1 Interaction Inhibitors Bearing an Indoline Scaffold. *Eur. J. Med. Chem.* **2020**, *186*, 111856.

(25)   Hu, Z.; Yu, P.; Du, G.; Wang, W.; Zhu, H.; Li, N.; Zhao, H.; Dong, Z.; Ye, L.; Tian, J. PCC0208025 (BMS202), a Small Molecule Inhibitor of PD-L1, Produces an Antitumor Effect in B16-F10 Melanoma-Bearing Mice. *PLoS One* **2020**, *15* (3), 1–15.

(26)   Magiera-Mularz, K.; Kocik, J.; Musielak, B.; Plewka, J.; Sala, D.; Machula, M.; Grudnik, P.; Hajduk, M.; Czepiel, M.; Siedlar, M.; Holak, T. A.; Skalniak, L. Human and Mouse PD-L1: Similar Molecular Structure, but Different Druggability Profiles. *iScience* **2021**, *24* (1), 101960.

(27)   Magiera-Mularz, K.; Skalniak, L.; Zak, K. M.; Musielak, B.; Rudzinska-Szostak, E.; Berlicki, Ł.; Kocik, J.; Grudnik, P.; Sala, D.; Zarganes-Tzitzikas, T.; Shaabani, S.; Dömling, A.; Dubin, G.; Holak, T. A. Bioactive Macrocyclic Inhibitors of the PD-1/PD-L1 Immune Checkpoint. *Angew. Chemie - Int. Ed.* **2017**, *56* (44), 13732–13735.

(28)   Cheng, B.; Ren, Y.; Niu, X.; Wang, W.; Wang, S.; Tu, Y.; Liu, S.; Wang, J.; Yang, D.; Liao, G.; Chen, J. Discovery of Novel Resorcinol Dibenzyl Ethers Targeting the Programmed Cell Death-1/Programmed Cell Death-Ligand 1 Interaction as Potential Anticancer Agents. *J. Med. Chem.* **2020**, *63* (15), 8338–8358.

(29)   Li, S.; Vilalta-Colomer, M.; Punna, S.; Malathong, V.; Singh, R.; Zhang, P. Preparation of Small Molecule Programmed Death Ligand 1 Phenylindanyloxybenzylamines Including N-(Phenylindanyloxyben- Zyl)-Amino Acid Derivatives, and Methods of Treating Cancer Using Them. **2020**, WO 2020047035 A1.

(30)   Narva, S.; Xiong, X.; Ma, X.; Tanaka, Y.; Wu, Y.; Zhang, W. Synthesis and Evaluation of Biphenyl-1,2,3-Triazol-Benzonitrile Derivatives as PD-1/PD-L1 Inhibitors. *ACS Omega* **2020**, *5* (33), 21181–21190.

(31)   Qin, M.; Cao, Q.; Wu, X.; Liu, C.; Zheng, S.; Xie, H.; Tian, Y.; Xie, J.; Zhao, Y.; Hou, Y.; Zhang, X.; Xu, B.; Zhang, H.; Wang, X. Discovery of the Programmed Cell Death-1/Programmed Cell Death-Ligand 1 Interaction Inhibitors Bearing an Indoline Scaffold. *Eur. J. Med. Chem.* **2020**, *186*, 111856.

Chapter 5
Finding Structurally new Ligands for STING Protein

STING (STtimulator of INterferon Genes) is an endoplasmic reticulum (ER)-resident transmembrane protein of 379 amino acids that was first identified as part of the ER translocation system. It consists of 4 transmembrane regions, 2 lumenal domain and 1 cytoplasmatic domain in which the binding site is located (Figure 1 and Figure 2). [1,2]

```
000    MPHSSLHPSIPCPRGHGAQKAALVLLSACLVTLWGLGEPPEHTLRYLVLH
050    LASLQLGLLLNGVCSLAEELRHIHSRYRGSYWRTVRACLGCPLRRGALLL
100    LSIYFYYSLPNAVGPPFTWMLALLGLSQALNILLGLKGLAPAEISAVCEK
150    GNFNVAHGLAWSYYIGYLRLILPELQARIRTYNQHYNNLLRGAVSQRLYI
200    LLPLDCGVPDNLSMADPNIRFLDKLPQQTGDHAGIKDRVYSNSIYELLEN
250    GQRAGTCVLEYATPLQTLFAMSQYSQAGFSREDRLEQAKLFCRTLEDILA
300    DAPESQNNCRLIAYQEPADDSSFSLSQEVLRHLRQEEKEEVTVGSLKTSA
379    VPSTSTMSQEPELLISGMEKPLPLRTDFS
```

Figure 1. Amino acid sequence of hSTING. The lumenal domains are reported in red, the transmembrane domains in yellow and the cytosolic domain in green.
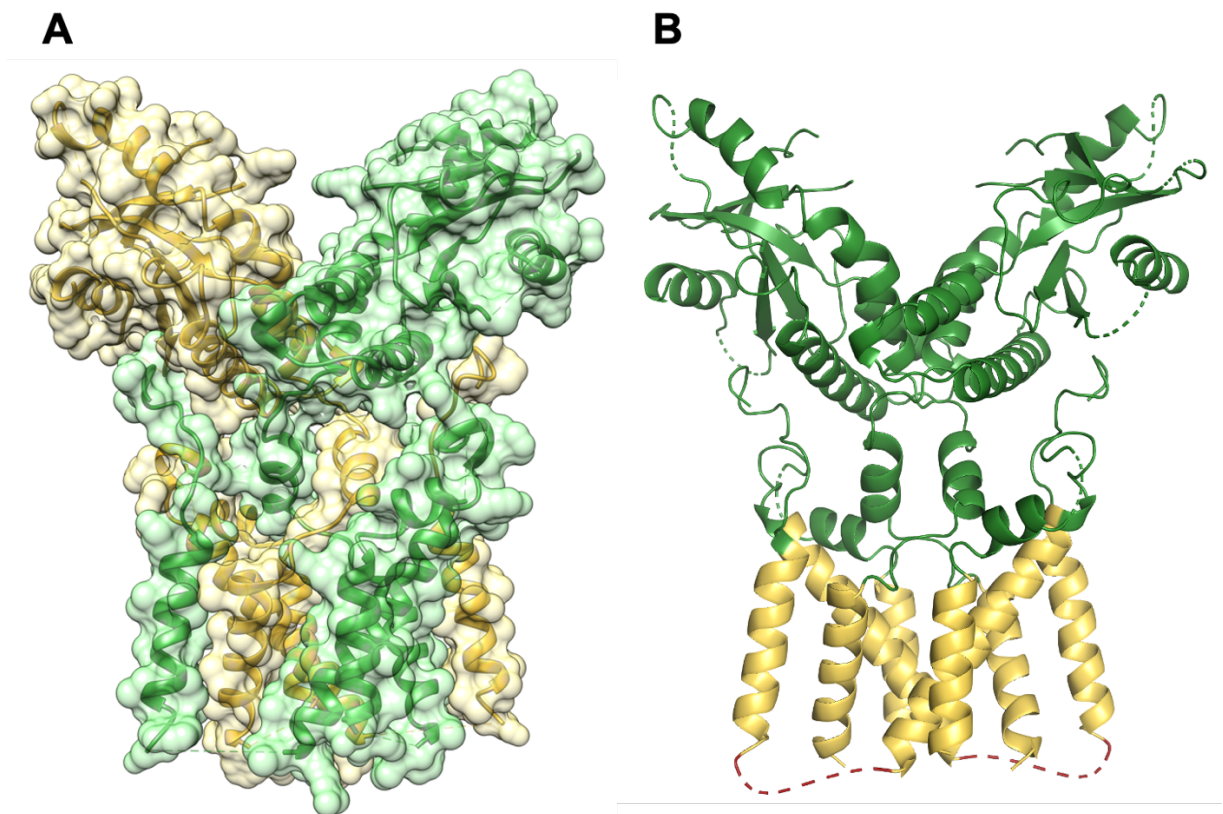

Figure. 2. Crystal structure of full-length inactive human STING by Cryo-Electron Microscopy (Cryo-EM) (PDB: 6NT5). (A) Views of full-length hSTING dimer is in yellow and green. (B) Views of amino acid sequence of STING. (lumenal domains are red, transmembrane domains are yellow and the cytosolic domain are green)

It is expressed in hematopoietic (T-cells, macrophages and dendritic cells) and also in various cells like endothelial and epithelial cell types; in addiction homologues of STING have been identified in invertebrates and in different eukaryotic species.[1,3–5]

This protein plays an important role in the innate immune pathway because is essential for controlling the transcription of numerous host defense genes type I interferons (IFNs-I) and pro-inflammatory cytokines, and also for the recognition of cyclic dinucleotides (CDNs) or mutant DNA species in the cytosol of the cell, so as to be identified as a potent target of anticancer therapies.[3,5–8] Within this system STING is a key sensor and the one of the most important mediators of the signaling triggered by cytosolic nucleic acid derived from DNA pathogens (viruses and bacteria) or self-DNA in the cytosol.[5,6] These cytosolic nucleic acids are powerful PAMPs (pathogen-associated molecular patterns)/ DAMPs (danger-associated molecular patterns) for which host organism possesses like STING a sensors and downstream adaptors to induce innate immune responses.[6,8,9] STING, unlike other nucleic acid sensors, does not directly bind DNA and instead recognizes cyclic dinucleotides (CDNs) of either exogenous (e.g., bacterial) or endogenous origin.[10]

STING is a central player in the innate immune response to nucleic acids,[11] particularly CDNs, because stimulates the transcription of numerous innate immune genes in response to various invading DNA pathogens or transfected DNA, indeed STING promotes immunity to DNA viruses and retro-viruses, suppresses replication of RNA viruses and activation of innate immune genes to prevent dangerous bacterial infection.[3] The CDNs bind STING in its C-terminal domain and activate it; furthermore, the presence of the cytosolic exogenous DNA and also endogenous damaged DNA in cytoplasm of mammalian cells is a danger signal that generates the production of second messenger cGAMP by the DNA sensor protein cyclic GMP-AMP synthase (cGAS) and induce a STING-dependent type I IFN response.[12–16]

STING activation induces its dimerization and translocation from ER to the Golgi by mechanism similar to autophagy, and then initiates the downstream TBK1-IRF3 cascade to induce type I interferons.[15–20] Within this system at first the association between STING-TBK1 leads to autophosphorylation of TBK1, its activation, and then STING phosphorylation by TBK1.[15,16,19–21]

STING phosphorylation is important for the recruitment of IRF3 in proximity to TBK1, and then to phosphorylate and activate IRF3. Activated IRF3 translocated into the nucleus and promotes expression of type I interferons. [15,16,19,22]

STING have also been shown to activate NF-κB pathway through phosphorylation of TKB1 and then its interaction and phosphorylation of IKK (IkB kinase). STING-TBK1-IKK axis, regulates the activation loop of IKKα/β releasing p65 to form active dimers with p50. Then the NF-kB complex translocated into the nucleus and promotes expression of type I interferons like the STING-TBK1-IRF3 axis. [15,16,19,20,23]

STING activation induces type I IFN (IFN-I) production and increased expression of IFN-stimulated genes (ISG). [4] The two major IFN-I, are IFN-α and β, are important for protecting the cell against for viral and bacterial infections and many tumor, indeed STING agonists have been used against the development of cancer by promoting antitumor immune responses (Figure 3A).[3]

Particularly the major STING antitumor effects depend by production of IFN-b production by antigen-presenting cells (APCs) that promotes CD8^{+} T cell priming against tumor-associated antigens. [16] Specifically, dendritic cells (DCs) absorb dying cancer cells and the tumor DNA activates STING pathway to induce the expression of interferons. Interferons stimulate the maturation of DCs and facilitates presentation of tumor associated antigens on MHCI. Finally, DCs migrates to lymph nodes and activates CD8+ T cells, which seek and attack tumors in target tissues (Figure 3B). [20] Based on these finding and cancer control via host immune cell activation, the antitumor therapy is based on activation of the STING pathway.
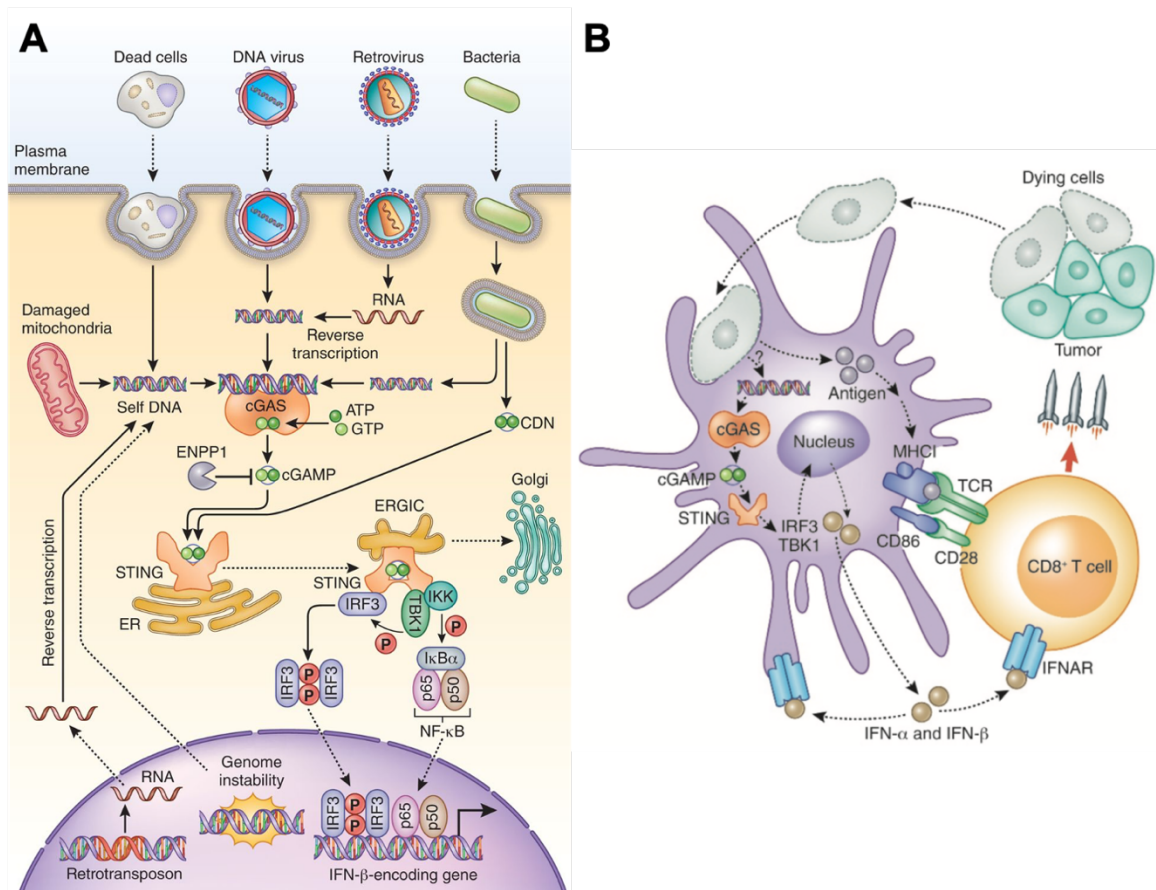
Figure. 3. (A)Regulation of the STING pathway. (B) Role of the STING pathway in antitumor immunity (adopted from Qi Chen et al. [20])

Recently it was shown that activation of STING pathways is required to have immunosuppressive effects through upregulation of programmed death-1 ligand (PD-L1) in different cancer in response to DNA damage; so combination of STING agonists with PD-1/PD-L1 antibodies or inhibitors was found to further boost antitumor immunity and to enforce control of tumor growth. [3,24]
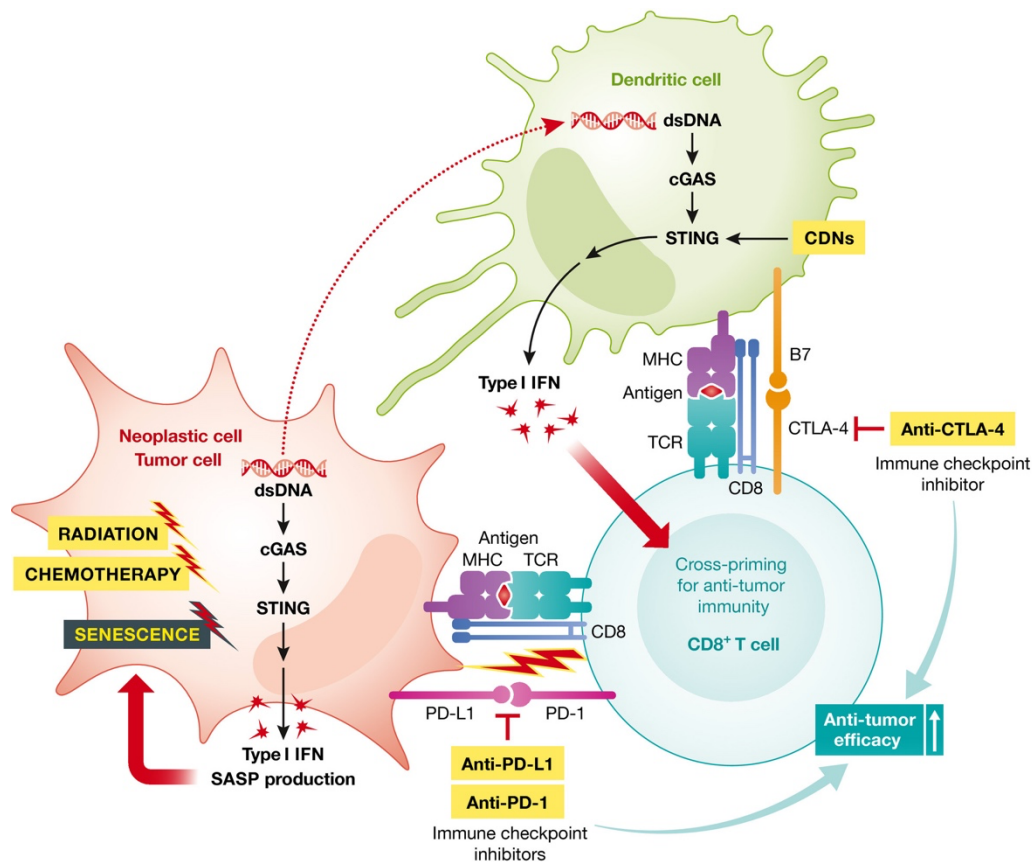
Figure. 4. Model of the tumor suppressive roles of the Sting and PD1/PD-L1 Pathways (adopted from Li Teng Khoo et al. [22])

There are many crystal structures of human STING (hSTING) complexed with its ligands. All crystal reveals that, after STING activation and its dimerization by ligand binding, the C-terminal portion of STING forms a V-shaped dimer and binds only one endogenous ligand at the dimer surface.[2,25]

STING exhibits two distinct conformations (open and closed) in solution. Structural studies of complex STING-ligand, suggest that ligands that induce the closed conformation of STING result more active.[25–27]
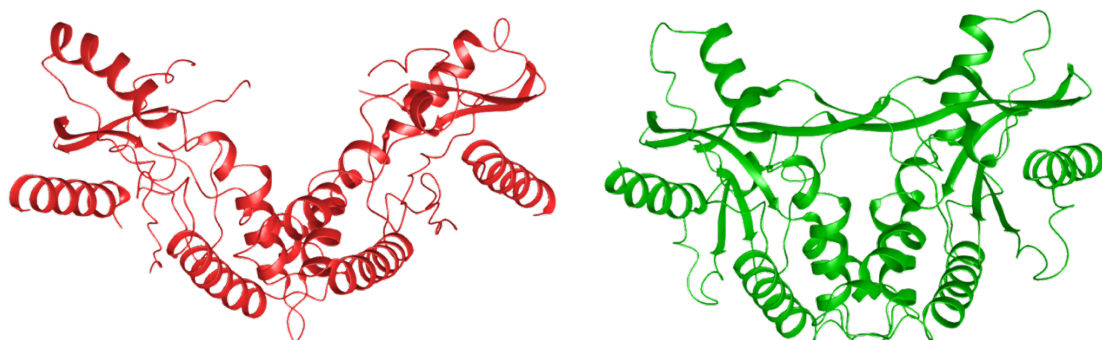
Figure. 5. Model of the STING conformations open (red) and closed (green)

The first STING ligands discovered were exogenous and endogenous CDNs such as cyclic di-AMP (c-di-AMP), secreted by bacteria like Listeria monocytogenes or cGAMP produced by cGAS.[3,5,28–30]

CDNs are ubiquitous second messenger molecules used in bacterial signal transduction in mammalian cells. Exogenous CDNs are c-di-GMP and c-di-AMP. Cyclic diguanylic acid (c-di-GMP) is the most prevalent intracellular signaling intermediate in bacteria and is the first CDNs identified. c-di-GMP is important for many cellular activities like cell-cycle regulation, differentiation and biofilm formation. Another important exogenous CDNs is cyclic diadenylic acid (c-di-AMP); it is involved in the regulation of cell growth, cell size and cell-wall homeostasis. Recently have been identified two new CDNs: 3'3'-cGAMP and 2'3'-cGAMP. The 3'3'-cGAMP is an exogenous CDNs produced by Vibrio Cholerae, instead 2'3'-cGAMP is an endogenous CDNs produced by cGAS. Mammalian cells synthesize 2'3'-cGAMP in response to cytosolic DNA interaction with cGAS (enzyme cyclic cGAMP synthase). [2,4,5,14,26,30–37] All the CDNs (Figure 6), endogenous and exogenous, binding in the same dimer surface, with hydrogen bonding and hydrophobic contacts. The different CDNs make take on STING different conformation. Starting to "open" conformation of dimer without ligand, passing to the V-shape with c-di-GMP (Similar to the structure of unliganded STING but a little more closed) and ending to the U-shape, or really "close" conformation, with cGAMP. [2,4,35–37,5,14,26,30–34] Unfortunately, these CDNs cannot be used in therapy because they are degraded by phosphodiesterase enzymes. [5,37,38] To overcome this problem, Dubensky, Kim, and colleagues at Aduro BioTech and Johns Hopkins University, designed new synthetic CDNs derivates that are more stable in vivo and enhanced binding with hSTING. These phosphodiesterase-resistant derivates presents two sulfur atoms instead of two non-bridging oxygen atoms and are diastereomer: (R;R)-S2-CDA and (R;S)-S2-CDA (Figure 6). The diastereomer (R,R)-S2-CDA are more active than (R;S)-S2-CDA and the unmodified parent molecules. [5,39–43] Starting to 3'3'-cAIMP, a parent molecule of 3'3'-cGAMP that present adenine and hypoxanthine instead of normal purine bases, have been deigned new synthetic CDNs derivates whose constituent nucleosides are adenosine and inosine and show vary substitution on ribose, on internucleotide linker and phosphate modification. The most interesting compound of this family are 3'3'-cAIMP (EC$_{50}$= 6.4 μM) and its analogues that contain one or two 2'-fluoro-2'-deoxyriboses and/or bis-

phosphorothioate likages (EC$_{50}$ 0.4-4.7 μM) because in human blood ex vivo induce more IFN I and proinflammatory cytokines than 2',3'-cGAMP. [5,43,44]

A much less complex small molecules structurally unrelated to CDNs are DMXAA and its related molecules like FAA (flavone acetic acid), XAA-5Me, XAA-8Me, CMA (carboxymethiyl-9-acridanone) and a-MG (alpha-Mangostin) (Figure 6).[5,43] DMXAA (Vadimezan) was synthesized by Denny and coworkers and was the first small molecule that exhibits immune modulatory activities in mouse STING. DMXAA was identified as a potential cancer therapeutic and in combination with paclitaxel and carboplatin and was evaluated in phase II of clinical trials but failed in human phase III trials.[5,25,42,43,45] Despite DMXAA binding the same pocket as natural CDNs in hSTING and the sequence identity between mSTING and hSTING is very high above all in the binding pocket, this compound not actives hSTING. In the same way its related compound FAA, XAA-5Me, XAA-8Me and CMA are selective agonists for mSTING against hSTING.[25,42,43]

Only one member of this class of small molecules binds and activate human STING through the activation of TBK1-IRF3 pathway and the production of type I interferon. This molecule is the dietary xanthine a-Mangostin, but its activity is less than natural CDNs and their synthetic derivates.[46]

Recently, Joshi M. Ramanjulu et all. have identified, three new compounds molecules that compete with the binding of cGAMP in the "open" state of human STING and active STING. These molecules are amidobenzimidazole and the most active is di-ABZI, the dimer of ABZI (Figure 9). Starting to ABZI, Joshi M. Ramanjulu et all, replaced the N1-hydroxyphenethyl moiety (N-1) with a linker between the two molecules to create a single dimeric ligand with an increase in binding affinity. The third and last compound of this family was obtained by di-ABZI lead optimization. it has, only on one side of the dimer, a carbonious linker with a final morpholine ring. These two compounds (di-ABZI and its derivate) are more potent than cGAMP.[47] At last, Xiaohui Zang et all, in their work have reported one small molecule that induces a proinflammatory cytokine response in a human-STING-manner.

This molecule, 6-bromo-N-(Naphtalen-1-yl)-benzo[d][1,3]dioxole-5-carboxamide (BNBC), specifically induce type I and III INFs dominant cytokine responses in primary human fibroblasts and PBMCs. Xiaohui Zang et all demonstrate that BNBC binds and actives specifically human STING and induces its pathway.[48]In the last year, the therapeutic interest towards hSTING has increased, in fact today there are many x-ray

complex between hSTING and monomer or dimer binder, such as hSTING/SR-717 complex [49] and hSTING/MSA-2 (monomer) complex ad its dimer derivates (Figure 6) [50] However, the recently available CDN–STING and binder-STING co-crystal structures together with the known differences among human and mouse STING represent a solid ground from which to start. Thus, herein, starting from the above-mentioned X-ray I aim at design and development of novel STING agonists through different computational methods: Virtual Screening (VS) and Core Hopping.
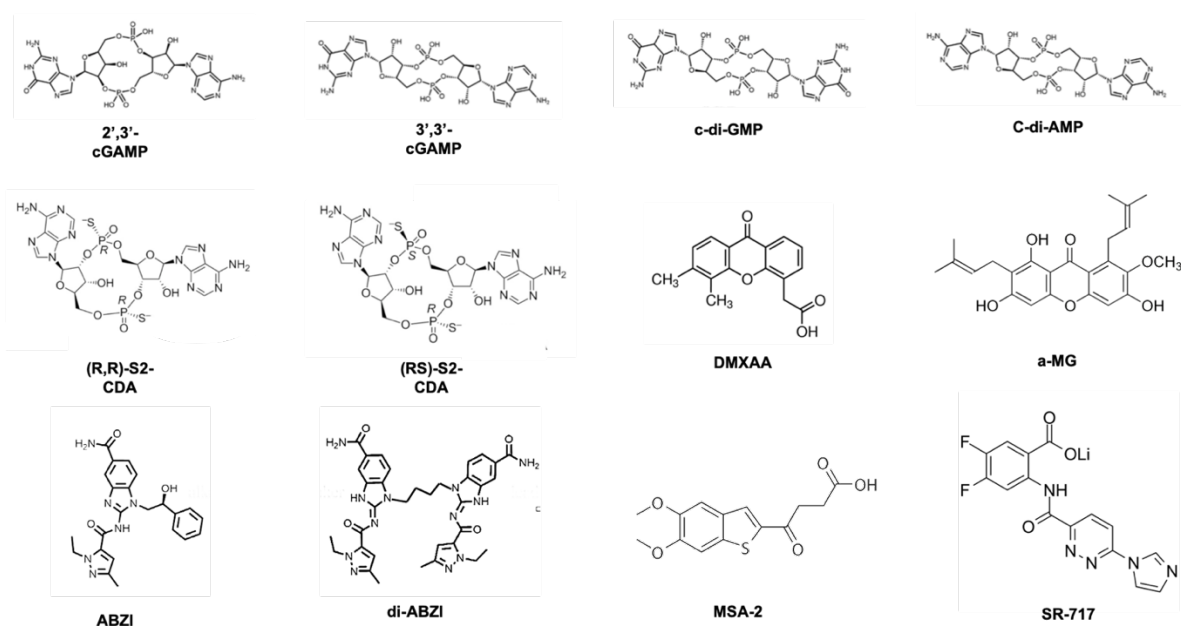
Figure 6. Chemical structures of representative STING binder

5.1. Results and Discussion

This paragraph describes all studies and all results obtained during my three years of PhD concerns the computational studies applied on hSTING to due to discover and develop new agonists and the successive analysis and experiments achieved by NMR ad integrated methodologies.

This protein was chosen considering the importance of hSTING in the treatment of several cancer in combination with the PD-1/PD-L1 axis.

As widely described in the previous, STING ligands are essentially cyclic dinucleotides (CDNs), which are ubiquitous small-molecule second messengers produced by bacteria and immune cells. However, native CDN molecules are sensitive to degradation by phosphodiesterases that are present in host cells or in the systemic circulation [40] and cannot be used in therapy. The exogenous modulation of the hSTING protein has been poorly explored so far, although it might have great therapeutic potential

In fact, a much less complex small molecule structurally unrelated to CDNs is the 5,6-dimethylxanthenone-4-acetic acid (DMXAA), which upon intratumor injection induced regression of established tumors in mice and generated substantial systemic immune responses, which were also capable of rejecting distant metastases and furthermore provided long-lived immunologic memory. [41] Unfortunately, DMXAA is capable of stimulating STING signaling in mice, but not in humans.

The two receptors differ for one amino acid (I230 in mSTING vs G230 in hSTING) located in the flexible loop that forms a lid above the c-di-GMP binding site, that stabilizes the near-sheets thus influencing the transition from the "open to ''closed'' conformation, [2,4,35–37,5,14,26,30–34] and in turn the STING activation. [2,25–27] Recently, new molecular compounds have been identified that compete with cGAMP binding both in the "open" (eg ABZI and it dimer derivates) [47] and "closed" state (e.g. SR-717) [49] of hSTING and activating it. However, the recently available CDN–STING and binder-STING co-crystal structures together with the known differences among human and mouse STING represent a solid ground from which to start.

Thus, herein, starting from the above-mentioned X-ray I aim at design and development of novel STING agonists through different computational methods: Core Hopping, Virtual Screening (VS) and rational design.

At the first time my attention focused on the search for new CDNs derivatives phosphodiesterase- resistant[5,37,38]. The endogenous STING activator (c-GAMP), co-crystalized with STING (PDB code: 4LOH) [31], was used as starting point and a rational sugar/phosphodiester substitution strategy was employed through the "Core hopping" facility of Schrödinger package. Core Hopping is based on the replacement of the central nucleus of starting compound with numerous others, and on consecutive molecular docking calculations of the molecules obtained. The choice of the cores will be dictated

also by the sufficient similarity between the chemical nature and shape of the novel scaffolds and those of physiological ligands, so not to alter the geometry for the two branches placement. (see Figure 2 in methods section) With this method were obtained new scaffolds presenting a different core from cGAMP. After an initial molecular docking study of these molecules, only those interact inside the receptor pocket in the same way as the endogenous ligand, present in the 4LOH crystal, were selected. Unfortunately, few of these structures were easy to synthesize because of their complexity but gave us new clues to develop. In close collaboration with a few synthesis groups, we have designed a number of different compounds.

In collaboration with the synthesis group of Dr. Stefano Tomassi of University of Napoli Federico II and Prof. Salvatore Di Maro of University of Campania Luigi Vanvitelli, we designed a number of compounds with a different core. Some representative compounds are displayed in the Figure 7 below.
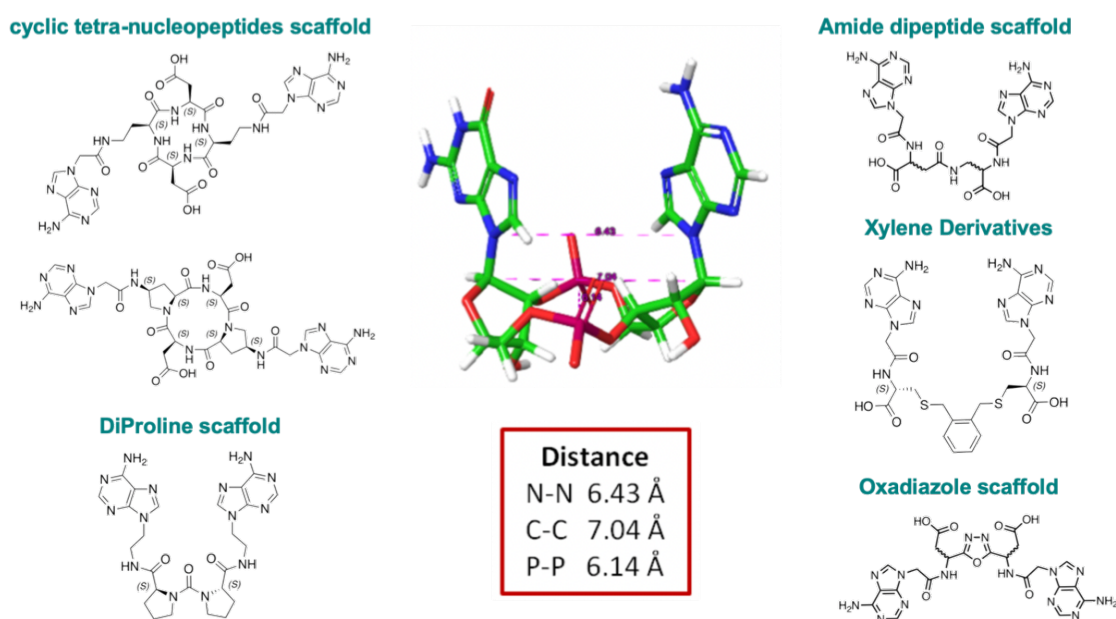
Figure 7. Representative structures of compounds with a different core

In collaboration with research group of Prof. Seneci of University of Milano, we designed a number of compounds with a sugar core. These compounds present disaccharides or monosaccharides cores. The most representative compound with disaccharide core presents a trehalose core, whereas the most representative compound with monosaccharide core presents a glucose core Figure 8.
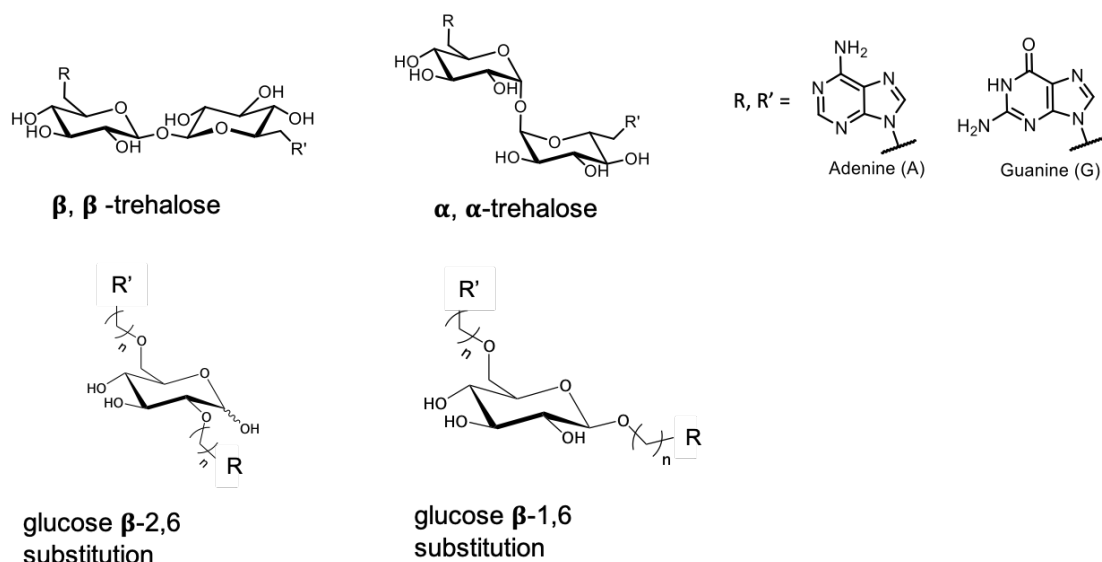
Figure 8. Representative structures of compounds with a sugar core

All compounds were docked in the open and in the closed STING conformation and just the best-scored were synthetized.

In order to elucidate at an atomistic level, the binding mode of our compounds at the hSTING receptor, molecular docking studies were performed. As for the protein tridimensional structure selection, the X-ray complex of hSTING dimer with the known STING activator c-GAMP (PDB code: 4LOH) was chosen. Docking of these compounds predicted that these molecules can be hosted, similarly to c-GAMP. In detail, the two nitrogenous bases of the new compounds in the upper part of the binding site, engage interactions with $_{A,B}$R238a and $_{A,B}$ Y167 analogously to what found for **c**-GAMP. While c-GAMP is stabilized through a network of direct and water-mediated hydrogen bonds with N242, S241, V239, Y163, E260 and Y261 leading to the closing of the receptor pocket, the new ligands designed directly bind some of these amino acids. This difference in binding gives us hope for the possible activation of sting by new compounds. Almost all the designed molecules have hydroxyl groups linked to the new core. These groups, In the bottom part of the binding pocket, engage interactions with S162 and/or T267 analogously to what found for c-GAMP
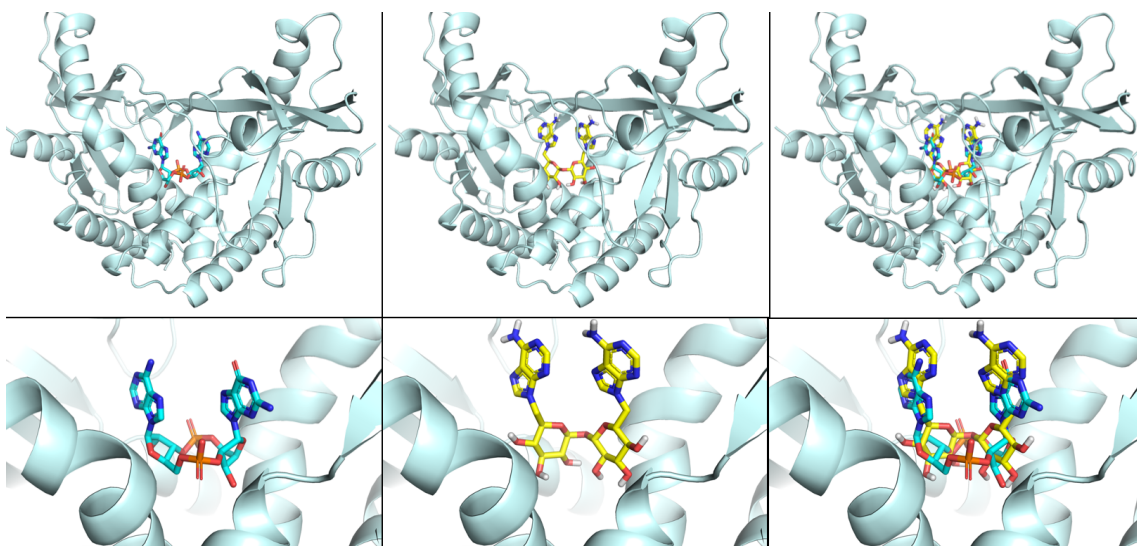
Figure 9 Docking studies of compound with trehalose core

Another approach to find small molecules as ligands for human STING was to perform a receptor- based virtual screening. It was performed with the aid of "Glide software" (Schrödinger package) and an "in house" database (about 10000 small organic molecules).

Starting from the X-ray complex of STING/c-GAMP (PDB code: 4LOH)[31], STING/DMXAA (PDB code: 4QXP)[25], STING/ABZI (PDB code: 6DXG)[47], STING/di-ABZI (PDB code: 6DXL) [47] and STING/SR717 (PDB code: 6XNP)[49], five receptor-based VS were performed. With this method were obtained new compounds presenting different scaffold. A further molecular docking study was carried out to screening the molecules obtained from previous receptor based VS. In this way were selected the molecules that engage interactions with the amino acids previously and have the same or similar binding mode of the ligand in the starting crystal. The obtained molecules have been divided in five groups, based on the crystal from which the receptor-based VS and the Docking have been carried out. Only the best-scored molecules were synthetized. The most representative compounds are displayed in the Figure 10.

Interesting is compound 10. This molecule is composed by two theophylline linked by disolfure bond. Docking of this compound was performed using the X-ray complex of hSTING dimer with c-GAMP (PDB code: 4LOH). In detail, the two theophylline in the upper part of the binding site, engage interactions with $_{A,B}$ R238 and $_{A,B}$ Y167, also interacts with the backbone of dimer on the bottom of the binding pocket through a

network of water-mediated hydrogen bonds analogously to the two nitrogenous bases of c-GAMP. In addition, its monomer (compound 13), and its derivates (compound 8-9) were found to be the best molecules of VS and molecular docking performed with X-ray complex of STING/DMXAA (PDB code: 4QXP) and STING/ABZI (PDB code: 6DXG). These molecules have been synthesized by the research group of Prof. Taliani of University of Pisa.

In the end, VS and Docking of compounds 15, 16, 17 and 18 were performed using the X-ray complex of STING/ABZI (PDB code: 6DXG) and STING/SR717 (PDB code: 6XNP).

These compounds, synthesized by research group of Prof. Silvestri of University of Roma, are interesting because these molecules can be easily dimerized as shown in figure 11. In this way we hope to obtain an increase of activities like the one obtained thanks to the dimerization of the ligand ABZI. Today a small library of dimers has been designed accordingly with receptor structure and docking results performed using X-ray complex of STING/di-ABZI (PDB code: 6DXL)
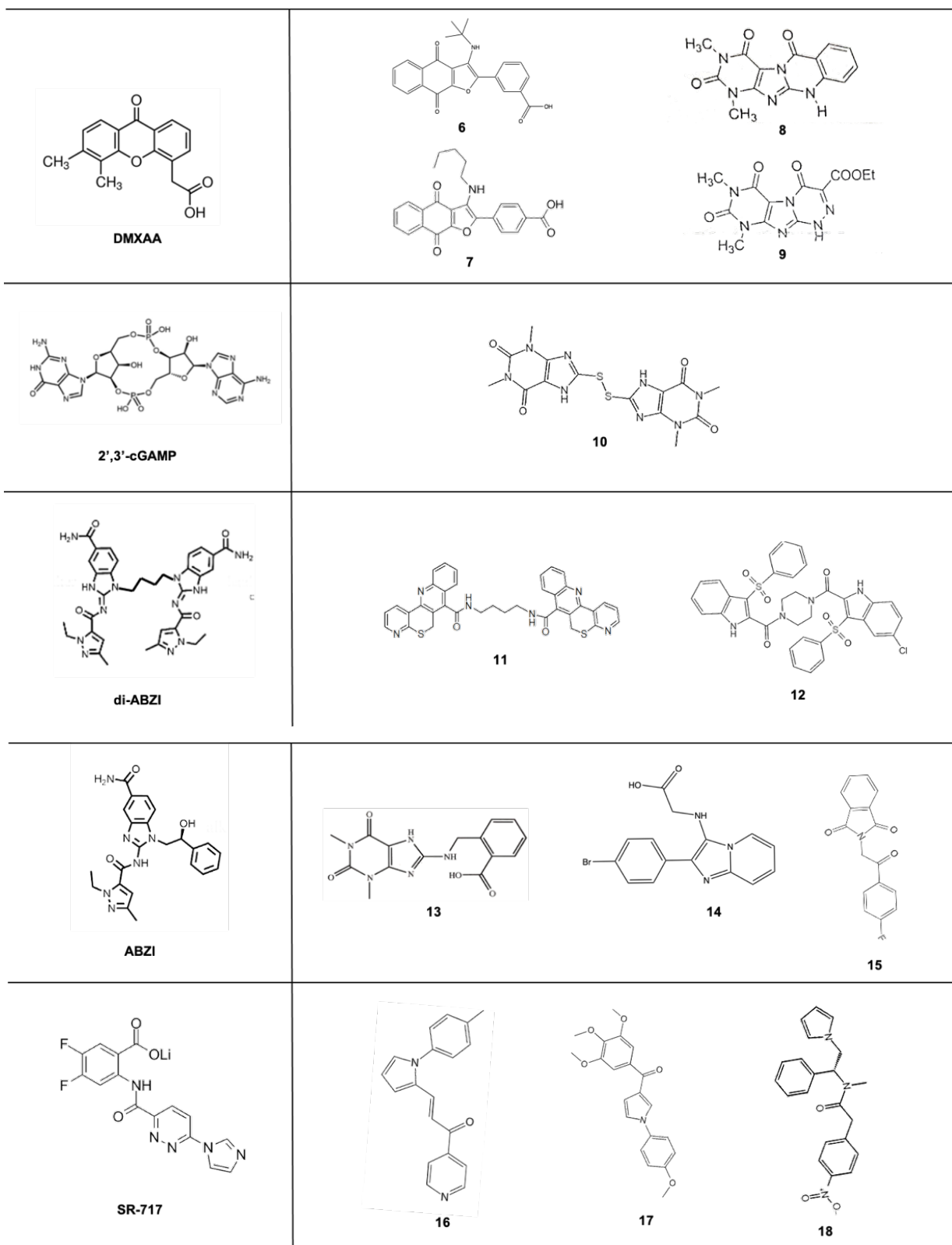
Figure 10. Representative structures obtained by VS
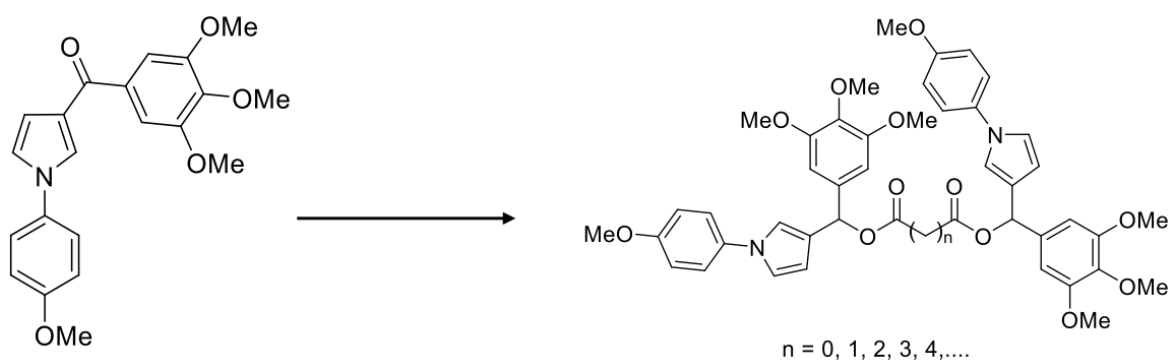
Figure 11. example of dimerization of compound 17

The compounds' series were synthesized, qualitatively tested by 1D ^{1}H-NMR, and then will be tested quantitatively through a homogeneous time-resolved fluorescence (HTRF) binding assay, which will provide an IC_{50} for each binder found through NMR

In second part of my PhD project, I've been working on expression, extraction and purification samples of hSTING in order to analyze it in free state and then evaluate its interaction with the designed ligands, through NMR experiments.

I started working on expression, extraction and purification samples of hSTING, as described by Xiao-Xia Du and Xiao-Dong Su in Detection of Cyclic Dinucleotides by STING (methods section 6.2.3)[51]

It is well known that the active form of hSTING^{CTD} expressed as described by Xiao-Xia Du and Xiao-Dong Su in Detection of Cyclic Dinucleotides by STING is a dimer of about 60 kDa. Therefore, it was essential to assess that the recombinant protein expressed was indeed dimer or monomer in order to select the most appropriate NMR experiments. Size exclusion chromatography and SDS-PSAGE were carried out on nl-hSTING sample.

As shown in figure 12 on SDS-page hSTING had MW of about 30 kDa and the elution volume of hSTING was found after one previous peak of supposed oligomers
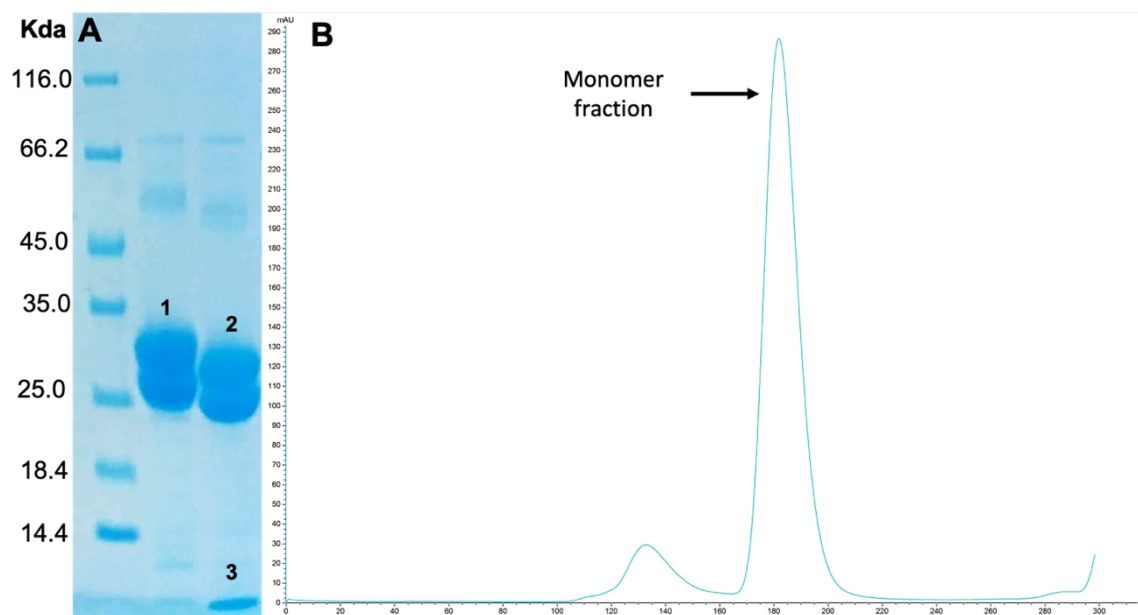
Figure 12. SDS-PAGE gel of nl-hSTING(A) before (A1) and before (A2 is hSTING and A3 is His-TAG) thrombin cleavage, and gel-filtration chromatogram (B) of nl-hSTING.

1D-^{1}H NMR and 2D ^{1}H–^{15}N HSQC spectra were acquired on free hSTING protein in order to evaluate whether the protein obtained was monomeric or dimeric. In addiction these spectra were performed in to confirm the correct folding and to identify the binding site of the protein.
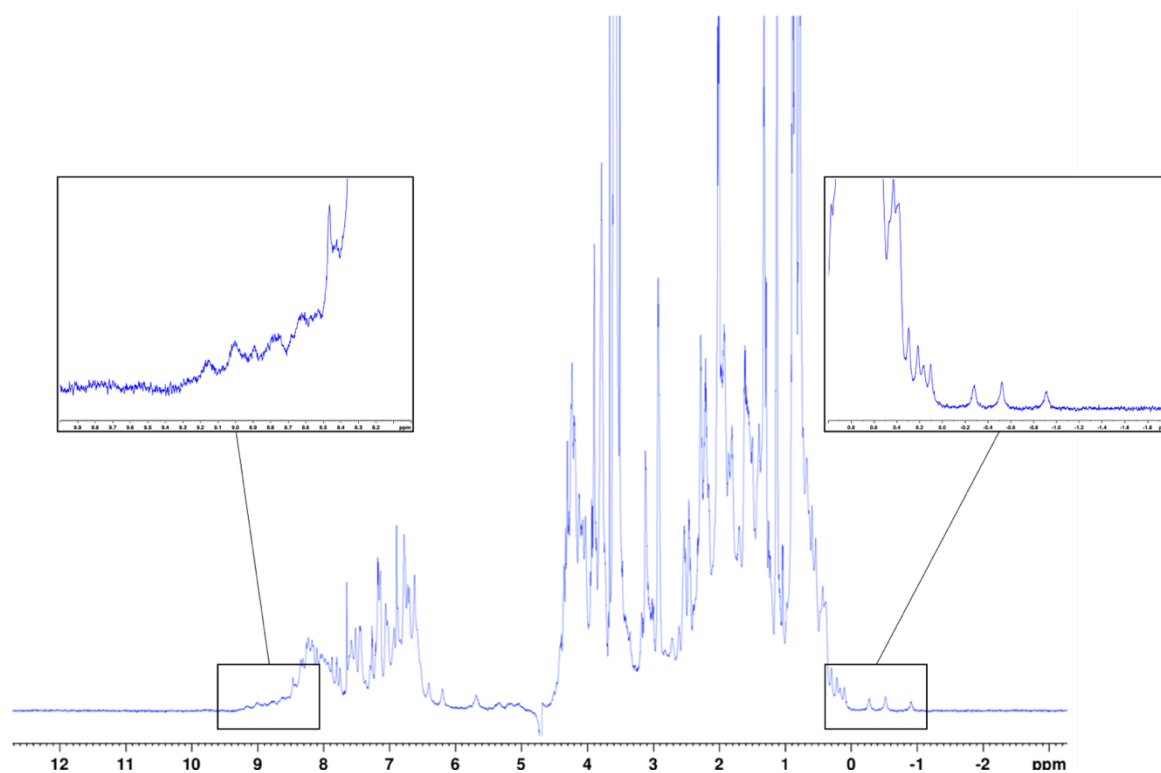
Figure 13 1D-^{1}H NMR spectra of 20 µM hSTING in 20 mM Tris-HCl, pH 8.0, 100 mM NaCl buffer and 10% D$_2$O,

As shown in imagine 13 of 1D-^{1}H NMR spectra of 20 μM hSTING in 20 mM Tris-HCl, pH 8.0, 100 mM NaCl buffer and 10% D$_2$O, the methyl signals under 0 ppm and the NH signals at 9 ppm indicate that protein is folded in the proper way. The methyl signal under 0 ppm indicates the presence of a hydrophobic region like a binding pocket and the good dispersion of NH signals at 9 ppm indicates the presence of tertiary and secondary structures of protein.

Analysis 1D-^{1}H spectrum, however, indicates that the hPD-L1 protein obtained with the expression and purification procedure previously shown is folded in the proper way, but doesn't give information about the conformational state

For this reason and in addiction to confirm the correct folding and to identify the binding site of the hSTING, HSQC spectra were acquired sample of 200 μM ^{15}N-hSTING in 20 mM Tris-HCl, pH 8.0, 100 mM NaCl buffer and 10% D$_2$O and 200 μM ^{2}D-^{13}C-^{15}N-hSTING in 20 mM MES-NaOH, pH 8.0, 100 mM NaCl buffer, 10mM TCEP buffer and 10% D$_2$O. Unfortunately, there is no reference HSQC spectrum of hSTING, but only of mSTING.

2D ^{1}H–^{15}N HSQC spectrum of the uniformly ^{15}N-labeled and ^{2}D-^{13}C-^{15}N- labeled hSTING are performed. The 2D ^{1}H-^{15}N and 2D-^{13}C-^{15}N- HSQC spectra of hSTING were not of very good quality, therefore a detailed characterization could not be possible. Unfortunately, there is no reference HSQC spectrum of hSTING with which to compare them, but only of mSTING.

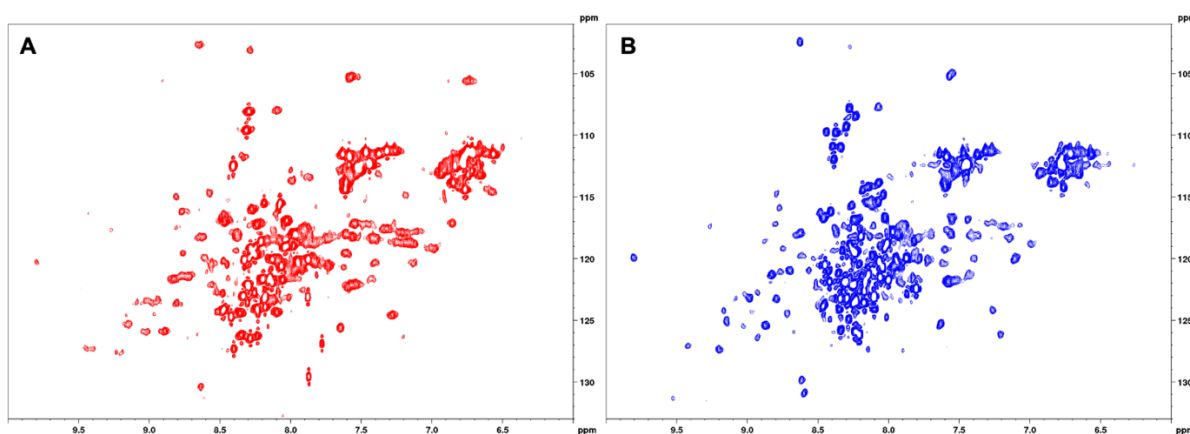**Figure 14** 2D ^{1}H–^{15}N HSQC spectra of 200 μM ^{15}N-hSTING (A,red) in 20 mM Tris-HCl, pH 8.0, 100 mM NaCl buffer and 10% D$_2$O and 200 μM ^{2}D-^{13}C-^{15}N-hSTING

(B,blu) in 20 mM MES-NaOH, pH 8.0, 100 mM NaCl buffer, 10mM TCEP buffer and 10% D_2O.

As shown in figure 14 the cross-peak of 2D ^1H-^{15}N and ^2D-^{13}C-^{15}N- HSQC are not good resolved. This shows that the protein in solution is in a dimeric state and that it is in a continuous conformational exchange between the open and the closed state. This explains why DMXAA was used to assign mSTING: to obtain a stable conformation. Since this result, it was fundamental to evaluate NMR experiments to be carried out, which were not based on protein observation but on ligands, unlike those carried out for the axis PD-1/PD-L1.

1D ^1H Ligand-based NMR experiments were used to detect the interaction between the hSTING protein not labelled, expressed and purified as previously described and our small library of synthesized compounds.

1D ^1H STD (Saturation Transfer Difference) and WaterLOGSY (Water-Ligand Observed by Gradient SpectroscopY, WL) spectra of 1 mM compounds were acquired in the presence of different hSTING 20μM, and the NMR proton phase of the compound signals were analyzed to discover new binding ligands. In the present NMR assay, we have compared the 1D ^1H STD an WL NMR spectra of new investigated ligands in the presence and absence of hSTING with those of the well-known binder ADU-S100, [5,39–43] which has been exploited as reference control in the presence of hSTING.

In Figure 15, the first spectrum (A, black) is the 1D ^1H-NMR spectrum of ADU-S100 in the presence of the hSTING protein. Analyzing the spectrum (B, blu) of the figure 15, which represents the WL spectrum of ADU-S100 in the presence of the protein hSTING, we can see how the aromatic signals of the ligand (9ppm-7ppm) are of opposite sign compared to that of the DMSO, a no-binder of hSTING used as a spy molecule. In the same way in the spectrum (C, red) of the Figure 16, which represents the STD of the ADU-S100 in the presence of the protein hSTING, we can notice the presence of the peaks relative to the proton resonances of the ligand. In addition, by comparing these spectra with those of ADU-S100 in the absence of the protein (Figure 16) we can note that in the WL (B, blu) the signals of both the ligand and the DMSO have the same phase; the spectrum STD (C,red) does not present ligand signals.
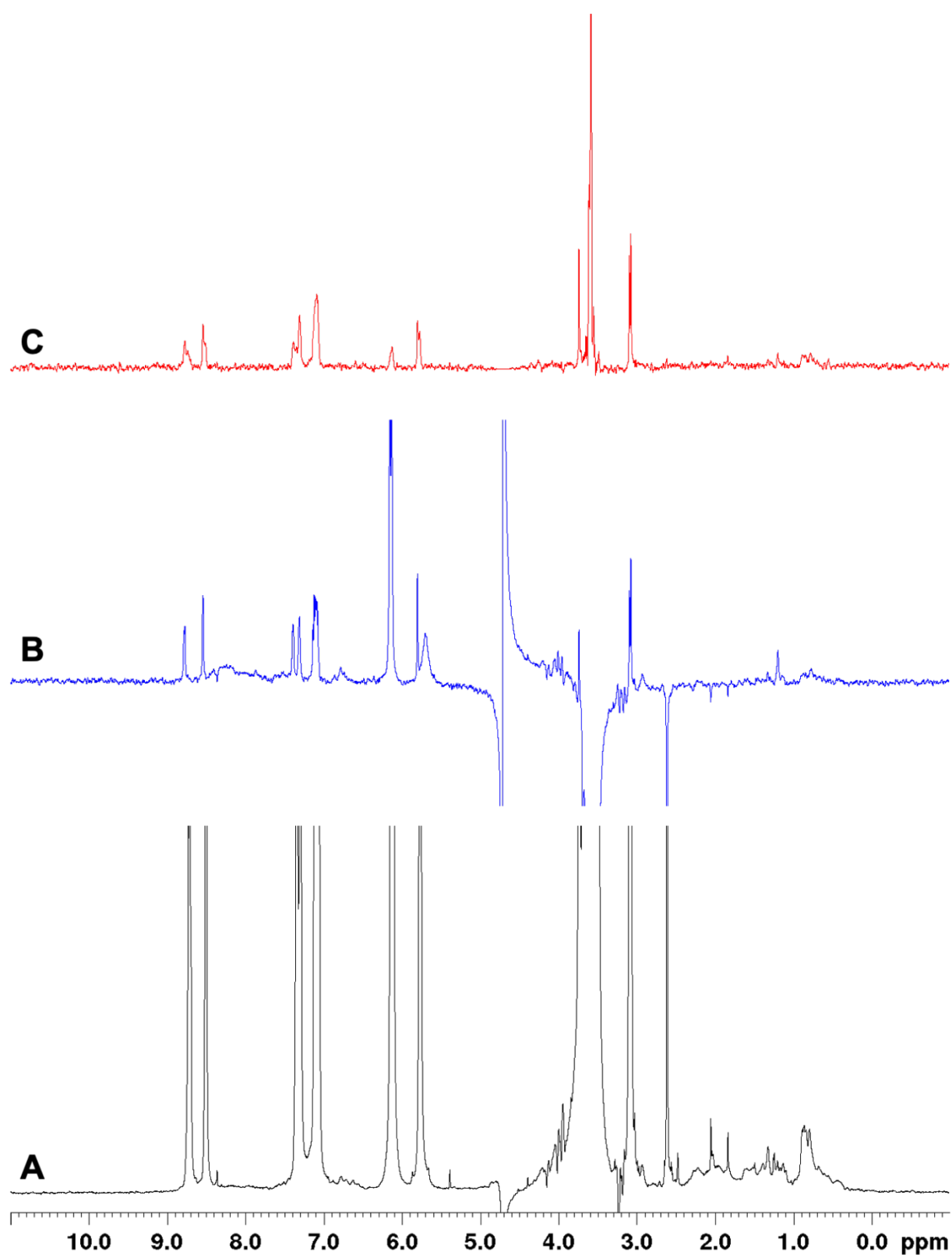
Figure 15. 1D-^{1}H NMR spectrum (A, black), WL spectrum (B, blu), STD spectrum (C, red) of ADU-S100 (1 mM) in presence of hSTING (20 μM)
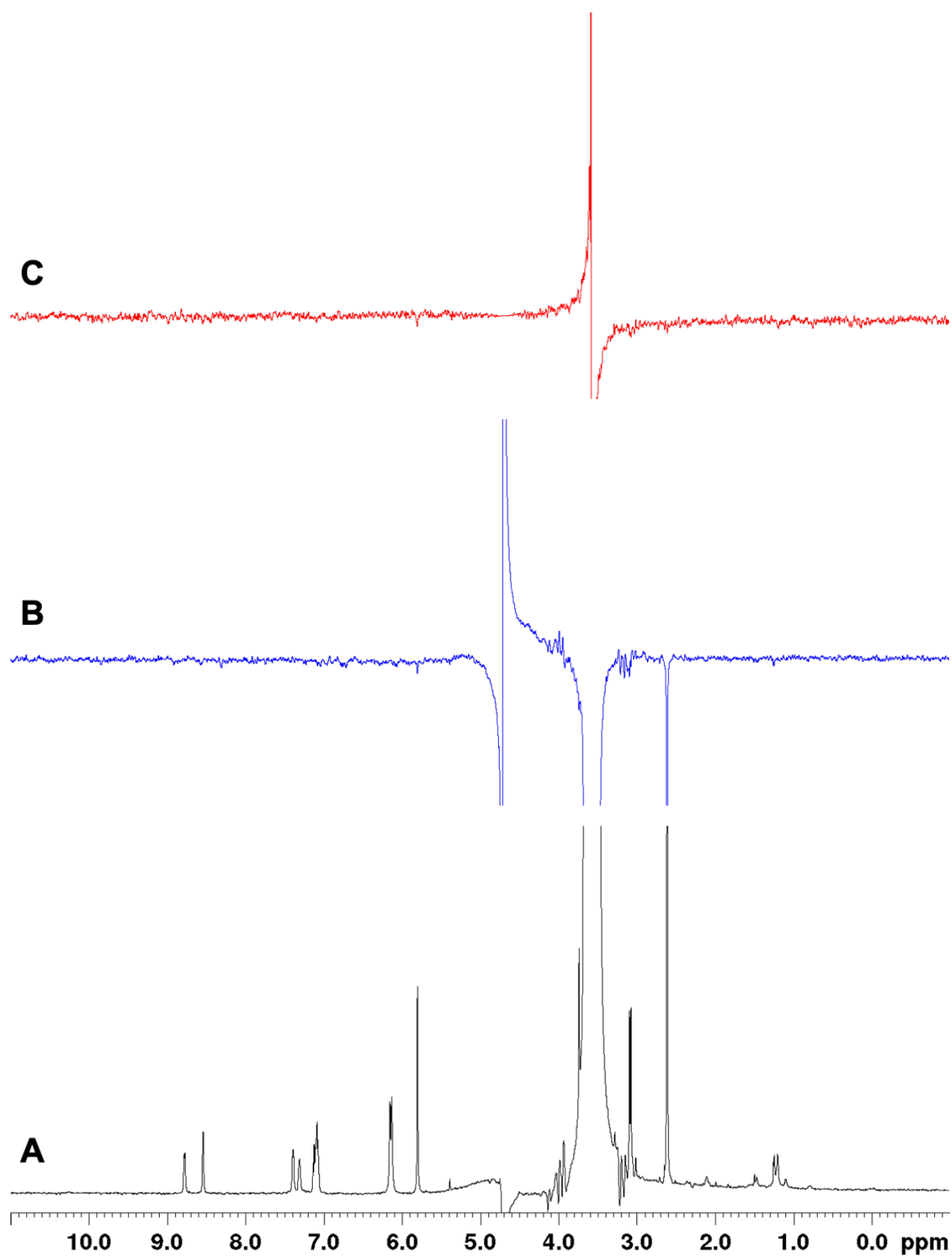
Figure 16. 1D-^{1}H NMR spectrum (A, black), WL spectrum (B, blu), STD spectrum (C ,red) of ADU-S100 (1 mM) in absence of hSTING

Similarly, samples were prepared containing hSTING (20 μM) in the presence of the ligands of our libraries (1mM) and were acquired the same experiments, STD and WL, in the same conditions.

53 compounds with different scaffold, belonged to different libraries, were screened. From analysis of 1D ^{1}H NMR STD and WL experiments, 20 compounds (**Table 1)** were found interact specifically with hSTING.

Figure 17 shows the spectra 1D ^{1}H-NMR hSTING + compound 21 (A, black); WL hSTING+ compound 21 (Bm blu); STD hSTING+ compound 21 (C, red). From the analysis of the WL NMR spectrum (B) we can note that the proton aromatic resonances of the compound 21 (9ppm-7ppm) have a phase opposite to the DMSO signal (2.60 ppm), as for ADU-S100. Analyzing the STD spectrum of compound 21 in the presence of the protein, we note the presence of aromatic signals (9ppm-7ppm) further confirming the interaction between the ligand and the protein. Again, to confirm the specificity of this interaction STD and WL NMR were acquired in the absence of hSTING (data not shown).
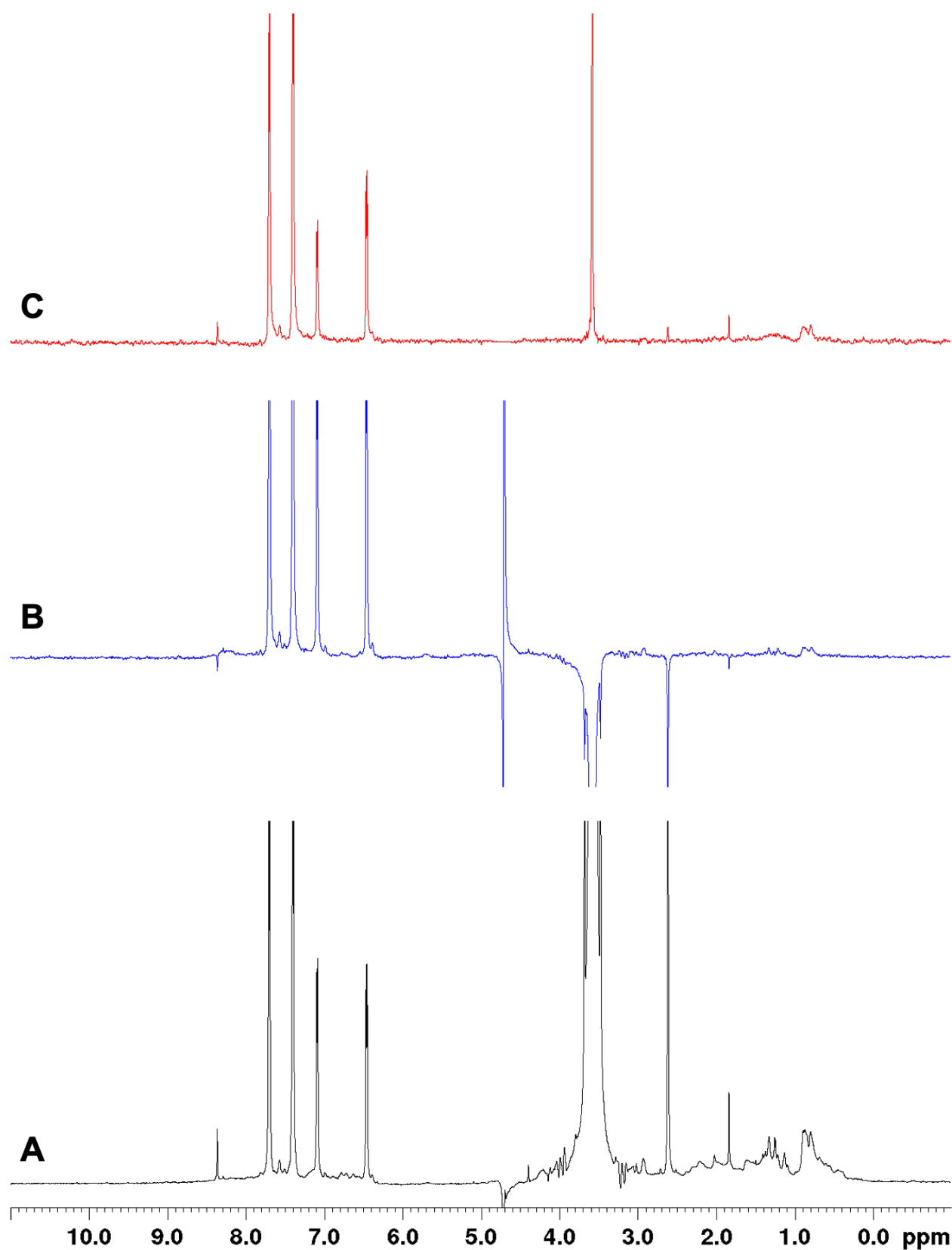
Figure 17. 1D-^{1}H NMR spectrum (A, black), WL spectrum (B, blu), STD spectrum (C, red) of compound 21 (1 mM) in presence of hSTING

Similar spectra have been obtained from the compounds in Table 1. Figure 18 show an example of STD and WL experiments of ligand binder and ligand not binder.
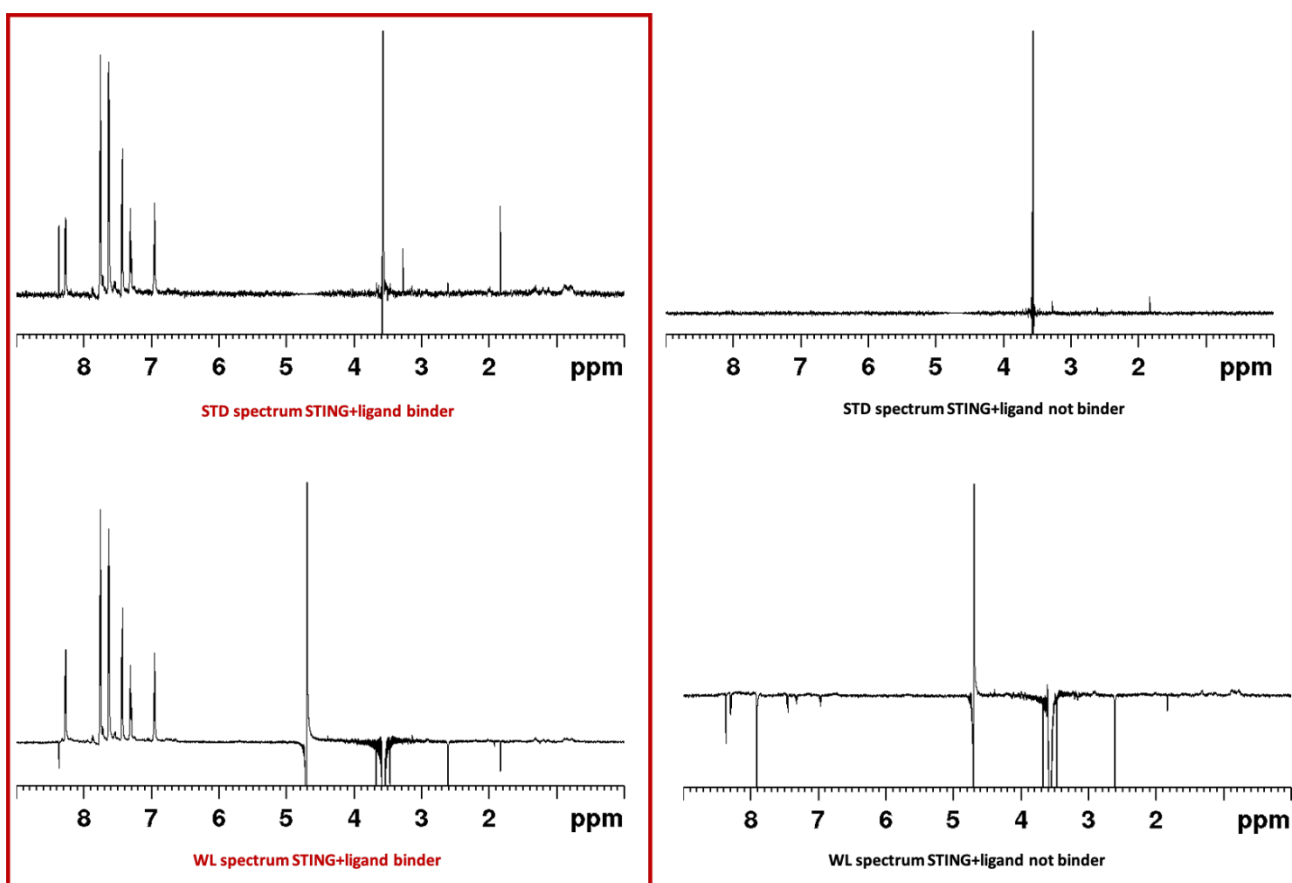
Figure 18 show the STD and WL of compound 22 (binder) in red square (left) and of compound not binder (right) of hSTING

Noteworthy, comparing the NMR spectra of hSTING/ADU-S100, hSTING/Compound 21, hSTING/Bider and hSTING/non binder in figure 15, 16, 17 and 18 it is clear how screening 1D ^{1}H ligand-based NMR STD and WL experiments was effective in the identification of new of hSTING binders, even if a quantitative evaluation of the binding potency is not feasible with this methodology.

The compounds identified as binder by 1D ^{1}H-NMR (Table1) will be tested quantitatively through a homogeneous time-resolved fluorescence (HTRF) binding assay, which will provide an IC_{50} and later tested in vitro in the same way described for PD-L1 inhibitors identified during my PhD project. In addiction HSQC NMR experiment were currently being carried out, in order to investigate the binding mode of our binder.

TABLE 1			
Structure	**Compound**	**Computational Studies**	**X-ray complex ref.**
	6	VS	STING/DMXAA (PDB code: 4QXP)
	7	VS	STING/DMXAA (PDB code: 4QXP)
	8	VS	STING/DMXAA (PDB code: 4QXP)
	9	VS	STING/DMXAA (PDB code: 4QXP)
	10	VS	STING/c-GAMP (PDB code: 4LOH
	12	VS	STING/di-ABZI (PDB code: 6DXL)
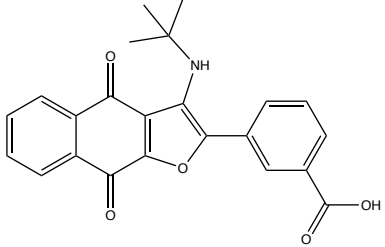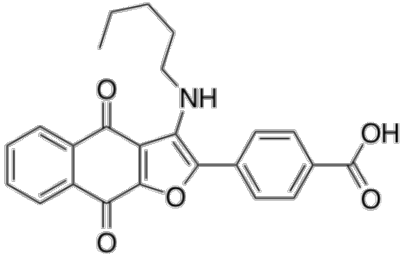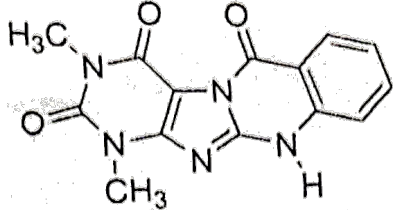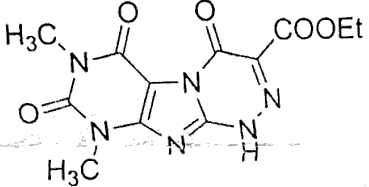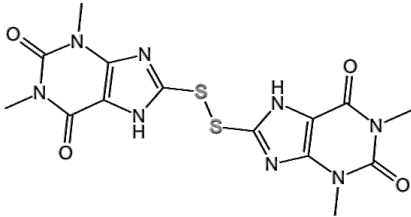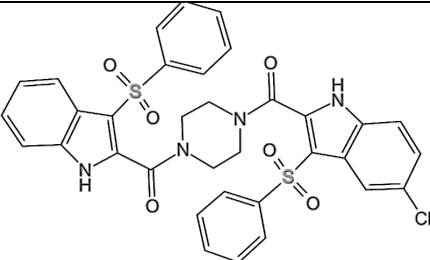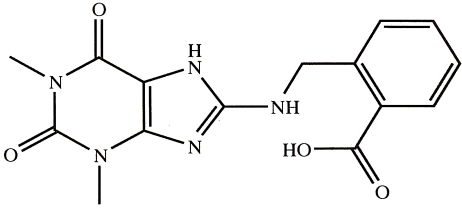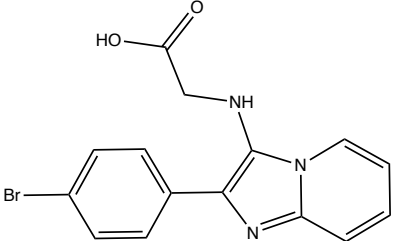
	13	VS	STING/ABZI (PDB code: 6DXG)
	14	VS	STING/ABZI (PDB code: 6DXG)
	15	VS	STING/SR717 (PDB code: 6XNP)
	16	VS	STING/SR717 (PDB code: 6XNP)
	17	VS	STING/SR717 (PDB code: 6XNP)
	18	VS	STING/SR717 (PDB code: 6XNP)
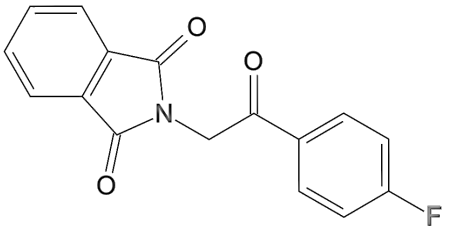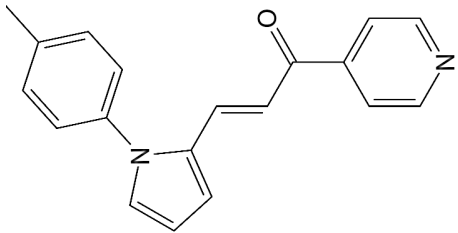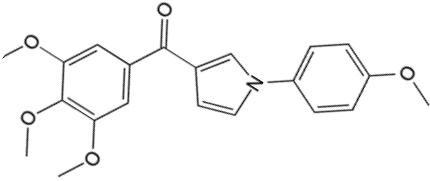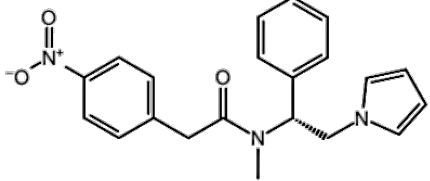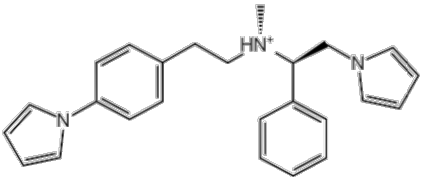
	19	VS	STING/SR717 (PDB code: 6XNP)
	20	VS	STING/di-ABZI (PDB code: 6DXL)
	21	VS	STING/ABZI (PDB code: 6DXG)
	22	VS	STING/ABZI (PDB code: 6DXG)
	23	VS	STING/ABZI (PDB code: 6DXG)
	24	VS	STING/DMXAA (PDB code: 4QXP)
	25	Core Hopping	STING/c-GAMP (PDB code: 4LOH)
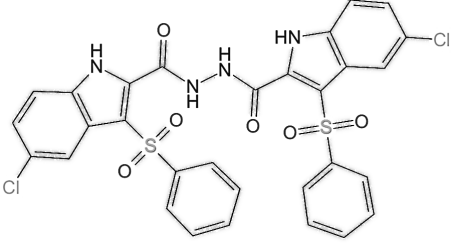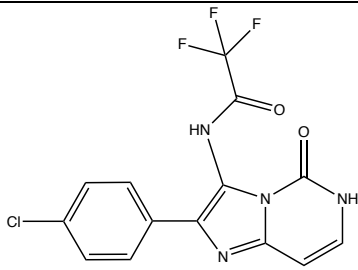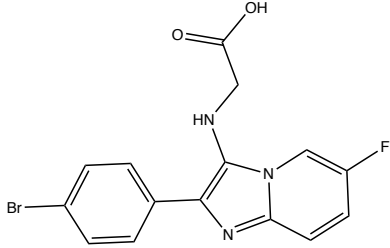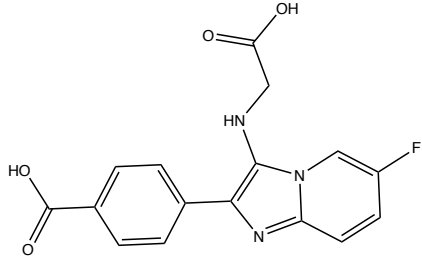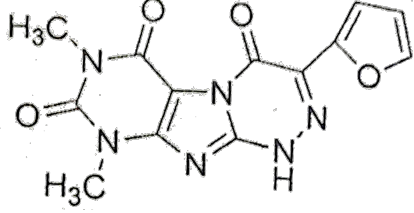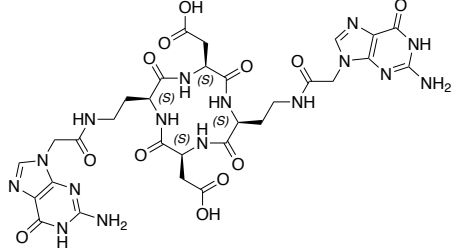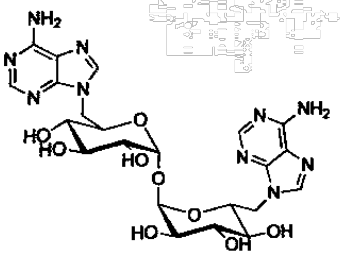
	26	Core Hopping	STING/c-GAMP (PDB code: 4LOH)

Table 1. Compounds identified as binder by 1D ^{1}H-NMR STD and WL experiments.

These compounds represented a starting point for rational design of libraries, in fact most promising molecules, after quantitatively tests, have undergone and will undergo reiterate cycles of design, synthesis and receptor binding test to improve their activity, selectivity and pharmacokinetic properties

As mentioned above, this last section of this paragraph describes further tests carried out, in collaboration with other research groups, to quantify and characterize the interaction between the hSTING and our compounds.

As a further confirm of the NMR assay results and to rank the novel ligands based on their *in vitro* ability to hSTING interaction, a homogeneous time-resolved fluorescence (HTRF) binding assay was used. This assay enables a simple and rapid characterization of inhibitors in a high-throughput format.

Basically, it uses tagged human recombinant hSTING and labelled anti-tag reagents for HTRF detection. More in detail, The HTRF STING binding assay is a competitive assay format which uses d2-labeled STING ligand, a 6His tagged human STING protein, and an anti 6His Cryptate-labeled antibody. The screening compound competes with the STING ligand-d2 and thereby prevents FRET from occurring. Thus, compounds able to bind hSTING interaction induce a reduction in HTRF signal. Among the newly synthesized compounds, two compounds (10 and 26) showed interaction with hSTING. Therefore, this compound was selected for subsequent biophysical and biological evaluations.

To assess the activator or inhibitory potential of these newly synthesized STING ligands, was used a human monocytic cell line, the Thp1, and evaluated their IFN response to these compounds in combination with a commercial cGAMP. Were taken in consideration parameters as: the transcriptional modulation of interferon stimulated genes

(e.g. MX1 and ISG15), and the phosphorylation and dimerization of several components of the STING pathway (STING itself, TBK1, IRF3, STAT). Shown are the results from a representative experiment: cGAMP alone strongly activated ISG expression and the STING pathway, while many ligands displayed the ability to counteract cGAMP and reduce the STING-dependent IFN response. Unfortunately, none of the compounds tested have shown to possess activator potential, but two of them revealed to have good inhibitory activity. Experiments performed so far indicate that the compound 10 possesses the highest inhibitory potential. In addition, compound 26 appears to possess the second highest inhibitory potential. These data are in accordance with the HTRF values, but analyses are still ongoing.
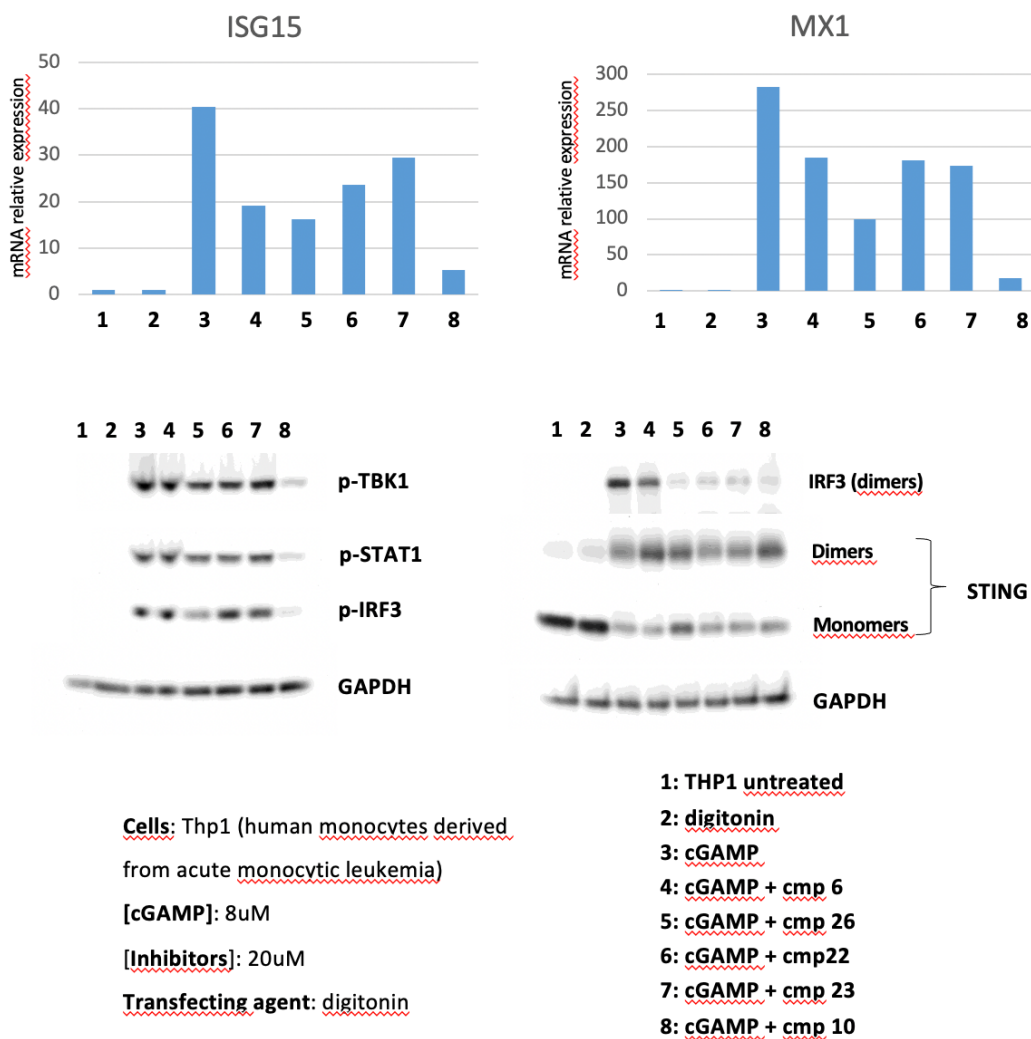
Figure 19 The INF response by novel STING Compound

5.2. Conclusion

STING activation has been found as the most promising approach to stimulate the innate immune system and improve tumor immunogenicity. STING is the pivotal protein on the innate immune cGAS–STING–TBK1 pathway implicated in the anti-tumor T cell response by recognizing tumor-derived CDNs. In fact, the recent studies were focused on STING agonistic approach and these efforts have provided a number of its agonists. Recently it was shown that activation of STING pathways is required to have immunosuppressive effects through upregulation of programmed death-1 ligand (PD-L1) in different cancer in response to DNA damage; so, combination of STING agonists with PD-1/PD-L1 antibodies or inhibitors was found to further boost antitumor immunity and to enforce control of tumor growth. In this respect, development of structurally new STING small ligands would be of the outmost importance. Herein, to do so, a combined approach of modeling/NMR was used. First Core Hopping ad five different Virtual Screening were carried. Then series of compounds was synthetized and assayed for their hSTING binding firstly by NMR, and then through HTRF assays. Two our compounds (10 and 26) showed a good interaction with hSTING on HTRF assay and were also subjected to further experiments to assess the activator or inhibitory potential and evaluated their IFN response in combination with a commercial cGAMP. These two compounds shown inhibitory activity, but analyses are still ongoing

5.3. References

(1)   Li, Y.; Wilson, H. L.; Kiss-Toth, E. Regulating STING in Health and Disease. *J. Inflamm. (United Kingdom)* **2017**, *14* (1), 1–21.

(2)   Yi, G.; Brendel, V. P.; Shu, C.; Li, P.; Palanathan, S.; Cheng Kao, C. Single Nucleotide Polymorphisms of Human STING Can Affect Innate Immune Response to Cyclic Dinucleotides. *PLoS One* **2013**, *8* (10), 1–16.

(3)   Barber, G. N. STING: Infection, Inflammation and Cancer. *Nat. Rev. Immunol.* **2015**, *15* (12), 760–770.

(4)   Bridget Larkin, Vladimir Ilyukha, Maxim Sorokin, Anton Buzdin, Edouard Vannier, and A. P. Activation of STING in T Cells Induces Type I IFN Responses and Cell Death Bridget. *J Immunol.* **2017**, *199* (2), 397–402.

(5)   Weinmann, H. Cancer Immunotherapy: Selected Targets and Small-Molecule Modulators. *ChemMedChem* **2016**, *11* (5), 450–466.

(6)   Sokolowska, O.; Nowis, D. STING Signaling in Cancer Cells: Important or Not? *Arch. Immunol. Ther. Exp. (Warsz).* **2018**, *66* (2), 125–132.

(7)   Qi, L.; Kash, J. C.; Dugan, V. G.; Jagger, B. W.; Lau, Y.; Crouch, E. C.; Hartshorn, K. L.; Taubenberger, J. K. STING Ligand C-Di-GMP Improves Cancer Vaccination against Metastatic Breast Cancer. *Cancer Immunol Res* **2012**, *412* (2), 426–434.

(8)   Deng, L.; Liang, H.; Xu, M.; Yang, X.; Burnette, B.; Arina, A.; Li, X. D.; Mauceri, H.; Beckett, M.; Darga, T.; Huang, X.; Gajewski, T. F.; Chen, Z. J.; Fu, Y. X.; Weichselbaum, R. R. STING-Dependent Cytosolic DNA Sensing Promotes Radiation-Induced Type I Interferon-Dependent Antitumor Immunity in Immunogenic Tumors. *Immunity* **2014**, *41* (5), 843–852.

(9)   Liu, X.; Wang, C. The Emerging Roles of the STING Adaptor Protein in Immunity and Diseases. *Immunology* **2016**, *147* (3), 285–291.

(10)   Paludan, S. R.; Bowie, A. G. Immune Sensing of DNA. *Immunity* **2013**, *38* (5), 870–880.

(11)   Burdette, D. L.; Vance, R. E. STING and the Innate Immune Response to Nucleic Acids in the Cytosol. *Nat. Immunol.* **2013**, *14* (1), 19–26.

(12)   Hopfner, K. P.; Hornung, V. Molecular Mechanisms and Cellular Functions of CGAS–STING Signalling. *Nat. Rev. Mol. Cell Biol.* **2020**, *21* (9), 501–521.

(13)   Yu, L.; Liu, P. Cytosolic DNA Sensing by CGAS : Regulation , Function , and

Human Diseases. *Signal Transduct. Target. Ther.* **2021**, *6* (170), 1–15.

(14)   Cai, X.; Chiu, Y. H.; Chen, Z. J. The CGAS-CGAMP-STING Pathway of Cytosolic DNA Sensing and Signaling. *Mol. Cell* **2014**, *54* (2), 289–296.

(15)   Balka, K. R.; De Nardo, D. Molecular and Spatial Mechanisms Governing STING Signalling. *FEBS J.* **2020**.

(16)   Zhu, Y.; An, X.; Zhang, X.; Qiao, Y.; Zheng, T.; Li, X. STING: A Master Regulator in the Cancer-Immunity Cycle. *Mol. Cancer* **2019**, *18* (1), 1–15.

(17)   Decout, A.; Katz, J. D.; Venkatraman, S.; Ablasser, A. The CGAS–STING Pathway as a Therapeutic Target in Inflammatory Diseases. *Nat. Rev. Immunol.* **2021**.

(18)   Nicole Dobbs, Nikolay Burnaevskiy, Didi Chen, Vijaya K Gonugunta, N. M. A. and N. Y. STING Activation by Translocation from the ER Is Associated with Infection and Autoinflammatory Disease. *Cell Host Microbe* **2015**, *18* (2), 157–168.

(19)   Yum, S.; Li, M.; Fang, Y.; Chen, Z. J. TBK1 Recruitment to STING Activates Both IRF3 and NF-KB That Mediate Immune Defense against Tumors and Viral Infections. *PNAS* **2021**, *118* (14), 1–9.

(20)   Chen, Q.; Sun, L.; Chen, Z. J. Regulation and Function of the CGAS-STING Pathway of Cytosolic DNA Sensing. *Nat. Immunol.* **2016**, *17* (10), 1142–1149.

(21)   Conggang Zhang, Guijun Shang, Xiang Gui, Xuewu Zhang, Xiao-chen Bai, Z. J. C. Structural Basis of STING Binding with and Phosphorylation by TBK1. *Nature* **2019**, *567* (7748), 394–398.

(22)   Tanaka, Y.; Chen, Z. J. STING Specifies IRF3 Phosphorylation by TBK1 in the Cytosolic DNA Signaling Pathway. *Sci. Signal.* **2012**, *5* (214), 1–12.

(23)   Abe, T.; Barber, G. N. Cytosolic-DNA-Mediated, STING-Dependent Proinflammatory Gene Induction Necessitates Canonical NF- B Activation through TBK1. *J. Virol.* **2014**, *88* (10), 5328–5341.

(24)   Khoo, L. T.; Chen, L. Role of the CGAS–STING Pathway in Cancer Development and Oncotherapeutic Approaches. *EMBO Rep.* **2018**, *19* (12).

(25)   Gao, P.; Zillinger, T.; Wang, W.; Ascano, M.; Dai, P.; Hartmann, G.; Tuschl, T.; Deng, L.; Barchet, W.; Patel, D. J. Binding-Pocket and Lid-Region Substitutions Render Human STING Sensitive to the Species-Specific Drug DMXAA. *Cell Rep.* **2014**, *8* (6), 1668–1676.

(26)   Wu, J.; Sun, L.; Chen, X.; Du, F.; Shi, H.; Chen, C.; Chen, Z. J. Cyclic GMP-AMP Is an Endogenous Second Messenger in Innate Immune Signaling by Cytosolic DNA. *Science (80-.).* **2013**, *339* (6121), 826–830.

(27)   Sun, L.; Wu, J.; Du, F.; Chen, X.; Chen, Z. J. Cyclic GMP-AMP Synthase Is a Cytosolic DNA Sensor That Activates the Type I Interferon Pathway. *Sciencexpress* **2013**, *339* (6121), 786–791.

(28)   Wan, D.; Jiang, W.; Hao, J. Research Advances in How the CGAS-STING Pathway Controls the Cellular Inflammatory Response. *Front. Immunol.* **2020**, *11* (615), 1–25.

(29)   Ahn, J.; Barber, G. N. STING Signaling and Host Defense against Microbial Infection. *Exp. Mol. Med.* **2019**, *51* (155), 1–10.

(30)   Woodward, J. J.; Lavarone, A. T.; Portnoy, D. A. C-Di-AMP Secreted by Intracellular Listeria Monocytogenes Activates a Host Type I Interferon Response. *Science (80-.).* **2010**, *328* (5986), 1703–1705.

(31)   Gao, P.; Ascano, M.; Zillinger, T.; Wang, W.; Dai, P.; Serganov, A. A.; Gaffney, B. L.; Shuman, S.; Jones, R. A.; Deng, L.; Hartmann, G.; Barchet, W.; Tuschl, T.; Patel, D. J. Structure-Function Analysis of STING Activation by c[G(20,50)PA(30,50)p] and Targeting by Antiviral DMXAA. *Cell* **2013**, *154* (4), 748–762.

(32)   Gao, P.; Ascano, M.; Wu, Y.; Barchet, W.; Gaffney, B. L.; Zillinger, T.; Serganov, A. A.; Liu, Y.; Jones, R. A.; Hartmann, G.; Tuschl, T.; Patel, D. J. Cyclic [G(2′,5′)PA(3′,5′)p] Is the Metazoan Second Messenger Produced by DNA-Activated Cyclic GMP-AMP Synthase. *Cell* **2013**, *153* (5), 1094–1107.

(33)   Romling, U.; Galperin, M. Y.; Gomelsky, M. Cyclic Di-GMP: The First 25 Years of a Universal Bacterial Second Messenger. *Microbiol. Mol. Biol. Rev.* **2013**, *77* (1), 1–52.

(34)   InvivoGen. Deciphering the STING Paradox STING,. *InvivoGen Rev. | STING* **2014**, *33*, 0–1.

(35)   Burdette, D. L.; Monroe, K. M.; Sotelo-Troha, K.; Iwig, J. S.; Eckert, B.; Hyodo, M.; Hayakawa, Y.; Vance, R. E. STING Is a Direct Innate Immune Sensor of Cyclic Di-GMP. *Nature* **2011**, *478* (7370), 515–518.

(36)   Ablasser, A.; Goldeck, M.; Cavlar, T.; Deimling, T.; Witte, G. Europe PMC Funders Group CGAS Produces a 2′-5′-Linked Cyclic Dinucleotide Second Messenger That Activates STING. *Nature* **2013**, *498* (7454), 380–384.

(37)   Zhang, X.; Shi, H.; Wu, J.; Zhang, X.; Sun, L.; Chen, C.; Chen, Z. J. Cyclic GMP-AMP Containing Mixed Phosphodiester Linkages Is an Endogenous High-Affinity Ligand for STING. *Mol. Cell* **2013**, *51* (2), 226–235.

(38)   Gao, J.; Tao, J.; Liang, W.; Zhao, M.; Du, X.; Cui, S.; Duan, H.; Kan, B.; Su, X.;

Jiang, Z. Identification and Characterization of Phosphodiesterases That Specifically Degrade 3'3'-Cyclic GMP-AMP. *Cell Res.* **2015**, *25* (5), 539–550.

(39)   Fu, J.; Kanne, D. B.; Leong, M.; Glickman, L. H.; McWhirter, S. M.; Lemmens, E.; Mechette, K.; Leong, J. J.; Lauer, P.; Liu, W.; Sivick, K. E.; Zeng, Q.; Soares, K. C.; Zheng, L.; Portnoy, D. A.; Woodward, J. J.; Pardoll, D. M.; Dubensky, T. W.; Kim, Y. STING Agonist Formulated Cancer Vaccines Can Cure Established Tumors Resistant to PD-1 Blockade. *Sci. Transl. Med.* **2015**, *7* (283).

(40)   Yan, H.; Wang, X.; KuoLee, R.; Chen, W. Synthesis and Immunostimulatory Properties of the Phosphorothioate Analogues of CdiGMP. *Bioorganic Med. Chem. Lett.* **2008**, *18* (20), 5631–5634.

(41)   Corrales, L.; Glickman, L. H.; McWhirter, S. M.; Kanne, D. B.; Sivick, K. E.; Katibah, G. E.; Woo, S. R.; Lemmens, E.; Banda, T.; Leong, J. J.; Metchette, K.; Dubensky, T. W.; Gajewski, T. F. Direct Activation of STING in the Tumor Microenvironment Leads to Potent and Systemic Tumor Regression and Immunity. *Cell Rep.* **2015**, *11* (7), 1018–1030.

(42)   Dhanak, D.; Edwards, J. P.; Nguyen, A.; Tummino, P. J. Small-Molecule Targets in Immuno-Oncology. *Cell Chem. Biol.* **2017**, *24* (9), 1148–1160.

(43)   Ding, C.; Song, Z.; Shen, A.; Chen, T.; Zhang, A. Small Molecules Targeting the Innate Immune CGAS–STING–TBK1 Signaling Pathway. *Acta Pharm. Sin. B* **2020**, *10* (12), 2272–2298.

(44)   Lioux, T.; Mauny, M. A.; Lamoureux, A.; Bascoul, N.; Hays, M.; Vernejoul, F.; Baudru, A. S.; Boularan, C.; Lopes-Vicente, J.; Qushair, G.; Tiraby, G. Design, Synthesis, and Biological Evaluation of Novel Cyclic Adenosine-Inosine Monophosphate (CAIMP) Analogs That Activate Stimulator of Interferon Genes (STING). *J. Med. Chem.* **2016**, *59* (22), 10253–10267.

(45)   McKeage, M. J.; Von Pawel, J.; Reck, M.; Jameson, M. B.; Rosenthal, M. A.; Sullivan, R.; Gibbs, D.; Mainwaring, P. N.; Serke, M.; Lafitte, J. J.; Chouaid, C.; Freitag, L.; Quoix, E. Randomised Phase II Study of ASA404 Combined with Carboplatin and Paclitaxel in Previously Untreated Advanced Non-Small Cell Lung Cancer. *Br. J. Cancer* **2008**, *99* (12), 2006–2012.

(46)   Zhang, Y.; Sun, Z.; Pei, J.; Luo, Q.; Zeng, X.; Li, Q.; Yang, Z.; Quan, J. Identification of α-Mangostin as an Agonist of Human STING. *ChemMedChem* **2018**, *13* (19), 2057–2064.

(47)   Ramanjulu, J. M.; Pesiridis, G. S.; Yang, J.; Concha, N.; Singhaus, R.; Zhang, S.

Y.; Tran, J. L.; Moore, P.; Lehmann, S.; Eberl, H. C.; Muelbaier, M.; Schneck, J. L.; Clemens, J.; Adam, M.; Mehlmann, J.; Romano, J.; Morales, A.; Kang, J.; Leister, L.; Graybill, T. L.; Charnley, A. K.; Ye, G.; Nevins, N.; Behnia, K.; Wolf, A. I.; Kasparcova, V.; Nurse, K.; Wang, L.; Li, Y.; Klein, M.; Hopson, C. B.; Guss, J.; Bantscheff, M.; Bergamini, G.; Reilly, M. A.; Lian, Y.; Duffy, K. J.; Adams, J.; Foley, K. P.; Gough, P. J.; Marquis, R. W.; Smothers, J.; Hoos, A.; Bertin, J. Design of Amidobenzimidazole STING Receptor Agonists with Systemic Activity. *Nature* **2018**, *564* (7736), 439–443.

(48)   Al., X. Z. et. Discovery and Mechanistic Study of a Novel Human STING Agonist. *ACS Infect Dis* **2019**, *5* (7), 1139–1148.

(49)   Chin, E. N.; Yu, C.; Vartabedian, V. F.; Jia, Y.; Kumar, M.; Gamo, A. M.; Vernier, W.; Ali, S. H.; Kissai, M.; Lazar, D. C.; Nguyen, N.; Pereira, L. E.; Benish, B.; Woods, A. K.; Joseph, S. B.; Chu, A.; Johnson, K. A.; Sander, P. N.; Martínez-peña, F.; Hampton, E. N.; Young, T. S.; Wolan, D. W.; Chatterjee, A. K.; Schultz, P. G.; Petrassi, H. M.; Teijaro, J. R.; Lairson, L. L. Antitumor Activity of a Systemic STING-Activating Non-Nucleotide CGAMP Mimetic. *Science (80-.).* **2020**, *369* (August), 993–999.

(50)   Pan, B. S.; Perera, S. A.; Piesvaux, J. A.; Presland, J. P.; Schroeder, G. K.; Cumming, J. N.; Wesley Trotter, B.; Altman, M. D.; Buevich, A. V.; Cash, B.; Cemerski, S.; Chang, W.; Chen, Y.; Dandliker, P. J.; Feng, G.; Haidle, A.; Henderson, T.; Jewell, J.; Kariv, I.; Knemeyer, I.; Kopinja, J.; Lacey, B. M.; Laskey, J.; Lesburg, C. A.; Liang, R.; Long, B. J.; Lu, M.; Ma, Y.; Minnihan, E. C.; O'Donnell, G.; Otte, R.; Price, L.; Rakhilina, L.; Sauvagnat, B.; Sharma, S.; Tyagarajan, S.; Woo, H.; Wyss, D. F.; Xu, S.; Bennett, D. J.; Addona, G. H. An Orally Available Non-Nucleotide STING Agonist with Antitumor Activity. *Science (80-.).* **2020**, *369* (August), 935–944.

(51)   Du, X. X.; Su, X. D. Detection of Cyclic Dinucleotides by STING. *Methods Mol. Biol.* **2017**, *1657*, 59–69.

Chapter 6

Materials and Methods

This chapter describes all several scientific field and all different theoretical and experimental techniques used for my PhD project. I used multidisciplinary approach in order to integrate different scientific fields for this aim: discover and develop inhibitors of MDM2 protein and PD-1/PDL-1 axis and new agonists capable of activating STING. Initially, I used several computational methodologies to discover and develop new molecules, then I focused on expression, purification and biochemical and structural characterization of the proteins. Finally, I decided to use 1D ^{1}H NMR screening experiment as a method to detect the interaction between my target proteins and the molecules obtained from modelling and synthesized.

6.1. Molecular modelling

Molecular modelling includes all methods and computational techniques used to simulate and study the structures and behaviors of molecules. These techniques are used in the fields of chemistry and biology for the study of both small biological systems and macromolecules. The use of the computer has thus allowed the application of molecular modeling for relatively complex systems. [1–4]

Most molecular modelling studies are developed in 3 stages. The first stage involves the selection of a model for inter- and intra-molecular description of the interactions of the system. The second stage includes simulations that allow to calculate, for example, the energy associated with a minimum conformation, the search for the correct conformation or even a simulation of molecular dynamics. The third and final step involves the analysis of the data and properties obtained during the calculations carried out in the second step. In the pharmaceutical chemistry, molecular modelling is used in various ways depending on the information available, but always with the aim of designing and/ or optimizing potential drugs against diseases of interest. [4–8]

In a simplified way we can see molecular modeling as a set of techniques that exploit concepts and theories of multiple fields of study, theoretical and applied, in order to study and obtain information about molecular systems.

6.1.1. Molecular Docking and Virtual Screening

Molecular docking is a computational technique that allows the study of the interaction between two molecules. It is used, in particular, to study the interaction of proteins with other molecules such as nucleic acids, small molecules and other proteins. In medicinal chemistry Molecular Docking is the computational procedure used for the prediction of interactions and binding mode of ligand within molecular target. This method is also used to perform virtual screening of large libraries of compounds, then to classify the results according to a score and finally propose structural hypotheses of the best ligand present in the library and how it binds to the protein. [4–8]

A normal Molecular Docking protocol (Figure 1) provides the choice and preparation of protein and ligand before performing the actual docking.
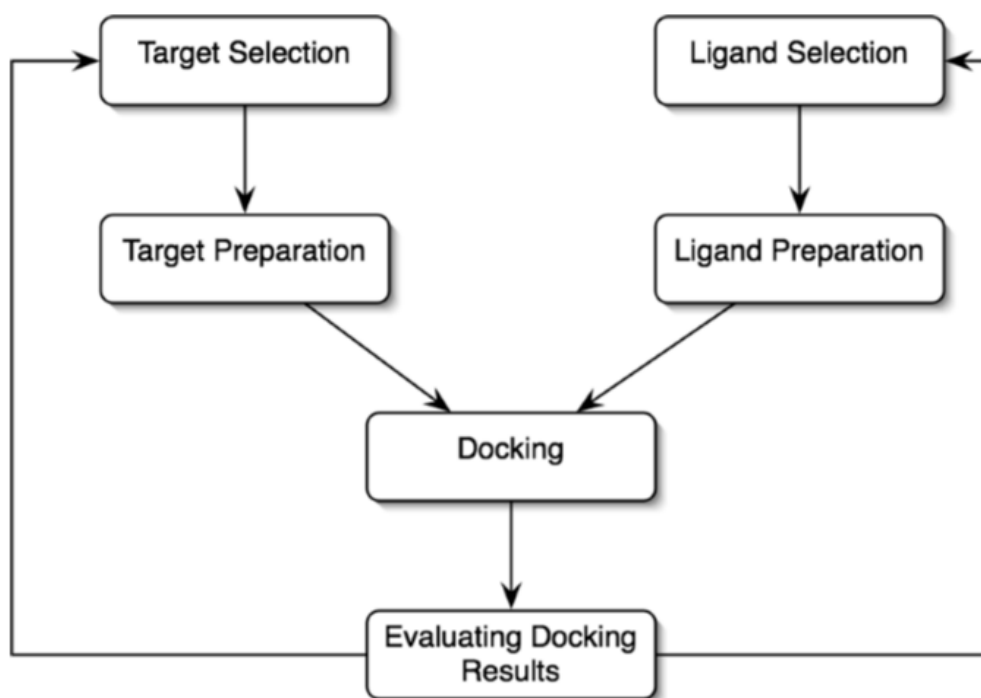
Figure 1. Molecular Docking workflow (adopted from M.Morris [2])

The docking process involves the use of an algorithm, which places ligands within the binding site of the macromolecule and then evaluates ligand-macromolecule interactions by assigning a specific score. The most aspect of docking is the evaluation of score and ranking of ligands. The calculations are very expensive, so the scoring functions implemented in the docking programs are simplified through the use of consensus

scoring. It combines information from different scores to balance errors in single scores. [4–8]

In pharmaceutical chemistry, Virtual Screening (VS) is the most used method to analyze large libraries of compounds in order to identify *Hits Compounds*. There are different types of VS, but the most used is the structure-based virtual screening (SBVS). The SBVS are based on molecular docking, and it is used to predict the binding of a large libraries of ligands into a specific target. [3,5,6,8]

A classical VS protocol provides:

- Choice and preparation of ligands libraries: large databases are filtered to create smaller databases and to remove potentially undesirable molecules.
- Molecular docking
- Analysis of results and hits selection. This is the critical step. For the selection of Hits Compounds it is not possible to rely only on the free energy values of each ligand calculated by the computer and then from the ranking obtained automatically. It is necessary to associate quantitative measures (calculated by the pc) with the visual analysis of the results such as the interaction of the ligand with the essential amino acids to obtain the biological effect and further interactions or similarity with the pose of the reference ligand. [3,5,6,8]

6.1.2. Core Hopping

De novo design strategies (*de novo drug design*) are very important in molecular modelling and are applied for the discovery of new leads, but especially for the optimization of *Hits Compounds*. To improve the activity of a compound are often made to vary the side chains attached to the central scaffold of the molecule, but in many cases, it is the side chains that bind to the protein. In this case, to improve the activity, the central nucleus of the molecule must be modified, leaving the lateral chains unchanged. This procedure is carried out with the Core Hopping (Figure 2). The strategy of Core Hopping is to screen the largest number of scaffolds replacing that of the original compound, without changing the side chains, and then docking the new structures in the receptor

pocket of the protein under study, through a previously developed molecular docking protocol. In case the structure of the protein, but especially of the receptor pocket, is available, the work with the Core Hopping is advantageous because the program automatically performs the process of molecular docking in the receptor pocket under examination, assigning a docking score to all new generated structures. If instead the structure of the receptor is not available, the new compounds are evaluated assigning a numerical value to each of them based on the overlap and alignment with the original compound of which the starting Core. There are two types of Core Hopping: Ligand-based e Glide-based. The Core Hopping Ligand-Based, compared to Glide-Based, turns out to be the most selective and restrictive procedure. [9–11]
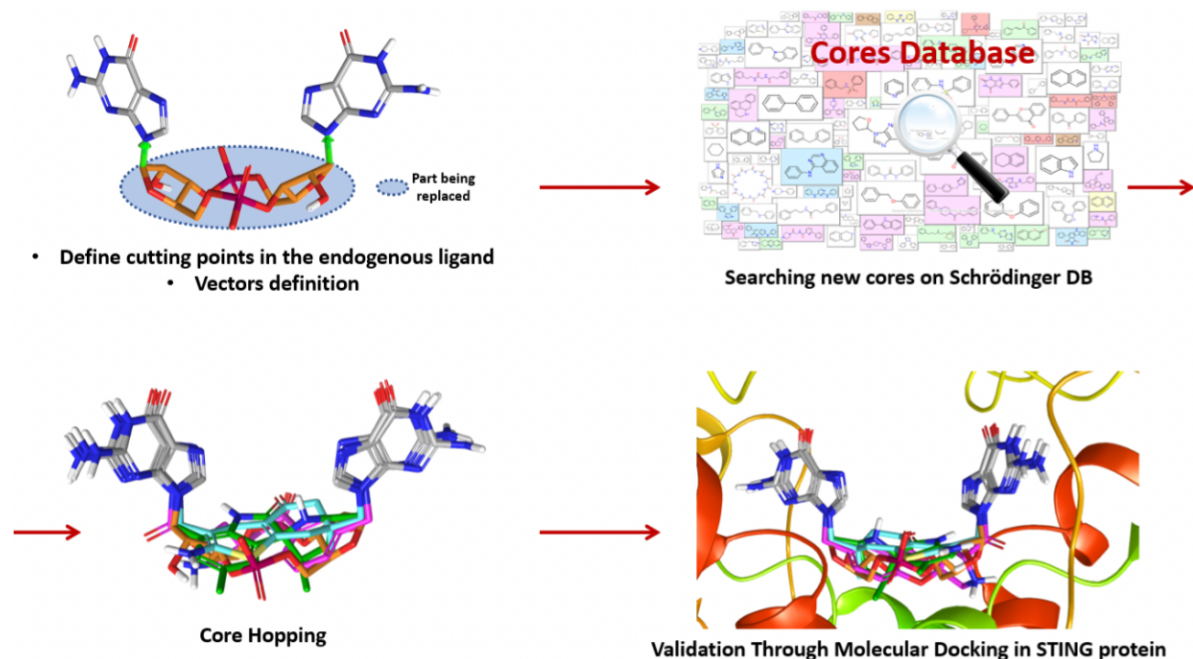
Figure 2. Core Hopping workflow.

6.1.3. MDM2

The first part of my PhD project was aimed to discover and develop new inhibitors for the MDM2/p53 complex. I was involved in of hMDM2 inhibitors design, starting from literature studies and previously VS work [12] done by the research group in which I work. In collaboration with the research groups of Simona Daniele of University of Pisa and Romano Silvestri of University of Roma, we designed a number of compounds derivates of RS3760 and also longer molecules endowed with a sulfonyl-phenyl branch.

The ligand 3D structures were built with the Maestro Build Panel. All the tautomeric and protomeric states at physiological pH (7.4 ± 1.5) were predicted using the Epik software implemented in the Ligprep tool.[13,14] The X-ray complex of MDM2 with Mi-65 inhibitor (PDB code: 3LBL) was selected due to the high degree of structural similarity between the co-crystalized ligand and our compounds. The receptor was prepared with the aid of the Protein Preparation Wizard panel of Maestro Suite (Schrödinger Release 2019-2: Schrödinger Suite 2019-1)[15] adding the missing hydrogen atoms and removing all the water molecules with less than two hydrogen-bonds to non-water molecules. In addition, the side chains ionization and tautomeric states were predicted, and the H-bonding network of the receptor refined minimizing the position of each hydrogen. The search grid was set around the co-crystallized ligand through the grid generation tool of the Glide 8.1 program. [16–18] Then, docking calculations were performed using Glide 8.1 in its XP variant and employing the OPLS3E force field [16–18] Thus, the top-ranked compounds were selected and visually double checked for a good chemical geometry.

6.1.4 PD-1/PD-L1 axis

The first part of my PhD project was aimed to discover and develop new inhibitors for the PD-1/PDL1 axis through computational methods. In particular, I was involved in of hPD-L1 inhibitors design, starting from literature studies. [19–40] The BMS-202/PD-L1 X-ray complex (PDB code: 5J89)[41] together with some biochemical data represented a precious starting point for ligand-based design or "me too" strategies. In collaboration of research group of Prof. Seneci of University of Milano, we looked for an accessible and synthetically flexible core replacement of BMS202 in order to obtained new ligand[24–30,37,41–45].

The ligand 3D structures were built with the Maestro Build Panel. All the tautomeric and protomeric states at physiological pH (7.4 ± 1.5) were predicted using the Epik software implemented in the Ligprep tool.[13,14] The X-ray complex of homodimeric PD-L1 with BMS202 (PDB code: 5J89) was selected due to the high degree of structural similarity between the co-crystalized ligand and our compounds. The receptor was prepared with the aid of the Protein Preparation Wizard panel of Maestro Suite (Schrödinger Release 2019-2: Schrödinger Suite 2019-1)[15] adding the missing hydrogen atoms and removing all the water molecules with less than two hydrogen-bonds to non-water molecules. In addition, the side chains ionization and tautomeric states were predicted, and the H-bonding network of the receptor refined minimizing the position of each hydrogen. The search grid was set around the co-crystallized ligand through the grid generation tool of the Glide 8.1 program. [16–18] Then, docking calculations were performed using Glide 8.1 in its SP variant and employing the OPLS3E force field [16–18] Thus, the top-ranked compounds were selected and visually double checked for a good chemical geometry.

6.1.5. STING

Another section of my PhD project concerned the application of computational methodologies in order to discover and develop new agonists capable of activating STING. Starting from hSTINg/binder X-ray complex and literature studies [46–75] , I aim at design and development of novel STING agonists through different computational methods: Core Hopping, Virtual Screening (VS) and rational design.

The ligand 3D structures were built with the Maestro Build Panel. All the tautomeric and protomeric states at physiological pH (7.4 ± 1.5) were predicted using the Epik software implemented in the Ligprep tool. [13,14] The receptor was prepared with the aid of the Protein Preparation Wizard panel of Maestro Suite (Schrödinger Release 2019-2: Schrödinger Suite 2019-1) [15] adding the missing hydrogen atoms and removing all the water molecules with less than two hydrogen-bonds to non-water molecules. In addition, the side chains ionization and tautomeric states were predicted, and the H-bonding network of the receptor refined minimizing the position of each hydrogen. The search grid was set around the co-crystallized ligand through the grid generation tool of the Glide

8.1 program. [(16–18)] The VS was performed using Glide 8.1 in its HTS variant and employing the OPLS3E force field [(16–18)]. The docking calculations was performed using Glide 8.1 in its SP variant and employing the OPLS3E force field [(16–18)] Thus, the top-ranked compounds were selected and visually double checked for a good chemical geometry.

As regarding the Core Hopping, the hSTING X-ray complex with c-GAMP (PDB code: 4LOH) has been selected as starting point for sugar/phosphodiester substitution strategy of CDNs binder. New cores of structures were prepared with using the core_library_2014.1-86640.sqlite of "Core hopping" facility of Maestro Suite (Schrödinger Release 2019-2: Schrödinger Suite 2019-1). [9–11] Then, the docking calculations was performed using Glide 8.1 in its SP variant and employing the OPLS3E force field [(16–18)] Thus, the top-ranked compounds were selected and visually double checked for a good chemical geometry.

6.2 Protein expression and purification

A further progress in my PhD project regarded expression, extraction and purification of N-teminal domain of hMDM2, extracellular domain of hPD-1 and PD-L1 and cytosolic domain of hSTING, the four proteins used as model. Protein expression is the biotechnological process in order to generate a specific protein by a vector. It is obtained by manipulating gene expression in an organism in which a large amount of a recombinant gene is expressed and then protein encoded by that gene. Commonly used protein production vector are *E. Coli* but some proteins can be difficult to obtain because it lacks intracellular organelles responsible for post-translational modifications of proteins expression.[76–78] Protein purification is a series of processes designed to isolate a specific protein from a complex mixture. [79–82] Protein purification is one of the most important and laborious processes for the characterization of protein function, structure of interest. The selection of methods of purification is made in relation to the type of protein expression by the vector. It can express the protein in the cytosol (soluble protein) or store it as insoluble inclusion bodies within the cytoplasm (insoluble protein). The extraction of the protein from the inclusion bodies is a very critical step, since the protein is denatured and then refolded through precise buffers and procedures.[83–86]

Samples of hMDM2, hPD-1, hPD-L1 and hSTING with different isotopic labeling patterns were prepared:

- not labeled hPD-1 (nl-hMDM2), ^{15}N uniformly labeled hPD-1 (^{15}N-hMDM2)
- not labeled hPD-1 (nl-hPD-1), ^{15}N uniformly labeled hPD-1 (^{15}N-hPD-1)
- not labeled hPD-L1 (nl-hPD-L1), ^{15}N uniformly labeled hPD-L1 (^{15}N-hPD-L1)
- not labeled hSTING, ^{15}N uniformly labeled hSTING (^{15}N-hSTING) and ^{2}D,^{13}C and ^{15}N uniformly labeled hSTING (^{2}D,^{13}C,^{15}N- hSTING)

The protocol for the expression was adapted according to the medium used for the different labeling [87]. The present chapter describes all the experimental procedures, also biophysical and NMR characterization of the proteins is showed too.

6.2.1 MDM2

The plasmid encoding hMDM2 (amino acids 1-117, MW of 15,1 kDa) construct and were cloned into two different pET-28a.

```
-50     ---------------------------------MAHHHHHHVDDDDK
000     MCNTNMSVPTDGAVTTSQIPASEQETLVRPKPLLLKLLKSVGAQKDTYTM
050     KEVLFYLGQYIMTKRLYDEKQQHIVYCSNDLLGDLFGVPSFSVKEHRKIY
100     TMIYRNLVVVNQQESSD---------------------------------
150     --------------------------------------------------
200     --------------------------------------------------
250     --------------------------------------------------
300     --------------------------------------------------
350     --------------------------------------------------
400     --------------------------------------------------
491     ----------------------------------------
```

Figura 3 Amino acid sequences of hMDM2 expressed

As shown in figure 3 the insertion of Met (M black in figure 3) is essential for the production of proteins: the start codon that initiates translation process in E.Coli is ATG (Met). [76] The plasmid encoding hMDM2, before the protein sequence (1-117) presents in the N-terminal part a 6xHIS-tag (blu in figure 3). The HIS-tag is used to initially purify the protein after the cellular lysis. Before using, the plasmid containing the gene was amplified by transforming in Top10 competent cells and purified through Midiprep and Miniprep techniques based on alkaline lysis method. [77,88]

medium in the shaker overnight to obtain the preculture. Different culture media and different expression approaches were used for the differently isotopic labeled hMDM2.

For the expression of nl-MDM2, the preculture of, pET-28a(+) transformed cells was poured into 1 LB medium supplied with Kanamicyn (0.1 mg mL^{-1}). A drop of antifoam was even added, and the culture was let shake at 37°C until OD reached 0.60. The protein overexpression was induced with 1mM IPTG and the culture further shaken at 37°C for 5h. Cells were harvested centrifugate at 7500 rpm for 15 min. The supernatant was discarded, whereas the pellet was resuspended in 50 mM Tris-HCl, pH 8.0, 50 mM TRIS-HCl 8 M GdmCl pH 8.0 (20 mL per liter of culture) and 8mM DTT.

The mixture was homogenized, then sonicated for 5 cycles, finally ultracentrifuged. The residual pellet was discarded, whereas the supernatant (GdmCl stock) was stored at 4°C. The GdmCl stock containing unfolded hMDM2 was slowly 15-fold diluted in 50 mM TRIS-HCl 500 mM NaCl pH 8.0 under vigorous magnetic stirring. A HiTrap HP column (Ni-column) was connected to a peristaltic pump, washed with H2O and equilibrated with 50 mL of 50 mM Tris-HCl, pH 8.0, 500 mM NaCl, 5 mM imidazole (without DTT) at a flow rate of approximately 3 mL / min and the solution containing the protein was then cyclically loaded onto a Ni-column for 3h. HiTrap HP column (Ni-column) containing the protein was connected into AKTA Pure system and then 2 elution steps were performed:

1. Wash impurities with 20–40 ml buffer 50 mM Tris-HCl, pH 8.0, 500 mM NaCl, 5 mM imidazole, 2,5 mM DTT, at a flow rate of 2.5 ml/min until UV absorption at 280 nm reaching baseline.
2. Elute the target proteins with a linear gradient buffer 50 mM Tris-HCl, pH 8.0, 500 mM NaCl, 500 mM imidazole, 2.5 mM DTT from 0% to 100%. Collect target protein according to UV 280 nm absorption.

The fractions containing hMDM2 were identified by Coomassie staining SDS-PAGE and collected.

The fractions were merged and therefore concentrated. The concentrations of hMDM2 in solution was achieved by UV-Vis spectroscopy using a Varian Cary 50 UV-Vis Spectrophotometer (Agilent) implemented with Cary WinUV software. Absorbance profile in the range of 250-350 nm was recorded and the value at 280 nm was used for

the estimation of protein amount. The molar extinction coefficient at 280 nm were $\varepsilon(ox)$ = 10555 M-1 cm-1 and $\varepsilon(red)$ = 10430 as calculated by the on-line ExPASy - ProtParam tool. In each experiment, a baseline correction was applied by acquiring a spectrum of the blank. The solution was concentrated and purified by size exclusion chromatography on a Hi-Load 26/60 Superdex 75pg column (GE Healthcare), previously equilibrated with 50 mM KH2PO4 50 mM Na2HPO4 150 mM NaCl pH 7.5 buffer. Elution was performed at 2.5 mL/min and fractions containing hMDM2 were collected. Therefore, the fractions containing hSMDM2 were collected and the concentrations were achieved by UV-Vis spectroscopy. The solutions of pure proteins were supplied with 0.1% NaN_3 and protease inhibitors (Roche), then stored at 4°C for NMR experiments. The protein folding was evaluated by NMR.

For the expression of ^{15}N-hSTING The preculture of, pET-28a(+) transformed cells was poured into 1L of M9 with:

1. 1ml of kanamycin (from 50 mg/mL stock in H2O)
2. 1,2 g of $(NH_4)_2SO_4$ (^{15}N) solubilized in in 10ml of H2O and filtered
3. 3g of glucose solubilized in in 10ml of H2O and filtered
4. 1ml of Thiamine (from 1 mg/mL stock in H2O)
5. 1ml of Biotin (from 1 mg/mL stock in H2O)
6. 100ul of $CaCl_2$ (from 2M stock in H2O)
7. 1ml of $MgSO_4$ (from 2M stock in H2O)

The culture in 1L of M9 was shaken at 37°C until OD reached 0.60, then induced with 1 mM IPTG and let shake at 37°C overnight. Despite the expression protocol, ^{15}N-hSTING was extracted and purified in the same way.

6.2.2 PD-1/PD-L1 axis

The proteins were expressed and purified as described by Holak et al. [37,89], implementing the extraction method through multiple cycles of sonication and buffers. The plasmid encoding hPD-L1 (amino acids 18-134, MW of 13,5 kDa) construct and the plasmid

encoding hPD-1 (amino acids 33-150, MW of 13,3 kDa) were cloned into two different pET-21b(+).


```
000   M-----------------------------------NPPTFSPALLVVTEGDNA
050   TFTCSFSNTSESFVLNWYRMSPSNQTDKLAAFPEDRSQPGQDCRFRVTQL
100   PNGRDFHMSVVRARRNDSGTYLCGAISLAPKAQIKESLRAELRVTERRAE
A 150 --------------------------------------------------
200   --------------------------------------------------
288   --------------------------------------------------

000   M------------------FTVTVPKDLYVVEYGSNMTIECKFPVEKQLDL
050   AALIVYWEMEDKNIIQFVHGEEDLKVQHSSYRQRARLLKDQLSLGNAALQ
100   ITDVKLQDAGVYRCMISYGGADYKRITVKVNAPY----------------
B 150 --------------------------------------------------
200   --------------------------------------------------
290   --------------------------------------------------
```

Figura 4 Amino acid sequences of hPD1 (A) and hPD-L1 (B) expressed

As shown in figure 4 the insertion of Met-0 is essential for the production of proteins: the start codon that initiates translation process in *E.Coli* is ATG (Met).[76] Before using, the plasmid containing the gene was amplified and purified through Midiprep and Miniprep techniques based on alkaline lysis method.[77,88]

After the amplification, the two different pET-21b(+) were expressed in *Escherichia coli* BL21(DE3) gold strain cells. The protocols for the expression and purification of the proteins are the same for hPD-L1 and PD-L1. The pET-21b(+) transformed cells were cultured in LB medium supplied with ampicillin (0.1 mg mL^{-1}) for not labeled protein, instead for the expression of ^{15}N uniformly labeled proteins, were cultured in M9 minimal medium, supplied with ampicillin (0.1 mg mL^{-1}), 2.0 mM MgSO4, 0.2 mM CaCl2, 3.0 g, 1ml of Thiamine (from 1 mg/mL stock in H2O), 1ml of Biotin (from 1 mg/mL stock in H2O) and 1.2 g ^{15}N-ammonium sulfate. In both medium a drop of antifoam was even added, and the culture was let shake at 37°C until OD reached 0.60. The protein overexpression was induced with 1 mM IPTG and the culture further shaken at 37°C for 16 h. Cells were harvested by centrifugation. The supernatant was discarded, whereas the pellet was resuspended in 20 mM Tris-HCl, pH 8.0 buffer (40 mL per liter of culture). Since the protein was expressed as inclusion bodies, it was extracted by several cycles in denaturating conditions, then refolded. In particular, after homogenizing, the suspension containing the inclusion bodies was sonicated for 10 cycles alternating 30 seconds of sonication and 3 minutes of resting, then ultracentrifuged. The supernatant (soluble

fraction) was discarded, whereas the pellet resuspended in 50 mM Tris-HCl, pH 8.0, 200 mM NaCl buffer (40 mL per liter of culture), supplied with 10 mM EDTA and 10 mM BME. The mixture was again homogenized, then sonicated for 5 cycles. The suspension was ultracentrifuged, then the supernatant (washing fraction) was discarded, whereas the pellet redissolved in 50 mM Tris-HCl, pH 8.0, 200 mM NaCl, 6 M GdmCl buffer (20 mL per liter of cultures) supplied with 10 mM BME. The mixture was homogenized, then sonicated for 5 cycles, finally ultracentrifuged. The residual pellet was discarded, whereas the supernatant (GdmCl stock) was stored at 4°C. The GdmCl stock containing unfolded hPD-L1 was slowly 15-fold diluted in 100 mM Tris-HCl, pH 8.0, 1 M L-arginine solution supplied with 0.25 mM oxidated glutathione and 0.25 mM reduced glutathione, under vigorous magnetic stirring. The solution of refolded protein was incubated at 4°C under magnetic stirring for 6 hours, then extensively dialyzed against 50 mM Tris-HCl, pH 8.0, 150 mM NaCl buffer. The protein solution was taken out from dialysis, then filtered with a 0.20 μm filter. The solution was concentrated and purified by size exclusion chromatography on a Hi-Load 26/60 Superdex 75pg column (GE Healthcare), previously equilibrated with 10 mM Tris-HCl, pH 8.0, 20 mM NaCl buffer. Elution was performed at 2.5 mL/min and fractions containing hPD-L1 or hPD-1 were identified by Coomassie staining SDS-PAGE and collected.

The concentrations of PD-1 or Pd-L1 in solution or were achieved by UV-Vis spectroscopy using a Varian Cary 50 UV-Vis Spectrophotometer (Agilent) implemented with Cary WinUV software. Absorbance profile in the range of 250-350 nm was recorded and the value at 280 nm was used for the estimation of protein amount. The molar extinction coefficient at 280 nm were ε(ox) = 17545 M-1 cm-1 and ε(red) = 17420 M-1 cm-1 for PD-L1 and ε(ox) = 8605 M-1 cm-1 and ε(red) = 8480 M-1 cm-1as calculated by the on-line ExPASy - ProtParam tool. In each experiment, a baseline correction was applied by acquiring a spectrum of the blank.

The solutions of pure proteins were supplied with 0.1% NaN$_3$ and protease inhibitors (Roche), then stored at 4°C for NMR experiments. The protein folding was evaluated by NMR.

Figure 5. Schematic PD-1 and PD-L1 expression and purification workflow.

6.2.3. STING

The proteins were expressed and purified as described by Xiao-Xia Du and Xiao-Dong Su in Detection of Cyclic Dinucleotides by STING [90], implementing the M9 minimal medium culture procedures.

The plasmid encoding hSTING^{CTD} (amino acids 140-379, MW of 30,65 kDa) construct STING^{CTD} was cloned into pET-28a and was provided by Prof. Xiao-Dong Su. The plasmid encoding hSTING^{CTD} was extracted from paper support and solubilized it in ddH2O

```
-50    ---------------MGSSHHHHHHSSGLVPRGSHMASMTGGQQMGRGSM
000    -------------------------------------------------------
050    -------------------------------------------------------
100    -----------------------------------------APAEISAVCEK
150    GNFNVAHGLAWSYYIGYLRLILPELQARIRTYNQHYNNLLRGAVSQRLYI
200    LLPLDCGVPDNLSMADPNIRFLDKLPQQTGDHAGIKDRVYSNSIYELLEN
250    GQRAGTCVLEYATPLQTLFAMSQYSQAGFSREDRLEQAKLFCRTLEDILA
300    DAPESQNNCRLIAYQEPADDSSFSLSQEVLRHLRQEEKEEVTVGSLKTSA
379    VPSTSTMSQEPELLISGMEKPLPLRTDFS
```

Figura 6. Amino acid sequence of hSTING^{CTD} expressed

As shown in figure 6 the insertion of Met (M black in figure 6) is essential for the production of proteins: the start codon that initiates translation process in E.Coli is ATG (Met). [76] The plasmid encoding hSTING^{CTD}, before the protein sequence (140-379) presents in the N-terminal part a 6xHIS-tag (blu in figure 6) followed by a cleavage thrombin site (pink in figure 6) and a T7-tag too (salmon in figure 6). The HIS-tag is used to initially purify the protein after the cellular lysis. The cleavage thrombin site is used to delete the HIS-tag. The T7 tag is a promoter for bacteriophage T7 RNA polymerase that make the protein expression more efficient. In addition, it is used for the labeling and detection of protein using immunoblotting, immunoprecipitation, and immunostaining techniques Before using, the plasmid containing the gene was amplified by transforming in Top10 competent cells and purified through Midiprep and Miniprep techniques based on alkaline lysis method. [77,88]

After the amplification, the pET-28a(+) encoding hSTING^{CTD} was expressed in *Escherichia Coli* BL21(DE3) gold strain cells, incubated and transformed them to obtain the new colonies on Kanamycin Plate. Later a single colony from the plate was selected and incubated in 10 ml LB medium in the shaker overnight to obtain the preculture. Different culture media and different expression approaches were used for the differently isotopic labeled hSTING.

For the expression of nl-hSTING, the preculture of pET-28a(+) transformed cells was poured into 1 LB medium supplied with Kanamicyn (0.1 mg mL^{-1}). A drop of antifoam was even added, and the culture was let shake at 37°C until OD reached 0.60. The protein overexpression was induced with 0.5mM IPTG and the culture further shaken at 18°C overnight. Cells were harvested centrifugate at 7500 rpm for 15 min. The supernatant was discarded, whereas the pellet was resuspended in 50 mM Tris-HCl, pH 8.0, 500mM NaCl, 5mM imidazole, previously supplied with 5mM DTT buffer (40 mL per liter of culture). After homogenizing, the suspension containing the protein was sonicated for 10 cycles alternating 30 seconds of sonication and 3 minutes of resting, then ultracentrifuged. The lysate was ultracentrifuged at 35000 rpm for 35 minutes, then the supernatant was diluted with 50 mM Tris-HCl, pH 8.0, 500 mM NaCl, 5 mM imidazole in order to dilute the concentration of DTT. A HiTrap HP column (Ni-column) was connected to a peristaltic pump, washed with H2O and equilibrated with 50 mL of 50 mM Tris-HCl, pH 8.0, 500 mM NaCl, 5 mM imidazole (without DTT) at a flow rate of approximately 3 mL / min

and the solution containing the protein was then cyclically loaded onto a Ni-column for 3h. HiTrap HP column (Ni-column) containing the protein was connected into AKTA Pure system and then 2 elution steps were performed:

1. Wash impurities with 20–40 ml buffer 50 mM Tris-HCl, pH 8.0, 500 mM NaCl, 5 mM imidazole, 2,5 mM DTT, at a flow rate of 2.5 ml/min until UV absorption at 280 nm reaching baseline.
2. Elute the target proteins with a linear gradient buffer 50 mM Tris-HCl, pH 8.0, 500 mM NaCl, 500 mM imidazole, 2.5 mM DTT from 0% to 100%. Collect target protein according to UV 280 nm absorption.

The fractions containing hSTING were identified by Coomassie staining SDS-PAGE and collected.

The fractions were merged and therefore concentrated, and buffer exchanged to 50 mM Tris-HCl, pH 8.0, 150 mM NaCl, 2.5 mM CaCl2, 2.5 mM DTT by using a DESALTING-column. The concentrations of hSTING in solution was achieved by UV-Vis spectroscopy using a Varian Cary 50 UV-Vis Spectrophotometer (Agilent) implemented with Cary WinUV software. Absorbance profile in the range of 250-350 nm was recorded and the value at 280 nm was used for the estimation of protein amount. The molar extinction coefficient at 280 nm were $\varepsilon(ox) = 22140$ M-1 cm-1 and $\varepsilon(red) = 21890$ as calculated by the on-line ExPASy - ProtParam tool. In each experiment, a baseline correction was applied by acquiring a spectrum of the blank. Finally, thrombin stock solution was added in order to cleavage HIS-tag and the mixture was incubated overnight at RT. The solution was concentrated and purified by size exclusion chromatography on a Hi-Load 26/60 Superdex 75pg column (GE Healthcare), previously equilibrated with 20 mM Tris-HCl, pH 8.0, 100 mM NaCl buffer. Elution was performed at 2.5 mL/min and fractions containing hSTING were collected. An SDS-PAGE was performed in order to verify the success of thrombin cleavage and establish which fractions contained the pure protein. From the gel, it was evident that the protein was properly cleavaged and purified, therefore the fractions containing hSTING were collected and the concentrations were achieved by UV-Vis spectroscopy. The solutions of pure proteins were supplied with 0.1% NaN$_3$ and protease inhibitors (Roche), then stored at 4°C for NMR experiments. The protein folding was evaluated by NMR.
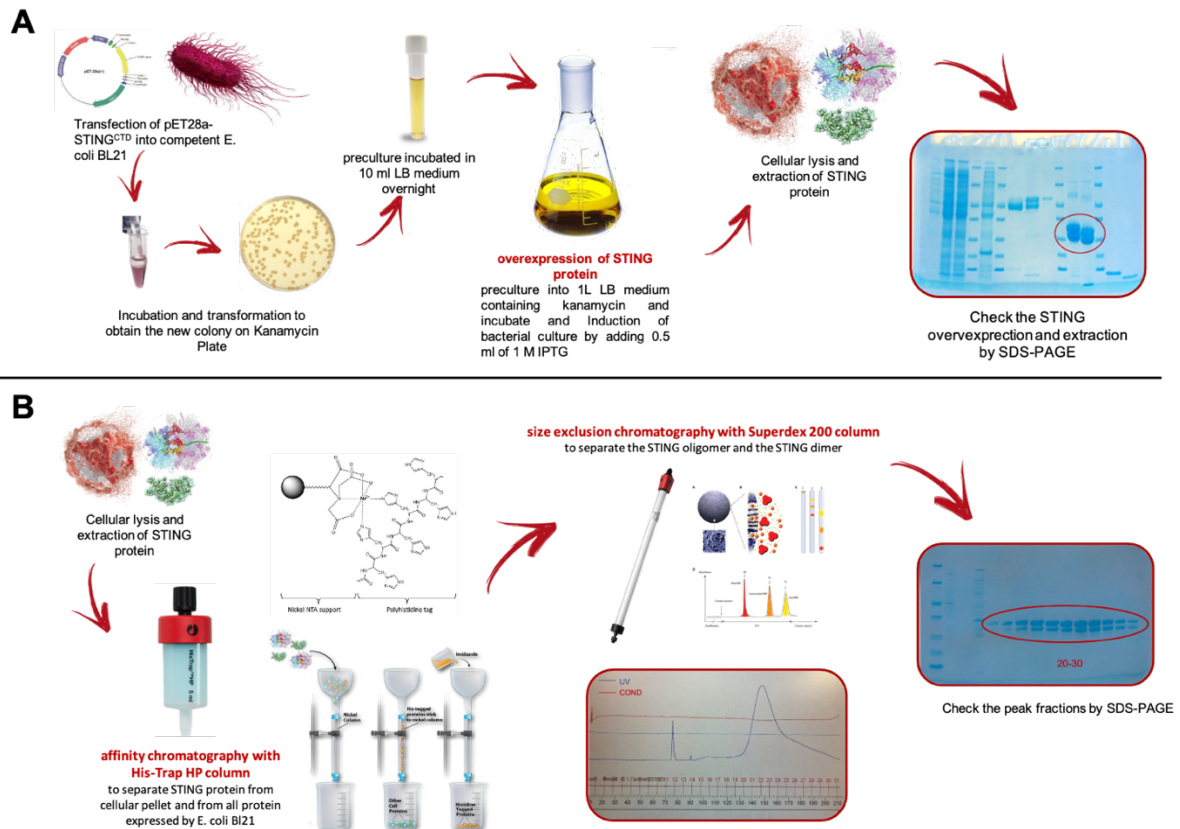
Figure 7. Schematic nl-hSTING expression and purification workflow.

For the expression of ^{15}N-hSTING, a Marley-like[87] method was applied. The preculture of, pET-28a(+) transformed cells was poured into 1 LB medium supplied with Kanamycin (0.1 mg mL^{-1}). A drop of antifoam was even added, and the culture was let shake at 37°C until OD reached 0.80. Then was centrifuged at 3000 rpm for 15 minutes, then the supernatant was discarded, whereas the pellet resuspended in 1L of M9 with:

1. 1ml of kanamycin (from 50 mg/mL stock in H2O)
2. 1,2 g of $(NH_4)_2SO_4$ (^{15}N) solubilized in in 10ml of H2O and filtered
3. 3g of glucose solubilized in in 10ml of H2O and filtered
4. 1ml of Thiamine (from 1 mg/mL stock in H2O)
5. 1ml of Biotin (from 1 mg/mL stock in H2O)
6. 100ul of $CaCl_2$ (from 2M stock in H2O)
7. 1ml of $MgSO_4$ (from 2M stock in H2O)

The culture in 1L of M9 was shaken at 37°C for 1h, then induced with 0,5 mM IPTG and let shake at 18°C overnight. Despite the expression protocol, ^{15}N-hSTING was extracted and purified in the same way.

Regarding the expression of ^{2}D,^{13}C,^{15}N- hSTING, pET-28a(+) transformed cells were inoculated into 10 mL ^{2}D,^{13}C,^{15}N-enriched Silantes OD2 medium supplied with kanamycin (from 50 mg/mL stock in D$_2$O). The preculture was shaken at 37°C overnight. The preculture was poured into 500 mL of Silantes DCN supplied with kanamycin (from 50 mg/mL stock in D$_2$O). The culture was shaken at 37°C until OD reached 0.55 (after 4.75 hours), then induced with 0.5 mM IPTG (from 1 M stock in D$_2$O) and let shake at 20°C overnight. Cells were harvested centrifugate at 7500 rpm for 15 min. The supernatant was discarded, whereas the pellet was resuspended in 50 mM Tris-HCl, pH 8.0, 500mM NaCl, 5mM imidazole, previously supplied with 5mM DTT buffer (40 mL per liter of culture). After homogenizing, the suspension containing the protein was sonicated for 10 cycles alternating 30 seconds of sonication and 3 minutes of resting, then ultracentrifuged. The lysate was ultracentrifuged at 35000 rpm for 35 minutes, then the supernatant was diluted with 50 mM Tris-HCl, pH 8.0, 500 mM NaCl, 5 mM imidazole in order to dilute the concentration of DTT.

The solution was then cyclically loaded onto a Ni-column. FT was collected, then four elution steps were performed:

1. 40 mL of binding buffer,
2. 40 mL of 50 mM Tris-HCl, pH 8.0, 500 mM NaCl, 2.5 mM DTT, 50 mM imidazole buffer,
3. 40 mL of 50 mM Tris-HCl, pH 8.0, 500 mM NaCl, 2.5 mM DTT, 300 mM imidazole buffer,
4. 40 mL of 50 mM Tris-HCl, pH 8.0, 500 mM NaCl, 2.5 mM DTT, 500 mM imidazole buffer.

An SDS-PAGE was carried out and it was found that almost all the protein was in the 300 mM imidazole fraction, which was therefore concentrated down to 10 mL and buffer exchanged to 50 mM Tris-HCl, pH 8.0, 150 mM NaCl, 2.5 mM CaCl2, 2.5 mM DTT by using a DESALTING-column.

The concentrations of hSTING in solution was achieved by UV-Vis spectroscopy, finally thrombin stock solution was added in order to cleavage HIS-tag and the mixture was incubated overnight at RT. The solution was concentrated and purified by size exclusion chromatography on a Hi-Load 26/60 Superdex 75pg column (GE Healthcare), previously equilibrated with 20 mM MES-NaOH, pH 8.0, 100 mM NaCl buffer, 10mM TCEP buffer. Elution was performed at 2.5 mL/min and fractions containing hSTING were collected. An SDS-PAGE was performed in order to verify the success of thrombin cleavage and establish which fractions contained the pure protein. From the gel, it was evident that the protein was properly cleavaged and purified, therefore the fractions containing hSTING were collected and the concentrations were achieved by UV-Vis spectroscopy. The solutions of pure proteins were supplied with 0.1% NaN_3 and protease inhibitors (Roche), then stored at 4°C for NMR experiments. The protein folding was evaluated by NMR.

6.3. NMR

In recent years, nuclear magnetic resonance (NMR) spectroscopy has been used in a huge number of pharmaceutical studies, [91–93] becoming the most important technique in the drug discovery process to identify new lead compounds. NMR spectroscopy is in fact the only biophysical technique that is able to detect and quantify intermolecular interactions in solution and, at the same time, provide important structural information with atomic-level resolution on the formation of protein complexes-ligand. [94–96] Typically, the initial step in drug discovery is the screening of a small libraries of compounds for the identification of possible lead. Afterwards, NMR spectroscopy can be used to validate the interaction of hits obtained from HTS or in silico assays. Where protein-based approaches are used, the orientation and position of the ligand can also be defined, and the binding confirmed. Theoretically, all spectroscopic NMR parameters can be used as indicators of ligand binding with a protein. Most used are chemical shift, relaxation times, diffusion constants and NOE changes. [97–100]

NMR-based screenings, combined with novel structural biology tools, have resulted in new NMR-high throughput screening (NMR-HTS) techniques to identify the interactions of large libraries of ligands with their target proteins, thus accelerating the drug discovery process, without relying on indirect convoluted biochemical assays. [95,98,101]

NMR-based screening can be performed both by monitoring the signals of the target macromolecule (macromolecule-based NMR) and those of the ligand (ligand-based NMR). [97,102]

6.3.1. Macromolecule-based NMR experiments

The NMR-screening macromolecules-based have the advantage to providing information about the macromolecule binding site. At the same time, they have some disadvantages such as use of large amounts of labeled protein with isotopes (^{15}N or ^{13}C).

In the Macromolecule-based NMR the effect of ligand-macromolecule interaction is monitored by comparing the NMR spectra of the macromolecule in the absence and in the presence of the ligand at different concentrations. [97,102] In fact, it is based on the observation of macromolecule nuclei chemical shift perturbations following ligand binding. The most used macromolecule-based NMR experiments are 1D ^1H Macromolecule-based NMR and HSQC.

1D ^1H Macromolecule-based NMR experiment is the most reliable, fast and direct NMR assay and the best method for evaluating ligand-protein interaction when dealing with libraries of several ligands and has the great advantage of not using labelled macromolecules. [101] This experiment NMR is based on comparing 1D ^1H spectra of the macromolecule in the absence and in the presence of the ligand. As shown in figure 8 the ^1H resonances of protein resonate in the region between -1ppm and 11 ppm, while those of the ligands between 1ppm and 10ppm, usually. For this reason, the most sensitive region of the protein's spectrum to detect the ligand-protein interaction is the aliphatic region (usually 0.7ppm / -1ppm, green zone in figure 8). The signals of the methyl protons usually are intense and acute peaks, therefore in presence of ligand interactions they are the first to have a chemical shift. [97]
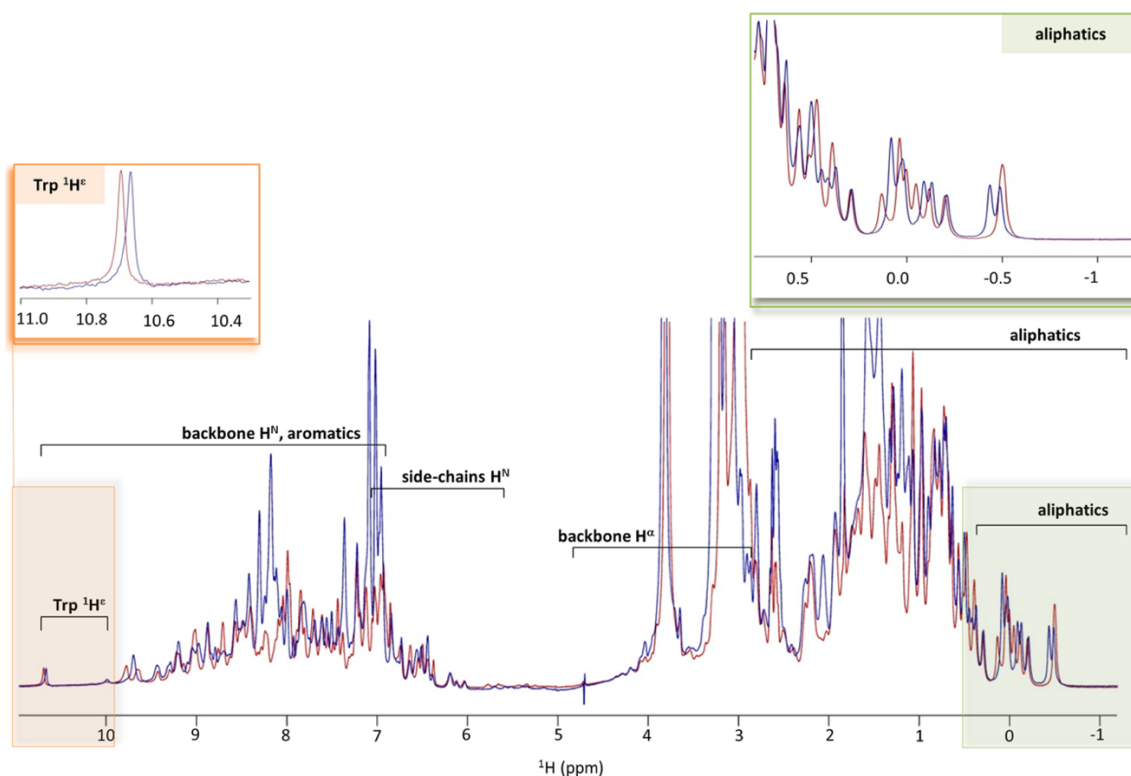
Figure 8. Example of 1D ^{1}H Macromolecule-based NMR experiment. The 1D ^{1}H NMR spectra of a protein in the absence (red) and presence (blue) of a ligand are reported. (Adopted from Elisa Barile and Maurizio Pellecchia) [96]

6.3.2. HSQC

1D ^{1}H NMR experiments give a lot of useful information; however, they are insufficient to get detailed information about protein folding and ligand-protein interaction. Bidimensional NMR experiments (2D NMR experiments) are used for these purposes. Just as 1D ^{1}H experiments, bidimensional experiments are based on comparison of macromolecule spectra in the absence and presence of the binder but using labelled molecules. In this way the information on intermolecular interactions can be obtained from comparison of chemical shift mapping of 2D spectra.

The most used bidimensional NMR experiment is the HSQC. Heteronuclear Single-Quantum Correlation (HSQC) is an 2D experiment that allows to identify the correlations between hydrogens and labelled heteroatoms directly linked to them. It is based on the acquisition of a ^{1}H-^{15}N (or ^{13}C) HSQC spectrum in the absence and presence of the ligand to compare the chemical shift mapping. (Figure 9) The interpretation of the spectrum is

simple: every cross-peak is generated by the coupling of a hydrogen with the heteroatom to which it is directly bound. In the HSQC spectrum of protein, every cross-peak is an amino acid. The interaction of the ligand with the protein generates a displacement of cross-peak of amino acids that are involved either directly in the bond or indirectly due to a conformational change in the structure of the protein. [103–106]

Figure 9. Examples of 2D protein-protein NMR assay. Panel A show 2D ^{1}H-^{15}N HSQC of free ^{15}N-hPD-L1. Panel B show 2D ^{1}H-^{15}N HSQC of ^{15}N-hPD-L1 in presence of hPD-1. Panel C show the overlays of two 2D ^{1}H-^{15}N HSQC and Selected chemical shift perturbations in well-resolved regions of each spectrum are highlighted.

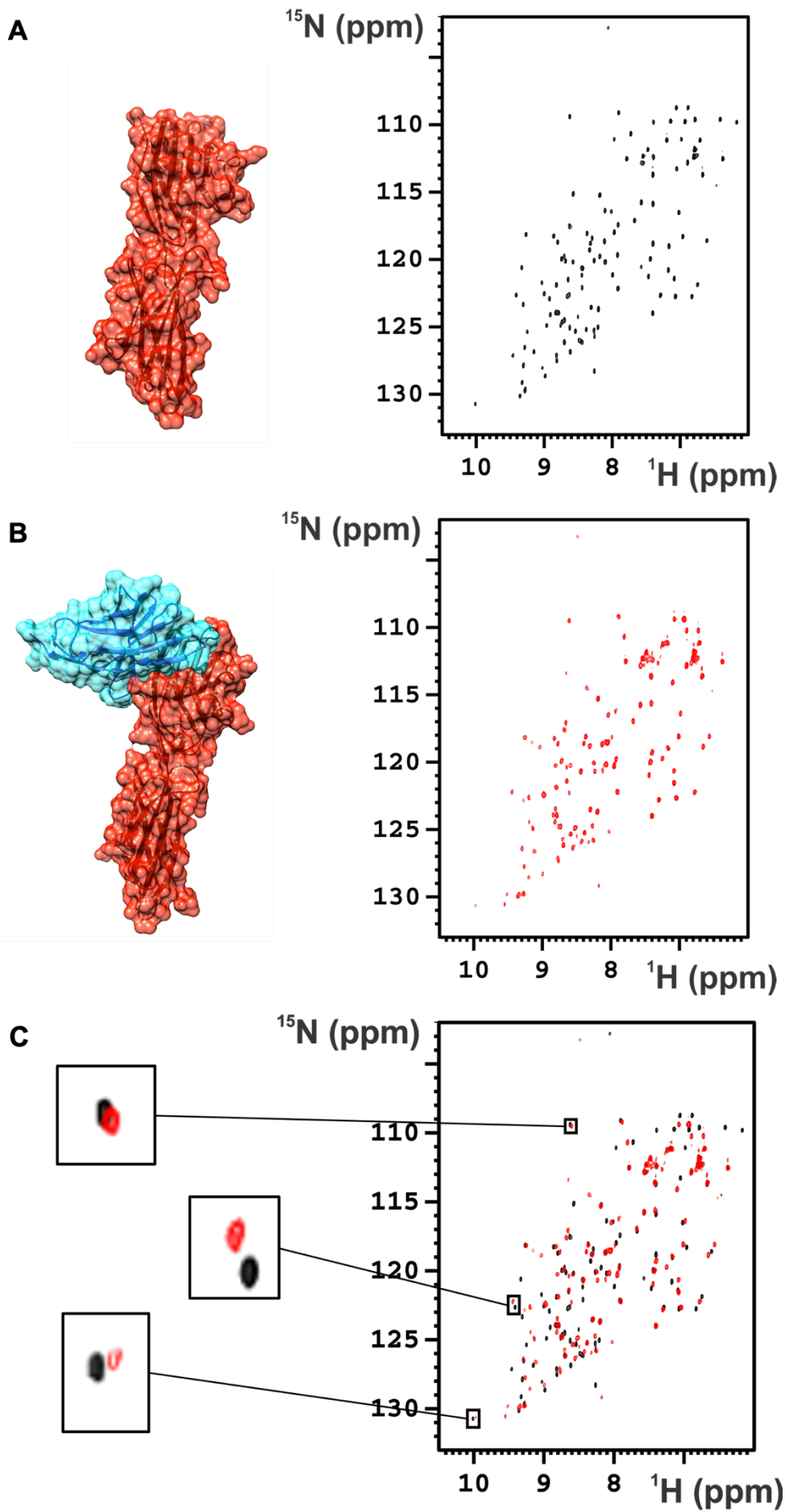## 6.3.3 Ligand-based NMR experiments

The NMR-screening ligand-based have the great advantage such as not labeling of the target macromolecule, require small amounts of macromolecule, no limitation of macromolecule size and in the end, allow the study of several compounds simultaneously. One of the disadvantages of these techniques is the solubility of the analyzed compounds, because these compounds are used in high concentrations in aqueous buffers. In the ligand-based NMR, the ligand-protein interaction is evaluated by comparing the NMR spectra of test ligands in the absence and presence of the target protein. [97,102]

A ligand in presence of a receptor protein (R), may be in equilibrium between two different states: free ligand (L) and bound ligand (RL). In bound state, the ligand acquires the hydrodynamic and NMR properties of the protein, acting as a high molecular weight compound. Therefore, if the ligand is in the bound form, the relaxation times, the diffusion coefficient and the magnetization transfer will be different from those of the free ligand and so the two NMR spectra of the ligands in absence and in presence of the target protein will be different. Instead, if the ligand doesn't bind the protein target, its properties will not change and therefore the two spectra will be equal. [100–102,107]

The most used ligand-based NMR experiments are STD (Saturation Transfer Difference) and WaterLOGSY (Water-Ligand Observed by Gradient SpectroscopY).

STD (Saturation Transfer Difference) is a ligand-based NMR technique able to identify potential binders of macromolecules such as proteins, DNA, membrane receptors, etc. This technique is based on the transfer of saturation from a macromolecule to a bound ligand that after exchange with the free ligand returns in solution, where it is detected. As shown in Figure 10, a first spectrum (I_{SAT}) is recorded with the selective saturation of the target macromolecule resonances (*on-resonance*), while a second reference spectrum (I_0) is acquired setting the values of radiation frequency far from those of protein and ligand saturations (*off-resonance*). The 1D ^{1}H spectrum difference that is obtained ($I_{STD} = I_0$ -

I_{SAT}) will show the signals of the target and the ligand. Usually, macromolecule is present in low concentrations and so it signals are not visible, but even if the signals were visible, they may be eliminated by using relaxation filters. It is important to note that molecules that do not bind the macromolecule will not receive magnetization and consequently will not show any signal in the STD spectrum. Therefore, this technique can be used to analyze mixtures of possible binders in the presence of the target macromolecule. When a macromolecule is irradiated with a selective pulse, saturation is transferred first from one proton to another in the macromolecule and then to the protons of the bound compound that are at the ligand-macromolecule interface. this mechanism is called spin diffusion. When the ligand dissociates from the target, it will transfer this saturation into solution where the free ligand signals can be displayed.[91,93,97,101,107]
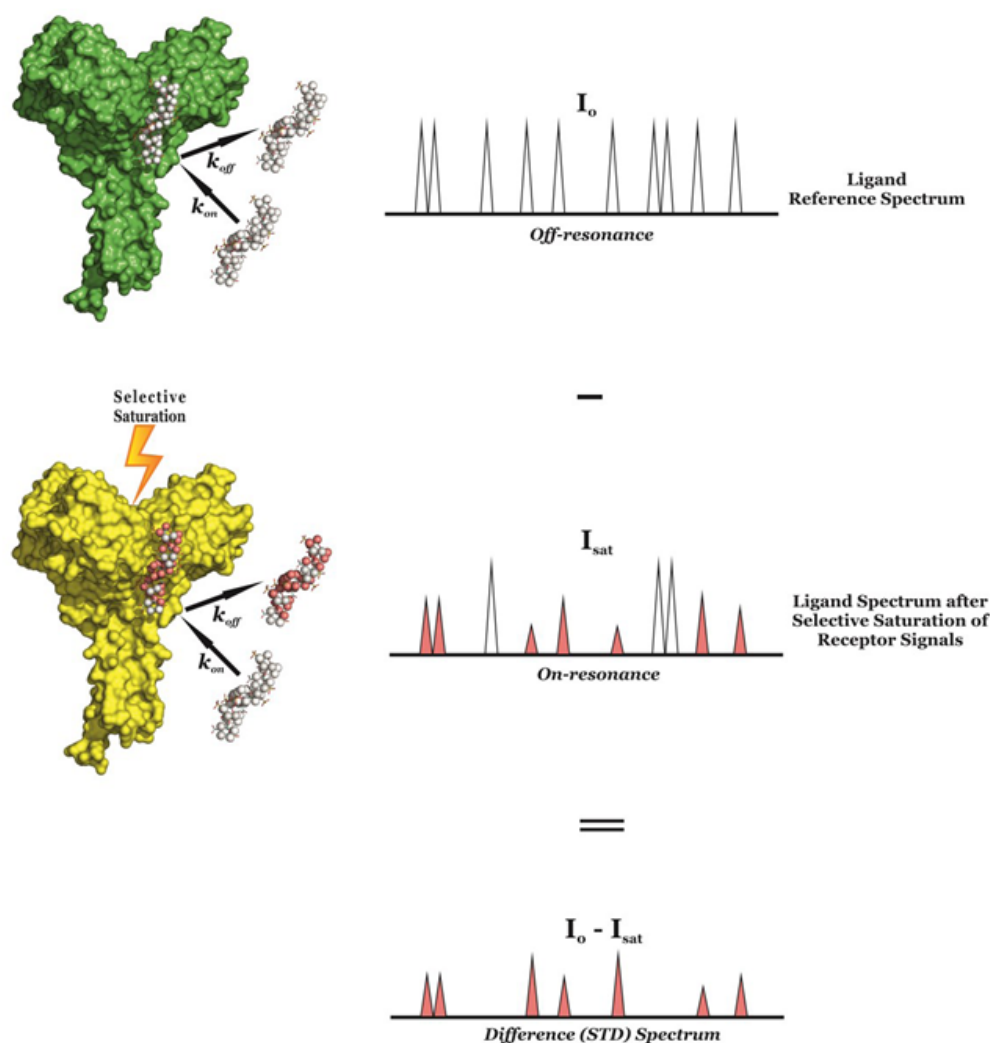
Figura 10. Schematic representation of STD experiment. (Adopted from Juan-Carlos Munoz-Garcia, Jesus Angulo Alvarez & Pedro Manuel Nieto Mesa on Glycopedia website)

The extent of ligand saturation depends on the ligand's residence time in the macromolecule's binding pocket. In fact, if the bond is very strong (e.g. Kd < 1nm) the transferring of saturation to the ligand is not very efficient. If the values of Kd are 100 nM or greater, the fast exchange of the ligand between the free and bound form will lead to a greater number of ligands in solution to which saturation will be transferred. [91,93,97,101,107]

WaterLOGSY (Water-Ligand Observed by Gradient SpectroscopY) is an experiment closely related to STD and widely used for the identification of protein-ligand interactions. The originality of WaterLOGSY is due to the magnetization transfer mechanism that occurs through water molecules in the binding site. In the STD experiment the ligand in the bound state is saturated by the macromolecule, instead in the WaterLOGSY it is saturated by water perturbation. In particular, the water signal is reversed and transferred to the ligand by intermolecular *cross-relaxation*. In this experiment, proton resonances of compounds that do not bind the macromolecule will appear with opposite phase compared to those of molecules that interact (figure11) [91,93,97,101,107]
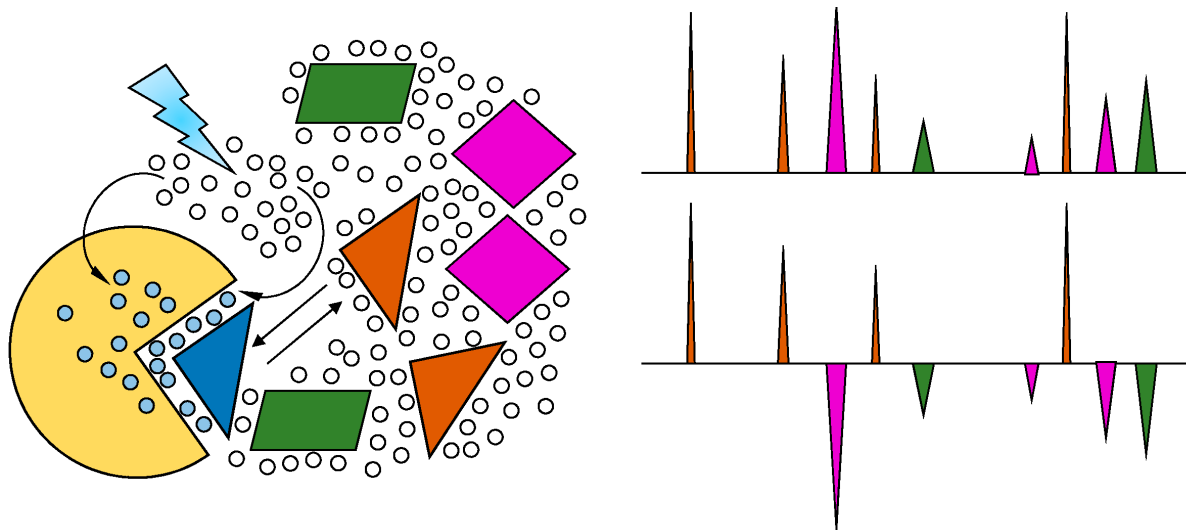
Figura 11. Schematic representation of WL experiment. (Adopted from Pomin, Vitor H. and Wang, Xu)[106]

Different experimental approaches have been used in this thesis work.

For hMDM2 we decided to use 1D ^{1}H Ligand-based NMR experiments STD (Saturation Transfer Difference) and WaterLOGSY (Water-Ligand Observed by Gradient SpectroscopY) to detect the interaction between the hMDM2 protein and the binder. In addiction we decided to use HSQC NMR experiments to investigate the binding mode of the most potent ligand of our library and to detect the interaction between the hMDM2 protein all possible binder.

For hPD-1/hPD-L1 axis we decided to use 1D ^{1}H Macromolecule-based NMR experiments as a method to detect the interaction between the hPD-L1 or hPD-1 protein and the small library of synthesized compounds. In addiction we decided to use HSQC NMR experiments to investigate the binding mode of the most potent ligand of our library.

As regard hSTING we decided to use 1D ^{1}H Ligand-based NMR experiments STD (Saturation Transfer Difference) and WaterLOGSY (Water-Ligand Observed by Gradient SpectroscopY) to detect the interaction between the hSTING protein and the small library of synthesized compounds. In addiction we decided to use HSQC NMR experiments to investigate the binding mode of the most potent ligand of our library.

6.3.4 MDM2

NMR Sample Preparation.
For the 1D ^{1}H-NMR free hSTING assay, 600 μL of 20 μM hMDM2 in 50 mM KH2PO4 50 mM Na2HPO4 150 mM NaCl pH 7.5 buffer and 10% D$_2$O was prepared.
In the 1D ^{1}H ligand-based NMR STD and WL screening experiments with our ligand's library, each sample was prepared in the same way: 1mM of ligand (previously solubilized in DMSO-d6) were added to 600 μL of 20 μM hSTING in 50 mM Na2HPO4 150 mM NaCl pH 7.5 buffer and 10% D$_2$O.
For the 2D ^{1}H-^{15}N HSQC experiments of free hSTING assay, 600 μL of 50 μM hsSTING in 50 mM Na2HPO4 150 mM NaCl pH 7.5 buffer and 10% D$_2$O was prepared.

NMR spectroscopy.

For the 1D ^{1}H-NMR all the experiments were acquired on a Bruker AVANCE NEO NMR spectrometer operating at 700 MHz (^{1}H Larmor frequency), equipped with a 5 mm TCI 3 channels HCN cryo-probehead and a room temperature probehead, optimized for ^{1}H sensitivity. The spectrometer is also equipped with SampleCase (autosampler) for NMR screening.

All spectra were acquired at 298 K, using 256 scans per spectrum with a recovery delay of 1.5 sec. The spectra were calibrated with respect to the water frequency; the H_2O signal was suppressed using excitation sculpting with gradients [108] and NMR spectra were phase adjusted and baseline corrected. The spectra were processed and analyzed with the Bruker TOPSPIN 4.0.7 software packages.

STD and WaterLOGSY NMR experiments: Saturation Transfer Difference (STD) spectra were acquired with 2048 scans, 2.0 s of saturation time and 40 ms of *spin lock* with *on-resonance* irradiation at -1.0 for selective saturation of protein resonances and *off-resonance* irradiation at 40 ppm for reference spectra. The saturation width of the used radiofrequency pulses was 200 Hz [6]. STD spectra were obtained by internal subtraction of the saturated spectrum from the reference spectrum by phase cycling with a spectral width of 9000 Hz, relaxation delay 1.0 s, 8 k data points for acquisition, and 16 k for transformation. STD effect is calculated as the signal to noise. WaterLOGSY NMR experiments were acquired with 2048 scans, 2.0 s of saturation time and 40 ms of *spin lock* for selective saturation of protein resonances.

For the 2D ^{1}H-^{15}N HSQC and 2D ^{2}D-^{13}C-^{15}N HSQC all experiments were acquired on a Bruker AVANCE III HD NMR spectrometer operating at 950 MHz (^{1}H Larmor frequency), equipped with cryogenically cooled probe. All spectra were acquired at 298 K, using 32 scans and 128 number of points in F1, ^{1}H spectral window of 16 ppm and ^{15}N spectral window of 30 ppm per spectrum with a recovery delay of 1.5 sec. The spectra were calibrated with respect to the water frequency; the H_2O signal was suppressed using excitation sculpting with gradients [108] and NMR spectra were phase adjusted and baseline corrected. The spectra were processed and analyzed with the Bruker TOPSPIN 4.0.7 software packages.

6.3.5. PD-1/PD-L1 axis

NMR Sample Preparation.

For the 1D ^{1}H-NMR free hPD-L1 and hPD-1 assays, 600 μL of 10 μM hPD-L1 and hPD-1 in 10 mM Tris-HCl, pH 8.0, 20 mM NaCl buffer and 10% D$_2$O were prepared.

For the 1D ^{1}H-NMR control experiment of hPD-L1 – BMS-202 interaction, 10 μM and 100 μM of BMS-202 previously solubilized in dimethyl sulfoxide-d6 (DMSO-d6) were added to 600 μL of 10 μM of hPD-L1 in 10 mM Tris-HCl, pH 8.0, 20 mM NaCl buffer and 10% D$_2$O.

In the 1D ^{1}H macromolecule-based NMR screening experiments with our ligand's library, each sample was prepared in the same way: 10 μM and 100 μM of a ligand (previously solubilized in DMSO-d6) were added to 600 μL of 10 μM hPD-L1 in 10 mM Tris-HCl, pH 8.0, 20 mM NaCl buffer and 10% D$_2$O.

For the 1D ^{1}H-NMR experiment of hPD-1 – most potent binder, 10 μM and 100 μM of compound 10 (previously solubilized in dimethyl sulfoxide-d6 (DMSO-d6)) were added to 600 μL of 10 μM of hPD-1 in 10 mM Tris-HCl, pH 8.0, 20 mM NaCl buffer and 10% D$_2$O.

For the 2D ^{1}H-^{15}N HSQC experiments of free hPD-L1 and hPD-1 assays, 600 μL of 50 μM hPD-L1 and hPD-1 in 10 mM Tris-HCl, pH 8.0, 20 mM NaCl buffer and 10% D$_2$O were prepared.

For the 2D ^{1}H-^{15}N HSQC control titration of hPD-L1 – BMS-202 interaction, increasing amounts (to reach concentrations of 6.25, 12.5, 18.75, 25, 50 μM) of BMS-202 previously solubilized in dimethyl sulfoxide-d6 (DMSO-d6) were added to 600 μL of 50 μM of hPD-L1 in 10 mM Tris-HCl, pH 8.0, 20 mM NaCl buffer and 10% D$_2$O.

For the 2D ^{1}H-^{15}N HSQC experiment of hPD-L1 – our binder interaction, increasing amounts (to reach concentrations of 6.25, 12.5, 18.75, 25, 50 μM) our binder (previously solubilized in dimethyl sulfoxide-d6 (DMSO-d6) were added to 600 μL of 50 μM of hPD-L1 in 10 mM Tris-HCl, pH 8.0, 20 mM NaCl buffer and 10% D$_2$O.

For the 2D ^{1}H-^{15}N HSQC control experiment of dissociation hPD-L1/hPD-1 complex with BMS-202, increasing amounts (to reach concentrations 4, 8, 12, 16, 32, 64 μM) of BMS-202 previously solubilized in dimethyl sulfoxide-d6 (DMSO-d6) were added to 600

µL of 32 µM of hPD-L1/hPD-1 complex in 10 mM Tris-HCl, pH 8.0, 20 mM NaCl buffer and 10% D_2O.

For the 2D ^{1}H-^{15}N HSQC control experiment of dissociation hPD-L1/hPD-1 complex with our ligand increasing amounts (to reach concentrations 4, 8, 12, 16, 32, 64 µM) of our binder previously solubilized in dimethyl sulfoxide-d6 (DMSO-d6) were added to 600 µL of 32 µM of hPD-L1/hPD-1 complex in 10 mM Tris-HCl, pH 8.0, 20 mM NaCl buffer and 10% D_2O.

For each analysis, the samples were then transferred to a 5 mm NMR tube.

NMR spectroscopy.

For the 1D ^{1}H-NMR all the experiments were acquired on a Bruker AVANCE NEO NMR spectrometer operating at 700 MHz (^{1}H Larmor frequency), equipped with a 5 mm TCI 3 channels HCN cryo-probehead and a room temperature probehead, optimized for ^{1}H sensitivity. The spectrometer is also equipped with SampleCase (autosampler) for NMR screening.

All spectra were acquired at 298 K, using 256 scans per spectrum with a recovery delay of 1.5 sec. The spectra were calibrated with respect to the water frequency; the H_2O signal was suppressed using excitation sculpting with gradients [108] and NMR spectra were phase adjusted and baseline corrected. The spectra were processed and analyzed with the Bruker TOPSPIN 4.0.7 software packages.

1D ^{1}H spectra of hPD-L1 were recorded prior and after the addition of each selected compound in a molar ratio of 1:1 with respect to the protein. A ligand excess (10-fold higher with respect to the protein) was also evaluated to detect weaker interactions. This method relies on monitoring chemical shift and line broadening changes of the signals of a protein in the aliphatic and aromatic regions, upon the protein interaction with a small molecule.

For the 2D ^{1}H-^{15}N HSQC all the experiments were acquired on a Bruker AVANCE III HD NMR spectrometer operating at 950 MHz (^{1}H Larmor frequency), equipped with cryogenically cooled probe. All spectra were acquired at 298 K, using 32 scans and 128 number of points in F1, ^{1}H spectral window of 16 ppm and ^{15}N spectral window of 30 ppm per spectrum with a recovery delay of 1.5 sec. The spectra were calibrated with

respect to the water frequency; the H_2O signal was suppressed using excitation sculpting with gradients [46] and NMR spectra were phase adjusted and baseline corrected. The spectra were processed and analyzed with the Bruker TOPSPIN 4.0.7 software packages. 2D ^1H-^{15}N HSQC of hPD-L1 were recorded prior and after the addition in increasing amounts of each selected compound. 2D ^1H-^{15}N HSQC of hPD-L1/hPD-1 complex was recorded prior and after the addition in increasing amounts of each selected compound. This method relies on monitoring chemical shift mapping of the cross-peak of a protein or complex, upon the protein interaction with a small molecule.

6.3.6. STING

NMR Sample Preparation.

For the 1D ^1H-NMR free hSTING assay, 600 μL of 20 μM hSTING in 20 mM Tris-HCl, pH 8.0, 100 mM NaCl buffer and 10% D_2O was prepared.

In the 1D ^1H ligand-based NMR STD and WL screening experiments with our ligand's library, each sample was prepared in the same way: 1mM of ligand (previously solubilized in DMSO-d6) were added to 600 μL of 20 μM hSTING in 20 mM Tris-HCl, pH 8.0, 100 mM NaCl buffer and 10% D_2O.

For the 2D ^1H-^{15}N HSQC experiments of free hSTING assay, 600 μL of 150 μM hsSTING in 20 mM Tris-HCl, pH 8.0, 100 mM NaCl buffer and 10% D_2O was prepared.

For the 2D ^1D-^{13}C-^{15}N HSQC experiments of free hSTING assay, 600 μL of 150 μM hsSTING in 20 mM Tris-HCl, pH 8.0, 100 mM NaCl buffer and 10% D_2O was prepared.

NMR spectroscopy.

For the 1D ^1H-NMR all the experiments were acquired on a Bruker AVANCE NEO NMR spectrometer operating at 700 MHz (^1H Larmor frequency), equipped with a 5 mm TCI 3 channels HCN cryo-probehead and a room temperature probehead, optimized for ^1H sensitivity. The spectrometer is also equipped with SampleCase (autosampler) for NMR screening.

All spectra were acquired at 298 K, using 256 scans per spectrum with a recovery delay of 1.5 sec. The spectra were calibrated with respect to the water frequency; the H_2O signal was suppressed using excitation sculpting with gradients [108] and NMR spectra were phase

adjusted and baseline corrected. The spectra were processed and analyzed with the Bruker TOPSPIN 4.0.7 software packages.

STD and WaterLOGSY NMR experiments: Saturation Transfer Difference (STD) spectra were acquired with 2048 scans, 2.0 s of saturation time and 40 ms of *spin lock* with *on-resonance* irradiation at -1.0 for selective saturation of protein resonances and *off-resonance* irradiation at 40 ppm for reference spectra. The saturation width of the used radiofrequency pulses was 200 Hz [6]. STD spectra were obtained by internal subtraction of the saturated spectrum from the reference spectrum by phase cycling with a spectral width of 9000 Hz, relaxation delay 1.0 s, 8 k data points for acquisition, and 16 k for transformation. STD effect is calculated as the signal to noise. WaterLOGSY NMR experiments were acquired with 2048 scans, 2.0 s of saturation time and 40 ms of *spin lock* for selective saturation of protein resonances.

For the 2D ^{1}H-^{15}N HSQC and 2D ^{2}D-^{13}C-^{15}N HSQC all experiments were acquired on a Bruker AVANCE III HD NMR spectrometer operating at 950 MHz (^{1}H Larmor frequency), equipped with cryogenically cooled probe. All spectra were acquired at 298 K, using 32 scans and 128 number of points in F1, ^{1}H spectral window of 16 ppm and ^{15}N spectral window of 30 ppm per spectrum with a recovery delay of 1.5 sec. The spectra were calibrated with respect to the water frequency; the H_2O signal was suppressed using excitation sculpting with gradients [108] and NMR spectra were phase adjusted and baseline corrected. The spectra were processed and analyzed with the Bruker TOPSPIN 4.0.7 software packages.

6.4. References

(1)   Salmaso, V.; Moro, S. Bridging Molecular Docking to Molecular Dynamics in Exploring Ligand-Protein Recognition Process: An Overview. *Front. Pharmacol.* **2018**, *9* (AUG), 1–16.

(2)   Lim-Wilby, G. M. M. and M.; Summary. Molecular Docking. *Encycl. Ref. Genomics Proteomics Mol. Med.* **2006**, *443*, 1149–1153.

(3)   Sethi, A.; Joshi, K.; Sasikala, K.; Alvala, M. Molecular Docking in Modern Drug Discovery: Principles and Recent Applications. *Drug Discov. Dev. - New Adv.* **2020**, No. July, 1–21.

(4)   Leach, A. R. Molecular Modeling: Principles and Applications. *Pearson Educ. Ltd.* **2001**, *1* (2), 1–773.

(5)   de Ruyck, J.; Brysbaert, G.; Blossey, R.; Lensink, M. F. Molecular Docking as a Popular Tool in Drug Design, an in Silico Travel. *Adv. Appl. Bioinforma. Chem.* **2016**, *9* (1), 1–11.

(6)   Wang, G.; Zhu, W. Molecular Docking for Drug Discovery and Development: A Widely Used Approach but Far from Perfect. *Future Med. Chem.* **2016**, *8* (14).

(7)   Prieto-Martínez, F. D.; Arciniega, M.; Medina-Franco, J. L. Molecular Docking: Current Advances and Challenges. *TIP Rev. Espec. en Ciencias Químico-Biológicas* **2018**, *21* (1), 65–87.

(8)   Meng, X.-Y.; Zhang, H.-X.; Mezei, M.; Cui, M. Molecular Docking: A Powerful Approach for Structure-Based Drug Discovery. *Curr. Comput. Aided-Drug Des.* **2012**, *7* (2), 146–157.

(9)   Release, S. S. Core Hopping 2.1 User Manual. *Schrödinger Press* **2015**, *2*, 1–34.

(10)   Shanthi Priya, S.; Doss, V. A. Core Hopping of Bis-Indole Derivatives to Identify an Effective Inhibitor for the Treatment of Bipolar Disorder. *Asian J. Biol. Life Sci.* **2021**, *9* (3), 402–407.

(11)   Wang, X. J.; Zhang, J.; Wang, S. Q.; Xu, W. R.; Cheng, X. C.; Wang, R. L. Identification of Novel Multitargeted PPARα/γ/δ Pan Agonists by Core Hopping of Rosiglitazone. *Drug Des. Devel. Ther.* **2014**, *8* (november), 2255–2262.

(12)   Giustiniano, M.; Daniele, S.; Pelliccia, S.; La Pietra, V.; Pietrobono, D.; Brancaccio, D.; Cosconati, S.; Messere, A.; Giuntini, S.; Cerofolini, L.; Fragai, M.;

Luchinat, C.; Taliani, S.; La Regina, G.; Da Settimo, F.; Silvestri, R.; Martini, C.; Novellino, E.; Marinelli, L. Computer-Aided Identification and Lead Optimization of Dual Murine Double Minute 2 and 4 Binders: Structure-Activity Relationship Studies and Pharmacological Activity. *J. Med. Chem.* **2017**, *60* (19), 8115–8130.

(13)   Shelley, J. C.; Cholleti, A.; Frye, L. L.; Greenwood, J. R.; Timlin, M. R.; Uchimaya, M. Epik: A Software Program for PKa Prediction and Protonation State Generation for Drug-like Molecules. *J. Comput. Aided. Mol. Des.* **2007**, *21* (12), 681–691.

(14)   Greenwood, J. R.; Calkins, D.; Sullivan, A. P.; Shelley, J. C. Towards the Comprehensive, Rapid, and Accurate Prediction of the Favorable Tautomeric States of Drug-like Molecules in Aqueous Solution. *J. Comput. Aided. Mol. Des.* **2010**, *24* (6–7), 591–604.

(15)   Madhavi Sastry, G.; Adzhigirey, M.; Day, T.; Annabhimoju, R.; Sherman, W. Protein and Ligand Preparation: Parameters, Protocols, and Influence on Virtual Screening Enrichments. *J. Comput. Aided. Mol. Des.* **2013**, *27* (3), 221–234.

(16)   Friesner, R. A.; Banks, J. L.; Murphy, R. B.; Halgren, T. A.; Klicic, J. J.; Mainz, D. T.; Repasky, M. P.; Knoll, E. H.; Shelley, M.; Perry, J. K.; Shaw, D. E.; Francis, P.; Shenkin, P. S. Glide: A New Approach for Rapid, Accurate Docking and Scoring. 1. Method and Assessment of Docking Accuracy. *J. Med. Chem.* **2004**, *47* (7), 1739–1749.

(17)   Halgren, T. A.; Murphy, R. B.; Friesner, R. A.; Beard, H. S.; Frye, L. L.; Pollard, W. T.; Banks, J. L. Glide: A New Approach for Rapid, Accurate Docking and Scoring. 2. Enrichment Factors in Database Screening. *J. Med. Chem.* **2004**, *47* (7), 1750–1759.

(18)   Harder, E.; Damm, W.; Maple, J.; Wu, C.; Reboul, M.; Xiang, J. Y.; Wang, L.; Lupyan, D.; Dahlgren, M. K.; Knight, J. L.; Kaus, J. W.; Cerutti, D. S.; Krilov, G.; Jorgensen, W. L.; Abel, R.; Friesner, R. A. OPLS3: A Force Field Providing Broad Coverage of Drug-like Small Molecules and Proteins. *J. Chem. Theory Comput.* **2016**, *12* (1), 281–296.

(19)   Miller, M. M.; Mapelli, C.; Allen, M.; Bowsher, M. S.; Boy, K.; Gillis, E. MACROCYCLIC INHIBITORS OF THE PD-1/PD-L1 AND CD80(B7-1)/PD-L1 PROTEIN/PROTEIN INTERACTIONS. *Bristol-Myers Squibb Co.* **2014**, *2* (12), WO 2014/151634 A1.

(20)   Chupak, L.; Zheng, X. Compounds Useful as Immunomodulators. *Bristol-Myers Squibb Co* **2015**, *12* (WO 2015/03 A1), WO2015034820 A1.

(21)   Guzik, K.; Tomala, M.; Muszak, D.; Konieczny, M.; Hec, A.; Błaszkiewicz, U.;

Pustuła, M.; Butera, R.; Dömling, A.; Holak, T. A. Development of the Inhibitors That Target the PD-1/PD-L1 Interaction—A Brief Look at Progress on Small Molecules, Peptides and Macrocycles. *Molecules* **2019**, *24* (11), 2071, 1–30.

(22)   Wang, T.; Wu, X.; Guo, C.; Zhang, K.; Xu, J.; Li, Z.; Jiang, S. Development of Inhibitors of the Programmed Cell Death-1/Programmed Cell Death-Ligand 1 Signaling Pathway. *J. Med. Chem.* **2019**, *62* (4), 1715–1730.

(23)   Cheng, B.; Xiao, Y.; Xue, M.; Cao, H.; Chen, J. Recent Advances in the Development of PD-L1 Modulators: Degraders, Downregulators, and Covalent Inhibitors. *J. Med. Chem.* **2020**, *63* (24), 15389–15398.

(24)   Cheng, B.; Ren, Y.; Niu, X.; Wang, W.; Wang, S.; Tu, Y.; Liu, S.; Wang, J.; Yang, D.; Liao, G.; Chen, J. Discovery of Novel Resorcinol Dibenzyl Ethers Targeting the Programmed Cell Death-1/Programmed Cell Death-Ligand 1 Interaction as Potential Anticancer Agents. *J. Med. Chem.* **2020**, *63* (15), 8338–8358.

(25)   Cheng, B.; Wang, W.; Niu, X.; Ren, Y.; Liu, T.; Cao, H.; Wang, S.; Tu, Y.; Chen, J.; Liu, S.; Yang, X.; Chen, J. Discovery of Novel and Highly Potent Resorcinol Dibenzyl Ether-Based PD-1/PD-L1 Inhibitors with Improved Drug-like and Pharmacokinetic Properties for Cancer Treatment. *J. Med. Chem.* **2020**, *63* (24), 15946–15959.

(26)   Guo, J.; Luo, L.; Wang, Z.; Hu, N.; Wang, W.; Xie, F.; Liang, E.; Yan, X.; Xiao, J.; Li, S. Design, Synthesis, and Biological Evaluation of Linear Aliphatic Amine-Linked Triaryl Derivatives as Potent Small-Molecule Inhibitors of the Programmed Cell Death-1/Programmed Cell Death-Ligand 1 Interaction with Promising Antitumor Effects in Vivo. *J. Med. Chem.* **2020**, *63* (22), 13825–13850.

(27)   Li, S.; Vilalta-Colomer, M.; Punna, S.; Malathong, V.; Singh, R.; Zhang, P. Preparation of Small Molecule Programmed Death Ligand 1 Phenylindanyloxybenzylamines Including N-(Phenylindanyloxyben- Zyl)-Amino Acid Derivatives, and Methods of Treating Cancer Using Them. **2020**, WO 2020047035 A1.

(28)   Konieczny, M.; Musielak, B.; Kocik, J.; Skalniak, L.; Sala, D.; Czub, M.; Magiera-Mularz, K.; Rodriguez, I.; Myrcha, M.; Stec, M.; Siedlar, M.; Holak, T. A.; Plewka, J. Di-Bromo-Based Small-Molecule Inhibitors of the PD-1/PD-L1 Immune Checkpoint. *J. Med. Chem.* **2020**, *63* (19), 11271–11285.

(29)   Narva, S.; Xiong, X.; Ma, X.; Tanaka, Y.; Wu, Y.; Zhang, W. Synthesis and Evaluation of Biphenyl-1,2,3-Triazol-Benzonitrile Derivatives as PD-1/PD-L1 Inhibitors. *ACS Omega* **2020**, *5* (33), 21181–21190.

(30)   Qin, M.; Cao, Q.; Wu, X.; Liu, C.; Zheng, S.; Xie, H.; Tian, Y.; Xie, J.; Zhao, Y.;

Hou, Y.; Zhang, X.; Xu, B.; Zhang, H.; Wang, X. Discovery of the Programmed Cell Death-1/Programmed Cell Death-Ligand 1 Interaction Inhibitors Bearing an Indoline Scaffold. *Eur. J. Med. Chem.* **2020**, *186*, 111856.

(31)   Chupak LS, Ding M, Martin SW, Zheng X, Hewawasam P, Connoly TP, Xu N, Yeung KS, Zhu J, Langley DR, Tenney DJ, S. P. Compounds Useful as Immunomodulators. *Bristol-Myers Squibb Co.* **2015**, *12* (WO 2015/160641 A2), WO 2015/160641 A2.

(32)   Zhang, Y.; Denhg, J.; Feng, Z.; Jiang, L.; Lu, X.; Shang, K.; Shou, J.; Wang, B.; Xu, X.; Xu, Y. Preparation and Application of Class of N-Containing Heterocyclic Compounds Having Immunoregulatory Function. *Shanghai Ennovabio Pharm. Co.* **2020**, WO 2020/024997 A1.

(33)   Zhang, Y.; Deng, J.; Feng, Z.; Huang, L.; Jiang, L.; Lu, X.; Shang, K.; Shou, J.; Wang, B.; Xu, X.; Xu, Y. Preparation and Application of Aromatic Compound Having Immunoregulatory Function. **2020**, WO 2020/025030 A1.

(34)   Miller, M. M.; Mapelli, C.; Allen, A. P.; Bowsher, M. S.; Gillis, E. P.; Langley, D. R.; Mull, E.; Poirier, M. A.; Sanghvi, N.; Sun, l.-Q; Tenney, D. J.; Yeung, K.-S.; Zhu, J.; Gillman, K. W.; Zhao, Q.; Grant-Young, K. A.; Scola, P. M.; Cornelius, l. A. M. MACROCYCLIC INHIBITORS OF THE PD-1/PD-L1 AND CD80 (B7-1)/PD-LI PROTEIN/PROTEIN INTERACTIONS. *Bristol-Myers Squibb Co.* **2016**, WO 2016/039749 A1.

(35)   Zarganes-Tzitzikas, T.; Konstantinidou, M.; Gao, Y.; Krzemien, D.; Zak, K.; Dubin, G.; Holak, T. A.; Dömling, A. Inhibitors of Programmed Cell Death 1 (PD-1): A Patent Review (2010-2015). *Expert Opin. Ther. Pat.* **2016**, *26* (9), 973–977.

(36)   Magiera-Mularz, K.; Skalniak, L.; Zak, K. M.; Musielak, B.; Rudzinska-Szostak, E.; Berlicki, Ł.; Kocik, J.; Grudnik, P.; Sala, D.; Zarganes-Tzitzikas, T.; Shaabani, S.; Dömling, A.; Dubin, G.; Holak, T. A. Bioactive Macrocyclic Inhibitors of the PD-1/PD-L1 Immune Checkpoint. *Angew. Chemie - Int. Ed.* **2017**, *56* (44), 13732–13735.

(37)   Guzik, K.; Zak, K. M.; Grudnik, P.; Magiera, K.; Musielak, B.; Törner, R.; Skalniak, L.; Dömling, A.; Dubin, G.; Holak, T. A. Small-Molecule Inhibitors of the Programmed Cell Death-1/Programmed Death-Ligand 1 (PD-1/PD-L1) Interaction via Transiently Induced Protein States and Dimerization of PD-L1. *J. Med. Chem.* **2017**, *60* (13), 5857–5867.

(38)   Konstantinidou, M.; Zarganes-Tzitzikas, T.; Magiera-Mularz, K.; Holak, T. A.; Dömling, A. Immune Checkpoint PD-1/PD-L1: Is There Life Beyond Antibodies?

Angew. Chemie - Int. Ed. **2018**, *57* (18), 4840–4848.

(39)   Kopalli, S. R.; Kang, T.-B.; Lee, K.-H.; Koppula, S. Novel Small Molecule Inhibitors of Programmed Cell Death (PD)-1, and Its Ligand, PD-L1 in Cancer Immunotherapy: A Review Update of Patent Literature. *Recent Pat. Anticancer. Drug Discov.* **2018**, *14* (2), 100–112.

(40)   Basu, S.; Yang, J.; Xu, B.; Magiera-Mularz, K.; Skalniak, L.; Musielak, B.; Kholodovych, V.; Holak, T. A.; Hu, L. Design, Synthesis, Evaluation, and Structural Studies of C2-Symmetric Small Molecule Inhibitors of Programmed Cell Death-1/Programmed Death-Ligand 1 Protein-Protein Interaction. *J. Med. Chem.* **2019**, *62* (15), 7250–7263.

(41)   Zak, K. M.; Grudnik, P.; Guzik, K.; Zieba, B. J.; Musielak, B.; Dömling, A.; Dubin, G.; Holak, T. A. Structural Basis for Small Molecule Targeting of the Programmed Death Ligand 1 (PD-L1). *Oncotarget* **2016**, *7* (21), 30323–30335.

(42)   Amaral, M.; Kokh, D. B.; Bomke, J.; Wegener, A.; Buchstaller, H. P.; Eggenweiler, H. M.; Matias, P.; Sirrenberg, C.; Wade, R. C.; Frech, M. Protein Conformational Flexibility Modulates Kinetics and Thermodynamics of Drug Binding. *Nat. Commun.* **2017**, *8* (1), 2276.

(43)   Perry, E.; Mills, J. J.; Zhao, B.; Wang, F.; Sun, Q.; Christov, P. P.; Tarr, J. C.; Rietz, T. A.; Olejniczak, E. T.; Lee, T.; Fesik, S. Fragment-Based Screening of Programmed Death Ligand 1 (PD-L1). *Bioorganic Med. Chem. Lett.* **2019**, *29* (6), 786–790.

(44)   Cheng, B.; Yuan, W. E.; Su, J.; Liu, Y.; Chen, J. Recent Advances in Small Molecule Based Cancer Immunotherapy. *Eur. J. Med. Chem.* **2018**, *157*, 582–598.

(45)   Skalniak, L.; Zak, K. M.; Guzik, K.; Magiera, K.; Musielak, B.; Pachota, M.; Szelazek, B.; Kocik, J.; Grudnik, P.; Tomala, M.; Krzanik, S.; Pyrc, K.; Dömling, A.; Dubin, G.; Holak, T. A. Small-Molecule Inhibitors of PD-1/PD-L1 Immune Checkpoint Alleviate the PD-L1-Induced Exhaustion of T-Cells. *Oncotarget* **2017**, *8* (42), 72167–72181.

(46)   Barber, G. N. STING: Infection, Inflammation and Cancer. *Nat. Rev. Immunol.* **2015**, *15* (12), 760–770.

(47)   Wan, D.; Jiang, W.; Hao, J. Research Advances in How the CGAS-STING Pathway Controls the Cellular Inflammatory Response. *Front. Immunol.* **2020**, *11* (615), 1–25.

(48)   Gao, P.; Ascano, M.; Zillinger, T.; Wang, W.; Dai, P.; Serganov, A. A.; Gaffney,

B. L.; Shuman, S.; Jones, R. A.; Deng, L.; Hartmann, G.; Barchet, W.; Tuschl, T.; Patel, D. J. Structure-Function Analysis of STING Activation by c[G(20,50)PA(30,50)p] and Targeting by Antiviral DMXAA. *Cell* **2013**, *154* (4), 748–762.

(49)   Gao, P.; Ascano, M.; Wu, Y.; Barchet, W.; Gaffney, B. L.; Zillinger, T.; Serganov, A. A.; Liu, Y.; Jones, R. A.; Hartmann, G.; Tuschl, T.; Patel, D. J. Cyclic [G(2′,5′)PA(3′,5′)p] Is the Metazoan Second Messenger Produced by DNA-Activated Cyclic GMP-AMP Synthase. *Cell* **2013**, *153* (5), 1094–1107.

(50)   Yi, G.; Brendel, V. P.; Shu, C.; Li, P.; Palanathan, S.; Cheng Kao, C. Single Nucleotide Polymorphisms of Human STING Can Affect Innate Immune Response to Cyclic Dinucleotides. *PLoS One* **2013**, *8* (10), 1–16.

(51)   Romling, U.; Galperin, M. Y.; Gomelsky, M. Cyclic Di-GMP: The First 25 Years of a Universal Bacterial Second Messenger. *Microbiol. Mol. Biol. Rev.* **2013**, *77* (1), 1–52.

(52)   Cai, X.; Chiu, Y. H.; Chen, Z. J. The CGAS-CGAMP-STING Pathway of Cytosolic DNA Sensing and Signaling. *Mol. Cell* **2014**, *54* (2), 289–296.

(53)   Bridget Larkin, Vladimir Ilyukha, Maxim Sorokin, Anton Buzdin, Edouard Vannier, and A. P. Activation of STING in T Cells Induces Type I IFN Responses and Cell Death Bridget. *J Immunol.* **2017**, *199* (2), 397–402.

(54)   Gao, J.; Tao, J.; Liang, W.; Zhao, M.; Du, X.; Cui, S.; Duan, H.; Kan, B.; Su, X.; Jiang, Z. Identification and Characterization of Phosphodiesterases That Specifically Degrade 3'3'-Cyclic GMP-AMP. *Cell Res.* **2015**, *25* (5), 539–550.

(55)   Fu, J.; Kanne, D. B.; Leong, M.; Glickman, L. H.; McWhirter, S. M.; Lemmens, E.; Mechette, K.; Leong, J. J.; Lauer, P.; Liu, W.; Sivick, K. E.; Zeng, Q.; Soares, K. C.; Zheng, L.; Portnoy, D. A.; Woodward, J. J.; Pardoll, D. M.; Dubensky, T. W.; Kim, Y. STING Agonist Formulated Cancer Vaccines Can Cure Established Tumors Resistant to PD-1 Blockade. *Sci. Transl. Med.* **2015**, *7* (283).

(56)   Yan, H.; Wang, X.; KuoLee, R.; Chen, W. Synthesis and Immunostimulatory Properties of the Phosphorothioate Analogues of CdiGMP. *Bioorganic Med. Chem. Lett.* **2008**, *18* (20), 5631–5634.

(57)   Corrales, L.; Glickman, L. H.; McWhirter, S. M.; Kanne, D. B.; Sivick, K. E.; Katibah, G. E.; Woo, S. R.; Lemmens, E.; Banda, T.; Leong, J. J.; Metchette, K.; Dubensky, T. W.; Gajewski, T. F. Direct Activation of STING in the Tumor Microenvironment Leads to Potent and Systemic Tumor Regression and Immunity. *Cell Rep.* **2015**, *11* (7), 1018–1030.

(58)   Ahn, J.; Barber, G. N. STING Signaling and Host Defense against Microbial Infection. *Exp. Mol. Med.* **2019**, *51* (155), 1–10.

(59)   Dhanak, D.; Edwards, J. P.; Nguyen, A.; Tummino, P. J. Small-Molecule Targets in Immuno-Oncology. *Cell Chem. Biol.* **2017**, *24* (9), 1148–1160.

(60)   Ding, C.; Song, Z.; Shen, A.; Chen, T.; Zhang, A. Small Molecules Targeting the Innate Immune CGAS–STING–TBK1 Signaling Pathway. *Acta Pharm. Sin. B* **2020**, *10* (12), 2272–2298.

(61)   Lioux, T.; Mauny, M. A.; Lamoureux, A.; Bascoul, N.; Hays, M.; Vernejoul, F.; Baudru, A. S.; Boularan, C.; Lopes-Vicente, J.; Qushair, G.; Tiraby, G. Design, Synthesis, and Biological Evaluation of Novel Cyclic Adenosine-Inosine Monophosphate (CAIMP) Analogs That Activate Stimulator of Interferon Genes (STING). *J. Med. Chem.* **2016**, *59* (22), 10253–10267.

(62)   Gao, P.; Zillinger, T.; Wang, W.; Ascano, M.; Dai, P.; Hartmann, G.; Tuschl, T.; Deng, L.; Barchet, W.; Patel, D. J. Binding-Pocket and Lid-Region Substitutions Render Human STING Sensitive to the Species-Specific Drug DMXAA. *Cell Rep.* **2014**, *8* (6), 1668–1676.

(63)   McKeage, M. J.; Von Pawel, J.; Reck, M.; Jameson, M. B.; Rosenthal, M. A.; Sullivan, R.; Gibbs, D.; Mainwaring, P. N.; Serke, M.; Lafitte, J. J.; Chouaid, C.; Freitag, L.; Quoix, E. Randomised Phase II Study of ASA404 Combined with Carboplatin and Paclitaxel in Previously Untreated Advanced Non-Small Cell Lung Cancer. *Br. J. Cancer* **2008**, *99* (12), 2006–2012.

(64)   Zhang, Y.; Sun, Z.; Pei, J.; Luo, Q.; Zeng, X.; Li, Q.; Yang, Z.; Quan, J. Identification of α-Mangostin as an Agonist of Human STING. *ChemMedChem* **2018**, *13* (19), 2057–2064.

(65)   Ramanjulu, J. M.; Pesiridis, G. S.; Yang, J.; Concha, N.; Singhaus, R.; Zhang, S. Y.; Tran, J. L.; Moore, P.; Lehmann, S.; Eberl, H. C.; Muelbaier, M.; Schneck, J. L.; Clemens, J.; Adam, M.; Mehlmann, J.; Romano, J.; Morales, A.; Kang, J.; Leister, L.; Graybill, T. L.; Charnley, A. K.; Ye, G.; Nevins, N.; Behnia, K.; Wolf, A. I.; Kasparcova, V.; Nurse, K.; Wang, L.; Li, Y.; Klein, M.; Hopson, C. B.; Guss, J.; Bantscheff, M.; Bergamini, G.; Reilly, M. A.; Lian, Y.; Duffy, K. J.; Adams, J.; Foley, K. P.; Gough, P. J.; Marquis, R. W.; Smothers, J.; Hoos, A.; Bertin, J. Design of Amidobenzimidazole STING Receptor Agonists with Systemic Activity. *Nature* **2018**, *564* (7736), 439–443.

(66)   Al., X. Z. et. Discovery and Mechanistic Study of a Novel Human STING Agonist. *ACS Infect Dis* **2019**, *5* (7), 1139–1148.

(67)   Chin, E. N.; Yu, C.; Vartabedian, V. F.; Jia, Y.; Kumar, M.; Gamo, A. M.; Vernier, W.; Ali, S. H.; Kissai, M.; Lazar, D. C.; Nguyen, N.; Pereira, L. E.; Benish, B.; Woods, A. K.; Joseph, S. B.; Chu, A.; Johnson, K. A.; Sander, P. N.; Martínez-peña, F.; Hampton, E. N.; Young, T. S.; Wolan, D. W.; Chatterjee, A. K.; Schultz, P. G.; Petrassi, H. M.; Teijaro, J. R.; Lairson, L. L. Antitumor Activity of a Systemic STING-Activating Non-Nucleotide CGAMP Mimetic. *Science (80-.).* **2020**, *369* (August), 993–999.

(68)   Pan, B. S.; Perera, S. A.; Piesvaux, J. A.; Presland, J. P.; Schroeder, G. K.; Cumming, J. N.; Wesley Trotter, B.; Altman, M. D.; Buevich, A. V.; Cash, B.; Cemerski, S.; Chang, W.; Chen, Y.; Dandliker, P. J.; Feng, G.; Haidle, A.; Henderson, T.; Jewell, J.; Kariv, I.; Knemeyer, I.; Kopinja, J.; Lacey, B. M.; Laskey, J.; Lesburg, C. A.; Liang, R.; Long, B. J.; Lu, M.; Ma, Y.; Minnihan, E. C.; O'Donnell, G.; Otte, R.; Price, L.; Rakhilina, L.; Sauvagnat, B.; Sharma, S.; Tyagarajan, S.; Woo, H.; Wyss, D. F.; Xu, S.; Bennett, D. J.; Addona, G. H. An Orally Available Non-Nucleotide STING Agonist with Antitumor Activity. *Science (80-.).* **2020**, *369* (August), 935–944.

(69)   Woodward, J. J.; Lavarone, A. T.; Portnoy, D. A. C-Di-AMP Secreted by Intracellular Listeria Monocytogenes Activates a Host Type I Interferon Response. *Science (80-.).* **2010**, *328* (5986), 1703–1705.

(70)   Weinmann, H. Cancer Immunotherapy: Selected Targets and Small-Molecule Modulators. *ChemMedChem* **2016**, *11* (5), 450–466.

(71)   InvivoGen. Deciphering the STING Paradox STING,. *InvivoGen Rev. | STING* **2014**, *33*, 0–1.

(72)   Burdette, D. L.; Monroe, K. M.; Sotelo-Troha, K.; Iwig, J. S.; Eckert, B.; Hyodo, M.; Hayakawa, Y.; Vance, R. E. STING Is a Direct Innate Immune Sensor of Cyclic Di-GMP. *Nature* **2011**, *478* (7370), 515–518.

(73)   Wu, J.; Sun, L.; Chen, X.; Du, F.; Shi, H.; Chen, C.; Chen, Z. J. Cyclic GMP-AMP Is an Endogenous Second Messenger in Innate Immune Signaling by Cytosolic DNA. *Science (80-.).* **2013**, *339* (6121), 826–830.

(74)   Ablasser, A.; Goldeck, M.; Cavlar, T.; Deimling, T.; Witte, G. Europe PMC Funders Group CGAS Produces a 2′-5′-Linked Cyclic Dinucleotide Second Messenger That Activates STING. *Nature* **2013**, *498* (7454), 380–384.

(75)   Zhang, X.; Shi, H.; Wu, J.; Zhang, X.; Sun, L.; Chen, C.; Chen, Z. J. Cyclic GMP-AMP Containing Mixed Phosphodiester Linkages Is an Endogenous High-Affinity Ligand for STING. *Mol. Cell* **2013**, *51* (2), 226–235.

(76)   Stanbury, P. F.; Whitaker, A.; Hall, S. J. The Production of Heterologous Proteins.

Princ. Ferment. Technol. **2017**, *3*, 725–775.

(77)   Mülhardt, C. & Beese, E. W. Fundamental Methods. *Mol. Biol. Genomics* **2007**, 11–36.

(78)   Walker, B. M. and J. E. Over-Production of Proteins in Escherichia Coli: Mutant Hosts That Allow Synthesis of Some Membrane Proteins and Globular Proteins at High Levels. *J. Mol. Biol.* **1996**, *260*, 289–298.

(79)   Stellwagen, E. Gel-Filtration. *Methods Enzymol.* **2009**, *463*, 373–385.

(80)   Hagel, L. & Haneskog, L. Size-Exclusion Chromatography. *eLS (American Cancer Soc.* **2010**.

(81)   Fekete, S., Beck, A., Veuthey, J.-L. & G. Theory and Practice of Size-Exclusion Chromatography for the Analysis of Protein Aggregates. *J Pharm Biomed Anal* **2014**, *101*, 161–173.

(82)   Schägger, H. Tricine–SDS-PAGE. *Nat. Protoc.* **2006**, *1*, 16–22.

(83)   Singh, A.; Upadhyay, V.; Upadhyay, A. K.; Singh, S. M.; Panda, A. K. Protein Recovery from Inclusion Bodies of Escherichia Coli Using Mild Solubilization Process. *Microb. Cell Fact.* **2015**, *14* (1), 1–10.

(84)   Govers, S. K.; Dutré, P.; Aertsen, A. In Vivo Disassembly and Reassembly of Protein Aggregates in Escherichia Coli. *J. Bacteriol.* **2014**, *196* (13), 2325–2332.

(85)   RAINER RUDOLPH AND HAUKE LILIE. In Vitro Folding of Inclusion Body Proteins. *FASEB J.* **1996**, *10* (January), 49–56.

(86)   Tsumoto, K.; Ejima, D.; Kumagai, I.; Arakawa, T. Practical Considerations in Refolding Proteins from Inclusion Bodies. *Protein Expr. Purif.* **2003**, *28* (1), 1–8.

(87)   Marley, J.; Lu, M.; Bracken, C. A Method for Efficient Isotopic Labeling of Recombinant Proteins. *J. Biomol. NMR* **2001**, *20* (1), 71–75.

(88)   Laboratoire, H. C. B. and J. D. A Rapid Alkaline Extraction Procedure for Screening Recombinant Plasmid DNA. *Nucleic Acids Res* **1979**, *7* (1), 1513–1523.

(89)   Zak, K. M.; Grudnik, P.; Guzik, K.; Zieba, B. J.; Musielak, B.; Dömling, A.; Dubin, G.; Holak, T. A. Structural Basis for Small Molecule Targeting of the Programmed Death Ligand 1 (PD-L1). *Oncotarget* **2016**, *7* (21), 30323–30335.

(90)   Du, X. X.; Su, X. D. Detection of Cyclic Dinucleotides by STING. *Methods Mol. Biol.* **2017**, *1657*, 59–69.

(91)   Sugiki, T.; Furuita, K.; Fujiwara, T.; Kojima, C. Current NMR Techniques for Structure-Based Drug Discovery. *Molecules* **2018**, *23* (1), 1–27.

(92)   Ziarek, J. J.; Peterson, F. C.; Lytle, B. L.; Volkman, B. F. Binding Site

Identification and Structure Determination of ProteinLigand Complexes by NMR: A Semiautomated Approach. *Methods Enzymol.* **2011**, *493* (2013 April 25), 241–275.

(93)   Meyer, B.; Peters, T. NMR Spectroscopy Techniques for Screening and Identifying Ligand Binding to Protein Receptors. *Angew. Chemie - Int. Ed.* **2003**, *42* (8), 864–890.

(94)   Weigelt, J.; Van Dongen, M.; Uppenberg, J.; Schultz, J.; Wikström, M. Site-Selective Screening by NMR Spectroscopy with Labeled Amino Acid Pairs. *J. Am. Chem. Soc.* **2002**, *124* (11), 2446–2447.

(95)   Shortridge, M. D.; Hage, D. S.; Harbison, G. S.; Powers, R. Estimating Protein-Ligand Binding Affinity Using High-Throughput Screening by NMR. *J. Comb. Chem.* **2008**, *10* (6), 948–958.

(96)   Dashti, H.; Westler, W. M.; Tonelli, M.; Wedell, J. R.; Markley, J. L.; Eghbalnia, H. R. Spin System Modeling of Nuclear Magnetic Resonance Spectra for Applications in Metabolomics and Small Molecule Screening. *Anal. Chem.* **2017**, *89* (22), 12201–12208.

(97)   Barile, E.; Pellecchia, M. NMR-Based Approaches for the Identification and Optimization of Inhibitors of Protein-Protein Interactions. *Chem. Rev.* **2014**, *114* (9), 4749–4763.

(98)   Baggio, C.; Cerofolini, L.; Fragai, M.; Luchinat, C.; Pellecchia, M. HTS by NMR for the Identification of Potent and Selective Inhibitors of Metalloenzymes. *ACS Med. Chem. Lett.* **2018**, *9* (2), 137–142.

(99)   Jahnke, W. Perspectives of Biomolecular NMR in Drug Discovery: The Blessing and Curse of Versatility. *J. Biomol. NMR* **2007**, *39* (2), 87–90.

(100)   Zartler, E. R.; Shapiro, M. J. Protein NMR-Based Screening in Drug Discovery. *Curr. Pharm. Des.* **2006**, *12* (31), 3963–3972.

(101)   Maity, S.; Gundampati, R. K.; Kumar, T. K. S. NMR Methods to Characterize Protein-Ligand Interactions. *Nat. Prod. Commun.* **2019**, *14* (5).

(102)   Gallo, M.; Matteucci, S.; Alaimo, N.; Pitti, E.; Orsale, M. V.; Summa, V.; Cicero, D. O.; Monteagudo, E. A Novel Method Using Nuclear Magnetic Resonance for Plasma Protein Binding Assessment in Drug Discovery Programs. *J. Pharm. Biomed. Anal.* **2019**, *167*, 21–29.

(103)   Ortega-roldan, J. L.; Blackledge, M. Characterizing Protein-Protein Interactions Using Solution NMR Spectroscopy. *Protein Complex Assem.* **2018**, No. September, 73–85.

(104)   Gell, D. A.; Mackay, J. P. NMR Spectroscopy in the Analysis of Protein-Protein

Interactions. *Mod. Magn. Reson.* **2008**, 1339–1346.

(105)   Becker, W.; Bhattiprolu, K. C.; Gubensäk, N.; Zangger, K. Investigating Protein–Ligand Interactions by Solution Nuclear Magnetic Resonance Spectroscopy. *ChemPhysChem* **2018**, *19* (8), 895–906.

(106)   Vaynberg, J.; Qin, J. Weak Protein-Protein Interactions as Probed by NMR Spectroscopy. *Trends Biotechnol.* **2006**, *24* (1), 22–27.

(107)   Pomin, V. H.; Wang, X. Glycosaminoglycan-Protein Interactions by Nuclear Magnetic Resonance (NMR) Spectroscopy. *Molecules* **2018**, *23* (2314), 1–25.

(108)   Hwang J., T. L. and S. Water Suppression That Works. Excitation Sculpting Using Arbitrary Wave-Forms and Pulsed-Field Gradients. *J. Magn. Reson. Ser. A* **1995**, *112* (2), 275–279.

Chapter 7
Conclusions

There is an urgent need to develop novel strategies for the treatment of cancer due to its high mortality. Thus, the discovery and the development of combination of anticancer drug and brand-new immunotherapeutic drugs able to induce a strong response against cancer cells through a combination of in silico drug design techniques, advanced synthetic methods and an accurate and extensive biological characterization, is expected to surely have a high-impact in cancer research.

All studies of my PhD project, here reported, were focused on discover and development of small molecules targeting three possible receptors recognized as new cancer targets: hMDM2 protein, PD-1/PDL-1 axis (Programmed cell Death protein-1/ Programmed Death-ligand 1), and on STING protein (STimulator of INterferon Genes).

Specifically, as regards the targeting of hMDM2, the main aim was to discover and develop novel selective and potent inhibitors. To do so, a combined approach of modeling/NMR was used. A ligand-based lead optimization was carried out and a number of compounds was synthetized and tested by NMR and immunoenzymatic assay. One these (RS3594) showed a highest affinity, with an IC_{50} value of 10 nM. RS3594, was combined with the CXCR4 antagonist, AMD3100, in human GBM cells and tested in GBM stem-like cells (neurospheres), which are crucial for tumor recurrence and chemotherapy resistance. The inhibition of the two pathways presents synergic effects confirm that the CXCR4/MDM2 block can represent a valuable strategy to reduce GBM proliferation and invasiveness, acting, most importantly, on the stem cell component. In addition, MDM2/p53 complex was chosen as a case study in order to evaluate the possibility for screening applications by protein- and ligand- based NMR. In this PhD thesis project, I described an efficient and simple method for the screening of PPI inhibitors (HOPPI-NMR), in which one of the two interacting proteins is replaced by a short peptide (hot-peptide). This method will provide new opportunities for the highly expanding field of medicinal chemistry devoted not only to the identification of effective PPI Inhibitors but also small molecule.

As regards the PD-1/PD-L1 axis, I was involved in a project having as aim the switching from monoclonal antibody (mAbs) to small molecule able to disrupt the interaction among the two above-mentioned proteins. Herein, a series of compounds was synthetized and assayed for their PD-L1 binding firstly by NMR screening, and then through HTRF

assays. One our compound endowed with a nanomolar IC_{50}, was also subjected to DSC experiments to compare its behavior with positive standard BMS202 in binding and stabilizing the PD-L1 protein. This compound demonstrated to strongly bind PD-L1 in biophysical assays, and on cell membranes, thus restoring the function of peripheral blood mononuclear cells (PBMCs) co-cultured with lung adenocarcinoma PC9 and HCC827 cells. Indeed, an increased interferon gamma (IFNγ) secretion and an augmented apoptotic induction on PC9 and HCC827 cancer cells was clearly visible upon treatment with it and was at least comparable to that observed with BMS-202. In addition, this our most potent bindes showed a lower cytotoxicity in healthy cells (lower off-target effects) than BMS202, thus paving the way for its subsequent preclinical optimization.

Concerning hSTING protein computational methods such as receptor-based VS, Core Hopping and De Novo design were applied go generate/finding structurally new ligands. These compounds were synthesized and assayed through an1D ^{1}H ligand-based screening NMR protocol (STD and WL experiments) and 20 of them were found interact specifically with hSTING. Then homogeneous time-resolved fluorescence (HTRF) binding assay was carried out and wo our compounds (10 and 26) showed a good interaction with hSTING. These were subjected to further experiments to assess the activator or inhibitory potential and evaluated their IFN response in combination with a commercial cGAMP. These two compounds shown inhibitory activity, but analyses are still ongoing

The choice of these proteins was not only relied on their relevance in therapies, but they also showed to be excellent model systems for a multidisciplinary approach in drug discovery.

In fact, in this PhD research project, we have defined a working model based on the application of computational design, synthesis, molecular biology techniques and NMR binding assays, that has demonstrated how this combined approach is of outmost importance to identify new binder and above all applicable to different targets. In particular, one more time molecular modelling (de novo design, Core Hopping and Virtual screening) combined NMR methodologies (1D ^{1}H NMR screening and 2D HSQC) turned out to be ones of the best tools in the drug discovery. Noteworthy, it is

clear how this our screening method was effective in the identification of new of MDM2, PDL1 and STING binder. This method may be used in the future for any similar system.

In conclusion, this PhD thesis show how the identification and characterization of structurally new, direct binders of these three protein targets is of outmost importance to understanding the full potentialities of small molecule in antitumor therapies both alone and in combination and demonstrated how the combined approach of Modelling/NMR is of outmost importance to identify new binder and above all applicable to different targets.

List of publications

1. Brancaccio, D.; Di Maro, S.; Cerofolini, L.; Giuntini, S.; Fragai, M.; Luchinat, C.; Tomassi, S.; Limatola, A.; **Russomanno, P**.; Merlino, F.; Novellino, E.; Carotenuto, A. HOPPI-NMR: Hot-Peptide-Based Creening Assay for Inhibitors of Protein-Protein Interactions by NMR. *ACS Med. Chem. Lett.* **2020**, *11* (5), 1047–1053.

2. D'Aria, F.; D'Amore, V. M.; Di Leva, F. S.; Amato, J.; Caterino, M.; **Russomanno, P**.; Salerno, S.; Barresi, E.; De Leo, M.; Marini, A. M.; Taliani, S.; Da Settimo, F.; Salgado, G. F.; Pompili, L.; Zizza, P.; Shirasawa, S.; Novellino, E.; Biroccio, A.; Marinelli, L.; Giancola, C. Targeting the KRAS Oncogene: Synthesis, Physicochemical and Biological Evaluation of Novel G-Quadruplex DNA Binders. *Eur. J. Pharm. Sci.* **2020**, *149* (April), 105337.

3. De Simone, A.; La Pietra, V.; Betari, N.; Petragnani, N.; Conte, M.; Daniele, S.; Pietrobono, D.; Martini, C.; Petralla, S.; Casadei, R.; Davani, L.; Frabetti, F.; **Russomanno, P**.; Novellino, E.; Montanari, S.; Tumiatti, V.; Ballerini, P.; Sarno, F.; Nebbioso, A.; Altucci, L.; Monti, B.; Andrisano, V.; Milelli, A. Discovery of the First-in-Class GSK-3β/HDAC Dual Inhibitor as Disease-Modifying Agent to Combat Alzheimer's Disease. *ACS Med. Chem. Lett.* **2019**, *10* (4), 469–474.

4. Daniele, S.; La Pietra, V.; Piccarducci, R.; Pietrobono, D.; Cavallini, C.; D'Amore, V. M.; Cerofolini, L.; Giuntini, S.; **Russomanno, P**.; Puxeddu, M.; Nalli, M.; Pedrini, M.; Fragai, M.; Luchinat, C.; Novellino, E.; Taliani, S.; La Regina, G.; Silvestri, R.; Martini, C.; Marinelli, L. CXCR4 Antagonism Sensitizes Cancer Cells to Novel Indole-Based MDM2/4 Inhibitors in Glioblastoma Multiforme. *Eur. J. Pharmacol.* **2021**, *897* (January), 173936.

5. ***Pasquale Russomanno**, Giulia Assoni Jussara Amato, Vincenzo Maria D'Amore, Riccardo Scaglia Diego Brancaccio Martina Pedrini, Giovanna Polcaro, Valeria La Pietra, Paolo Orlando, Marianna Falzoni, Linda Cerofolini, Stefano Giuntini, Marco Fragai, Bruno Pagano, Ettore Novellino, Angela Zampellal Francesco Sabbatino, Stefano Pepe, Pierfausto Seneci, Daniela Arosio, Luciana Marinelli. Targeting the*

Tumor-Immune Interface: Making Way For Triazine-Based Small Molecules as Novel PD-L1 Inhibitors. ***(Manuscript sent)***